

Green Energy and Technology



David Borge-Diez
Enrique Rosales-Asensio *Editors*

Geothermal Heat Pump Systems



Springer

Green Energy and Technology

Climate change, environmental impact and the limited natural resources urge scientific research and novel technical solutions. The monograph series Green Energy and Technology serves as a publishing platform for scientific and technological approaches to “green”—i.e. environmentally friendly and sustainable—technologies. While a focus lies on energy and power supply, it also covers “green” solutions in industrial engineering and engineering design. Green Energy and Technology addresses researchers, advanced students, technical consultants as well as decision makers in industries and politics. Hence, the level of presentation spans from instructional to highly technical.


****Indexed in Scopus**.**


****Indexed in Ei Compendex**.**

David Borge-Diez · Enrique Rosales-Asensio
Editors

Geothermal Heat Pump Systems

Editors

David Borge-Diez 
Department of Electrical, Systems
and Automation Engineering
University of León
León, Spain

Enrique Rosales-Asensio 
Department of Electrical Engineering
University of Las Palmas de Gran Canaria
Las Palmas de Gran Canaria, Spain

ISSN 1865-3529

ISSN 1865-3537 (electronic)

Green Energy and Technology

ISBN 978-3-031-24523-7

ISBN 978-3-031-24524-4 (eBook)

<https://doi.org/10.1007/978-3-031-24524-4>

© The Editor(s) (if applicable) and The Author(s), under exclusive license to Springer Nature Switzerland AG 2023

This work is subject to copyright. All rights are solely and exclusively licensed by the Publisher, whether the whole or part of the material is concerned, specifically the rights of translation, reprinting, reuse of illustrations, recitation, broadcasting, reproduction on microfilms or in any other physical way, and transmission or information storage and retrieval, electronic adaptation, computer software, or by similar or dissimilar methodology now known or hereafter developed.

The use of general descriptive names, registered names, trademarks, service marks, etc. in this publication does not imply, even in the absence of a specific statement, that such names are exempt from the relevant protective laws and regulations and therefore free for general use.

The publisher, the authors, and the editors are safe to assume that the advice and information in this book are believed to be true and accurate at the date of publication. Neither the publisher nor the authors or the editors give a warranty, expressed or implied, with respect to the material contained herein or for any errors or omissions that may have been made. The publisher remains neutral with regard to jurisdictional claims in published maps and institutional affiliations.

This Springer imprint is published by the registered company Springer Nature Switzerland AG
The registered company address is: Gewerbestrasse 11, 6330 Cham, Switzerland

Contents

Geospatial Distribution of the Efficiency and Sustainability of Different Energy Sources for Geothermal Heat Pumps in Europe	1
Ignacio Martín Nieto, David Borge-Diez, Cristina Sáez Blázquez, Arturo Farfán Martín, and Diego González-Aguilera	
Low-Enthalpy Geothermal Applications	19
Tine Aprianti, Kandadai Srinivasan, and Hui Tong Chua	
Energy Geostructures	67
Norma Patricia López-Acosta, David Francisco Barba-Galdámez, and Kitzia Judith Arizmendi-López	
Multiparametric Evaluation of Electrical, Biogas and Natural Gas Geothermal Source Heat Pumps	103
Cristina Sáez Blázquez, David Borge-Diez, Ignacio Martín Nieto, Arturo Farfán Martín, and Diego González-Aguilera	
Transient Thermal-Resistance-Capacitance Model for U-Tube Ground Heat Exchanger	123
Quan Liao and Wenzhi Cui	
Technical Optimization of the Energy Supply in Geothermal Heat Pumps	157
Cristina Sáez Blázquez, David Borge-Diez, Ignacio Martín Nieto, Arturo Farfán Martín, and Diego González-Aguilera	
The Role of Geothermal Heat Pump Systems in the Water–Energy Nexus	185
Carlos Rey Mahia, Felipe Pedro Álvarez Rabanal, Stephen J. Coupe, and Luis Ángel Sañudo Fontaneda	
Performance Prediction of Hybrid GSHP System Considering Ground Thermal Balance	217
Shiyu Zhou and Wenzhi Cui	

5th Generation District Heating and Cooling Networks as a Heat Source for Geothermal Heat Pumps	259
Robin Zeh, Matthias Schmid, Björn Ohlsen, Stefan Venczel, and Volker Stockinger	
Techno-Economic Assessment of Shallow Geothermal Heat Pump System with Energy Piles	293
Yuanlong Cui, Jie Zhu, and Hui Tong	

Geospatial Distribution of the Efficiency and Sustainability of Different Energy Sources for Geothermal Heat Pumps in Europe



Ignacio Martín Nieto, David Borge-Diez, Cristina Sáez Blázquez, Arturo Farfán Martín, and Diego González-Aguilera

Abstract This research work aims at the multinational study, in Europe, of the emissions and energy costs generated by the operation of low enthalpy geothermal systems, with heat pumps fed by different energy sources. From the economic point of view, gas natural and biogas prizes are, usually, lower than electricity ones. So, it may be advantageous to use these energy sources to feed the heat pumps instead of electricity. From the environmental point of view, it's intended to highlight the fact that under certain conditions of electricity production (electricity mix.), more CO₂ emissions are produced by electricity consumption than using other a priori less “clean” energy sources such as natural gas. In order to establish the countries where each of the different heat pumps may be more cost-efficient and environmentally friendly, multi-source data have been collected and analyzed. The results show that in the whole majority of cases, the electric heat pump is the most recommendable solution. However, there are some countries (such as Poland and Estonia), where the gas engine heat pump may be a better alternative.

Keywords Electric heat pumps · Gas driven heat pumps · Electricity mix · Economic and environmental analysis

Nomenclature and Formulae

HP	Heat pump
COP	Coefficient of performance
SPF	Seasonal performance factor
GSHP	Ground source heat pump geothermal system
EHP	Electric heat pumps

I. M. Nieto · A. F. Martín · D. González-Aguilera
Department of Cartographic and Land Engineering, University of Salamanca, Higher Polytechnic School of Avila, Hornos Caleros 50, 05003 Avila, Spain

D. Borge-Diez (✉) · C. S. Blázquez
Department of Electric Systems and Automatic Engineering, University of León, León, Spain
e-mail: david.borge@unileon.es

GEHP	Gas engine heat pump
LPG	Liquefied petrol gas
W	Mechanical energy from the compressor (MWh)
Q_c	Thermal energy from the condenser (MWh)
Q_e	Thermal energy from the evaporator (MWh)
C_1	Coefficient of performance of the electric motor or the gas engine motor of the HP
C_2	Average performance of the thermoelectric transformation of the primary energy into electricity.
HCV	Higher calorific value
IDEA	Institute for the diversification and energy saving
EUROSTAT	Statistical office of the European Union
EP	Electricity prices (€/kWh)
EEC	Emissions (CO ₂) by electricity consumption (g CO ₂ /kWh)
NGP	Natural gas prices (€/kWh)
ENGCO	Emissions (CO ₂) by natural gas consumption (g CO ₂ /kWh)

1 Introduction

Many European countries are heavily committed in developing a sustainable and decarbonized energy system [1]. This may be due, in large part, to the lack of oil and natural gas resources in most of the countries of Europe. In the challenge to reduce the CO₂ emissions, the building stock plays a very important role because it is responsible for the 36% of emissions in the E.U.

Heating and cooling systems powered by electricity instead of fossil fuels may become more and more important in the future due to the upcoming policies of CO₂ emissions control [2]. In this environment, the low enthalpy geothermal systems may emerge as one of the best solutions available due to the wide locations where is possible to install these systems and the high efficiency of them [3].

The above-mentioned systems do not depend on great geothermal anomalies; they can be installed in many other places where a certain heat conductivity of the ground and some initial temperature conditions can be found [4]. In exchange for this wide availability, these systems are not able to use geothermal energy in a direct way; they need to include a heat pump in their core.

These heat pumps may work with electricity or with natural gas or even biogas. The first group may be the most environmentally friendly, however, under certain circumstances, the natural gas and biogas driven heat pumps can be more efficient in terms of CO₂ emissions and annual costs.

The idea of the present work is to make a comparison between heat pumps belonging to low enthalpy geothermal systems, working under different conditions (technical, economic and energetic), in many different European countries.

Heat pumps (HPs) constitute a very important part of the aforementioned installations [5] so one of the main concerns about using them in low enthalpy geothermal systems is associated with their primary energy consumption. The performance of an HP is commonly characterized by the Coefficient of Performance (COP) and the Seasonal Performance Factor (SPF). Both are performance coefficients, defined by the ratio between the heat obtained through the HP and the primary energy consumed by it (most of it goes to the activation and operation of the compressor's power unit). The COP is obtained using instantaneous values, while in the SPF are considered annual behaviors [6, 7]. For the present work, we have used the COP of the chosen HPs to make the comparisons due to data availability; nevertheless, we think that using the SPF instead wouldn't change the results in a significant way.

The general workflow followed in this study is shown in the next diagram (Fig. 1).

We must also remember that the COP of a HP conditions the design of the well field associated to the geothermal system. A higher COP means that the field must supply much more energy to the system so a much larger well field is needed. In the HPs driven by natural gas and biogas, the COPs are much lower; this reduces the drilling length of the well field. so the initial investment is smaller [8].

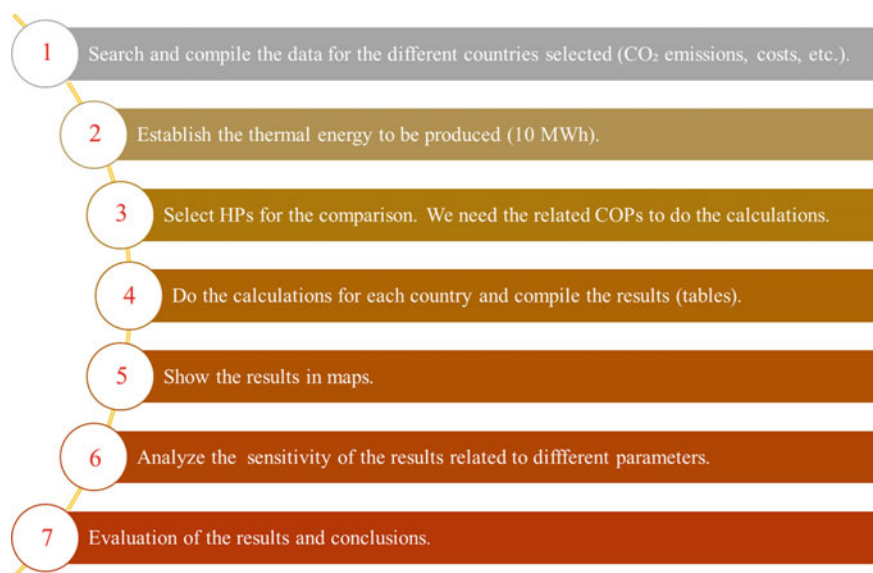


Fig. 1 Description of the workflow followed in the present research

2 Heat Pumps Technology

Ground source heat pumps geothermal systems (GSHPs) use the ground as a heat source or sink depending on seasonal working conditions. In heating mode (winter), heat is extracted from the ground by the set of boreholes, the energy taken from the ground is then lifted by the heat pump up into the building/s. For cooling applications (summer), this process can be reversed, injecting the heat extracted from the building into the ground.

In order to perform the thermal delivery from the ground to the building, the heat pump performs a cyclic process with the following phases (in the heating cycle, for the cooling cycle is the same in reversed order):

1. Liquid refrigerant inside the heat pump, absorbs heat in the evaporator from the ground loop, turning into gas.
2. The refrigerant is put through a compressor, which raises the pressure of the gas, increasing its temperature.
3. The hot gas flows through condenser coils inside the building to be heated, and since it is at a higher temperature than this space, it transfers heat to the room and condenses back into a liquid.
4. The liquid finally flows back through a valve (expansion valve), which reduces its pressure in order to cool it down so it can repeat the cycle.

In step 2 (Fig. 1) we have a compressor, the way of powering the compressor shaft will condition the type of heat pump (HP) we may choose. Although the cycle described above is the same in all HPs, depending on the primal energy, there are some differences between HPs which are worth commenting on.

Heat pumps are usually categorized as electric heat pumps (EHPs) or gas engine heat pumps (GEHPs) [9]. Most of the current heat pump models in the market are driven by electric motors. Regarding gas engine heat pumps, this equipment is recently used as an alternative to the conventional electric heat pumps. They use natural gas, liquefied petrol gas (LPG) or biogas and are able to recover the waste heat released by the engine to enhance the total heating capacity (this characteristic makes it possible to significantly reduce the drilling length of the well field) [10].

For an EHP operating in heating mode we can establish energy efficiency as follows. We may start quite intuitively, thinking about the balance between the energy we introduce and the heat we are going to get. Thus, a COP (Coefficient of performance) which is the most widespread coefficient to compare performances of heat pumps (European Standard EN-14825–2016 of good practices in the calculation of HPs performance), can be defined, as follows (Eq. 1).

$$COP = \frac{Q_c}{W} = \frac{Q_c}{Q_c - Q_e} = \frac{1}{1 - \frac{Q_e}{Q_c}} \quad (1)$$

The concept of performance of our system can be extended to the electrical supply and performance of our compressor (electric), defining what is known as global coefficient of performance (Eq. 2):

$$COP_{global} = C_1 * C_2 * COP$$

(2)

The coefficient of performance of the electric motors (C_1) of heat pumps in the domestic regime is around 90%. C_2 depends on the electric mix of the situation where the HP is operating [11].

Data from the EHP selected for this study are presented, in order to be able to implement the comparison in a table (Tables 1 and 2) later on, the typical COP of these heat pumps is around 4–4.5 [12].

There are heat pumps on the market (GEHPs) which perform the thermodynamic heat exchange cycle described above driven by a compressor which in turn is driven

Table 1 General features of electric heat pumps versus gas engine heat pumps

	EHP	GEHP
Energy consumption	Electric consumption	Natural gas, biogas consumption
Compressor shaft's engine performance	Around 90% and up	Around 30–35%
COP	1.5–1.7	4–4.5
Refrigeration circuit	Not required	Required (heat recovery systems)
Equipment cost	High	Very high
Operation costs	Electricity price	Gas or biogas price
Weight of the equipment	Normal	Very high
CO ₂ emissions	Electricity mix of the area	Natural gas 252 g/kWh; biogas 0 g/kWh

Table 2 Characteristics of the heat pumps used for the comparative

EHP		GEHP	
Watkotte GmbH Basic Line Ai1 Geo		AISIN (Toyota group) GHP 8hp	
COP EN14511 B0/W35 ^a	4.6	COP ^b	1.57
Refrigerant	R410A ^c	Refrigerant	R410A
Power consumption output	5.7 kW	Power consumption	8hp (5.96 kW)
Electrical engine performance	92%	Gas engine	3 cylinder, 4-stroke
		Gas engine performance	32%
		Engine displacement	952 cm ³
		Water cooling engine, heat recovery systems	

^a A device using brine as heat source and water as heat transfer for example is called a brine/water heat pump. In the case of brine/water heat pumps, the nominal standard conditions at low temperature are for brine at 0 °C (B0, B = brine, a mixture of anti-freeze and water) and a heating water temperature of 35 °C (W35, W = water). This boundary condition is abbreviated to B0W35

^b No brine temperature is given, due to the pre-heating cycle previous to the evaporator inlet

^c Mixture of difluoromethane (CH₂F₂, called R-32) and pentafluoroethane (CHF₂CF₃, called R-125), patented by Allied Signal (now Honeywell International Inc.) in 1991

by an internal combustion engine (most commonly fueled by natural gas or biogas). In this case, Eq. (2) turns into Eq. (3).

$$COP_{global} = C_1 * COP \quad (3)$$

The thermodynamic performance obtained from that Otto cycle engine, C_1 from Eq. (3) here is usually around 30–35% [13]. This reduces the COP of the heat pump thinking in terms of the energy provided (from the natural gas) and the energy obtained from the land to be transferred to the building. The COP from GEHPs is usually around 1.5–1.7 (more detailed data about the GEHP selected for this study can be found in Table 2).

The effect of the lower performance of the Otto cycle engine, from the GEHPs, compared to the electric one of the EHPs electric heat pumps, may induce GSHP designers to think that the EHP is a better choice in any case, however, we must take into account some considerations:

- The price per kWh of natural gas and biogas is much cheaper than the price per kWh of electricity in general in most countries of Europe.
- The sizing of the geothermal well field is reduced more or less by a half (depending on the thermal conductivity of the project's site). This means a very significant lowering of the initial investment in the installation. Recall that the initial investment is one of the main drawbacks when considering a geothermal system instead the other alternatives [14].
- The heat produced in the internal combustion engine driving the compressor's shaft, excess heat that cannot be used as mechanical energy, is usually used to heat the geothermal fluid from the wells before being introduced in the evaporator intercooling system of the heat pump. This increases significantly the performance of the internal heat pump process. It can be used also to feed the domestic hot water circuit of the installation.

So the heat pumps selected for this study are described in Table 1. All the characteristics are from a real heat pump which can be purchased and included in a geothermal system.

The same characteristics for the GEHP and the biogas HP are assumed, although there are some differences between the two energy sources explained in the next section. These differences may require specific design of the devices in the biogas HPs which are not yet available in the market.

3 Analysis Description

The objective of this study, as presented in the introduction, is to compare the economic and environmental performances of different HPs in different European countries. This will be done by considering a certain quantity of thermal energy (equal for all cases) in order to describe how this thermal energy is delivered by each one

of the different heat pumps in each case and then reveal the economic and environmental costs of the process. The annual energy demand in Europe of a single-family home strongly depends on the climate area where this is located [10, 15]. In the cited article [10], there are described the thermal needs of the same building located in the three different climate areas established by the European Directive 2009/28/CE [16]. The annual thermal needs in these three equal buildings are: 39.088, 71.742 and 88.882 MWh per year. As can be seen, the usual thermal needs in Europe for a regular home are in the order of magnitude of some tens of MW per year. So, 10 MWh of thermal energy has been established as the reference energy to be produced in this comparison by the different systems.

3.1 Heat Pump Selection

For this study, two types of domestic heat pumps have been selected in order to perform the analysis on a real basis, in Table 2 are the characteristics of both devices.

The GEHP will be asked also to work with Biogas for the shake of this study, although this technology is not fully developed, it could be one of the best solutions from the economic and the environmental points of view. To be able to work with biogas some considerations about the system must be assumed. First of all, at the moment there aren't any HPs in the market ready to be fed with biogas yet, so for this study the data from the GEHP selected in Table 2 will be used as if were possible to feed that HP with biogas. Secondly, the consumption of the GEHP fed with biogas will be greater than with natural gas to get the same amount of energy, this is because the biogas higher calorific value (HCV) is lower than the natural gas HCV. According to the Institute for the Diversification and Energy Saving "IDAE" [10] the biogas HCV is 46.21% lower than the natural gas HCV, so the volumetric gas consumption will be 46.21% higher in this case. However, the COP of the biogas GEHP will remain the same because it only depends on the energy balance of the thermodynamic process, and here the thermal energy supplied by the natural gas and the biogas are the same.

3.2 Input Energies

A brief look at the energies used in the operation of the correspondent HPs. Main characteristics and sources are given, in order to establish the framework for the economic and environmental calculations in the next section.

3.2.1 Natural Gas

An equal natural gas composition is established for all countries, consisting of 99% methane and 1% of other components, mainly CO₂ [17].

Energy data, comes from the IDAE, in its report on calorific powers of fuels, where it quotes sources from EUROSTAT and the International Energy Agency (IEA). HCV of natural gas is set to 9667 kcal/Nm³ (11.23 kWh/Nm³).

Regarding the emissions, data from IDAE, in its guide of CO₂ emissions for each energy source [18], has been considered. Then 0.252 kg CO₂/kWh of final energy will be the used in further calculations. These energy and CO₂ emissions data can be extended to all countries, since we have set equal natural gas conditions.

3.2.2 Biogas

The IDAE data for calorific powers of fuels mentioned in Sect. 3.2.1 has been used as a reference here also. HCV of 5200 kcal/Nm³ (6.04 kWh/Nm³) for biogas is set, from that same source.

The biogas type composition is 53.5% Methane and 46.5% CO₂. The energetic consequence of this chemical composition, established as standard for all countries, is clear if we compare the calorific values of the natural gas and biogas. This is also mentioned in previous sections.

3.2.3 Electricity

In order to calculate CO₂ emissions by electric energy use, data from the International Energy Agency have been used. The fraction of the CO₂ emissions that should come from electricity production only have been proportionally separated, taking into account the amounts of generation that come from renewable energies and those that do not (data in I.A.E. Statistics by country).

The process of obtaining the CO₂ emissions factor by electricity production in each country, has started from the separation of total emissions by electricity and large-scale heating. Here it has been taken into account that the data on the production of electricity from fossil fuels (those that contribute to these emissions), is given to us in the form of electrical energy, a performance factor in that transformation of 0.4 have been considered in order to evaluate the thermal energy used, and to be able to establish a proportion which determines the electrical contribution to the total emissions of the data.

4 Costs and Emissions Comparative

In Table 3 the countries selected and the CO₂ emissions and household prices for the three types of energies considered to feed the different HPs are presented.

Emissions and costs in the three cases of primal energy feed to the HPs in different countries selected can be found in Table 4. Emissions from biogas combustion are usually considered to be zero, because of the neutral cycle contemplated during its production. For the costs and emissions in EHP and GEHP fed by natural gas, the associated calculations have been performed as follows.

For the EHP, Eqs. (4) and (5):

$$\text{Costs (€/10 MWh)} = \frac{EP (\text{€/kWh}) * 1000 \left(\frac{kWh}{MWh} \right) * 10}{COP} \quad (4)$$

$$\text{Emissions (kgCO}_2\text{/10 MWh)} = \frac{EEC \left(\frac{gCO_2}{kWh} \right) * 10}{COP} \quad (5)$$

For the GEHP, Eq. (6):

$$\text{Costs (€/10 MWh)} = \frac{NGP (\text{€/kWh}) * 1000 \left(\frac{kWh}{MWh} \right) * 10}{COP} \quad (6)$$

$$\text{Emissions (kgCO}_2\text{/10 MWh)} = \frac{ENG C \left(\frac{gCO_2}{kWh} \right) * 10}{COP} \quad (7)$$

Biogas prizes are an estimation based on prizes offered in Spain by some biogas producers extended to all the other countries by keeping the ratio of the prize with the natural gas (this seems to fit in the countries with biogas prizes available to compare).

As shown, while biogas prices are related to the natural gas prices or taken directly from suppliers, biogas emissions are considered zero.

With all the data from Table 3 and the formulas referred above, we can introduce Table 4.

There are some remarkable results in Table 4. Regarding the economic aspect, biogas costs are, by far, the cheapest of all the three options. EHPs prices to get 10 MWh are commonly higher than the ones from GEHPs except for three countries: The Netherlands, Sweden and Czech Republic (Figs. 3 and 4).

From the emissions point of view, Table 4 shows that there are two countries (Poland and Estonia), where EHPs CO₂ emissions are higher than GEHPs emissions as suggested in previous sections. We can see also that there are some countries where both emissions are quite similar (Fig. 4).

Combining together cost and emissions, Poland and Estonia showed a lower costs and lower emissions scenario for GEHPs against EHPs. Greece shows lower costs

Table 3 Countries, CO₂ emissions and household prices for electricity, natural gas and biogas

Countries	EEC (g CO ₂ /kWh) ^a	ENGCE (g CO ₂ /kWh) ^b	EP (€/kWh) ^c	NGP (€/kWh) ^c	Biogas prices (€/kWh) ^c
Belgium	169.6	252.0	0.2824	0.0547	0.0042
Bulgaria	470.2	252.0	0.0979	0.0368	0.0028
Czech Republic	512.7	252.0	0.1573	0.0583	0.0045
Denmark	166.1	252.0	0.3126	0.0583	0.0064
Germany	440.8	252.0	0.2987	0.0661	0.0051
Estonia	818.9	252.0	0.1348	0.0346	0.0027
Ireland	424.9	252.0	0.2369	0.0652	0.0050
Greece	623.0	252.0	0.1672	0.0564	0.0027
Spain	265.4	252.0	0.2383	0.0677	0.0050
France	58.50	252.0	0.1748	0.0650	0.0043
Croatia	210.0	252.0	0.1311	0.0428	0.0052
Italy	256.2	252.0	0.2067	0.0731	0.0050
Latvia	104.9	252.0	0.1531	0.0424	0.0033
Lithuania	18.0	252.0	0.1097	0.0413	0.0032
Luxemburg	219.3	252.0	0.1671	0.0454	0.0035
Hungary	260.4	252.0	0.1123	0.0344	0.0026
Netherlands	505.2	252.0	0.1706	0.0779	0.0060
Austria	85.1	252.0	0.1966	0.069	0.0053
Poland	773.3	252.0	0.1410	0.0392	0.0030
Portugal	324.7	252.0	0.2246	0.0913	0.0070
Romania	306.0	252.0	0.1333	0.0332	0.0026
Slovenia	254.1	252.0	0.1613	0.0599	0.0046
Slovakia	132.3	252.0	0.1566	0.046	0.0035
Finland	112.8	252.0	0.1612	0.0310	0.0024
Sweden	13.3	252.0	0.1891	0.1129	0.0087
U.K.	281.1	252.0	0.1887	0.0553	0.0042

^a Source “Data and Statistics by country, CO₂ emissions from electricity and heat by energy source,” (2018). International Energy Agency (IEA), 31–35 rue de la Fédération 75,739, Paris, France

^b “Factores de emisión de CO₂ y coeficientes de paso a energía primaria de diferentes fuentes de energía final consumidas en el sector de edificios en España.”. Instituto para la Diversificación y Ahorro de la Energía, “IDAE” 2018

^c International Monetary Fund. World Economic Outlook Database, October 2018. Eurostat Database, 2019

Table 4 Costs and emissions

Countries	Costs (€) ^a			Emissions (kg CO ₂) ^a		
	EHP	GEHP	BIO-GEHP	EHP	GEHP	BIO-GEHP
Belgium	706.00	348.41	26.76	424.00	1605.10	0
Bulgaria	244.75	234.39	18.00	1175.50	1605.10	0
Czech Republic	393.25	371.34	28.52	1281.75	1605.10	0
Denmark	781.50	530.57	40.75	415.25	1605.10	0
Germany	746.75	421.02	32.34	1102.00	1605.10	0
Estonia	337.00	220.38	16.93	2047.25	1605.10	0
Ireland	592.25	415.29	31.90	1062.25	1605.10	0
Greece	418.00	359.24	27.59	1557.50	1605.10	0
Spain	595.75	431.21	33.12	663.50	1605.10	0
France	437.00	414.01	31.80	146.25	1605.10	0
Croatia	327.75	272.61	20.94	525.00	1605.10	0
Italy	516.75	465.61	35.76	640.50	1605.10	0
Latvia	382.75	270.06	20.74	262.25	1605.10	0
Lithuania	274.25	263.06	20.21	45.00	1605.10	0
Luxemburg	417.75	289.17	22.21	548.25	1605.10	0
Hungary	280.75	219.11	16.83	651.00	1605.10	0
Netherlands	426.50	496.18	38.11	1263.00	1605.10	0
Austria	491.50	439.49	33.76	212.75	1605.10	0
Poland	352.50	249.68	19.18	1933.25	1605.10	0
Portugal	561.50	581.53	44.67	811.75	1605.10	0
Romania	333.25	211.46	16.24	765.00	1605.10	0
Slovenia	403.25	381.53	29.31	635.25	1605.10	0
Slovakia	391.50	292.99	22.50	330.75	1605.10	0
Finland	403.00	197.45	15.17	282.00	1605.10	0
Sweden	472.75	719.11	55.23	33.25	1605.10	0
U.K.	471.75	352.23	27.05	702.75	1605.10	0

^a To produce 10 MWh (thermal energy) as explained in Sect. 3

from GEHPs and similar emissions and The Netherlands presents similar emissions but higher costs from GEHPs.

Evolutions expected and extended conclusions are detailed in the next sections.

5 Sensitivity Analysis

This section presents a sensitivity analysis to evaluate how different factors may influence the costs and the emissions of the different HPs considered. We will be proposing changes in the main factors guided by the recent circumstances around them, and also taking into account the political and social environment.

5.1 Sensitivity Related to COP Improvement in EHPs

A 25% improvement in the COP of the EHPs (from 4 to 5 in our case) could be possible in the near future according to the past behavior, so seems interesting to take into account this scenario.

This COP enhancement may come from new and improved designs on this device and also because of the improvements in the design of the geothermal systems where an improvement in the working conditions may affect the COP [19].

With this COP improvement in the EHPs, the map from Figs. 2 and 3 changes a lot (Fig. 4). We have 12 countries now (instead of two) where the cost to get 10 MWh of thermal energy is higher from the GEHPs than from the EHPs.

Regarding the emissions in this scenario, is interesting to compare Fig. 3 with Fig. 5. Whereas in the first case there are two countries with higher emissions from the electricity mix than from the gas engine heat pumps, in the new scenario, there is only one country in this situation, Estonia, and two other countries where emissions are similar (difference is less than 25%), Poland and Greece, The Netherlands have now clearly lower emissions from EHPs.

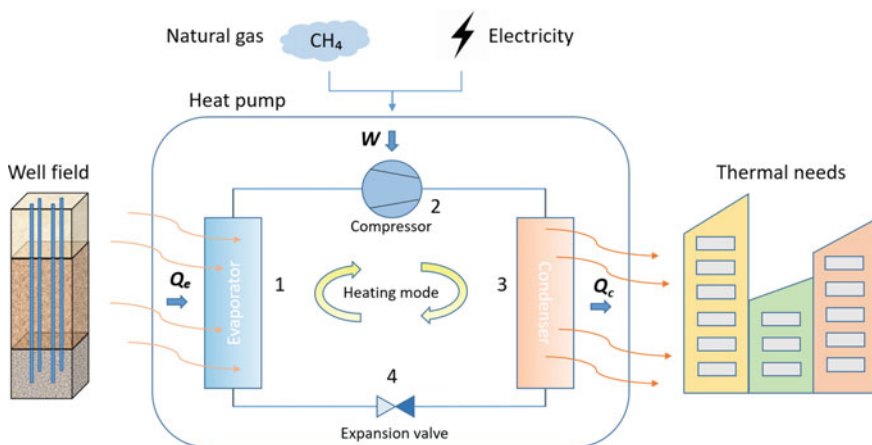


Fig. 2 Phases in the cyclic process inside a heat pump in heating mode (Q_e heat exchanged in the evaporator and Q_c heat exchanged in the condenser)

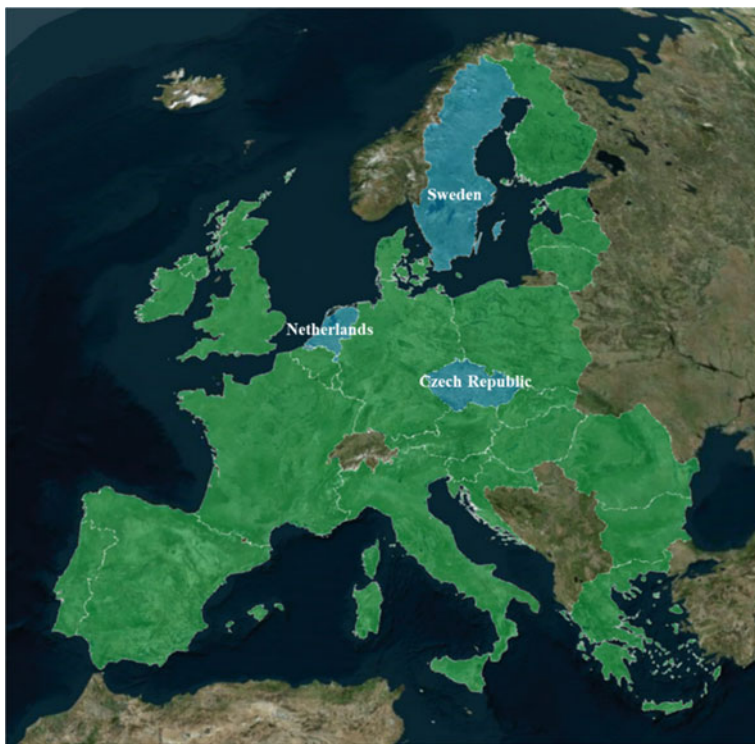


Fig. 3 From Table 4, countries with higher costs from EGP in green. Netherlands, Sweden and Czech Republic, in blue, have higher costs from GEHP (biogas powered HPs has lower costs in all the countries)

5.2 Sensitivity Related to COP Improvement in GEHPs

Due to the low market penetration of these models of HPs, is not realistically expected an improvement in the COP of these systems based on research and development in the factories. In addition to this, the political environment in Europe is not favoring these kinds of devices although the geothermal systems should be considered important in the future plans for the heating & air-conditioning industry.

It is also worth mentioning that an important improvement in the COP of these systems will mean that one of the main advantages of the GEHPs could be compromised. This is the ability to reduce in a considerable way the drilling length of the well field.

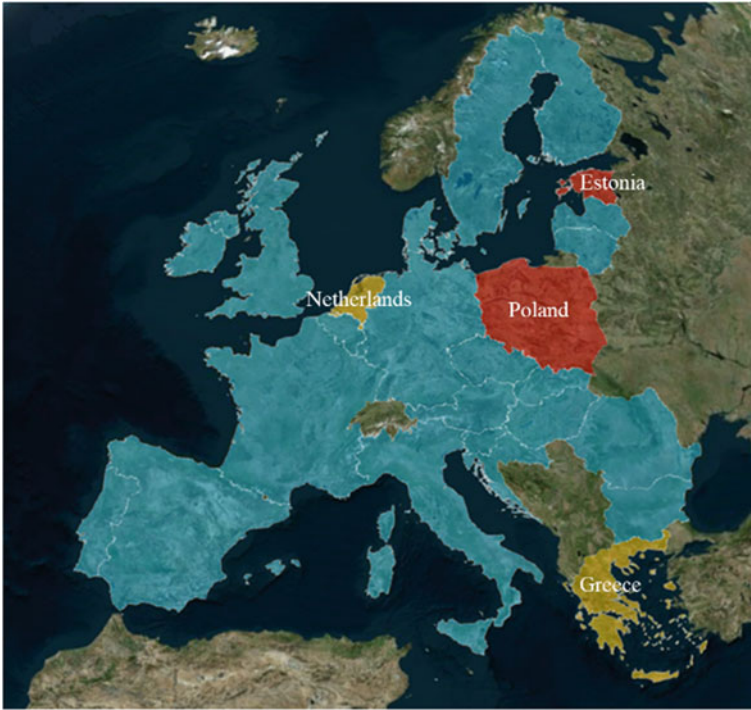


Fig. 4 From Table 4, countries with higher emissions from GEHP in light-blue. Poland and Estonia in red, have higher emissions from EHPs than from GEHPs. Netherlands and Greece, in light-orange, their emissions from EHPs and GEHPs differ less than 20% (biogas powered HPs have, of course, no emissions in all the countries)

5.3 Sensitivity Related to Emissions in Electricity Production

This scenario is especially important for the countries in Fig. 3 where emissions from EHP are higher than the ones from GEHPs, in those cases is where an improvement in the emissions from electricity production can produce a change concerning the solutions with less emissions.

Figure 6 shows the evolution of the CO₂ emissions from electricity production in these four countries.

In two countries, Poland and Estonia, the emissions from GEHPs were less than the ones from EHPs. As Fig. 6 shows in both cases, there isn't any clear decreasing signal in the evolution of the emissions through the last 4–5 years. So, it is unlikely to find a significant change in the near future [20] Fig. 7.

The two other countries from Fig. 3, Greece and The Netherlands, are special because their emissions from EHPs are lower but quite near the ones from GEHPs. Here a downward trend in the emissions is observed, especially in The Netherlands. This may affect the selection of GEHPs since the costs are also higher there.

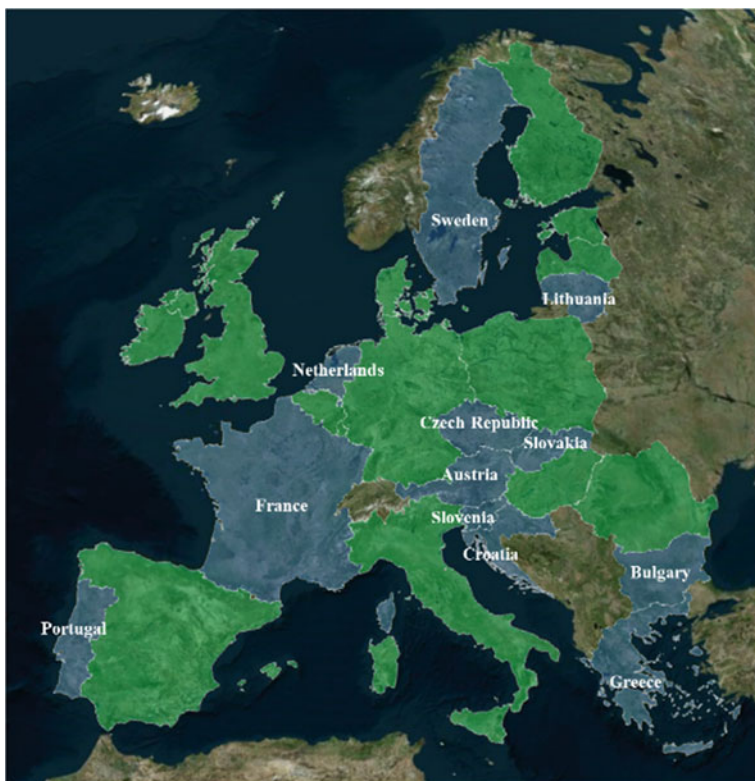


Fig. 5 Green countries represent higher costs from EHPs. Blue countries represent higher costs from GEHPs

6 Conclusions

It is clear from all the data collected and compiled in this work, that the biogas driven HPs are the best solution from the economic and environmental points of view. Development and widespread of these types of GSHP systems would contribute to the low emission policies to be implemented in Europe in the near future [21].

Apart from this, in most countries, EHPs are much more common than GEHPs. The results from this work seem to agree with this selection of most Europeans. However, although emissions are clearly higher from GEHPs, the reduction of the drilling length, with the reduced initial investment derived from this, may be an important factor to consider. Also, the annual costs seem to be lower from gas natural in most countries. Maybe the purchase price of the GEHP is higher but this is fully balanced with the price reduction in the construction of the well field.

In Table 5 we find the four countries where the selection of the type of HP may be not so straight forward.



Fig. 6 Blue countries where CO₂ emissions from EHPs are lower than from GEHPs. Red countries where emissions from GEHPs are lower than from EHPs. Orange countries equal to blue ones except that the difference is less than 25%

It is clear that Poland and Estonia, under the current circumstances (not expecting to change so much in the near future [13]) the GEH P is the ideal selection, from the economic and environmental points of view.

In The Netherlands, the gas price is against the GEHPs, and the emissions are lower from EHPs and going in that direction also in the future The usual selection would be electrical. The Greek case is similar, here even the annual costs are lower for the GEHPs. However, future developments in CO₂ emissions from electricity production and COP improvements in EHPs seem to recommend the electric choice also.

We can conclude that, for some countries, and under certain circumstances, it may be a good idea to recommend the GEHPs in order to reduce the thermal energy costs and the CO₂ emissions at the same time. The cut-out in the initial investment is also an advantage to take into consideration.

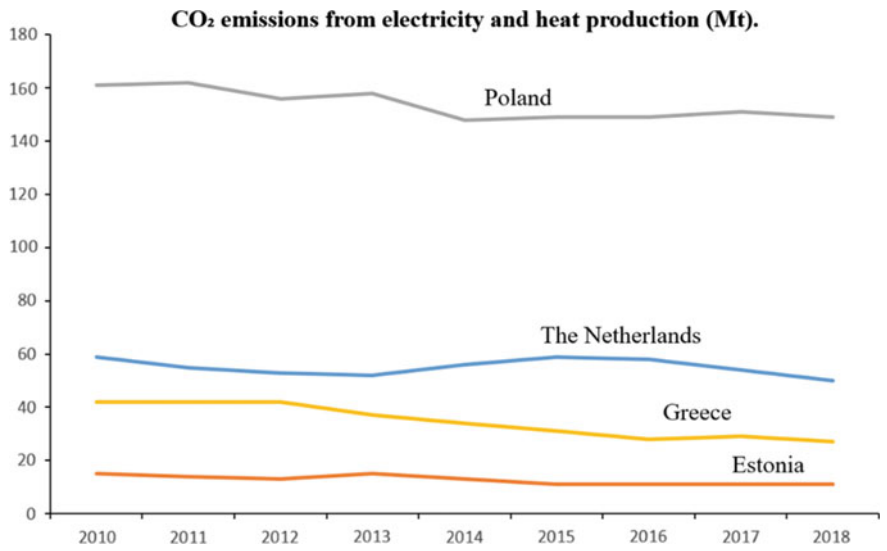


Fig. 7 Evolution of the CO₂ emissions by electricity production in the countries selected. IEA. CO₂ emissions by energy source

Table 5 Countries where GEHPs may be more suitable from the economic and environmental points of view

	10 MWh (thermal energy)			
	Costs (€)		Emissions (kg CO ₂)	
	EHP	GEHP	EHP	GEHP
Countries				
Estonia	337	220.38	2047.25	1605.1
Poland	352.5	249.68	1933.25	1605.1
Greece	418	359.24	1557.5	1605.1
Netherland	426.5	496.18	1263	1605.1

Apart from these exceptional cases, in most countries in Europe an EHP may be a better option (mainly due to the emissions factor), and will be getting even better in the near future.

Acknowledgements Authors would like to thank the Department of Cartographic and Land Engineering of the Higher Polytechnic School of Avila, University of Salamanca, for allowing us to use their facilities and their collaboration during the experimental phase of this research. Authors also want to thank the University of Salamanca and Santander Bank for providing a pre-doctoral Grant (Training of University Teachers Grant) to the corresponding author of this study what has made possible the realization of the present work.

References

1. Bouzarovski S, Tirado Herrero S (2017) The energy divide: Integrating energy transitions, regional inequalities and poverty trends in the European Union. *Eur Urban Reg Stud* 24(1):69–86
2. DIRECTIVE (EU) 2018/2001 of the European parliament and of the council of 11 December 2018 on the promotion of the use of energy from renewable sources
3. Rybach L (2014) Geothermal power growth 1995–2013—A comparison with other renewables. *Energ* 7(8):4802–4812
4. Colmenar-Santos A, Palomo-Torrejón E, Rosales-Asensio E, Borge-Diez D (2018) Measures to remove geothermal energy barriers in the European Union. *Energ* 11(11):3202
5. Neuberger P, Adamovský R (2017) Analysis of the potential of low-temperature heat pump energy sources. *Energies* 10(11):1922
6. Borge-Diez D, Colmenar-Santos A, Pérez-Molina C, López-Rey Á (2015) Geothermal source heat pumps under energy services companies finance scheme to increase energy efficiency and production in stockbreeding facilities. *Energ* 88:821–836
7. Fraga C, Hollmuller P, Schneider S, Lachal B (2018) Heat pump systems for multifamily buildings: potential and constraints of several heat sources for diverse building demands. *Appl Energy* 225:1033–1053
8. Angrisani G, Diglio G, Sasso M, Calise F, d'Accadia MD (2016) Design of a novel geothermal heating and cooling system: Energy and economic analysis. *Energy Convers Manage* 108:144–159
9. Lian Z, Park SR, Huang W, Baik YJ, Yao Y (2005) Conception of combination of gas-engine-driven heat pump and water-loop heat pump system. *Int J Refrig* 28(6):810–819
10. Blázquez CS, Borge-Diez D, Nieto IM, Martín AF, González-Aguilera D (2019) Technical optimization of the energy supply in geothermal heat pumps. *Geothermics* 81:133–142
11. Weisser D (2007) A guide to life-cycle greenhouse gas (GHG) emissions from electric supply technologies. *Energ* 32(9):1543–1559
12. Self SJ, Reddy BV, Rosen MA (2013) Geothermal heat pump systems: Status review and comparison with other heating options. *Appl Energy* 101:341–348
13. Mozurkewich M, Berry RS (1982) Optimal paths for thermodynamic systems: the ideal Otto cycle. *J Appl Phys* 53(1):34–42
14. Sáez Blázquez C, Farfán Martín A, Nieto IM, González-Aguilera D (2018) Economic and environmental analysis of different district heating systems aided by geothermal energy. *Energ* 11(5):1265
15. Boyano A, Hernandez P, Wolf O (2013) Energy demands and potential savings in European office buildings: Case studies based on EnergyPlus simulations. *Energ Build* 65:19–28
16. Directive 2009/28/EC of the European Parliament and of the Council of 23 April 2009 on the promotion of the use of energy from renewable sources and amending and subsequently repealing Directives 2001/77/EC and 2003/30/EC
17. Instituto para la Diversificación y Ahorro de la Energía (2014) IDAE, Factores de emisión de CO₂ y coeficientes de paso a energía primaria de diferentes fuentes de energía final consumidas en el sector edificios en España
18. IDAE (2016) Factores de emisión de CO₂ y coeficientes de paso a energía primaria de diferentes fuentes de energía final consumidas en el sector de edificios en España. Instituto para la Diversificación y Ahorro de la Energía
19. AENOR (2019) UNE-EN 14825:2019. Air conditioners, liquid chilling packages and heat pumps, with electrically driven compressors, for space heating and cooling—Testing and rating at part load conditions and calculation of seasonal performance
20. European Environment Agency. Overview of electricity production and use in Europe. Chapter: Is electricity production in Europe becoming less carbon intensive? Published 18 Dec 2018
21. DIRECTIVE (EU) (2018) 2018/844 of The European Parliament and of the Council, amending Directive 2010/31/EU on the energy performance of buildings and directive 2012/27/EU on energy efficiency. Off J Eur Union

Low-Enthalpy Geothermal Applications



Tine Aprianti, Kandadai Srinivasan, and Hui Tong Chua

Abstract This chapter discusses two low-enthalpy geothermal applications in Perth, Western Australia. The first application pertains to using tepid groundwater for the municipal heating of Olympic-size outdoor swimming pools. The second application examines the viability of ground source heat pumps (GSHP) against air source heat pumps (ASHP). In the first application, the objective is to develop an accurate sizing methodology to improve the capital effectiveness for geothermal swimming pools. The predicted pool-water temperature and heating demands are compared against on-site measurements at a Leisure Centre. This model can replicate 71 and 73% of the measured heating capacity data within ± 25 kW for the 30-m pool and ± 35 kW for the 50-m pool, respectively. In the second application, we assess the feasibility of implementing a GSHP vis-à-vis an ASHP for domestic applications. For the second application, the GSHP has a constant coefficient of performance (COP) of $3.8 \pm 6.7\%$, while that of ASHP ranges from 2.2 to $2.7 \pm 6.5\%$. For cooling, the GSHP has a constant COP of $3.1 \pm 13\%$, while that of ASHP varied between 1.4 and $2.4 \pm 11.5\%$. When a GSHP is considered with a planned installation of a borehole for irrigation, the payback period ranges from near-immediate to four years.

Keywords Electric heat pumps · Heating and cooling · Ground source heat pump · Economic and environmental analysis

T. Aprianti · K. Srinivasan · H. T. Chua (✉)

Chemical Engineering Department, The University of Western Australia, 35 Stirling Hwy, Perth, WA 6009, Australia

e-mail: huitong.chua@uwa.edu.au

T. Aprianti

Chemical Engineering Department, Universitas Sriwijaya, Jl. Raya Palembang-Prabumulih KM.32 Inderalaya, Ogan Ilir, Sumatera Selatan, Palembang 306622, Indonesia

Nomenclature and Formulae

A	Pool surface area (m^2)
C_8	Cloud cover factor (oktas)
$C_{cloud\ effect}$	A scaling parameter to reflect the effect of cloud cover
C_p	Specific heat capacity (kJ/kg K)
D_{AB}	Binary diffusion coefficient for water and air at 1 atm (m^2/s)
E	Irradiance (W/m^2)
F	View factor
g	Gravitational acceleration (m/s^2)
Gr	Grashof number
h	Heat transfer coefficient ($\text{W/m}^2 \text{ K}$)
h_{fg}	Heat of vaporisation of water (kJ/kg)
h_m	Mass transfer coefficient (m/s)
k	Thermal conductivity (W/m K)
L	Length of the pool (m)
\dot{m}	Mass flow rate of water (kg/s)
\dot{n}	Mass transfer rate (kg/s)
Nu	Nusselt number
Pr	Prandtl number
p	Pressure (Pa)
Q	Heat transfer (kW)
Ra	Rayleigh number
Re	Reynolds number
Sc	Schmidt number
Sh	Sherwood number
T	Temperature (K)
t	Temperature ($^{\circ}\text{C}$)
U	Wind speed (m/s)
W	Width of pool (m)

Greek Symbols

α	Absorptivity of the pool
ε	Emissivity
ρ	Density (kg/m^3)
σ	Stefan-Boltzmann constant ($\text{W/m}^2 \text{ K}^4$)
ϕ	Relative humidity (%)
μ	Viscosity (kg/m s)
θ	Angle of incidence of wind (degrees)
ν	Kinematic viscosity (m^2/s)

Subscripts

<i>a</i>	Air
<i>BOM</i>	Bureau of Meteorology
<i>cs</i>	Clear sky
<i>dew</i>	Dew point
<i>diff</i>	Diffusivity
<i>evap</i>	Evaporation
<i>conv</i>	Convection
<i>f</i>	Film
<i>fc</i>	Forced convection
<i>geo</i>	Geothermal
<i>nc</i>	Natural convection
<i>hx,o</i>	Heat exchanger outlet
<i>m</i>	Mass transfer
<i>MSL</i>	Mean sea level
<i>rad</i>	Radiation
<i>refill</i>	Refill water
<i>s</i>	Interface of pool water and air
<i>w</i>	Water

1 Introduction

Geothermal energy is championed as one of the renewable energy sources along with solar, wind, and wave/tidal. Yet, high enthalpy geothermal energy, from which electricity can be produced using steam or organic Rankine cycles, is available in only very few places which are less inhabited than places where electricity is in demand. However, low enthalpy geothermal energy (at $<100\text{ }^{\circ}\text{C}$) is available more commonly, which can be gainfully used to augment energy conservation though not energy generation. Subterranean aquifers can be judiciously exploited, for example, in the heating and cooling of buildings and heating of large swimming pools. These subterranean sources are available at reasonable depths (up to ca. 1000 m), which do not render drilling and pumping costs prohibitive. By virtue of being subterranean, one can reasonably assume these geothermal reservoirs as constant temperature sources or sinks. Thermodynamically, if source or sink temperatures or both can be maintained constant, the performance of engines or heat pumps will be efficient. Unlike solar, wind, or wave, geothermal has a round-the-clock availability which makes it worth exploring. Comparing the costs a priori, both solar and wind require a large swathe of land area, which may be at a premium economically and environmentally in well-inhabited settlements. On the other hand, geothermal sources require small footprints, but the costs of drilling, maintenance of pipelines, and heat transfer equipment have to be considered. While energy generation with renewable sources will dominate this

century, it is also pertinent that the energy is also conserved using renewable energy sources such as low enthalpy geothermal sources.

The objective of this chapter is to present outcomes from several projects where this low enthalpy geothermal energy has been used for supplementing heating inventories of Olympic size swimming pools in winter and is being mulled for substantially reducing electricity bills of cooling and heating at even domestic levels. Although the case studies herein pertain to the Perth Metropolitan Area in Western Australia, the techniques are adoptable all over the globe where near-constant temperature aquifers are present. The chapter is divided into two major sections addressing the aforementioned two distinct applications of low enthalpy geothermal energy.

2 Geothermal Olympic-Size Outdoor Swimming Pools

2.1 Introduction

Due to increasing recognition of the importance of exercise in maintaining good health, ever more Australians are resorting to swimming as an option. This is evidenced by the number of medals won by Australia in swimming events of all international competitions, right from the Olympics to the Commonwealth games. While it used to be a seasonal activity in yesteryears, now it is a year-round activity all over Australia. It is imperative that the pool water temperature be maintained between 26 and 28 °C irrespective of the season. In particular, for competitive swimming, these temperature limits are even more imperative. This is a difficult task for outdoor swimming pools in winters when the ambient temperatures across non-tropical Australia are quite low. Swimming pools maintained by local governments allocate huge budgets for heating them, and gas-fired hot-water boilers are generally used. A collateral liability of the operation of swimming pools is the replenishment of evaporated water. Thus, public swimming pools are confronted with two major environmental issues, namely, greenhouse gas emissions from the boiler and water consumption. While the latter is inevitable, the former can be reduced substantially by using geothermal aquifers.

A study of the distribution of heating energy in 855 swimming pools in Italy indicates that heat lost due to Evaporation accounts for 60% of the total heating requirements, with another 38% being used to replace the water after heating [1]. The conventional methodology adopted to heat the pool water is to use an on-site gas-fired boiler, a heat pump, or solar power. An alternative method of meeting these heating needs sustainability is to use geothermal aquifers [2]. This choice banks on the constancy of groundwater temperature being circa 46.5–48.5 °C when taken from a depth of about 1 km in the Perth Metropolitan Area. Boreholes are drilled for pumping the water up and returning it with adequate spacing to avoid thermal breakthrough [3, 4]. There are several expansive aquifers in and around Perth, Western Australia, and the success of geothermal heating can be seen by its use in at least 14 existing

swimming pools in the Perth region alone [2]. Despite the initial capital expense, compared to solar and wind, geothermal systems require a much smaller land area and are immune to weather conditions.

Highly variable environmental conditions ranging from cold nights and clear sky to gales immensely enhance heat loss from swimming pools in Australian winters. In fact, in winters, when heating is mostly required, the availability of solar energy is the least. Further, wind energy cannot be directly used for heating up water. Seasonal fluctuations in the availability of renewable energy sources impel supplementing heating with backup boilers, which may not be powered by clean energy. If renewable energy sources are used, the heating capacity of systems must be pessimistically sized to meet the requirements of the pool in order to reduce the need for backup boilers. In this context, geothermal energy will stand out to be the main renewable energy that can be used in this application. Some heating capacity design methods in vogue are empirical [5–8] and use non-location-specific atmospheric weather conditions, which could lead to either over or underestimating heating inventories. Although the most significant contributor to energy consumption is the heat loss due to Evaporation, there is no standard method of quantifying it and other heat losses in the pool [9]. It is imperative that a model needs to be able to assess all losses accurately so that it can be adapted for pools of all sizes and locations. An attempt in this direction has been made by Lovell et al. [10], who developed a model and benchmarked it against data available from experimental measurements in a 50 m Olympic size swimming pool.

While the Lovell et al. model is an initiation, it is observed that some refinements are necessary to make it more generally applicable. The present model addresses some of the lacunae [6–8, 11] by enhancing the methodology of estimating heat transfer by radiation, solar inputs, cloud, and precipitation conditions. This is to emphasise the importance of radiation from and to the pool under the influence of surrounding structures. These refinements were benchmarked using data from the 50 m pool of Lovell et al. [10] and also another 30 m pool adjacent to that pool. A significant difference between the two is in the surrounding structures. In addition, this section compares results from yet another model developed by Smith et al. [12]. Whatever method of estimating heating inventories is used, it will be preferable to oversize the heating system to avoid the use of boilers. In this context, again, low enthalpy geothermal heating turns out to be the front runner because all that one needs is oversizing the heat exchanger and pump, which have minimal effects on overall costs, provided the heating capacity is designed appropriately. Hereunder has presented a systematic analysis of those heating inventories for two different-sized swimming pools.

2.2 The Beatty Park Leisure Centre Outdoor Swimming Pools

The Beatty Park Leisure Centre is a swimming pool complex in the North Perth suburb of Western Australia. Originally known as the Beatty Park Aquatic Centre,

it was built as the main swimming event venue for the 1962 British Empire and Commonwealth Games, alongside the Perry Lakes Stadium athletics complex. Prior to the construction of the centre, the area was part of Beatty Park, a large reserve. A major redevelopment took place from 2011 to 2013. This renovation included the installation of geothermal boreholes for heating the upgraded pools [13] (Figs. 1, 2, 3 and 4).

Yet, on completion, the geothermal heating system struggled to meet the pool temperature requirements. This shortfall eventually mandated the retrofit of additional gas-fired boiler capacities [16]. This underestimation of heating needs has motivated the present research. Details of the two pools are given in Table 1. Geothermal heating is adopted for both pools. The control method used is a simple on-off strategy of the submersible pump.

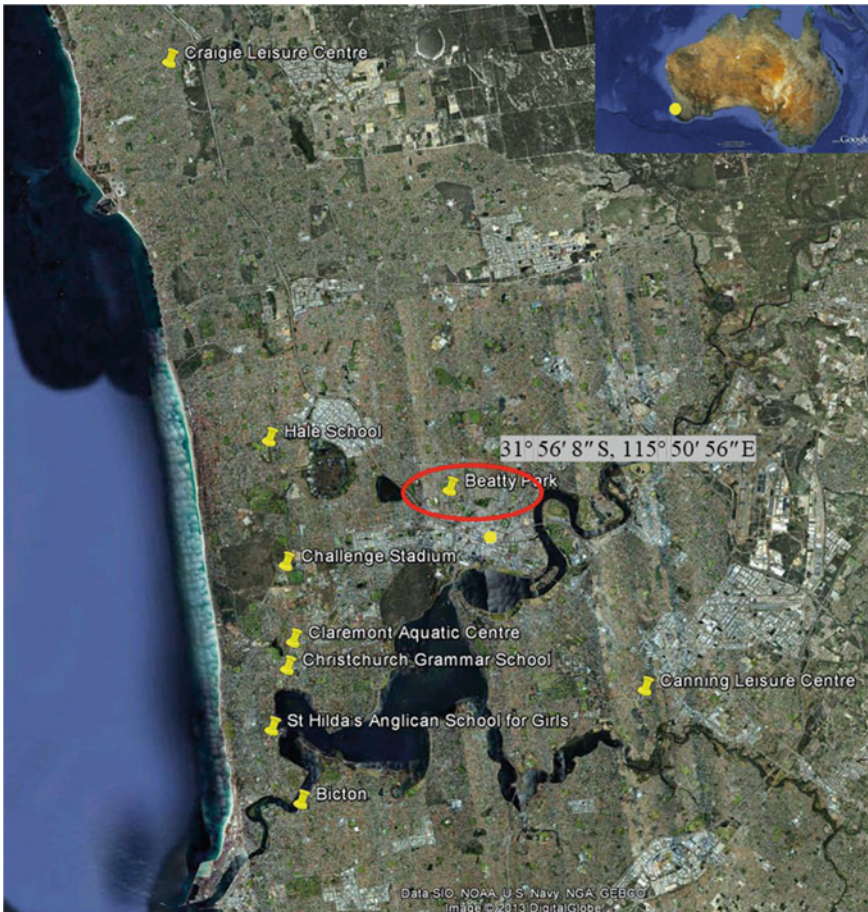


Fig. 1 The Beatty Park Leisure Centre location in Perth, Australia [14]



Fig. 2 Photographs of 50 m and 30 m swimming pools at the Beatty Park Leisure Centre, Perth, Western Australia. This complex uses a geothermal heating system for the swimming pool water, which replaced gas-fired boilers in 2011. This change aims to reduce the cost of heating by approximately AUD 300,000 per year [15]

The geothermal heating system that draws tepid water from deep underground to heat all of the swimming pools uses an SP125-104NE (Grundfos) submersible pump with a 93 kW Franklin Hi-Temp motor with 40 kW pumping power at the maximum pumping rate. A 1,156 m deep geothermal borehole taps into the Yarragadee aquifer [2], producing water temperatures in the range of 47.5–48.5 °C at the wellhead [17]. The water is reinjected into the same aquifer at 799 m depth via a separate injection borehole so as not to give rise to cross-contamination of the groundwater in the aquifer and prevent thermal breakthrough [2]. Both geothermal and injection borehole are shown in Fig. 5.

Insulated belowground pipework transmits tepid water to each pool, with the geothermal energy transferred to each pool heating system via plate heat exchangers installed in the plant room.

The geothermal heat-exchange systems extract warm groundwater, circulate the groundwater through heat exchangers to keep the pool water at the desired temperature, and then reinject the heat-depleted groundwater at 30 °C back into the source aquifer via a shallower injection well to maintain a neutral water balance as shown in Fig. 6.



Fig. 3 Redeveloped 50 m and 30 m pools at the Beatty Park Leisure Centre, Perth [15]

2.3 *Energy Balance*

In addition to combined convective and evaporative losses, the present paper enhances the ability to predict the radiative components described in our earlier model [10]. These changes are uniformly applied to other empirical and semi-empirical convective and evaporative models [5–8, 12, 16] such that a meaningful comparison could be made against measured data.

All models share the same energy balance as proposed by Rakopoulos and Vazeos [19], which summarises various components of heat load as follows:

$$Q_{pool} = Q_{evap} + Q_{convection} + Q_{conduction} + Q_{radiation} + Q_{refill} - Q_{solar} \quad (1)$$

Several empirical and semi-empirical formulae are used to estimate evaporative and convective losses from a pool surface. Invariably conduction losses are neglected as they are comparatively very small. Equations for Evaporation and convection used by several sources are listed in Appendix A. Solar incoming radiation and radiative components of pool surface heat losses depend on the solar angles as seen by the pool surface, shielding by surrounding structures, cloud cover, depth of the pool, and rainfall [4].

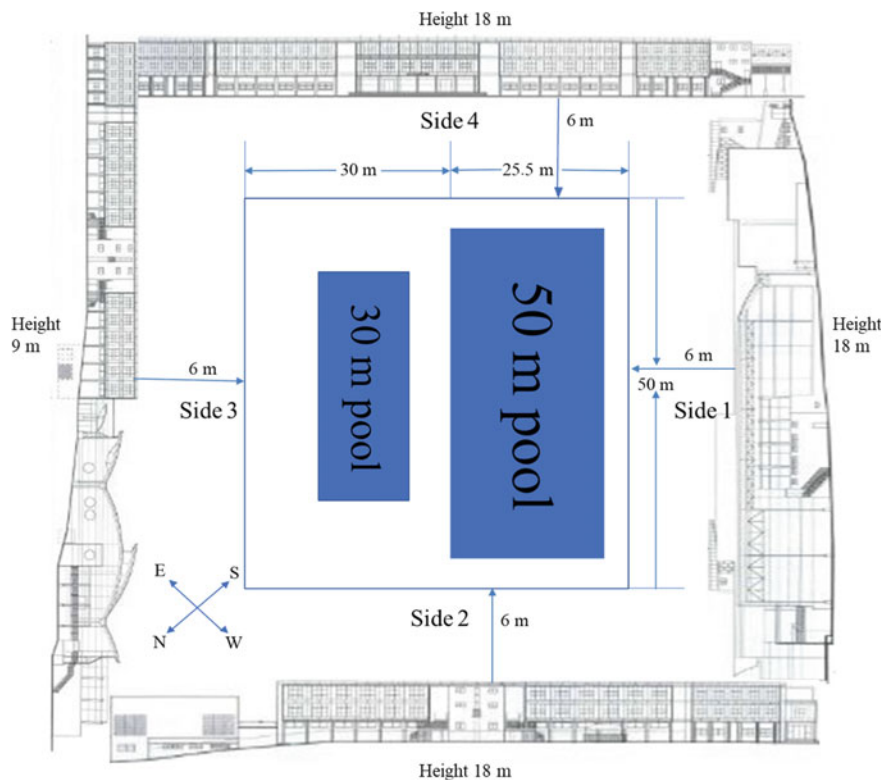


Fig. 4 The orientation of the pools for view factor calculations

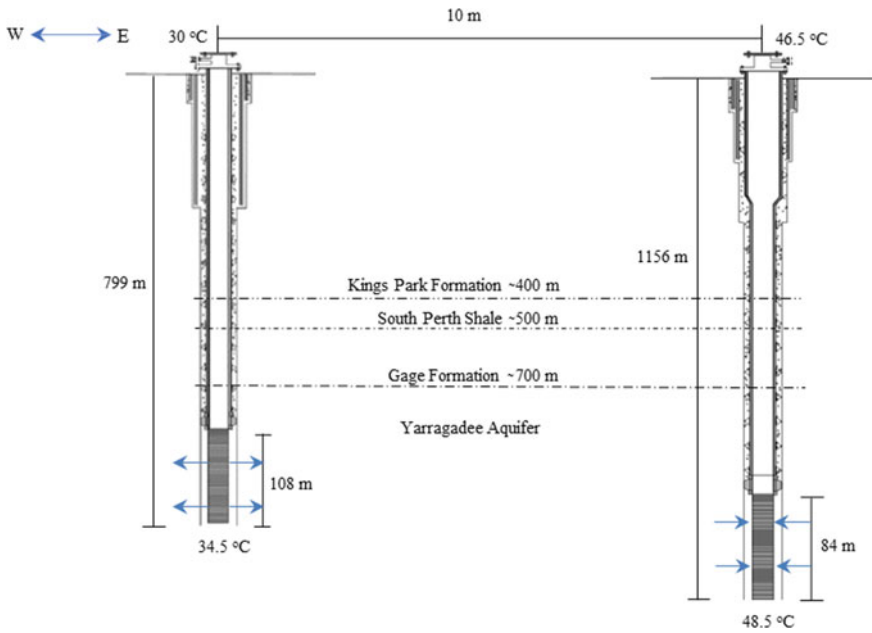
2.4 Model Data

2.4.1 Weather Data

Climatic data is paramount to the accuracy of all models. These are obtained from the local meteorological weather station. Data from the nearest station (Perth Metro) of the Bureau of Meteorology (BOM) is adopted for the location. These data, recorded at half-hour intervals, comprise dry bulb and dew point temperatures, relative humidity, wind direction and velocity (at 10 m above sea level), and mean sea level pressure. Rainfall data is given cumulatively every half hour from 9 AM each day. Although cloud cover data is available, it is not at half-hour intervals. The present model interpolates the recorded data between 9 AM and 3 PM instead of using data at 9 AM or 3 PM. It is assumed that the coverage before 9 AM and after 3 PM is the same on either side of those durations.

Table 1 Pool parameters at the Beatty Park Leisure Centre

Length (m)	50	30
Width (m)	25.5	20.5
Average depth (m)	1.5	2
Total volume (m ³)	1912	1230
Design flowrate of pool pump (L/s)	8.5	6.8
<i>Common features for both pools</i>		
Set water temperature (°C)	26.5	
Orientation of the pool	45° (0° is E–W)	
Latitude	−31.9°S	
Longitude	115.85°E	
Height above mean sea level	24 m	
Average annual rainfall	786 mm	

**Fig. 5** Injection borehole (left) and geothermal borehole (right). Figure not to scale [14]

2.4.2 Geothermal Addition

Since both pools are heated by geothermal energy, this heat addition is calculated as shown below

$$Q_{geo} = \dot{n} c_{p,w} (T_{hx,o} - T_w) \quad (2)$$

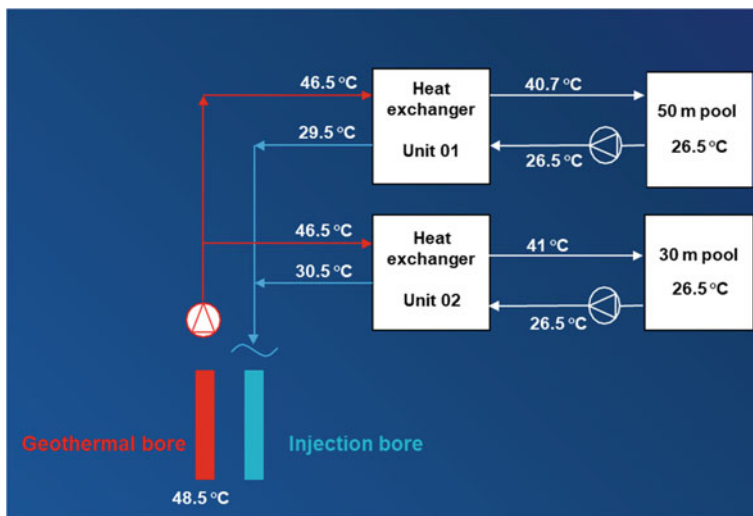


Fig. 6 The geothermal heating design [14]

In order to measure the heating requirement, the pump status obtained from on-site recorded data is used in conjunction with the constant flow rate data for each pool (listed in Table 1) and the temperature differential data across the heat exchangers [10].

2.5 Model Analysis

Data collected between March 2017 and December 2019 from the 30 m and 50 m pool at Beatty Park Leisure Centre with a hiatus from March to September 2018 when the pool heating system underwent refurbishment is used to compare all the models and is presented hereunder.

2.5.1 Predicted Temperature Comparisons

Figure 7 shows that most of the expected temperature values have a near-normal distribution. Different models show either an over-or under-prediction of pool water temperatures. A standard value of ± 1 °C deviation between predicted and measured pool water temperatures is chosen for further discussion. Qualitatively, the frequency distribution of all models is analogous except for the model of ASHRAE [20], AS3634 [18], and Smith et al. [12]. In the present model, there is a slight bias towards temperature over-prediction. Quantitatively, the present, Richter [7] and McMillan's [6] model show similar distributions around zero, whereas Woolley et al.'s model

[8] is pivoted around 1 °C, causing an over-prediction of the temperature. The 30 m pool temperatures are strongly under-predicted by the ASHRAE model [20] and over-predicted by the AS3634 model [18]. There is also, broadly, internal consistency for each model for both pools. The differences can be attributed, *prima facie*, to wind direction effects which are different for the 50 and 30 m pools because of surrounding structures. As far as radiation is concerned, the 50 m pool has more proximity to surrounding structures than the 30 m pool. In this regard, the view factor of the surrounding structures in relation to the 30 m pool is 0.26, while that in relation to the 50 m pool is 0.31.

A quantitative comparison of temperature variations among various models for the 30 m pool is shown in Table 2. It demonstrates that the present model has 77% of temperature differences within ± 1 °C. In comparison, the other two models, McMillan [6] and Richter [7], have 66% and 62% compliance, respectively, within the same range. Many of the deviations projected by Woolley et al.'s [8], ASHRAE [20], and AS3634 models [18] are outside of the measured values and have a relatively low percentage of compliance compared to the other models. Table 2 also quantitatively compares the temperature variations from all models for the 50 m pool.

The present, Richter [7], and McMillan's [6] models are fairly consistent in the number of data points within 1 °C. This is also reflected in the RMS (root mean square) values of temperature deviations. On the other hand, the remaining models show a larger deviation. This can be attributed to the treatment of velocity contribution in the calculation of heat/mass transfer coefficients. From Fig. 2, it can also be inferred that the present, McMillan [6], and Richter's [7] model predict a warmer pool water temperature for the 30 m pool. This results from an underestimation of heat losses or overestimation of solar heat gain. The latter can arise from the shielding of surrounding building structures which is rather difficult to model precisely. An underestimation of heat losses could now be attributed to the treatment of the radiative loss component, which has been uniformly applied to all models. Additional reasons can be that exact meteorological data at the location are not known, and an approximation was made with data from a nearby station.

Richter's model [7] has a somewhat under prediction of pool temperature as against the present, McMillan's [6], and Woolley et al.'s [8] model for the 50 m pool. However, for the 30 m pool, it is almost the same as the other models. The ASHRAE [20] and Smith's model [12] consistently under-predict pool water temperatures for both pools, whereas for AS3634 [18], it is the reverse.

2.5.2 Predicted Heating Capacity Comparisons

Histograms comparing the heating capacity differences between estimated and measured data are shown in Fig. 7. In all these figures, it is assumed that the makeup water temperature is at 20 °C, although its contribution to the total heating requirement is negligibly small. Table 3 shows the statistical data for all models. A notional heating requirement of 500 kW for the 30 m pool and 700 kW for the 50 m pool

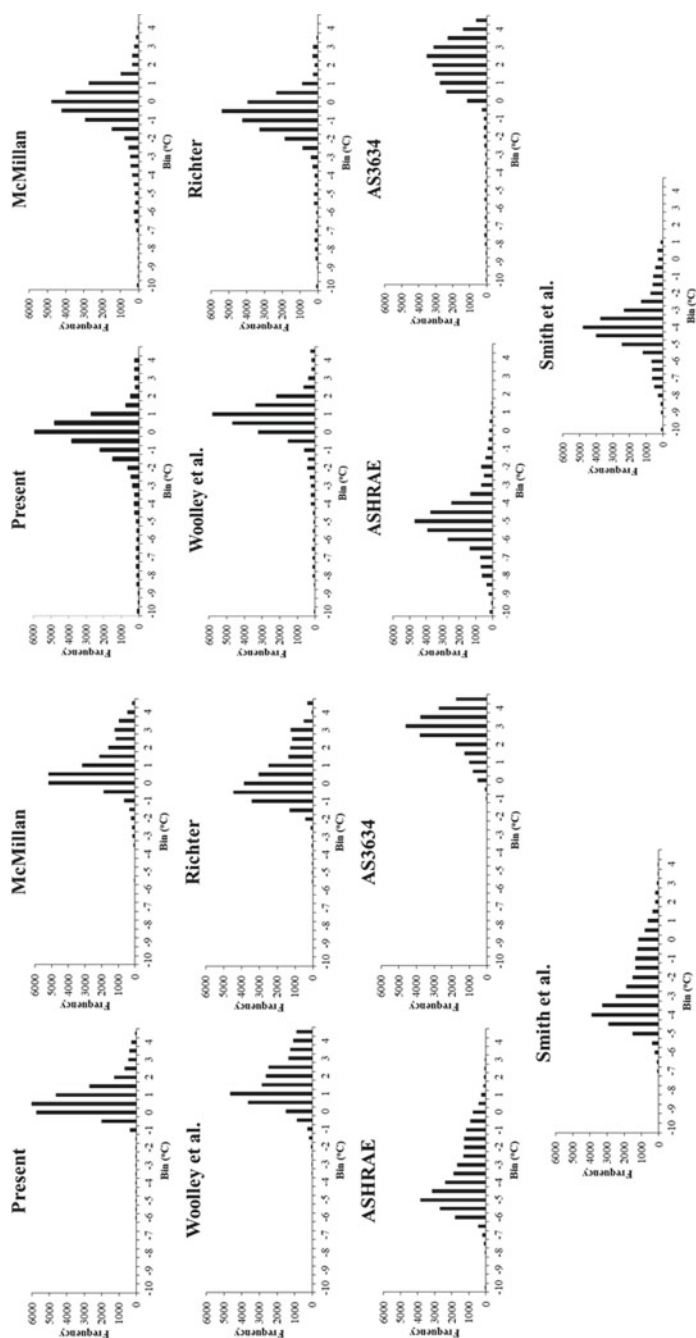


Fig. 7 Frequency distribution of the difference between measured and predicted temperatures by different models of the 30 m pool (left) and 50 m pool (right)

Table 2 Deviations of predicted water temperature from measured data

Model	% within ± 1 °C		RMS temperature deviations (°C)	
	30 m pool	50 m pool	30 m pool	50 m pool
Present	77	74	1.3	2.0
McMillan [6]	62	71	2.0	2.0
Richter [7]	66	63	1.8	2.2
Woolley et al. [8]	42	60	2.7	2.1
AS3634 [18]	10	26	3.7	2.8
ASHRAE [20]	14	4	4.1	5.3
Smith et al. [12]	20	7	3.3	4.4

Table 3 Percentage of predicted heating capacity values of both pools

Model	% within ± 25 kW	% within ± 35 kW	RMS temperature deviations (kW)	
	30 m pool	50 m pool	30 m pool	50 m pool
Present	71	76	34.0	40.6
McMillan [6]	69	58	55.8	46.3
Richter [7]	65	72	33.7	46.5
Woolley et al. [8]	59	61	29.4	45.2
AS3634 [18]	29	34	87.3	168.1
ASHRAE [16]	7	9	81.4	74.7
Smith et al. [12]	5	8	81.1	139.2

is observed based on measured data. It is also assumed that the heating data has an uncertainty of 5%. The RMS values of deviations are also listed therein.

Figure 8 shows that in the present model, 71% of heating requirements are within ± 25 kW for the 30 m pool and 76% within ± 35 kW for the 50 m pool. These degrees of agreement are inversely correlated to temperature spectra because an over-estimation of the pool water temperature requires a lesser heating capacity. The present model is fairly consistent quantitatively and qualitatively. A deviation of the order of 30% between predicted and measured data is due to the model taking only four principal directions for wind, whereas, in reality, it is multidirectional. In addition, wind direction can fluctuate sharply in a short time, which will affect the wind velocity and length parameters involved in convective heat and mass transfer.

The near-normal distribution seen in Fig. 7 is absent in Fig. 8. This is due to the on/off control method used for the pump and diurnally variable heating demands, which could vary at more frequent intervals than modelled. The heating inventories predicted by various models depend on the amount of Evaporation and the pool water temperature according to each model. Importantly, for the present model, the total energy losses due to heat and mass transfer are not a simple linear summation of

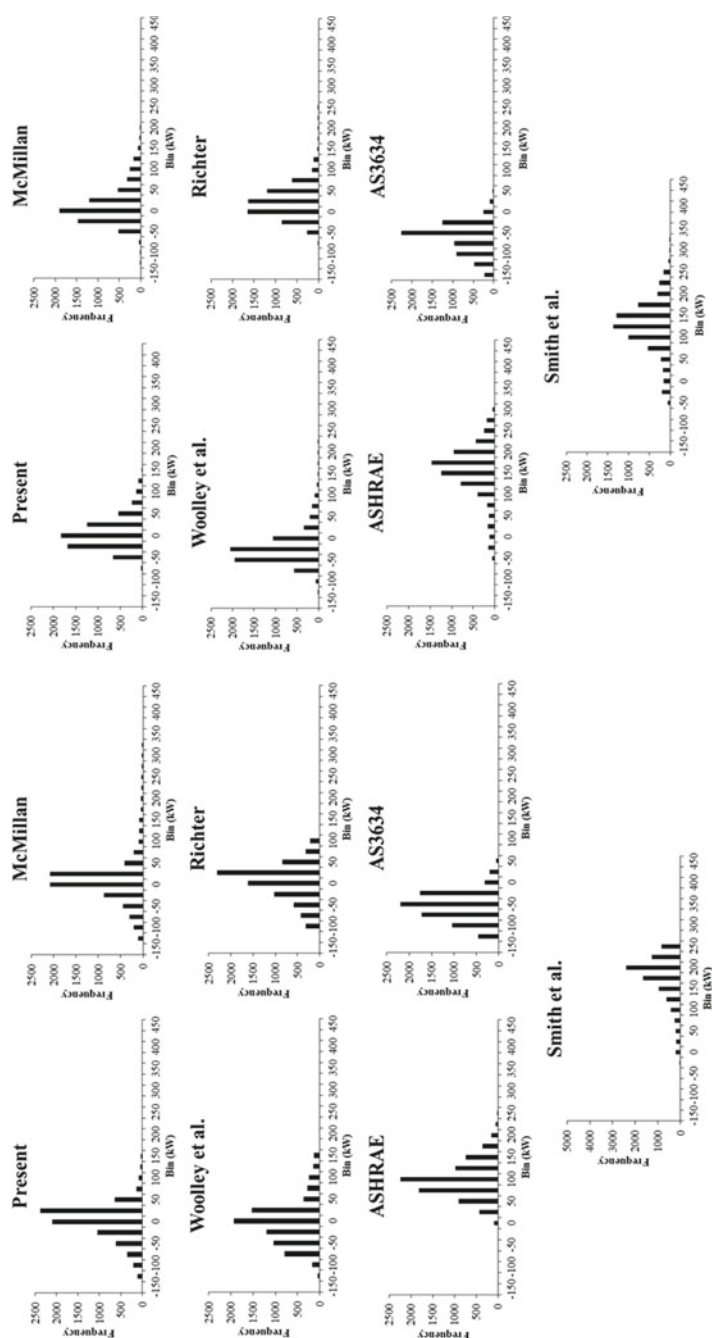


Fig. 8 Frequency distribution of the variation between predicted and measured heating capacity by different models for 30 m (left) and 50 m (right) pools

forced and natural convection effects but are combined via a power-law relation (see Appendix equation A.14).

Figures 9 and 10 show the distribution of heat losses due to Evaporation and convection for each of the pools from various models. It can be seen that evaporative losses dominate in each model though the relative magnitudes of forced and natural convection evaporation are significantly different among the models. In fact, these variations get reflected in the spectral distribution of heating inventories shown in Fig. 8.

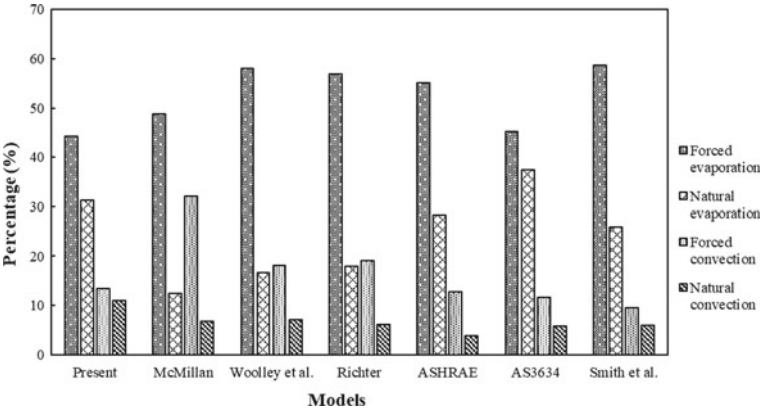


Fig. 9 Comparison of heat losses predicted by different models of the 30 m pool

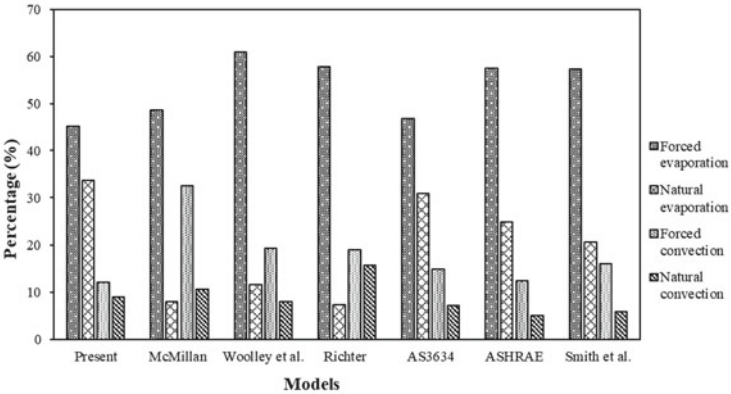


Fig. 10 Comparison of heat losses predicted by different models of the 50 m pool

2.5.3 Predicted Heating Capacity Comparisons

Regarding the heat loss distribution from various sources for each pool, as shown in Figs. 9 and 10, it can be seen that the present model and that of AS3634 [18] for both 30 m and 50 m pools are comparable, although the magnitude of heat transfer varies vastly. The differences in magnitude seem to be predominantly due to the treatment of natural convection evaporation. The other differences are due to forced convection evaporation.

Throughout the three-year duration, the contribution to the total heat loss due to Evaporation, convection, and radiation for the 30 m pool are approximately 66%, 21%, and 13%, respectively (Fig. 11), and are approximately 68%, 18%, and 14% for the 50 m pool (Fig. 12). The total energy loss due to mass transfer is due to both forced and natural convection-driven Evaporation, with the former amounting to 59% for 30 m pool and 57% for 50 m pool. Analogously, the total energy loss due to heat transfer is also due to both forced and natural convection, with the former amounting to 55% for 30 m pool and 57% for 50 m pool.

Further partitioning of convection components is shown in Figs. 11 and 12. There is qualitative conformity with previous literature results, which predict them to be 50–60% of total losses [1].

Figures 13 and 14 show the temporal distribution of various components of energy loss (convection, Evaporation, and radiation) and energy input (solar and geothermal) for both pools for a few days in the season that requires maximum heating in June 2019. It is apparent that heat transfer by convection and radiation put together are significant and could lead to over or under-estimation of heating requirements. While the contribution of radiation seems to be nearly the same for both pools, the effect of convection appears to be somewhat larger in the 30 m pool. This can be attributed to the effect of surrounding buildings around each. While the 50 m pool is more

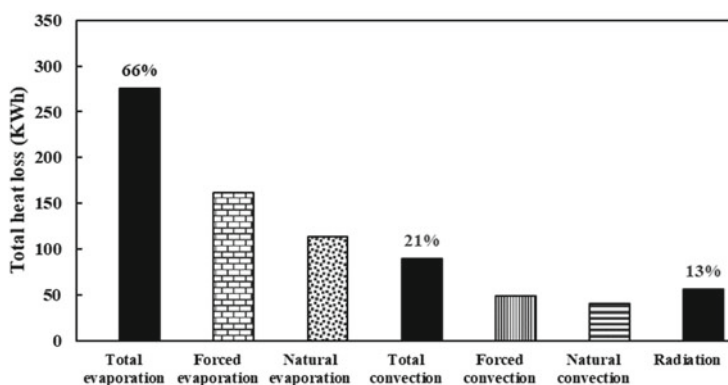


Fig. 11 Comparison of heat losses contributions mechanisms by the present model of the 30 m pool

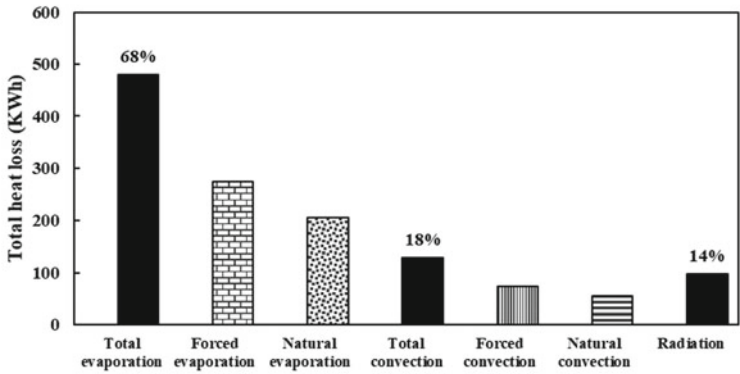


Fig. 12 Comparison of heat losses contributions mechanisms by the present model of the 50 m pool

or less open, the 30 m pool is surrounded by some buildings. It is quite involved to model their effects and often unnecessary because the heating plant has to be conservatively sized. These buildings also affect the radiation components which have been accounted for in all the models studied.

In spite of the above analysis, as seen earlier, only approximately 70–80% of actual heating used seems to tally with present model calculations when the uncertainty is 5%. Consequently, it is advisable to size the heating requirements pessimistically by augmenting heating capacities by 10–15% above the calculated values as per the present model. This is where geothermal pools are easily adoptable against

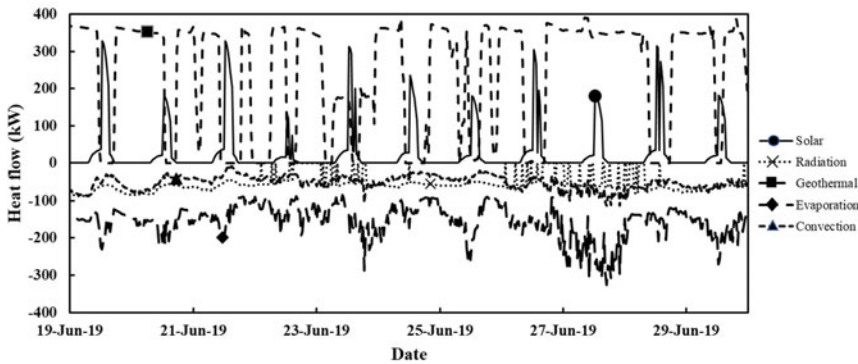


Fig. 13 Calculated and measured heat flow distributions by the present model of the 30 m pool over 10 days in June 2019

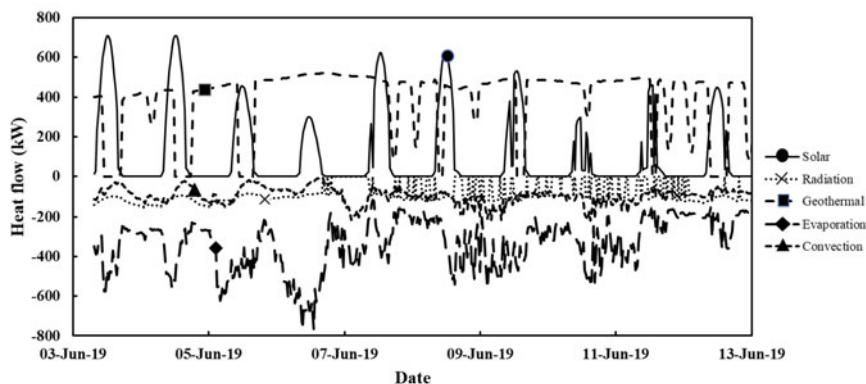


Fig. 14 Calculated and measured heat flow distributions by the present model of the 50 m pool over 10 days in June 2019

solar-heated pools. The drilling costs are nearly independent of the amount of water pumped.

Because of the vast resource of geothermal groundwater, pumps can be oversized and driven by variable frequency drives. It is also amenable to good control techniques which address seasonal heating demands.

Figure 15 shows the corresponding heat exchanger water supply temperature to the pool during the same period as in Fig. 13. As mentioned before, the pool pump uses on–off control, the effect of which is reflected in the heat exchanger water supply temperature intermittency. However, it can be seen that the groundwater supply temperature remains fairly constant at 40.7–41.0 °C when the pool pump is activated. This on–off control makes the pool temperature consistently maintained at 26.5 °C. This series of experimental water supply temperatures are applied commonly to all the pool models for a consistent comparison.

3 Conclusions

From comparisons made between 30 and 50 m pool data among various models, it is clear that the present model is able to predict the pool water temperature and heating capacity requirements fairly well and consistently. This can be attributed to the attention to actual local weather conditions instead of generalised data and effects of surrounding structures. In spite of this, only 77% and 74% of the measured data agree to within ± 1 °C for the 30 m and 50 m pools at the Beatty Park Leisure Centre. Analogously, 71% and 76% of measured heating capacities seem to comply within $\pm 5\%$ of the installed capacity for both pools. It is expected that the present calculation scheme will help the industry to appreciate the importance of local weather data and assess heating demands with a smaller uncertainty. Pessimistic sizing of heating

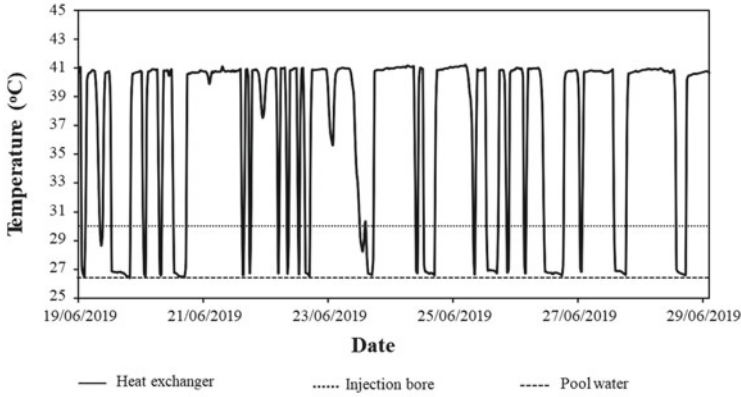


Fig. 15 Water supply temperature to/from the pool over 10 days in June 2019

inventories will be important, keeping in view the performance reliability for public usage. To this end, geothermal pools could be a good choice because capacity control can be fine-tuned through pumps coupled to variable frequency drives.

Appendix A

The wind speed data from the Bureau of Meteorology (BOM) has to be corrected for the pool surface for all models except AS3634, which has its own correction method. For the swimming pools analysed, the category 3 multiplier is 0.38 for height ≤ 3 m and 0.44 for 10 m. The value of corrected wind speed for the pool surface is,

$$U = \frac{0.38}{0.44} U_{BOM} \quad (\text{A.1})$$

A.1 Evaporation

A.1.1 Evaporation Due to Natural Convection Mass Transfer

Heat loss due to natural convection evaporation is given by the following equation:

$$Q_{evap,nc} = \dot{n}_{w,s} h_{fg} \quad (\text{A.2})$$

where $\dot{n}_{w,s}$ is the mass transfer rate given by

$$\dot{n}_{w,s} = h_{evap,nc} A (\rho_{w,s} - \phi \rho_{w,\infty}) \quad (\text{A.3})$$

Sherwood number (Sh), characteristic length (L), and binary diffusion coefficient (D_{AB}) are used to determine the evaporative mass transfer constant ($h_{mn,c}$):

$$h_{m,nc} = \frac{Sh}{D_{AB} L} \quad (A.4)$$

Sherwood number, in turn, is arrived at using the criteria [21]:

$$\text{If } 10^4 < Ra_m < 10^7 \rightarrow Sh = 0.54 Ra_m^{0.25} \quad (A.5)$$

$$\text{If } 10^7 < Ra_m < 10^{11} \rightarrow Sh = 0.15 Ra_m^{0.33} \quad (A.6)$$

Grashof and Schmidt numbers required for calculating the Rayleigh number are estimated using the following equations [21]:

$$Gr = \frac{g(\rho_{a,s} - \rho_{a,\infty})L_{nc}^3}{\rho_{a,\infty} \nu^2} \quad (A.7)$$

$$Sc = \frac{\mu}{\rho D_{AB}} \quad (A.8)$$

The equation for the binary diffusion coefficient is calculated using the following empirical correlation [22].

$$D_{AB} = \frac{1.049 \times 10^{-4} T_f^{1.774}}{1000 p_{MSL}} \quad (A.9)$$

where T_f is in K and p_{MSL} in kPa.

A.1.2 Evaporation Due to Forced Convection Mass Transfer

The present model treats the forced convection component differently from other models in the literature. The wind direction is explicitly accounted for as follows [10]:

For the incidence angle of $\theta = 22.5^\circ$ or 45° ,

$$Q_{evap,fc} = 2c_m [W \sin(\theta)]^{\frac{9}{5}} + d_m W [L - W \tan(\theta)] \left[\frac{W}{\cos(\theta)} \right]^{-\frac{1}{5}} \quad (A.10)$$

for $\theta = 67.5^\circ$

$$Q_{evap,fc} = 2c_m [L \cos(\theta)]^{\frac{9}{5}} + d_m L \left[W - \frac{L}{\tan(\theta)} \right] \left[\frac{L}{\sin(\theta)} \right]^{-\frac{1}{5}} \quad (A.11)$$

where

$$c_m = \frac{5}{9} 0.037 (\rho_{w,s} - \phi \rho_{w,\infty}) D_{AB} Sc^{\frac{1}{3}} \left(\frac{U_\infty}{\nu} \right)^{\frac{4}{5}} \left[\frac{2}{\sin(2\theta)} \right]^{\frac{4}{5}} h_{fg} \quad (A.12)$$

$$d_m = 0.037 (\rho_{w,s} - \phi \rho_{w,\infty}) D_{AB} Sc^{\frac{1}{3}} \left(\frac{U_\infty}{\nu} \right)^{\frac{4}{5}} h_{fg} \quad (A.13)$$

Natural and forced evaporation effects are combined as per the power-law relation below:

$$Q_{evap} = \left(Q_{evap,fc}^{\frac{7}{2}} + Q_{evap,nc}^{\frac{7}{2}} \right)^{\frac{2}{7}} \quad (A.14)$$

A.2 Heat Transfer

Heat transfer by convection is treated analogously, where Sc is replaced with Pr and Sh with Nu .

A.3 Radiation

The radiative transfer to the sky is calculated as shown below:

$$Q_{rad} = \frac{\sigma \varepsilon_w A (T_w^4 - T_{sky}^4) (1 - F_{w-structure})}{(1 - \varepsilon_w)(1 - F_{w-structure}) + \varepsilon_w} \quad (A.15)$$

where F is the view factor calculated from the geometries and orientation of the pool. The pool water surface emissivity is taken as 0.96 [10]. The sky temperature is calculated using the ambient air temperature and sky emissivity (ε_{sky}),

$$T_{sky} = (\varepsilon_{sky} T_{\infty}^4)^{\frac{1}{4}} \quad (A.16)$$

where

$$\varepsilon_{sky} = \varepsilon_{cs} (1 + 0.17792 C_8 - 0.224 C_8^2 + 1.4336 C_8^3) \quad (A.17)$$

$$\varepsilon_{cs} = 0.787 + 0.764 \ln \left(\frac{T_{dew}}{273.15} \right) \quad (A.18)$$

C_8 (measured in units of octas), which are available from BOM data, represents the effect of cloud cover.

A.4 Refill

The loss of water from the pool due to Evaporation by all the aforementioned mechanisms has to be replenished from the conventional municipal water supply. The following equation is used [10] to calculate refill:

$$Q_{refill} = \dot{n} c_{p,w} (t_w - t_{refill}) \quad (A.19)$$

t_{refill} is the temperature of the added water, which is taken as 20 °C and is the total mass transfer rate given by

$$\dot{n} = \dot{n}_{fc} + \dot{n}_{nc} \quad (\text{A.20})$$

A.5 Solar Insolation

Using the methodology from ASHRAE [20], all models studied herein use the following equation to calculate solar insolation:

$$Q_{solar} = \alpha_{pool} A (E_{beam} + E_{diff}) C_{cloud\ effect} \quad (\text{A.21})$$

where

$$C_{cloud\ effect} = -0.0024C_8^3 + 0.0108C_8^2 - 0.0242C_8 + 1.0001 \quad (\text{A.22})$$

The pool is unable to absorb the irradiance from a direct sunbeam when precipitation happens since raindrops absorb the solar energy and diffuse it out. As such, when this happens, solar insolation is set to zero in all models.

4 Viability of Ground Source Heat Pumps (GSHP) Against Air Source Heat Pumps (ASHP) for Domestic Applications

Nomenclature and Formulae

c	Velocity (m/s)
c_p	Specific heat of moist air (kJ/kg °C)
h	Specific enthalpy (kJ/kg)
P	Power (kW)
q	Volumetric flow rate (l/s)
Q	Cooling/heating capacity (kW)
t	Temperature (°C)
ν	Specific volume of moist air (m ³ /kg)
W	Humidity ratio (kg/kg of dry air)

Greek Letters

ϕ	Relative humidity
τ	Time (min)

Subscripts

1	Inlet of FCU
2	Outlet of FCU
a	Ambient

<i>c</i>	Cooling
<i>h</i>	Heating
<i>in</i>	Input
<i>w2</i>	Saturated liquid water

5 Introduction

According to the Australian energy authority [23], electricity markets in the twenty-first century showed a growing tendency to 210 TWh until around 2008–2009, then a minor fall to 195.7 towns. However, the residential and commercial sectors accounted for approximately 13% of total energy usage [24]. Possible explanations for this drop include consumer reaction to higher electricity bills, the advent of energy-efficient appliances, and improved housing design. This development can be interpreted as an indication of how willing Australians are embracing more energy-efficient measures in their houses. The trend undoubtedly encourages Australians to consider other methods of heating and cooling their houses, as heating and cooling can account for up to 40% of a household energy consumption [25].

The adoption of ground source heat pumps (GSHPs) is one feasible technique to reduce energy consumption. GSHPs use the constant subsurface temperature as a heat source for heating and a heat sink for cooling, thereby insulating heating and cooling device performance from diurnal and seasonal changes in ambient temperatures [26]. This aspect should be considered not only in terms of lowering the amount of energy required to operate GSHPs but also in terms of making them more ecologically friendly [27]. Direct geothermal energy utilisation has been widespread in a variety of industries, including pool heating [3, 10, 28] in Australia.

The usage of GSHPs for domestic heating and cooling is now on the rise [29], particularly in Australia. For example, in 2012, a project using GSHP systems was launched in Melbourne with the goal of boosting the geothermal industry in the state [30]. In 2019, AUD 1.7 million commercial-scale demonstrations of renewable ground-source heat pumps were installed in the Fairwater master-planned residential development in Blacktown, Western Sydney [31, 32], with an emphasis on residential clusters for heating and cooling applications [33]. High capital investments, uncertainty about the best design, and low consumer confidence can all be deterrents to adopting this technology [34].

The design of various types of GSHP requires a geological survey [35]. The water quality and quantity, in particular, must be examined a priori in open-loop systems (as is the case in this study). Open-loop or closed-loop GSHP systems are available [29]. GSHPs have been compared to traditional heating and cooling systems in prior research. The GSHP has a 32–54% higher coefficient of performance (*COP*) for cooling than the ASHP and a 36–38% higher *COP* for heating [36]. The basic energy consumption of the heat pump system is 71% less than that of a reference installation based on ordinary gas-fired boilers and water-cooling machines, according to a study of an aquifer thermal storage system in a Belgian hospital [37]. The heat pump *COP*

during the cooling period is 6.0–10.9 at partial load, while the whole system *COP* is 4.3–7.4, according to a study conducted at Pusan National University in Korea to evaluate the performance of a GSHP system. The heat pump *COP* at partial loads during the heating season is 4.3–8.3, whereas the whole system *COP* is 3.0–6.2 [38]. The closed-loop GSHP and variable refrigerant flow (VRF) systems installed in ASHRAE Headquarters in Atlanta were described by Southard et al. [39]. They reported a significant increase in heating *COP* of 4.6 for the GSHP system compared to 3.1 for the VRF system and a significant increase in cooling *COP* of 3.3 from 2.1 for the VRF system. A study was carried out to see if high conductivity phase change material (PCM) could be used in the borehole heat exchanger of a GSHP to shorten the borehole length and enhance the coefficient of performance (*COP*) [40]. The maximum *COP* values of a GSHP calculated assuming an ideal reverse Carnot cycle for cooling mode increased by roughly 81% with PCM and by 112% with graphite enhanced PCM, according to the results of its experiments.

Molavi and McDaniel [41] conducted a comprehensive analysis of GSHPs for retail buildings in the northeast the United States and found that, while they all offer environmental benefits, a lack of information and risk assessment is preventing wider adoption of this concept. Self et al. [42] have reviewed and confirmed the advantages of open-loop systems over other configurations. In a school facility during the winter season of 2008, Song et al. [43] compared GSHP to an ASHP. Their research discovered that ground temperatures at shallow depths of 2–5 m are greatly affected by external temperatures, whereas ground temperatures at depths below 20 m remain constant at roughly 16 °C. According to this study, the GSHP has a *COP* of 5.1 for a heat pump and 4.2 for the entire system, which includes the circulation pump. The overall *COP* of the GSHP system is 31% greater than that of the ASHP system. The better *COP* is owing to a 10 °C higher temperature at the evaporator in the GSHP system, resulting in a reduced pressure difference for the refrigerant compressor.

Michopoulos et al. [44] compared vertical GSHP to conventional systems in single and multi-family dwellings in many sites in Cyprus with varying climatic circumstances. These technologies were looked at for both heating and cooling purposes. In two typical residential structures in Cyprus, simulations were run to calculate the amount of electricity consumed by both GSHP and conventional systems. The findings demonstrate that the principal energy savings for GSHP systems are strongly dependent on geography, with reductions of up to 33.6% in colder areas and 23.5% in warmer places. It has also been discovered that multi-family dwellings save more energy than single-family homes.

The heating performance of three vertical closed-loop water-to-air GSHP systems built in three new single-family detached houses in Innisfail (80 km north of Toronto, Canada) was monitored, examined, and evaluated over one heating season by Abdel-Salam et al. [45]. The findings suggest that GSHPs can handle peak heating demands without the use of an extra heating element. The *COPs* for the three seasons are 4.2, 4.0, and 3.4, respectively. In a rebuilt campus building in Korea, a comparison reveals that the sum total running costs of a GSHP system is around one-third that of the

current heating and cooling systems [46]. The effect of various system characteristics on GSHP performance is investigated using a computer model [47]. Based on a comparative economic evaluation that is conducted to analyse the feasibility of utilising a GSHP in place of traditional heating/cooling systems and an ASHP, the conclusion reveals that GSHP is economically advantageous to conventional systems. The Solar Energy Institute at Ege University in Izmir, Turkey, on the other hand, investigated the cooling performance of a vertical GSHP system installed in a 65 m² room [48]. Due to the oversizing of several system parts, the cooling coefficient of the GSHP performance and the entire system is relatively low when compared to other heat pumps operating under conditions at or near design values.

While there is no doubt that GSHPs provide significant environmental and operational benefits, the price of drilling, pumping, and piping, as well as their running costs and heat exchanger derating, have proven to be stumbling blocks. In the residential sector, there is a need for a comprehensive assessment that takes into consideration of all aspects. Through a simulation of a typical residence in Cyprus, Christodoulides et al. [49] addressed this issue and concluded that GSHPs would not be cost-effective because payback durations would be in the order of 20 years. Despite the GSHP greater initial cost, the benefits of lower CO₂ emissions and lower operating expenses may outweigh the disadvantages [50].

A review of the literature suggests that GSHPs may not be a viable alternative for home use, owing to the high expense of drilling. When a borewell is included as part of a home reticulation or water supply, however, such expenditures are essentially eliminated for GSHP operations. This is the scenario in Perth and its environs, where there were 190,000 garden bores in 2017 [51]. In India, this is also the case in many urban areas. Bangalore, for example, has 400,000 authorised borewells [52]. Heating and cooling are a necessity in all of those urban populations.

In addition, using groundwater for GSHPs provides the advantage of using that valuable resource at a net-zero abstraction level. There has been relatively little attempt to substantiate a comparison of GSHP and ASHP in the residential sector through actual measurements in this context. In Perth, two nearly identical houses were built next to one other, one with a GSHP in open-loop mode and the other with a conventional ASHP, to fill this gap. A comparison of the two systems performance is based on real-world data collected over more than two years and across all seasons. It has been demonstrated that there is a significant direct saving of energy and associated expenses, as well as environmental benefits as a corollary.

6 Experimental Systems

The physical systems are made up of two nearly similar single-story residential homes that were erected in 2016 in Perth, Australia (31.8°S, 115.8°E) and featured frontal views, as shown in Fig. 16.



Fig. 16 Two almost identical houses. Left: ASHP, right: GSHP

6.1 Common Construction Details of the Houses

Both houses are constructed on a 375 m² plot of land with a built-up space of around 270 m² and are facing west. They are structurally identical and resemble a typical Western Australian house. Each residence contains four bedrooms, two bathrooms, a movie room, a double garage, and a kitchen/living room area. The outer walls of the dwellings are double brick with an air gap between them. The bulk of Perth metropolitan homes are constructed in this manner.

Both the interior and exterior of the houses are completed in the same manner. Both residences have Colorbond® steel roofs that are insulated with R4.1 insulation. The ceiling is 10 mm plasterboard with a 1.5 kW solar panel system installed. The front of the house has a double lock-up garage, and the laundry is behind it. The master bedroom is located in the front of the house. The second and third bedrooms, as well as a second bathroom that separates the fourth bedroom, are located in the back of the home. The cinema room is located next to the fourth bedroom. The kitchen, dining room, and living room, which are next to the bedrooms and movie room, are the most important areas in the house. The layout of each house, as well as the ducting used within it, is seen in Fig. 17a. The house with a GSHP unit comprises an SCW construction and a water Furnace NVK-012, 15 kW can be seen in Fig. 17b. Both residences have two windows at the front. Two windows and one sliding glass door are built into the back of the dwellings. The residences have five windows on one side and four enormous windows on the other, which assist in bringing light into the living room, and a sliding glass door for the laundry. All of the windows have conventional glass and are framed with aluminium, as shown in Fig. 17c. The living room windows have roller shutters, whereas the rest of the house windows, save the bathrooms and laundry room, have normal blinds. The findings of air leakage tests show leakages of 1.20 and 1.47 l/s per m² for the GSHP and ASHP properties, respectively, at a 50 Pa pressure differential. Members of the public own both houses.

As can be expected in a suburban setting, resident usage and biological patterns vary, which may result in some variances in heating/cooling system demand.

The capacities of the systems in both houses differ by 3 kW, as can be seen from the preceding description, with the GSHP house having a higher capacity. The builder and equipment provider took these decisions, possibly to be cautious because GSHPs were new to the market. Both residences use centralised all-air systems with their

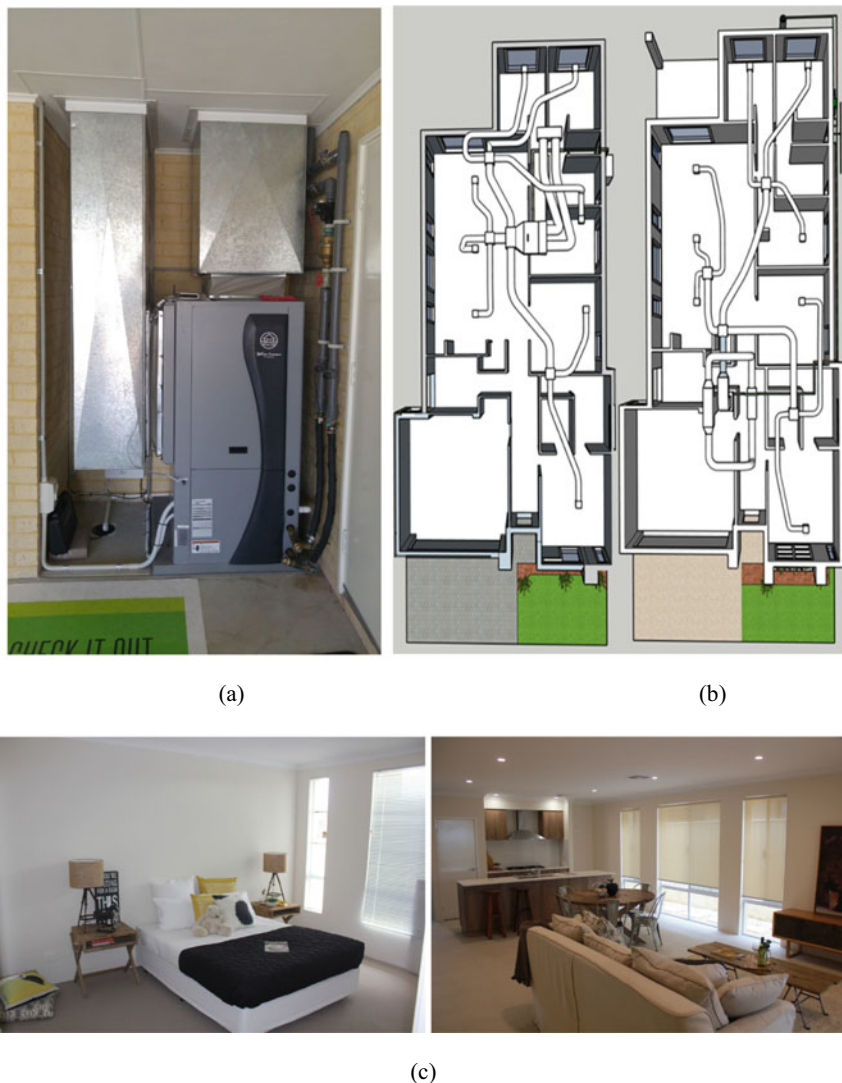


Fig. 17 a Schematic ducting plan for both houses. Left: ASHP, right: GSHP; b The GSHP unit (Water Furnace NVK-012, 15 kW) located in the garage; c Representative interior of both houses

own air handling units (AHUs) and terminal units. AHU fan power had been factored into *COP* calculations.

6.2 GSHP System Description

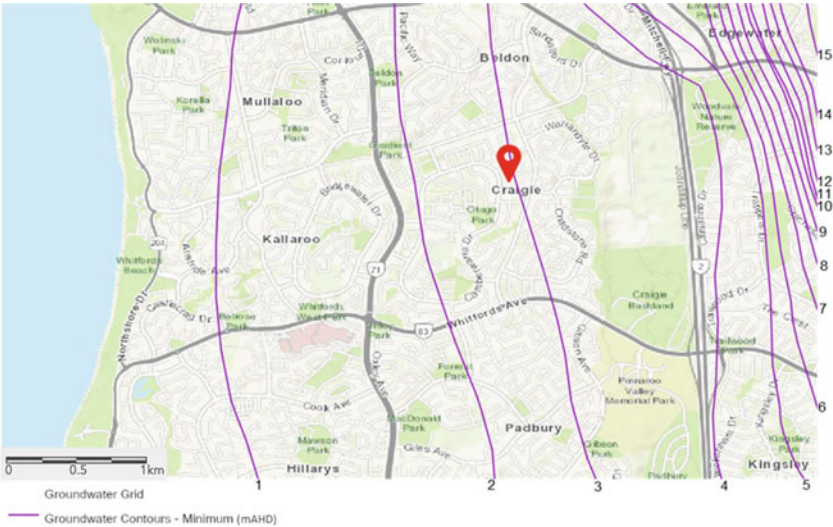
A standing column well (SCW), also known as a doublet system, is used in the GSHP system to access and return groundwater as a heat source for heating and a heat sink for cooling. A 200-mm diameter borehole was dug to a depth of 57 m, with the water table at 34.4 m for this system. At a depth of 35 metres below ground level, the returned groundwater is reinjected into the aquifer. This technique aims to prevent thermal breakthroughs while simultaneously lowering drilling expenses. The temperature of the groundwater is relatively steady at 22 °C. The water quality in Perth aquifers is generally excellent for geothermal applications. Salinities in the Yarragadee aquifer range from fresh to brackish. The salinity level rises generally with depth. Up to 1100 m below ground level, it is roughly 1 g/l, while at 1300 m below ground level, it is 30 g/l [51]. With a salinity of 0.25 g/l, the water quality at the research location is good, with little risk of iron staining and no risk of acid sulphate class [52]. As a result, an open-loop GSHP system is suitable for the chosen location. A concentric tube heat exchanger is used for heat transfer between bore water and the refrigerant. The groundwater contours map of Craigie, northern suburb area of Perth, where the two houses located is illustrated in Fig. 18a. The GSHP system using doublet system is depicted in Fig. 18b, c. A Caprari CapSub-3 System 2 model 30–65 submersible pump with a nominal power rating of 900 W is shown in Fig. 18d.

6.3 ASHP System Description

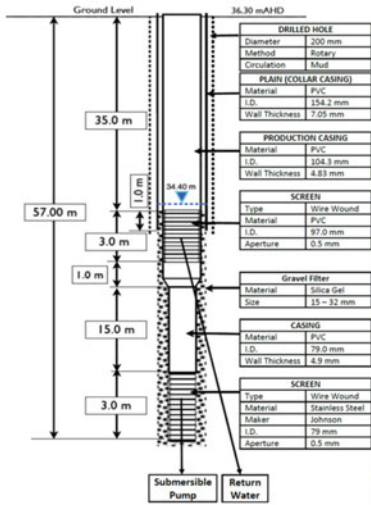
The ASHP house is installed with a Samsung Duct S AC120HBHFKH/SA indoor unit, and an inverter-based Samsung Duct S AC120HCAFKH/SA outdoor unit, with a refrigerant charge of 2.9 kg of R410A and a standard cooling capacity of 12 kW. This ASHP system is a typical split ducted unit that is found in many residential homes in Western Australia.

7 Instrumentation

The sensors installed are summarised in Table 4. The Onset HOBO RX3000 Remote monitoring station was employed as the data logger. The systems utilised a cloud background that allowed data to be accessed via the HOBOLink portal; data was recorded every 15 minutes to accommodate for sensor response time.



(a)



(b)



(c)

Fig. 18 **a** Groundwater contour map area of Craigie, Perth [53]; **b** Schematic arrangement of GSHP subterranean water sourcing; **c** Drilling operation for the doublet system; **d** The completed borehole that is located at the backyard of the GSHP house; **e** CapSub-3 System 2 model 30–65 submersible pump

**Fig. 18** (continued)**Table 4** Details of instrumentation

Model	Sensor	Measuring range	Accuracy	Response time
Onset S-THB-M008	Temperature	−40 °C to 75 °C	±0.21 °C from 0 °C to 50 °C	5 min in air moving 1 m/s
	Relative humidity	100% RH at −40 °C to 75 °C	±2.5% from 10 to 90% RH	5 min in air moving 1 m/s with a protective cap
HOBO S-TMB-M006	Water temperature	−40 °C to 100 °C	<±0.2 °C from 0 to 50 °C	<1 min typical in stirred water bath
Kimo CTV210	Air velocity	0 to 30 m/s	from 0.15 m/s to 3 m/s: ± 3% of reading ± 0.03 m/s	T ₆₃ = 1.6 s
Onset T-MAG-0400	Current transformers	Input from 1 to 75 A, output from 0–333 mV	10% to 130% of rated current	N/A

7.1 Sensor Calibration

The sensors in both residences were calibrated by Delta Building Automation. The data from the HOBO RX3000 remote monitoring station was also examined to guarantee that the measurements were accurate, as shown in Fig. 19a. The overall air flow, which was the sum of flow rates from all the grills in different rooms, had to be correlated with a single velocity measurement in the fan coil unit (FCU) discharge duct due to the domestic nature of both buildings. Flow rates at each discharge grill were monitored using a flow hood (Testo 420) and reconciled with air velocity prior

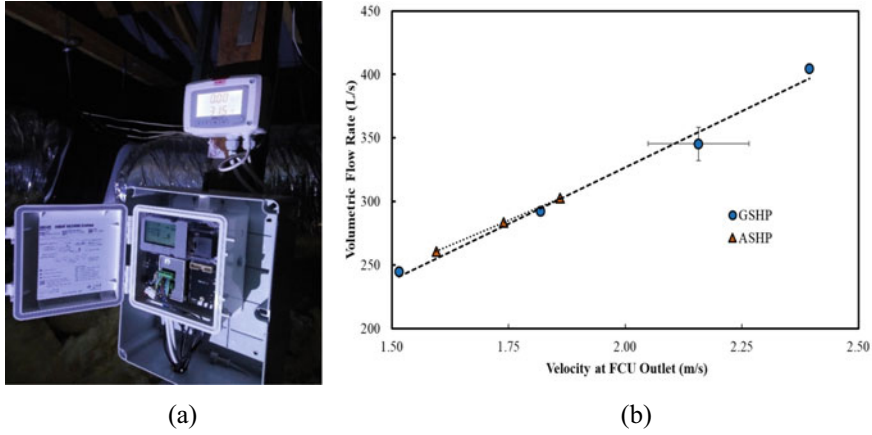


Fig. 19 **a** HOBO RX3000 remote air flow monitoring station in the attic; **b** Calibration chart of velocity conversion at FCU outlet to total volumetric flow rate

to the commissioning of both houses. Figure 19b shows the obtained airflow calibration curves. When the fan operation stabilised, all data was taken while in steady condition.

$$q \left(\frac{\text{L}}{\text{s}} \right) = 177.5 \, c \, (\text{m/s}) - 28.1 \quad (3)$$

$$q \left(\frac{\text{L}}{\text{s}} \right) = 157.9 \, c \, (\text{m/s}) + 8.9 \quad (4)$$

For both GSHP and ASHP houses, the related uncertainty was calculated to be 6.3% and 6.2%, respectively. Air turbulence was responsible for the high level of uncertainty. The Appendix B contains the error analysis. Following trial runs in August 2017, continuous data collection began in October 2017 and lasted through to July 2019.

7.2 Data Collection and Processing

For both houses, the following metrics were recorded at 15-minute intervals:

- current drawn by heat pump compressors, FCU, ASHP outdoor unit, and GSHP submersible pump.
- FCU inlet and outlet temperatures, ambient, living room temperatures in both houses, and groundwater inlet and outlet temperatures for the GSHP. A solar radiation shield (Onset RS3B) was used to protect outdoor temperature sensors.

Table 5 Criteria for steady-state operating conditions

GSHP house	Conditions	ASHP house	Conditions
$P_{Bore\ Pump}$	>15 W	P_{Fan}	>60 W
$P_{Heat\ Pump}$	>250 W	P_{in}	>1000 W
P_{in}	>1100 W	c	>0.2 m/s
c	>0.2 m/s		

- Supply air velocities at FCU outlet.
- Relative humidity at FCU inlet and outlet, ambient, and living rooms.

8 Analysis

8.1 Comparison of Operating Conditions

Table 5 lists the criteria that were used to filter the downloaded data. For comparative studies, only steady-state data lasting at least 45 minutes was used. To prevent the inclusion of data during unsteady operation, data was also eliminated when the FCU inlet/outlet temperature varied by more than 1 °C from the previous reading or when the computed FCU inlet/outlet absolute humidity drifted by more than 1 g/kg of dry air. The average power factor for variable-frequency-drive-based GSHP was 0.79, whereas the inverter-based ASHP system had a power factor of 1.00 (both measured with Fluke 1738).

8.2 Heating and Cooling Capacities and COP

The specific volume, absolute humidity, specific enthalpy, and specific heat of moist air were calculated using the ASHRAE psychrometric calculation scheme [54]. For ambient conditions, Wangara, Perth weather data was used (atmospheric pressure, temperature, and relative humidity).

The average heating and cooling capacity were calculated by numerically integrating instantaneous data for 45 min as follows:

$$Q_h = \frac{1}{45 \text{ min}} \int_0^{45 \text{ min}} \left(\frac{q}{v} \right) c_p (t_2 - t_1) d\tau \quad (5)$$

$$Q_c = \frac{1}{45 \text{ min}} \int_0^{45 \text{ min}} \left(\frac{q}{v} \right) [(h_1 - h_2) - (W_1 - W_2)h_{w2}] d\tau \quad (6)$$

The uncertainties in the heating and cooling capacities were computed using the NIST method [55] and found to be 7.5% for heating and 8.2% for cooling, respectively, which is primarily attributable to inaccuracies in flow rate estimation (details are given in Appendix). Electrical power input was also handled in a similar manner. The coefficients of performance (*COPs*) were then computed as follows:

$$COP_h = \frac{Q_h}{\frac{1}{45 \text{ min}} \int_0^{45 \text{ min}} P_{in} d\tau} \quad (7)$$

$$COP_c = \frac{Q_c}{\frac{1}{45 \text{ min}} \int_0^{45 \text{ min}} P_{in} d\tau} \quad (8)$$

Because electrical power measurement has a modest margin of uncertainty, the total relative uncertainty in *COPs* can be predicted to be similar to that of heating and cooling capacities.

9 Results and Discussion

9.1 Basic Data

Figure 20 depicts the ambient conditions for both systems steady-state operation durations. When the systems are turned on in the winter and summer, the ambient relative humidity appears to be quite consistent. Figures 21, 22, 23 and 24 show the processed steady-state primary data of temperature and relative humidity at the inlet and outlet of FCUs, as well as ambient temperature and supply air velocity at the FCU exits. The information offered there spans approximately two years (two summers and two winters).

9.2 Air Entering the FCU

Figures 21 and 22 show the state of air inside and outside the FCU when they were utilised for heating and cooling, respectively. In each of these figures, uniformity in indoor settings (as correlated by FCU in) can be seen, with settings ranging from 20–27 °C and 35–55% RH for heating and 22–29 °C and 30–55% RH for cooling mode. This trend corresponds to user behaviours in Western Australia, where temperatures are set slightly lower in the winter and slightly higher in the summer to save money on energy. Despite the fact that the correlations between air velocity at FCU

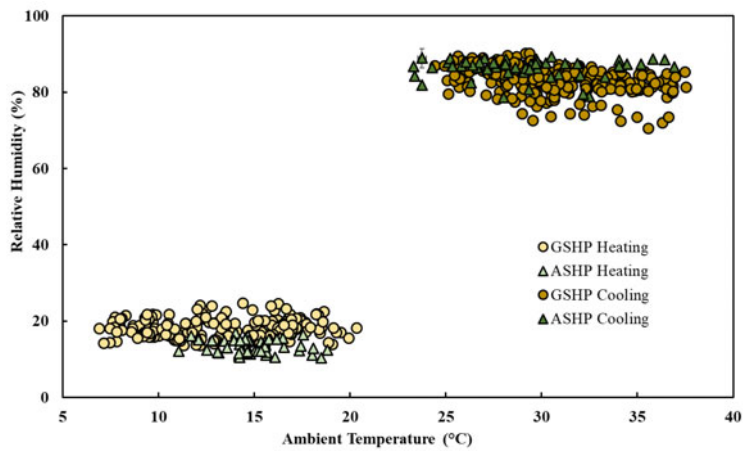


Fig. 20 Ambient conditions for both houses

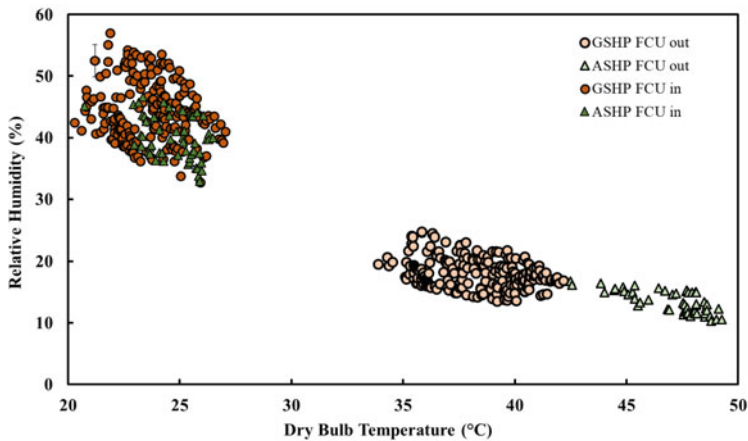


Fig. 21 Primary data for conditions of air across FCUs of GSHP and ASHP during heating

and volumetric flow rate for the two houses are different (Eqs. 1 and 2), Fig. 19b demonstrates that the actual flow rates are comparable.

The temperature setting by the users is approximately identical to the FCU inlet conditions. Both houses have hugely different FCU outlet states. When compared to the ASHP house (44–49 °C), the GSHP house has a lower magnitude (34–42 °C) (Fig. 21). This is due to the individual heat pump systems condensing temperatures and compression superheats. While the GSHP uses a constant temperature ground-water source (at the heat pump evaporator), the ASHP evaporator is vulnerable to ambient temperatures that are significantly lower than groundwater temperatures in the winter.

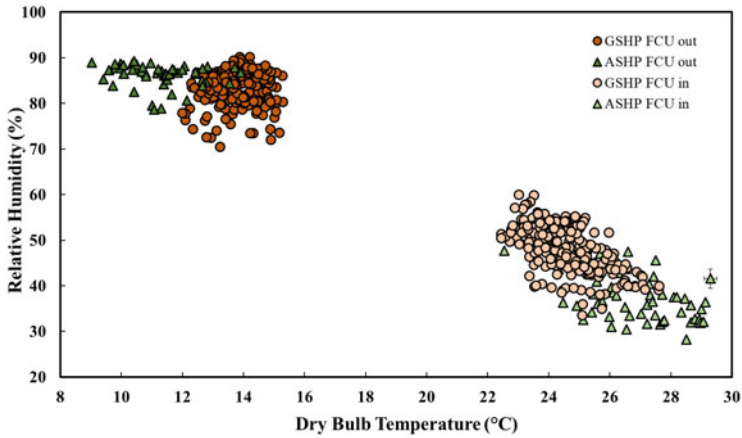


Fig. 22 Primary data for conditions of air across FCUs of GSHP and ASHP during cooling

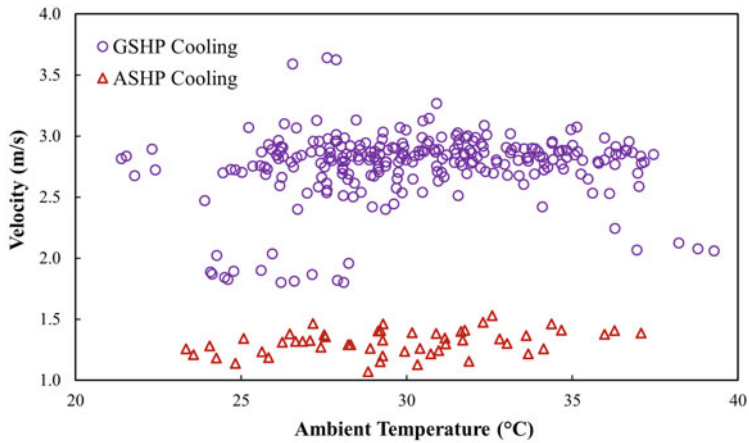


Fig. 23 Primary data for air velocity at FCUs and ambient temperature for heating conditions

The thermostat settings and the heating load both determine the discharge pressure. As a result, an ASHP system compression ratio is higher than a GSHP system. As a result, when the suction superheats of ASHP and GSHP compressors are the same (usually 5–10 °C), the corresponding discharge superheats in the former will be higher than in the latter. This is exacerbated by the decrease in compressor isentropic efficiency when condenser and evaporator compression ratios rise. Furthermore, compressor volumetric efficiency is inversely proportional to compression ratios. To meet the heating demand, the ASHP compressor must operate at greater discharge pressure. The FCU output status of the two systems clearly reflects this. Because there

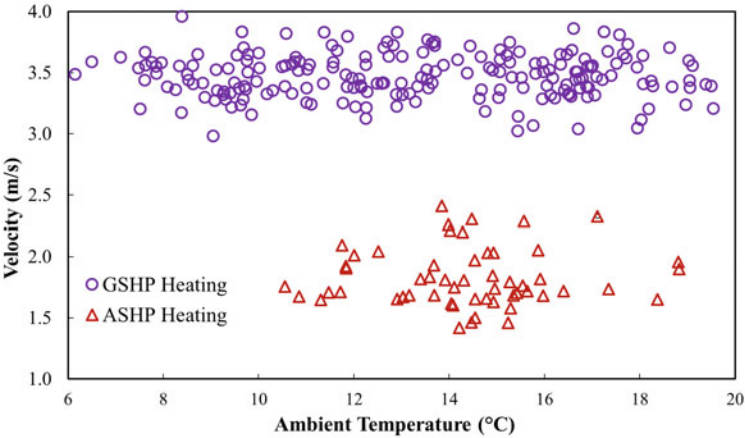


Fig. 24 Primary data for air velocity at FCUs and ambient temperature for cooling conditions

is no humidification or dehumidification in FCUs during heating, relative humidity practically tracks temperature in the opposite direction.

9.2.1 Comparative Analysis of the Cooling Mode of Two Systems

In cooling mode, the GSHP condenser maintains a relatively steady and lower temperature, similar to that of bore water. This will usually be lower than the temperature at which the ASHP runs. The majority of the data gathered for FCU outlet cooling is within 12–16 °C for GSHP and 9–13 °C for ASHP, as shown in Fig. 22. This condition is similar to the heating situation. The compression ratios in GSHP will be lower than those in ASHP, regardless of whether they are used for heating or cooling. The evaporator in an ASHP must run at a lower temperature to meet the cooling demand, as shown by the FCU outlet temperature in Fig. 22.

The operation of FCUs is another aspect of the performance. Air flow rates across them control this. Figures 23 and 24 show the heating and cooling velocity across the FCUs in ASHP and GSHA households. The volumetric flow rate over the coil of the GSHP is higher, while the cross-sectional area of the FCU is smaller. GSHP achieves better heat transfer than ASHP due to higher air velocity across the coil. As a result of this process, in order to meet the cooling demand, the cooling given to the air over the coil in ASHP must be greater than in GSHP, as seen by lower temperatures at the FCU output (Fig. 22). Furthermore, the FCU inlet temperature in the ASHP house is sometimes greater than in the GSHP house, which can be related to occupant settings that may be in different age groups.

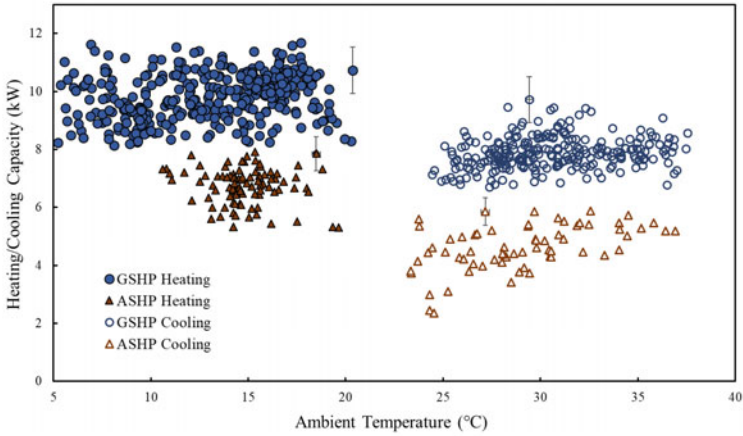


Fig. 25 Heating and cooling capacities are delivered by GSHP and ASHP at various ambient temperatures

9.2.2 Comparison of Heating and Cooling Capacities

Over the course of two years, Fig. 25 depicts the heating and cooling capacity of both systems. Despite the fact that the temperature settings in both homes are the same and the residences are identical, the systems capabilities are vastly different. This can be ascribed to actual heating and cooling loads due to resident usage patterns, which are dependent on the number of occupants, the number of zones that are actually used, and interior sources such as refrigerators, microwaves, gas stoves, television sets, computers, and so on. Diurnal/seasonal fluctuations in cooling/heating demands on the systems cause the data to be scattered. Residents in the ASHP house appear to be more conservative in their settings than those in the GSHP house. The difference in the nature of heating/cooling demands between GSHP and ASHP houses is something to notice. Figure 25 depicts the qualitative behaviour of the two systems in relation to the surrounding environment. The ASHP home follows the ambient temperature with a weak trend. As a result, a preferable criterion for evaluation will be the *COP*, which will be discussed later.

9.3 Groundwater Temperature

On a worldwide scale, groundwater is a limited and valuable resource. As a result, it is crucial to consider how a GSHP system could impact this resource. During nearly two years of heating and cooling operations, the temperature of groundwater entering and exiting the evaporator and condenser is shown in Fig. 26. During the transitional seasons, there are gaps in the data, indicating that the system is not active

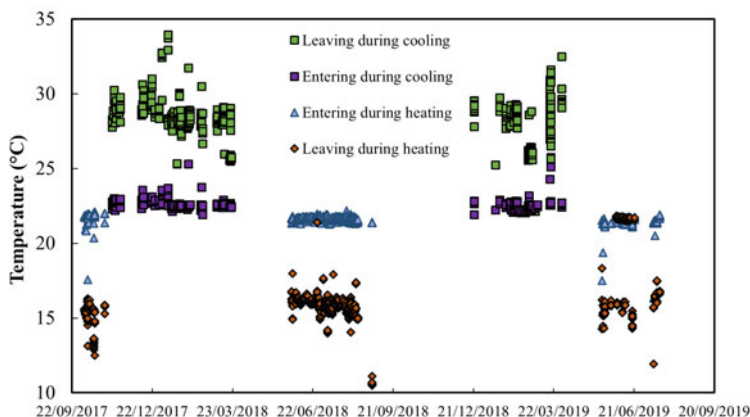


Fig. 26 Water temperatures across FCU over two years for GSHP

(spring and autumn). Local communities have selected this as an energy-saving option as well. Throughout the period, the temperature of groundwater entering the evaporator/condenser has remained relatively constant at around 22–23 °C. On the other hand, it has a temperature rise during cooling (water-cooled condenser) and a temperature fall while heating (water-heated evaporator). Fluctuations in these outlet temperatures are caused by variations in the cooling load at any given time, which are mostly dependent on ambient conditions and resident usage patterns, such as the number of zones used, internal loads, and so on.

A secondary advantage of GSHP is that the compressor operates at a constant temperature differential, resulting in a constant and lower pressure ratio than with ASHP. The GSHP, as previously stated, has higher volumetric and isentropic efficiencies than the ASHP. The longevity of compressor valves and lubrication uniformity are examples of intangible benefits. This can be illustrated further by comparing the *COPs* listed below.

9.4 *COPs of GSHP and ASHP Systems*

Figure 27 depicts the *COPs* of both systems for heating and cooling modes of operation over a two-year monitoring period. Because each data point is related to diurnal and seasonal external factors, such as sunshine, cloud cover, variations in surface conditions of surfaces, ambient air velocity, and so on, there is significant scatter in the data. In each scenario, typical error bands associated with data are presented for one point. As previously stated, the *COP* of GSHP is essentially unaffected by ambient temperature, varying only by about 0.8 between heating and cooling, which is close to the theoretical limit of 1. ASHP, on the other hand, appears to increase with

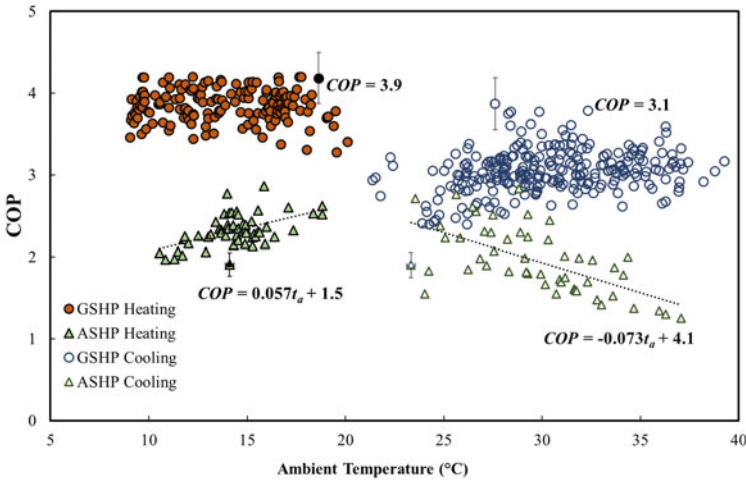


Fig. 27 A comparison of *COP* of GSHP and ASHP at various ambient temperatures

ambient temperature during heating and decrease with ambient temperature during cooling. Only when the outdoor temperature is close to that of the groundwater does the *COP* of the ASHP matches that of the GSHP. When compared to ASHP, GSHP systems are predicted to have higher *COPs* throughout the course of a year of operation, resulting in lower power consumption and associated Scope 2 emissions. This is especially true in Perth, where the summers are scorching hot and the winters are cold, as shown in Figs. 20 and 27 also depicts the *COP* trend lines.

In the GSHP house, the *COPs* for heating and cooling are heightened significantly, as shown in Fig. 27. Accordingly, the GSHP house would have saved roughly AUD\$1050 per year in energy expenditures if it had used ASHP instead. At 28.8 cents per kWh, this equals 3646 kWh of electricity. Based on 0.7 kg of CO₂/kWh for Perth, the environmental benefits will be around 2.5 t of CO₂ emission reduction. Based on 7 t/dwelling/year [56], this equates to a nearly 35% reduction in greenhouse gas emissions. If most Perth homes had installed borewells for reticulation, it would not be difficult to estimate the impact of GSHP. It is also possible to deduce that installing a GSHP in an existing home with a borewell can result in significant financial and environmental benefits. Furthermore, the impact of groundwater quality on the heat exchanger and piping performance in GSHP systems must be assessed. However, the water quality in this investigation was sufficient to avoid derating during its operation.

10 Conclusions

The current experimental program was designed to compare the performance of an open-loop GSHP system to a traditional ASHP in the residential sector of Perth, Western Australia. In each category, just one house was compared. When used for both heating and cooling, the GSHP system clearly outperformed the ASHP system. The GSHP system had an average *COP* of 3.1 for cooling, which was practically independent of ambient temperatures. The *COP* of the ASHP system, on the other hand, varied from 1.3 to 2.8, depending on external temperatures. Similarly, the *COP* of the GSHP system stayed fairly constant at 3.9 for heating, whereas the *COP* of the ASHP system varied from 1.9 to 2.9 depending on external conditions. These findings revealed that the GSHP system was up to 100% and 60% more efficient than the ASHP system when used for cooling and heating, respectively. If a borewell is included with a home, it is clear that GSHP is a better alternative than ASHP.

Acknowledgements The authors would like to thank David Lister from the Beatty Park Leisure Centre. He has been very generous and kind in providing us with access to the swimming pools and helping us with all information required. Tine Aprianti would like to thank LPDP (Indonesia Endowment Fund for Education) for the scholarship award and to The University of Western Australia and The University of Sriwijaya for their great support.

The Cool Earth Project is a collaborative research between The University of Western Australia, DevelopmentWA, GeoExchange, Carbonomics, ABN Group and The Vibe at Craigie. The authors acknowledge the advice rendered by Paul Jackson and Graham Boyle of The Australian Institute of Refrigeration, Air Conditioning and Heating (AIRAH), the assistance of QED Environmental Services in conducting the leak tests for the houses and Adrian Middleton of Delta Automation for his support and assistance in checking the sensors and calibrating the air flow rates, and also the kind assistance from Greg Ryan of DevelopmentWA. Tine Aprianti expresses her most sincere thanks to the Indonesia Endowment Fund for Education (LPDP) for the scholarship award and to The University of Western Australia and The University of Sriwijaya for their great support.

Human Research Ethics Declaration The present research is subject to the Human Research Ethics oversight of The University of Western Australia (Project number RA/4/1/7833).

11 Appendix B

The uncertainty associated with the results are due to (i) instrument uncertainties, (ii) correlation uncertainties from the velocity measured at FCUs to the total airflow rate,

and (iii) mathematical uncertainties due to averaging and data processing. Uncertainties in properties such as specific heat capacities of fluids and densities of fluids are ignored, although the effect of temperature and relative humidity uncertainty on them has been accounted for Volumetric flow rate uncertainty (Table B.1).

- Velocities were measured at FCUs throughout the experiments and correlated against the total airflow rates in Fig. 3.4 and Eqs. (3.1 and 3.2).
- The following table summarises the uncertainties in assessing the volumetric flow rates of both the GSHP and ASHP houses.

Cooling and heating capacity uncertainties

Estimation of the heating capacity uncertainty stems from the uncertainties in q (which are 6.3% and 6.2% (as shown above) for GSHP and ASHP house, respectively), t_1 , t_2 , and v in Eq. 3.3.

The estimation of the cooling capacity uncertainty stems from the uncertainties in q , t_1 , t_2 , v , W_1 , and W_2 in Eq. 3.4.

In the above cases, the uncertainty in v arises from t_1 , t_2 , and W_1 again.

It is assumed that the atmospheric pressure is constant at 1013 mbar throughout because Perth is on the coast, and it changes only marginally and has minimal effect on v .

Uncertainty in the heating capacity can be written as

$$\frac{\Delta Q_h}{Q_h} = \sqrt{\left(\frac{\Delta q}{q}\right)^2 + 2\left(\frac{\Delta t}{t_2 - t_1}\right)^2 + 2\left(\frac{\Delta t}{273.15 + 0.5(t_2 + t_1)}\right)^2 + 2\left(\frac{\Delta W}{W}\right)^2}$$

Table B.1 The uncertainties in assessing the volumetric flow rates of both the ground source heat pump (GSHP) and air source heat pump (ASHP) houses

	Fan speed	Airflow uncertainty (l/s)	Velocity uncertainty (m/s)	Correlation uncertainty from velocity (l/s)	Total uncertainty (l/s)	% error
GSHP	1	10.8	0.08	13.4	17.2	7.0
	2	11.4	0.08	15.0	18.9	6.5
	3	12.2	0.09	16.8	20.8	6.0
	4	13.1	0.10	18.1	22.3	5.5
	Average % error					6.3
ASHP	1	10.8	0.08	12.7	16.7	6.4
	2	11.2	0.08	13.4	17.5	6.2
	3	11.5	0.09	14.0	18.1	6.0
	Average % error					6.2

The uncertainty in temperature is accounted 4 times as follows: twice for the difference between t_1 and t_2 because each has an uncertainty, one for its effect on v , and one for its effect on c_p . The humidity effect is accounted for twice as follows: Once for v and once for c_p . It is also reasonable to assume that the uncertainty in W will map directly as relative humidity (\square).

A Sample calculation for heating capacity uncertainty

For the GSHP house on 3 June 2018, for a heating capacity of 10.0 kW, the temperatures at the inlet and outlet of FCU were $t_2 = 35.98^\circ\text{C}$ and $t_1 = 22.28^\circ\text{C}$.

$$t_2 - t_1 = 35.98 - 22.28 = 13.70^\circ\text{C}$$

$$273.15 + 0.5(t_2 + t_1) = 302.28\text{ K}$$

$$\frac{\Delta q}{q} = 0.063, \quad t = 21^\circ\text{C}, \quad \frac{\Delta W}{W} = \frac{\Delta \phi}{\phi} = 0.025,$$

$$\frac{\Delta Q_h}{Q_h} = \sqrt{0.063^2 + 2\left(\frac{0.21}{13.70}\right)^2 + 2\left(\frac{0.21}{302.28}\right)^2 + 2(0.025)^2} = 7.5\%$$

The relative uncertainty in COP is expected to be about the same as the uncertainty in power is negligible.

In the case of cooling, the uncertainty in humidity will be multiplied four times. Accordingly

$$\frac{\Delta Q_c}{Q_c} = \sqrt{\left(\frac{\Delta q}{q}\right)^2 + 2\left(\frac{\Delta t}{t_2 - t_1}\right)^2 + 2\left[\frac{\Delta t}{273.15 + 0.5(t_2 + t_1)}\right]^2 + 4\left(\frac{\Delta W}{W}\right)^2}$$

A Sample calculation for the cooling capacity uncertainty

For the ASHP house, on 7 November 2017, its cooling capacity was 4.4 kW, and the temperatures at the inlet and outlet of FCU were $t_1 = 25.09^\circ\text{C}$ and $t_2 = 9.19^\circ\text{C}$.

$$t_2 - t_1 = 9.19 - 25.09 = -15.30^\circ\text{C}$$

$$273.15 + 0.5(t_2 + t_1) = 290.29\text{ K}$$

$$\frac{\Delta q}{q} = 0.062, \quad t = 21^\circ\text{C}, \quad \frac{\Delta W}{W} = \frac{\Delta \phi}{\phi} = 0.025,$$

$$\frac{\Delta Q_c}{Q_c} = \sqrt{0.062^2 + 2\left(\frac{0.21}{-15.30}\right)^2 + 2\left(\frac{0.21}{290.29}\right)^2 + 4(0.025)^2} = 8.2\%$$

Table B.2 Standard deviations for *COP* between the fit and individual data points in Fig. 27

	Heating	Cooling
GSHP	0.24	0.29
ASHP	0.16	0.31

While the uncertainties associated with each of the points in Fig. 27 were 7.5% for heating and 8.2% for cooling, respectively. The scatter seen in those plots is due to external factors affecting heating and cooling loads. While heating loads are relatively unaffected by solar loads, the heat loss from external walls during winter is affected by the ambient air velocity, which changes quite considerably in Perth during winter, and the temperature difference between the house setting and ambient. During summer, in addition to these ambient weather conditions, the solar loads change vastly diurnally and seasonally.

The correlations given in Fig. 27 need to be seen in the light of the above factors. The standard deviations between the fit and individual points there are as follows (Table B.2).

A larger standard deviation in the case of GSHP heating can also be attributed to the usage pattern of residents and appliances activated by residents. It could also depend on the age of the inhabitants, with elderly people setting a higher temperature in winters.

References

1. Zuccari F, Santiangeli A, Orecchini F (2017) Energy analysis of swimming pools for sports activities: cost effective solutions for efficiency improvement. *Energy Procedia* 126:123–130. <https://doi.org/10.1016/j.egypro.2017.08.131>
2. Pujol M, Ricard LP, Bolton G (2015) 20 years of exploitation of the Yarragadee aquifer in the Perth Basin of Western Australia for direct-use of geothermal heat. *Geothermics* 57(2015):39–55. <https://doi.org/10.1016/j.geothermics.2015.05.004>
3. Christ A, Rahimi B, Regenauer-Lieb K, Chua HT (2017) Techno-economic analysis of geothermal desalination using Hot Sedimentary Aquifers: a pre-feasibility study for Western Australia. *Desalination* 404:167–181. <https://doi.org/10.1016/j.desal.2016.11.009>
4. Wang X, Bierwirth A, Christ A, Whittaker P, Regenauer-Lieb K, Chua HT (2013) Application of geothermal absorption air-conditioning system: a case study. *Appl Therm Eng* 50(1):71–80. <https://doi.org/10.1016/j.applthermaleng.2012.05.011>
5. Hahne E, Kübler R (1994) Monitoring and simulation of the thermal performance of solar heated outdoor swimming pools. *Sol Energy* 53(1):9–19. [https://doi.org/10.1016/S0038-092X\(94\)90598-3](https://doi.org/10.1016/S0038-092X(94)90598-3)
6. McMillan W (1971) Heat dispersal—lake Trawsfynydd cooling studies. Symposium on freshwater biology and electrical power generation 1:41–80. <https://doi.org/10.1002/wat2.1172>
7. Richter D (1979) Temperatur- und Wärmehaushalt des thermisch belasteten Stechlin- und Nehmitzsees, no. 123. Berlin: Akademie-Verlag
8. Woolley J, Harrington C, Modera M (2011) Swimming pools as heat sinks for air conditioners: model design and experimental validation for natural thermal behavior of the pool. *Build Environ* 46(1):187–195. <https://doi.org/10.1016/j.buildenv.2010.07.014>
9. Jimenez SA, Carrillo V, Alvarado MA (2015) Swimming Pool heating systems: a review of applied models. *Tecciencia* 10(19):17–26. <https://doi.org/10.18180/tecciencia.2015.19.4>

10. Lovell D et al (2019) Thermal performance prediction of outdoor swimming pools. *Build Environ* 160. <https://doi.org/10.1016/j.buildenv.2019.106167>
11. Ruiz E, Martínez PJ (2010) Analysis of an open-air swimming pool solar heating system by using an experimentally validated TRNSYS model. *Sol Energy* 84(1):116–123. <https://doi.org/10.1016/j.solener.2009.10.015>
12. Smith CC, Lof GOG, Jones RW, Kittler R, Jones R (1998) Rates of evaporation from swimming pools in active use/discussion. *ASHRAE Trans* 104:514
13. Beatty Park (2014). https://en.wikipedia.org/wiki/Beatty_Park. Accessed 17 Feb 2022
14. Pujol M (2014) Hale school geothermal. https://www.airah.org.au/Content_Files/Divisionmeetingpresentations/WA/12-03-14-WA-Hale-School.pdf
15. Vincent WA, Perth TO (2011) Special council meeting 3 May 2011. <https://www.vincent.wa.gov.au/council-meetings/special-council-meeting/17-may-2011/397/documents/20110517.pdf>. Accessed 23 Jan 2022
16. Foster B (2016) Beatty Park geothermal pool heater fault to cost Vincent council \$700,000 (2016). <https://www.watoday.com.au/national/western-australia/beatty-park-geothermal-pool-heater-fault-to-cost-vincent-council-700000-20160506-goodcl.html#:~:text=Adodgy heating system at, to heat their three pools.> Accessed 23 Jan 2022
17. Jewell C (2013), Beatty Park redevelopment saves Vincent 5000mW per year (2013). <https://thefifthstate.com.au/articles/beatty-park-redevelopment-saves-vincent-5000mw-per-year/>. Accessed 17 Feb 2022
18. Australian Standard © Solar heating systems for swimming pools, AS 3634–1989 (Reconfirmed 2013). Australian Standard. [Online]. Available <https://www.saiglobal.com/PDFTemp/Previews/OSH/As/as3000/3600/3634.pdf>
19. Rakopoulos CD, Vazeos E (1987) A model of the energy fluxes in a solar heated swimming pool and its experimental validation. *Energy Convers Manag* 27(2):189–195. [https://doi.org/10.1016/0196-8904\(87\)90075-6](https://doi.org/10.1016/0196-8904(87)90075-6)
20. A. S. of H. R. and A.-C. E. Inc, Refrigerants, SI Edition. American Society of Heating, Refrigerating and Air-Conditioning Engineers, Inc. (ASHRAE) (2017)
21. Bergman TL, Incropera FP (eds) (2011) Fundamentals of heat and mass transfer, 7th edn. John Wiley, Hoboken, NJ
22. Rossie K (1953) Die diffusion von Wasserdampf in Luft bei Temperaturen bis 300 °C, *Forsch. auf dem Gebiet des Ingenieurwesens A*, 19(2):49–58. <https://doi.org/10.1007/BF02558326>
23. <https://www.aer.gov.au/wholesale-markets/wholesale-statistics/national-electricity-market-electricity-consumption>. Accessed 14 Feb 2021
24. Department of Industry, Science, Energy and Resources, Australian Energy Update 2020, September 2020, Australian Energy Statistics, ISSN (Online): 2203–8337
25. Lucia U, Simonetti M, Chiesa G, Grisolia G (2016) Ground-source pump system for heating and cooling: review and thermodynamic approach. *Renew Sustain Energy Rev* 70:867–874. <https://doi.org/10.1016/j.rser.2016.11.268>
26. Egg J, Howard BC (2011) Geothermal HVAC: green heating and cooling. McGraw-Hill, New York, 2011, [Online]. Available <http://accessengineeringlibrary.com/browse/geothermal-hvac-green-heating-and-cooling>
27. Naicker SS, Rees SJ (2018) Performance analysis of a large geothermal heating and cooling system. *Renew Energy* 122(February):429–442. <https://doi.org/10.1016/j.renene.2018.01.099>
28. Lund JW, Freeston DH, Boyd TL (2011) Direct utilization of geothermal energy 2010 worldwide review. *Geothermics* 40(3):159–180. <https://doi.org/10.1016/j.geothermics.2011.07.004>
29. <https://industry.gov.au/Office-of-the-ChiefEconomist/Publications/Documents/GA21797.pdf>. Accessed 14 Feb 2021
30. Lu Q, Narsilio GA, Aditya GR, Johnston IW (2017) Economic analysis of vertical ground source heat pump systems in Melbourne. *Energy* 125:107–117. <https://doi.org/10.1016/j.energy.2017.02.082>

31. Australian Renewable Energy Agency (2019) Renewable geothermal heat pumps trialled at Blacktown greenfield estate. ARENA media, Australian Government. https://arena.gov.au/assets/2019/01/ARENA-Media-Release_Climate-KIC-to-trial-geothermal-pumps-at-Fairwater-residential-estate-in-Blacktown-250119x.pdf. Accessed 20 Jan 2021
32. Hannam P (2017) Suburban test-bed for geothermal heating and cooling. The Sydney Morning Herald. Fairfax Media Publications Pty Limited, p. 8, 2017, [Online]. Available <https://www.smh.com.au/environment/sustainability/geothermal-a-technology-that-blows-hot-and-cold-in-sydneys-booming-west-20170410-gvherz.html>
33. Kirkby AL (2011) The ground source heat pump at geoscience Australia. Preview 2011(153):29–30. <https://doi.org/10.1071/pvv2011n153p29>
34. Lu Y, Hooman K, Atrens AD, Russell H (2017) An experimental facility to validate ground source heat pump optimisation models for the Australian climate. Energies 10(1). <https://doi.org/10.3390/en10010138>
35. Luo J, Rohn J, Xiang W, Bertermann D, Blum P (2016) A review of ground investigations for ground source heat pump (GSHP) systems. Energy Build. 117:160–175. <https://doi.org/10.1016/j.enbuild.2016.02.038>
36. Michopoulos A, Zachariadis T, Kyriakis N (2013) Operation characteristics and experience of a ground source heat pump system with a vertical ground heat exchanger. Energy 51:349–357. <https://doi.org/10.1016/j.energy.2012.11.042>
37. Vanhoudt D, Desmedt J, Van Bael J, Robeyn N, Hoes H (2011) An aquifer thermal storage system in a Belgian hospital: long-term experimental evaluation of energy and cost savings. Energy Build 43(12):3657–3665. <https://doi.org/10.1016/j.enbuild.2011.09.040>
38. Kim E, Lee J, Jeong Y, Hwang Y, Lee S, Park N (2012) Performance evaluation under the actual operating condition of a vertical ground source heat pump system in a school building. Energy Build 50:1–6. <https://doi.org/10.1016/j.enbuild.2012.02.006>
39. Southard L, Liu X, Spittler J (2014) Performance of the HVAC systems at the ASHRAE headquarters building. Part I: measured energy usage. ASHRAE J
40. Lyne Y, Paksoy H, Farid M (2019) Laboratory investigation on the use of thermally enhanced phase change material to improve the performance of borehole heat exchangers for ground source heat pumps. Int J Energy Res 43(9):4148–4156. <https://doi.org/10.1002/er.4522>
41. Molavi J, McDaniel J (2016) A review of the benefits of geothermal heat pump systems in retail buildings. Procedia Eng. 145:1135–1143. <https://doi.org/10.1016/j.proeng.2016.04.147>
42. Self SJ, Reddy BV, Rosen MA (2013) Geothermal heat pump systems: status review and comparison with other heating options. Appl Energy 101:341–348. <https://doi.org/10.1016/j.apenergy.2012.01.048>
43. Song J et al (2010) Heating performance of a ground source heat pump system installed in a school building. Sci China Technol Sci 53(1):80–84. <https://doi.org/10.1007/s11431-009-0422-8>
44. Michopoulos A, Voulgari V, Tsikaloudaki A, Zachariadis T (2016) Evaluation of ground source heat pump systems for residential buildings in warm Mediterranean regions: the example of Cyprus. Energy Effic 9(6):1421–1436. <https://doi.org/10.1007/s12053-016-9431-1>
45. Abdel-Salam MRH, Zaidi A, Cable M (2021) Field study of heating performance of three ground-source heat pumps in Canadian single-family houses. Energy Build, 110959. <https://doi.org/10.1016/j.enbuild.2021.110959>
46. Lim J-H (2010) Application of geothermal heat pumps in a renovated campus building. Int J Energy Res 34(5):445–453. <https://doi.org/10.1002/er.1648>
47. Healy PF, Ugursal VI (1997) Performance and economic feasibility of ground source heat pumps in cold climate. Int J Energy Res 21(10):857–870. [https://doi.org/10.1002/\(SICI\)1099-114X\(199708\)21:10%3C857::AID-ER279%3E3.0.CO;2-1](https://doi.org/10.1002/(SICI)1099-114X(199708)21:10%3C857::AID-ER279%3E3.0.CO;2-1)
48. Hepbasli A (2002) Performance evaluation of a vertical ground-source heat pump system in Izmir, Turkey. Int J Energy Res 26(13):1121–1139. <https://doi.org/10.1002/er.839>
49. Christodoulides P, Arestib L, Florides G (2019) Air-conditioning of a typical house in moderate climates with Ground Source Heat Pumps and cost comparison with Air Source Heat Pumps. Appl Thermal Eng 158:113772. <https://doi.org/10.1016/j.applthermaleng.2019.113772>

50. Maddah S, Goodarzi M, Safaei MR (2020) Comparative study of the performance of air and geothermal sources of heat pumps cycle operating with various refrigerants and vapor injection. *Alexandria Eng J* 59(6):4037–4047. <https://doi.org/10.1016/j.aej.2020.07.009>
51. <https://www.water.wa.gov.au/urban-water/bores>. Accessed 4 May 2021
52. <https://www.bbc.com/future/article/20201006-india-why-bangalore-is-digging-a-million-wells>. Accessed 11 May 2021
53. <https://www.water.wa.gov.au/maps-and-data/maps/perth-groundwater-atlas>. Accessed 27 June 2022
54. ASHRAE Handbook of Fundamentals, vol. 30329, no. 404. Atlanta: American Society of Heating, Refrigerating and Air-Conditioning Engineers, Inc. (2009)
55. Taylor BN, Kuyatt CE (1994) Guidelines for evaluating and expressing the uncertainty of NIST measurement results. NIST Technical Note 1297 (1994), Physics Laboratory, National Institute of Standards and Technology, Gaithersburg, MD 20899–0001
56. <https://www.yourhome.gov.au/energy#:~:text=The%20average%20Australian%20home%20is. greenhouse%20gas%20emissions%20each%20year>. Accessed 11 May 2021



**Norma Patricia López-Acosta, David Francisco Barba-Galdámez,
and Kitzia Judith Arizmendi-López**

Abstract Energy geostructures are a special type of closed Ground Source Heat Pump (GSHP) system in which heat exchange pipes are installed in the foundation elements (e.g., piles, walls) to extract or inject thermal energy from/to the ground. Due to its dual function and high-energy efficiency, this technology is an alternative to reduce the environmental impact of the growing energy demand for space conditioning while avoiding the high initial cost of traditional GSHP systems. This chapter summarizes the basic concepts of energy geostructures, with emphasis on energy piles, including heat transfer mechanism, site investigations procedures, thermal and mechanical analysis approaches. Additionally, the chapter discusses the most recent design considerations and some construction recommendations.

Keywords Energy piles · Thermal analysis · Mechanical behavior · Construction recommendations

1 Introduction

Energy consumption for air conditioning in residential and commercial buildings has increased in recent years. This growing demand has a serious impact on the environment, largely due to the use of low-performance conventional heating and cooling systems that work with electricity generated primarily from fossil fuels [1]. Among the most promising techniques in the field of renewable energies to solve this problem are Ground Source Heat Pumps systems (GSHPs), which use electricity to transfer heat from the subsoil to the building. This process is carried out through a cyclic system that includes three components: (a) primary (heat exchanger with the ground), (b) secondary (heat exchanger with the conditioned space), and (c) heat pump. By using a sustainable energy source (shallow geothermal energy), Ground Source Heat Pumps help reduce energy consumption and maintenance costs

N. P. López-Acosta (✉) · D. F. Barba-Galdámez · K. J. Arizmendi-López
Instituto de Ingeniería, Universidad Nacional Autónoma de México, Circuito Escolar CU,
Coyoacán 04510, Ciudad de México, México
e-mail: nlopeza@iingen.unam.mx

of heating–cooling systems. Despite the various advantages that this technology provides, its use has been limited due to its high initial costs [2].

In this context, energy geostructures (geotechnical structures used as heat exchangers) emerge as a valuable alternative, especially the so-called energy piles. These consist of foundation elements coupled with a heat exchanger and function as the primary system of the GSHP. Thus, by using elements initially required for structural and geotechnical reasons, the costs associated with traditional systems are reduced.

Despite being a relatively new technology, energy geostructures have already been implemented in several countries. The Laizer Tunnel and the Uniqa Tower in Vienna (Austria), the Dock Midfield terminal at Zurich Airport (Switzerland), Norddeutsche Landesbank Hannover and the Berlin School Center (Germany), Lambeth College (UK), Stockton College (USA), and Sapporo City University (Japan) are some applications of energy piles in the world. In addition to the above countries, Scotland, Canada, Italy, the Netherlands, Belgium, France, Poland, Sweden, Norway, Denmark, Australia, Hong Kong, China, South Korea, and Mexico are at an early stage of the development of this technology [3].

This chapter presents an overview of the state of the art of Energy Geostructures with an emphasis on energy piles. The types of heat exchangers, the heat transfer mechanisms, and the effects of temperature changes on the thermo-mechanical behavior of soil and energy piles are detailed. In addition, the various factors that govern the design of these systems are presented, along with their main assumptions and some recommendations.

2 Energy Pile Fundamentals

2.1 Ground Source Heat Pump Systems (GSHPs)

Ground Source Heat Pump (GSHP) systems are heating or cooling systems that utilize the thermal gradient between the ground and the environment to heat or cool buildings and facilities by coupling Ground Heat Exchangers (GHEs). In general, GSHPs can be installed in most geological conditions (except for areas where groundwater is protected), making them one of the most promising technologies in the field of renewable energies for building conditioning [1].

Geothermal heat pumps consist of three main components: (1) primary circuit, (2) secondary circuit, and (3) heat pump. The primary circuit consists of a closed system of pipes installed inside elements in contact with the ground. A heat-conducting fluid is pumped through these pipes to allow energy exchange with the soil. The secondary circuit is a closed network of heating pipes embedded in the floors and walls of the structure [4]. Both circuits are connected through a heat pump that is responsible for raising (in the case of heating) the temperature extracted from the ground to a usable level for the building (usually from 10–15 °C to 25–35 °C) from the supply of a small amount of electrical energy [5].

2.2 *Types of Ground Heat Exchangers (GHEs)*

According to its principle of operation, a GSHP is simply a heat pump that transfers heat between building interiors and the ground. Thus, in winter GSHPs extract thermal energy from the ground and transfers it to the building interior, while in summer, they take heat from the interior and inject it into the ground [6]. There are different types of GHEs to extract/inject thermal energy from/into the ground: open-loop systems and closed-loop systems. In open systems, groundwater is used as a heat carrier and is pumped directly from the source (aquifer or river) to the heat pump. Its main limitations are the high maintenance costs and the likelihood of groundwater contamination [7]. In closed systems, the heat transfer between the building and the ground is carried out indirectly from a closed pipe circuit. According to De Moel et al. [8], these systems are more versatile and economically more cost-effective in the long term. In addition, they can be installed in most geological conditions.

2.2.1 **Open-Loop Systems**

Open systems are characterized by the fact that groundwater, which flows freely in the subsoil, functions as a source and heat exchanger. In general, two boreholes are drilled, one for groundwater extraction and one for subsequent re-injection. In heating mode, water is pumped from the groundwater well to transmit thermal energy to the building. The heat is then distributed through the secondary circuit. The extraction of energy causes the water to decrease in temperature. Finally, the heat carrier fluid is injected back into the source through the secondary well.

According to Sanner [9], this type of system is recommended in high permeability soils with an adequate chemical quality of groundwater. In fact, in these systems, problems are often associated with corrosion and clogging of pipes due to the deposition of dissolved minerals in the water [10]. Therefore, it is important to look for catchment areas with low iron content.

2.2.2 **Closed-Loop Systems**

Closed systems use pipes installed inside elements in contact with the ground through which a heat carrier fluid (water, mixtures of water and antifreeze, or saline solutions) is pumped to allow energy exchange with the ground. These systems are divided into two categories: horizontal and vertical.

In horizontal systems, the pipes are laid in a trench at a depth of about 1–2 m. In this case, the thermal recharge provided by solar radiation is transferred to the heat carrier fluid circulating through the pipes. Therefore, it is important not to cover the surface above the heat collector [11]. Generally, the pipes are of high-density polyethylene (HDPE), and their diameter varies from 25 to 40 mm. The pipe arrangement is variable. Some installation alternatives are the slinky and straight

type, connected in series or in parallel. Parallel connections are the most common, as they use smaller volumes of heat transfer fluid and consume less pumping energy [12]. However, series arrangements require fewer pipes. On the other hand, slinky type pipes are employed when higher pipe installation density is required due to land space limitations [13].

Vertical systems are used when the land area is limited or when the surface is rocky. The pipes are installed in a borehole with a diameter of 100–150 mm, and their depth usually varies between 50 and 150 m [11]. In this area the ground temperature is constant and approximately equal to the annual average temperature, which allows it to be a stable heat source to cover the energy demand. However, its implementation has been restricted due to its high drilling costs. An alternative to overcome this limitation is to incorporate the closed-loop system into the structural foundation elements.

Energy geostructures are a special type of closed system Geothermal Source Heat Pumps (GSHPs), in which the heat exchange pipes are installed in structural elements (piles, slabs, walls, etc.) [14]. Given their dual nature, they reduce installation and land use costs associated with traditional systems. The most common application of these systems are the so-called energy piles, i.e., piles that function as heat exchangers.

2.3 Heat Exchange Operation

In the heat exchange process, the main objective of GHEs is to use the ground as a heat source or sink. Thus, GHEs can be operated in two ways [15]:

- **Pure injection/extraction:** In these systems, the heat flow is unidirectional (extraction during winter or injection in summer), allowing the soil to return to its initial thermal condition when conditioning is not required. According to Brandl [5], this type of system is recommended in soils of high permeability in the presence of water flow with high hydraulic gradients.
- **Seasonal heat storage:** These systems induce annual cyclical variations in ground temperature, creating a thermal equilibrium during a complete heating–cooling period. Consequently, they are the most sustainable and economically profitable mechanisms. Their application is facilitated in saturated soils with low permeability in the presence of water flow with low hydraulic gradients.

2.4 Energy Pile Materials and Configurations

Energy piles fulfill a structural function, while allowing the use of surface geothermal energy in accordance with the requirements of the buildings. These objectives must be taken into account during the selection of materials, since they directly influence

the thermo-mechanical behavior and the energy efficiency of the pile. Moreover, the operation principle of these structures is different from that of conventional GHE since they have shorter lengths.

Among the most used materials for the construction of energy piles are the following: reinforced concrete, steel, and grout [8]. The favorable thermal characteristics of concrete (high thermal conductivity and heat capacity) allow improving the thermal productivity of heat exchange systems [7]. Therefore, concrete energy piles are the most widely used elements in the world [5]. In contrast, steel piles have not gained as much interest from researchers. Recently, Lee et al. [2] proposed a novel method of energy piles equipped with steel pipes that function as heat exchangers and main reinforcements. The results of their research show that piles with steel pipes have better thermal performance than piles with HDPE pipes.

The pipe arrangement within the energy piles plays an important role in the thermal behavior of the system. The most common configurations for the primary circuit piping are (Fig. 1): U single, double, triple or W-type, the latter being the ones that can dissipate more heat. However, a U-type arrangement offers better workability and economic efficiency. Usually, U-pipes are of high-density polyethylene (HDPE) or cross-linked polyethylene (PEX). These pipes are typically $\frac{3}{4}$ or 1 inch (27 or 34 mm) in diameter [16]. Double or triple arrangements are employed to improve heat transfer efficiency by increasing the number of pipes. Nevertheless, it is necessary to consider the installation of separators to avoid thermal interactions between them [17]. Currently, the application of helix (or spiral) pipes is gaining considerable popularity. According to Park et al. [18], from an economic and heat exchange efficiency point of view the helix configuration is preferable. In addition, reducing the pitch of the spiral can improve heat transfer. It is recommended to avoid using a pitch less than 250 mm due to excessive pressure drops and less pronounced heat transfer enhancement [19].

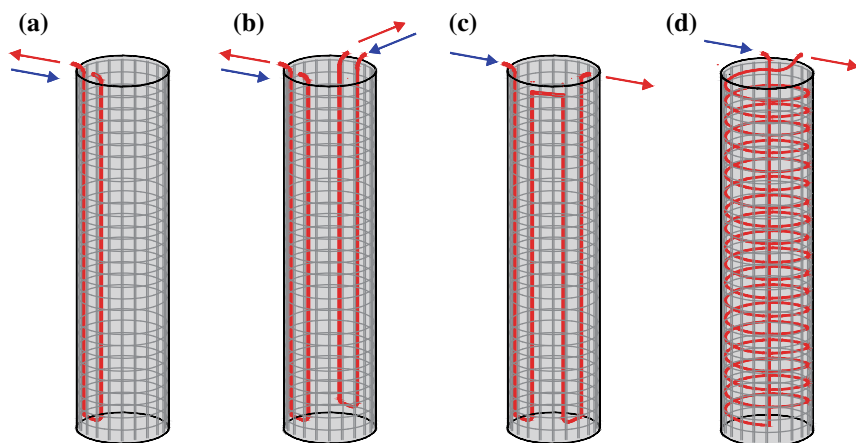


Fig. 1 Different arrangements of heat exchanger pipes: **a** U single, **b** U double, **c** W-type and, **d** Helix

Table 1 Benefits of the use of energy geostructures (adapted from [8])

Benefit	Description
Economic	In the long term, it reduces the costs of air conditioning systems compared to conventional systems, with payback periods of 5–10 years depending on the type of soil, its properties, and the prices of other energy sources (natural gas, oil, coal, etc.)
Energetic	Due to its high COP values, it decreases electricity demand
Technological	It can be installed in most geological conditions and its implementation is not restricted to urban areas
Environmental	It reduces greenhouse gas emissions by avoiding the consumption of fossil fuels and using a clean, renewable energy source
Social	It reduces noise (due to the absence of fans) and provides greater safety (since it does not require the use of explosive gases for its operation) with respect to other air conditioning systems

2.5 Benefits and Limitations

The benefits of implementing energy geostructures are diverse and include economic, energy, technological, environmental, and social aspects. These are summarized in Table 1.

Like any other technology, energy geostructures present some limitations and disadvantages. De Moel et al. [8] mention their high initial cost, the possible generation of thermal imbalances in the soil due to excessive heat extraction or injection, and the current limitations in the analysis and design methods. Finally, it is important to emphasize that, in the case of energy piles, the installation of energy absorption systems does not generate limitations with respect to the length of the element. On the contrary, their energy potential increases with depth. For economic reasons, a minimum length of 6 m is recommended [4].

2.6 Applications and Developments

Energy geostructures play an important role in several countries to meet the growing demand for space conditioning, including Austria, Germany, Switzerland, United Kingdom, Japan, and China [20]. One of the largest projects in Austria is the LT24 lot of the Lainzer Tunnel, which uses energy piles installed in its side walls. The system consists of 59 energy piles with a diameter of 1.2 m and an average length of 17.1 m. The elements are equipped with absorber pipes connected to collection pipes, which lead to six heat pump units that supply the heating demand of an adjacent school building [21].

Two major projects in Switzerland have employed energy piles, the Dock Midfield terminal at Zurich airport and the Swiss Technological Convention Center at the Swiss Federal Institute of Technology in Lausanne. The foundation system of the

Dock Midfield airport consists of 440 piles, of which 300 were equipped as energy piles. Thus, 85% of the annual heating demand is covered by the heat pump, while the cooling demand is supplied by a combination of energy piles and a conventional cooling system [22]. Moreover, the Lausanne project has been used for various investigations related to the effects of temperature on the mechanical response of the structure and the thermo-hydraulic behavior of the surrounding soil [23, 24].

In recent years, several buildings have been equipped with energy piles in Germany as the Norddeutsche Landesbank in Hannover, the Main Tower and Galileo buildings in Frankfurt, and the International Solar Center in Berlin. The Main Tower is a 200 m high building and is founded on 213 piles, 112 of which function as energy piles [23]. The foundation of the Berlin International Solar Center consists of 200 energy piles that supply 15% of the heating demand and 100% of the cooling demand with a seasonal heat storage system [25].

In the United Kingdom, some projects that have employed energy piles such as Keble College, One New Change, and Lambeth College. The Keble College building in Oxford was the first structure equipped with energy piles in the UK [26]. It was built in 2001 and has operated smoothly ever since. At Lambeth College, a total of 146 energy piles were installed at 25 m depth to supply a five-story building. Bourne-Webb et al. [27] analyzed the impact of heating and cooling cycles on the pile performance, as well as the thermodynamic response of the system.

3 Thermal Behavior of Energy Piles

3.1 General Principles

Heat transfer between energy piles and their surroundings is time-dependent. Such behavior is a consequence of a variation in the conditions surrounding the system and lasts until a steady state temperature distribution is reached [28]. In this context, it is important to analyze the transient heat transfer to determine the impact of this phenomenon on the performance of energy piles. The fundamental approach for evaluating heat transfer as a function of time is to simulate the temperature distribution in bodies and their surroundings as a transient process. Therefore, several analytical and numerical methods have been developed to represent the complex interactions that take place during this process.

The main advantage of analytical methods is that they facilitate the calculation process, since they assume simple heat exchange conditions. On the other hand, numerical methods require more computational resources and execution time. However, their results have a high degree of accuracy.

3.2 Heat Transfer Within Energy Piles

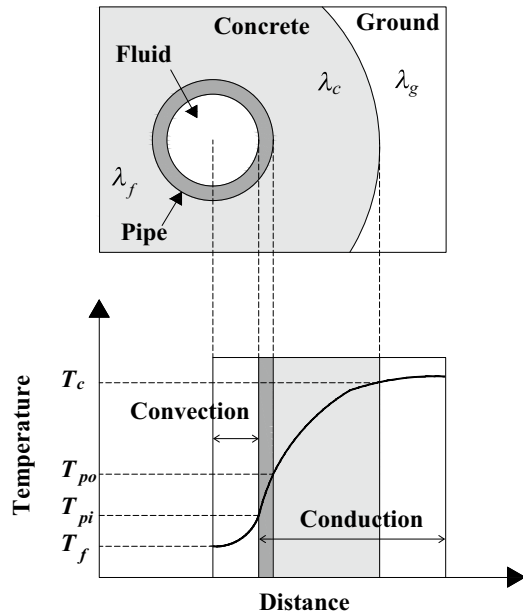
As in saturated soils, the two main heat transfer mechanisms observed in energy piles are convection and conduction. Heat conduction is the process in which thermal energy is transmitted from one region of a medium to another, due to the interaction between molecules [5]. Whereas convection occurs between thermodynamic systems that move relatively to each other, commonly fluids. Convection can be divided into two types: diffusion and advection (mass movement of fluids).

Abdelaziz et al. [29] describe the transfer process in energy piles as follows: (a) convection between the fluid and the inner walls of the conduction pipes, (b) conduction through the pipes, (c) conduction through the concrete of the piles, and (d) conduction and convection (if any) in the soil. In general, conduction is the dominant process in the soil. However, if groundwater flow is present, advection may also be important [30]. Figure 2 illustrates the heat transfer mechanism described above. In this figure λ_f , λ_c and λ_g represent the thermal conductivity of the pipe, concrete, and soil, respectively, while T_f , T_c , T_{pi} , T_{po} are the temperature of the fluid, the concrete-soil contact, the inner and outer wall of the pipe, respectively.

The mathematical equation describing the convection process is based on Newton's law of cooling:

$$\frac{Q}{A} = h(T_{pi} - T_f) \quad (1)$$

Fig. 2 Mechanism of heat transfer in energy piles (adapted from [14])



where Q is the heat transfer rate, A is the area, h is the heat transfer coefficient and $(T_{pi} - T_f)$ is the temperature difference across the convection surface. In steady conditions, Fourier's law describes the relationship between the rate of heat transfer and the temperature profile as [14]:

$$\frac{Q}{A} = -\lambda \frac{\Delta T}{L} \quad (2)$$

where λ is the thermal conductivity, L is the length and ΔT the temperature difference. In heat transfer analysis, the soil response is usually assumed to be in a transient state. Under these conditions, the heat transfer depends on the thermal diffusivity (α), the geometry, and the rate at which temperature changes. Therefore, the transient conduction is expressed as:

$$\frac{dT}{dt} = \alpha \frac{d^2T}{dx^2} \quad (3)$$

where $\alpha = \frac{\lambda}{c_s \rho}$, c_s is the specific heat capacity, ρ is the soil density, and $\frac{d^2T}{dx^2}$ is the temperature Laplacian.

3.3 Thermal Analysis of Energy Piles

3.3.1 Scale Analysis

In the study of energy piles, it is important to address the full spectrum of temporal and spatial scales that occur during heat transfer, since most analytical solutions are based on the temporal characteristics of the thermal process. Space scales are necessary to evaluate thermal interactions between adjacent energy piles. Temporal scales are used to evaluate changes in soil loads during system operation, they indicate the time in which the system reaches steady conditions.

According to Li and Lai [31], four spatial and eight temporal scales are present in the thermal process, which mainly depend on the thermal properties of the soil. The first spatial scale is related to the energy pile diameter r_b , and the time in which it develops ($t_b \sim r_b^2 / \alpha_b$) is on the order of hours to a few days, during which the effect of the heat capacity of the backfill material is significant. The second scale corresponds to the mean distance between two adjacent energy piles (L) and its time scale ($t_L \sim L^2 / \alpha_s$) is on the order of a month, during which the thermal interaction between adjacent energy piles is significant. The largest space scale comprises the site where the borehole system is installed in the horizontal direction and the distance where significant thermal interaction occurs in the vertical direction. A length of $H/2$ is considered, where H is the length of the energy pile. The associated time ($t_H \sim H^2 / 4\alpha_s$) is as long as the lifetime of the energy pile. There is another important

time scale ($t_r \sim H/u$) called residence time which usually lasts for several minutes and represents the time in which the heat capacity of the fluid must be addressed [31].

3.3.2 Idealizations and General Assumptions

To simulate the time-dependent heat transfer that characterizes energy piles, it is necessary to make some assumptions to simplify the calculation process. The main criteria are described below [28, 32]:

- The ground is considered to have a finite or semi-infinite extent, depending on whether or not the influence of the surface is considered.
- The ground has a uniform initial temperature in any modeled domain.
- The boundary conditions for the wall of the energy pile or the heat transfer pipe are either a constant flux or a constant temperature.
- When considering the effect of groundwater flow, a homogeneous flow with parallel streamlines to the surface is assumed.
- The ground can be treated as a medium with an equivalent thermal conductivity, $\lambda_{g,e}$.

3.3.3 Analytical Models

Conventional analytical models consider the temperature inside the heat exchanger to be in a steady state, which allows the heat flow around the pipes to be calculated using a constant resistance. Generally, this assumption is applied in the design of borehole heat exchangers. However, piles have larger diameters and differences in thermal properties between the pile and the surrounding soil must be taken into account when analyzing heat transfer. The thermal conductivity and heat capacity values of concrete, soil, and plastic are different. Therefore, the heat flow rate is not constant [33].

The problem of time-dependent heat transfer by GHEs can be expressed as [32]:

$$q_l = \frac{T_f(t) - T_g}{R(t)} = \frac{\Delta T}{R(t)} \quad (4)$$

where q_l is the heat transfer rate of the GHE per unit length, T_f is the average temperature of the circulating fluid, T_g is the effective undisturbed temperature of the ground, and R is the total thermal resistance. The thermal resistance considered is usually decomposed into a time-independent and a time-dependent part as:

$$R(t) = R_s + G(x, t) \quad (5)$$

where R_s is the time-independent part of the thermal resistance R , and $G(x, t)$ is the time-dependent part usually referred to as g -function (with x the coordinates of a considered point and t the time). Based on Eqs. 4 and 5, the temperature change

(ΔT) can be calculated as:

$$\Delta T = q_l R(t) = q_l [R_s + G(x, t)] \quad (6)$$

To determine the average temperature of the ground loops considered in the above equations, T_f is assumed to be approximately equal to the average of the inlet and outlet temperatures of the heat transfer fluid [34]. Thus, the inlet ($T_{f,i}$) and outlet ($T_{f,o}$) temperatures can be obtained as:

$$T_{f,i}(t) = T_f(t) + \frac{q_l H}{2\rho_f c_f V_f} \quad (7)$$

$$T_{f,o}(t) = T_f(t) - \frac{q_l H}{2\rho_f c_f V_f} \quad (8)$$

In general, heat transfer analysis consists of first determining G and R_s . Based on these data, the temperatures T_f , $T_{f,i}$, and $T_{f,o}$ can be calculated. These values and the flow rate represent the limits for the geothermal heat exchanger models.

According to Loveridge [35], heat transfer in concrete should be assumed to be a transient process. Loveridge and Powrie [14] developed models that consider transient heat storage within the pile, different time scales, and piping arrangements. In these correlations, the temperature response of the surrounding soil is time-dependent and is represented by pile g -function and the behavior of the pile itself is simulated by another concrete g -function [17]. Thus, the overall temperature response function of a heat exchanger can be expressed as:

$$\Delta T = q_l R_p + q_l R_c G_c + \frac{q_l}{2\pi \lambda_g} G_g \quad (9)$$

where q_l is the heat transfer rate per meter length of the energy pile, R_p is the thermal resistance of the pipes (including the fluid), R_c is the thermal resistance of the concrete, G_c is the concrete g -function describing the transient concrete response, and G_g is the pile g -function for the transient response of the ground surrounding the energy piles. Table 2 presents the most used analytical models for thermal analysis of GHE. These methods allow defining g -functions to calculate the time-dependent heat transfer around the bodies.

3.3.4 Duhamel's Theorem

Duhamel's theorem or superposition principle is used to find the solution to heat conduction problems over time [36, 40], as the heat transfer rate varies continuously depending on the heating or cooling demand of the building. According to Duhamel's theorem, time-varying load problems can be studied relatively easily using the solution to the problem for a unit-step load [36]:

Table 2 Analytical models for thermal analysis of heat exchangers (adapted from [31])

Analytical model	Comments
Infinite line source model [36]: $G(t, r_b) = \frac{1}{4\pi\lambda_g} \int_{r_b}^{\infty} \frac{\exp(-u)}{u} du = \frac{1}{4\pi\lambda_g} E_1\left(\frac{r_b^2}{4\alpha_g t}\right)$	<ul style="list-style-type: none">• 1-D thermal analysis• It does not simulate the thermal process inside the pile• Not recommended for analyses involving short to medium time scales
Finite line source model [37]: $G(t, r_b) = \frac{1}{4\pi\lambda_g} \int_0^H \left[\frac{\operatorname{erfc}\left(\frac{\sqrt{r_b^2 + (z-z')^2}}{2\sqrt{\alpha_g t}}\right)}{\sqrt{r_b^2 + (z-z')^2}} - \frac{\operatorname{erfc}\left(\frac{\sqrt{\frac{r_b^2}{4} + (z-z')^2}}{2\sqrt{\alpha_g t}}\right)}{\sqrt{\frac{r_b^2}{4} + (z-z')^2}} \right] dz'$	<ul style="list-style-type: none">• 2-D thermal analysis for periods longer than one year• Considers thermal interaction between adjacent boreholes• Considers finite pile length• It is suitable for predicting long-term responses• The influence of the ground surface is considered
Infinite cylindrical surface source model [38]: $G(t, r_b) = \frac{1}{\pi^2 r_b \lambda_g} \int_0^{\infty} \left(e^{-\alpha_g u^2 t} \right) \frac{J_0(ur_b) Y_1(ur_b) - Y_0(ur_b) J_1(ur_b)}{u^2 [J_1^2(ur_b) + Y_1^2(ur_b)]} du$	<ul style="list-style-type: none">• 1-D thermal analysis• Considers the radial dimension of the heat exchanger• Does not simulate the thermal process inside the pile
Infinite moving line-source model [39]: $G(t, r_b) = \frac{1}{4\pi\lambda_g} I_0\left(\frac{U r_b}{2\alpha_g}\right) \int_0^{\frac{r_b^2}{4\alpha_g t}} \frac{1}{\eta} \exp\left(-\frac{1}{\eta} - \frac{U^2 r_b^2 \eta}{16\alpha_g^2}\right) d\eta$	<ul style="list-style-type: none">• It considers the effect of the characteristic groundwater velocity (U) on the response of the GHEs

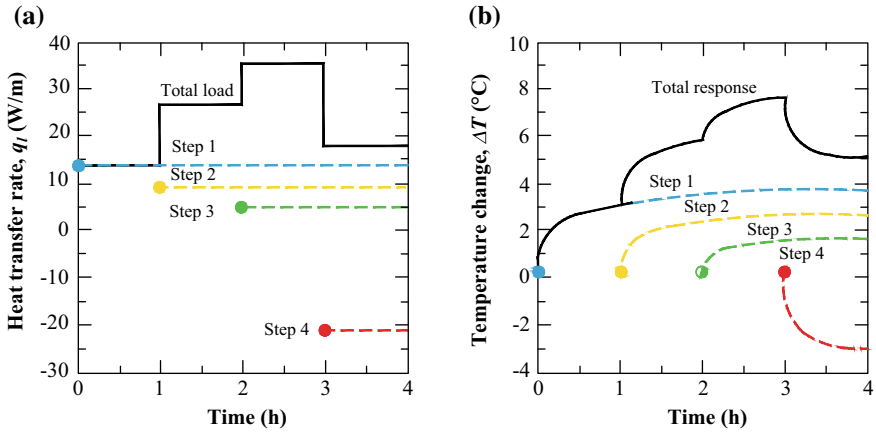


Fig. 3 **a** Hourly loads represented as step functions and **b** Individual responses to step pulses superimposed to give temperature response (adapted from [28])

$$T_1(x, t) = T_g + \int_0^t q_l(\tau) \frac{\partial G(x, t - \tau)}{\partial t} d\tau \quad (10)$$

where T_1 is the temperature at the point under consideration x , $q_l(t)$ is the time-dependent function of the heat exchange rate of an energy pile, and τ is a variable of integration with time dimensions. The function G represents the response function for the unit step change in the thermal load of the energy pile. Duhamel's theorem considers that the heating and cooling loads can be decomposed into constant-valued step pulses, resulting in the total load profile (Fig. 3). The mathematical equation describing such behavior is [40]:

$$T_1(x, t) = T_g + \sum_{j=0}^{N-1} \Delta q_j G(x, t - j \Delta t) \quad (11)$$

where $\Delta q_j = q_{j+1} - q_j$ is the stepwise change in q_l at the beginning of the $(j + 1)$ -th time interval. The Eqs. 10 and 11 imply that the temperature response of any time-varying thermal load q_l is easily determined once the g -function for the step load response is available [32].

3.3.5 Numerical Models

Numerical modeling is the most advanced tool for the study of energy geostructures. These methods allow the simulation of the effects of freezing and thawing on the soil, the components of energy geostructures, the variability of temperature changes, and

the soil nonlinearity under different thermal conditions. Therefore, they are becoming more cost-effective and widely used tools to solve differential governing equations with different boundary conditions [17]. The main models for thermal analysis of heat exchangers are the finite difference method, the finite volume method, and the finite element method.

Numerical models are impractical for engineering applications for three main reasons: they require more computational resources, long execution time, and skilled personnel are needed to implement them. Furthermore, due to the large variety of lengths and time scales that need to be dealt with heat transfer, these methods are often not feasible for designing energy geostructures [41]. Consequently, their use has been restricted to research projects. Thus, there are relatively few published studies in which this procedure is used [42–47], most of which have shown promise but are not used as design tools yet.

4 Mechanical Behavior of Energy Piles

The thermo-mechanical response of energy piles was first described by Laloui et al. [48] and systematized by Bourne-Webb et al. [27, 49] and Amatya et al. [50]. Experimental data in thermo-mechanical loading tests on energy piles show that, when subjected to heating and cooling cycles, the piles expand and contract around a null point. In this case, the null point is defined as the point where the pile does not experience relative displacement to the ground during the application of thermal loads.

The location of the null point depends on the stiffness of the boundaries (provided by the superstructure at the head and the presence of a stiff soil layer at the toe) and the friction mobilized at the shaft [51]. Thus, being partially restrained, the pile experiences axial strains smaller than the free-body condition (ε_L), the largest located at its ends, reducing towards the null point.

In the case of free bodies, the free thermal axial strain ε_L is proportional to the coefficient of thermal expansion of the material α_{exp} (1/K) and the temperature change ΔT :

$$\varepsilon_L = \alpha_{exp} \cdot \Delta T \quad (12)$$

For partially restrained bodies, the blocked axial strain ε_r is defined as the difference between the free axial strain ε_L and the observed strain ε_o .

$$\varepsilon_r = \varepsilon_L - \varepsilon_o \quad (13)$$

By preventing the thermal strain, a stress σ_T is created, which is considered as an additional load to be evaluated in the design of the pile [20]. If the element is assumed to be a homogeneous and elastic material, the corresponding stress (σ_T) and thermal load (P_T) can be obtained from Young's modulus of the material E_m and

the cross-sectional area of the pile A [50]:

$$P_T = -E_m A \varepsilon_r = \sigma_T A \quad (14)$$

In Eq. 14 the negative sign indicates that the interaction with the soil generates a force that restrains the strain of the pile [50]. Therefore, the total load in energy piles P_{total} is the sum of the mechanical load P_M and the thermal load P_T :

$$P_{total} = P_M + P_T \quad (15)$$

The magnitude and distribution of these loads depend on the surrounding soil and the strain restraints that add up at the pile head and toe. An alternative option to evaluate the thermal stresses generated in energy piles is using the concept of the degree of freedom η , which is defined as the ratio between the observed axial unit strain ε_o and the free strain ε_L :

$$\eta = \frac{\varepsilon_o}{\varepsilon_L} \quad (16)$$

The value of η varies between zero (fully restrained pile) and one (free body). Based on this parameter, the blocked axial strain ε_r is determined as follows:

$$\varepsilon_r = (1 - \eta)\varepsilon_L = (1 - \eta)\alpha_{exp} \Delta T \quad (17)$$

Therefore, the thermal load can be calculated as follows:

$$P_T = -E_m A \varepsilon_r = -E_m A (1 - \eta) \alpha_{exp} \Delta T \quad (18)$$

Amatya et al. [50] proposed several simplified conceptual models depending on the type of end restraints, assuming that the mobilized shaft friction is constant and that the soil does not experience thermal expansion ($\alpha_{exp,g} = 0$). For unrestrained piles located in homogeneous soil, the model consists of:

- The pile head load mobilizes the shaft friction, and the axial load decreases linearly with depth (Fig. 4a).
- During the cooling cycles, the pile contracts, generating tensile stresses (Fig. 4b). The thermal and mechanical stresses mobilized have the same direction above the null point and the opposite direction below it. Thus, depending on the magnitude of the temperature change and the level of restraint imposed by the soil, tensile forces can be generated at the bottom of the pile.
- During the heating cycles, the pile expands, generating compressive stresses (Fig. 4c). The direction of the thermal and mechanical stresses mobilized is opposite to that described in the previous point. In this case, significant increases in the compressive strength of the element may occur.

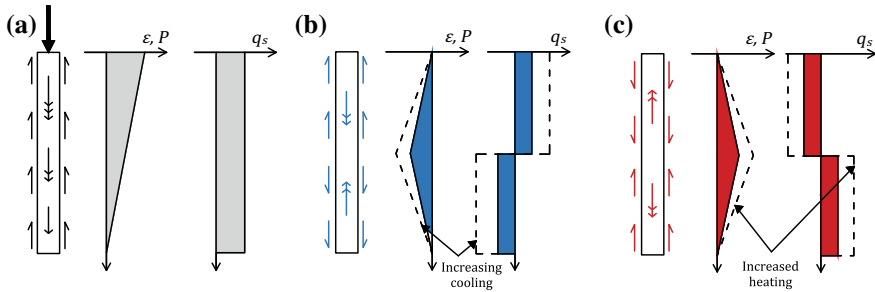


Fig. 4 Mechanism of response of a pile to thermal loads: **b** cooling cycle and **c** heating cycle (ϵ : axial strain in the pile; P : axial load in the pile; q_s : shaft friction) (adapted from [50])

5 Design of Energy Piles

5.1 General Considerations

Due to their dual function (as a foundation element and heat exchanger), the design of energy piles requires the interaction of thermal, geotechnical, and structural analyses [52]. In geotechnical and structural designs, it is necessary to verify the behavior under serviceability and ultimate conditions. The serviceability conditions are associated with the adequate performance of the structure, while the ultimate conditions imply the system collapse.

From a thermal perspective, the design involves estimating the amount of energy the system can exchange with the surrounding soil to satisfy the thermal loads of the building fully or partially [53, 54]. Thus, the information required for thermal design is the geometry of the piles (dimensions, loop characteristics, separation/spatial distribution), the thermal properties of the materials, the operating conditions of the system, the distribution of the thermal loads, and the characterization of the groundwater flow in the study area.

The main characteristics of the structure (e.g., the length and separation of the energy piles) depend on the structural and geotechnical designs of the foundation. Therefore, a 100% supply of the required heating and cooling energy cannot be guaranteed. Instead, auxiliary systems must be used to fulfill the energy demand (a hybrid system). To accurately determine the maximum thermal energy that the geothermal system can provide using the already structurally designed energy piles is challenging, considering that the limited existing design approaches can be time-consuming or not as reliable as required [53].

5.2 *Current Standards*

Currently, no country has included energy geostructures in its geotechnical standards or design codes. In response to this, various industries and professional organizations in Europe have developed guidelines or general criteria for the design and installation of such systems, especially for energy piles [55]. Among these are:

- **VDI 4640 Part 2** [56]. German guideline for the design and installation of geothermal heat pumps. It does not provide further details on energy geostructures and merely suggests that energy piles can be studied as borehole heat exchangers.
- **SIA D0190** [57]. Swiss Guideline for the design, construction, and maintenance of thermoactive structures. It provides specific information on construction details (pipe arrangement, materials, etc.) and design considerations such as additional loads and differential settlement effects.
- **Ground Source Heat Pump Association** [58]. Guide published in the UK that gives recommendations for the design, installation, and selection of materials for energy piles. The guide discusses the roles and responsibilities of the various parties involved in this type of project and the fundamental thermal and geotechnical aspects of energy pile analysis.

In addition, The French National Research Agency (ANR) proposed a set of recommendations presenting theoretical references and case studies for the design, construction, and application of energy geostructures. This design methodology is based on the French design standard and the Eurocode for the evaluation of ultimate and serviceability limit states [59].

5.3 *Thermal Design*

As mentioned in Sect. 3, traditionally the thermal design of energy piles is based on the concepts applied to GHEs. In this context, the design methodologies are very similar from a thermal point of view and are described below.

5.3.1 *Methodologies Classification*

The design of the energy piles can be determined directly or iteratively adjusted until it meets the user's specifications. The above will depend on the design methodology adopted [41]. Based on the time step used, the design methods can be classified on the following levels (the highest level corresponds to a higher level of resolution):

- **Level 0 (General Rules)**. They relate the length of the heat exchanger to the maximum heating/cooling loads of the building and the installed equipment capacity. Although this methodology is a practical way to design energy piles, its use can lead to inaccurate results. The above is mainly related to the fact that the

time constant of the surrounding soil is usually on the order of years. Thus, the entering fluid temperature of the heat pump fluid increases/decreases with time and is not related to peak loads but to annual loads. The only conditions under which this method can work are when there is a strong relationship between peak loads and annual loads, or reasonably constant soil thermal properties between locations for which the rule of thumb is applied.

- Level 1 (Two pulses). This method uses a single design period for the heating season and another for the cooling season [60]. Its duration must be determined by the designer.
- Level 2 (Six pulses). In this solution, three pulses are used for heating and three for cooling: an annual pulse, a monthly pulse and a peak pulse of duration defined by the designer [61].
- Level 3 (Monthly and monthly peak pulses). Represents the loads as total monthly cooling and heating loads, to which the monthly peak thermal loads are superimposed. The monthly peak loads are represented as a rectangular pulse with the magnitude and duration.
- Level 4 (Hourly simulation). In this method, the GHE is sized by means of an iterative hourly simulation [62].

To study the heat transfer process, these methodologies use analytical solutions such as Infinite line source model, Infinite cylindrical surface source model, Finite line source model, and *g*-functions (Table 2). Their choice depends on the loads, the borehole/energy pile configuration, and the system being analyzed. Here, the use of uniform heat flow when calculating *g*-functions tends to overestimate the dimensions of the energy pile, whereas assuming uniform pile wall temperature results in smaller dimensions.

In the case of energy piles, it is convenient to analyze heat transfer using thermal resistances or quasi-resistance values. For example, heat transfer between the heat carrier fluid in the pipes and the borehole/energy pile wall usually approaches a quasi-steady-state condition. The calculation of borehole/energy pile thermal resistance includes shape factors and multipole methods. A detailed summary of these can be found in Javed and Spitler [63]. Recently, Claesson and Javed [64] have proposed the first analytical method specifically design to calculate the thermal resistance of energy piles.

Generally, the behavior of the heat pump is considered as a polynomial model relating heat rejection to cooling and heat extraction to heating provided as a function of the temperature of the heat pump entering fluid [41]. Thus, the design explicitly takes into account the dependence between temperature and efficiency, as well as the imposed loads.

5.3.2 Input Parameters

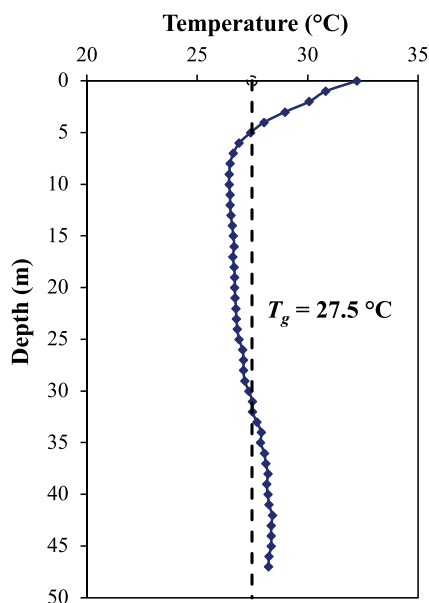
Undisturbed ground temperature

The undisturbed ground temperature (Fig. 5) is an important parameter as it determines the required size of the energy piles and the temperature limits needed for system operation. The size of the element is usually inversely proportional to the difference between the ground temperature and the maximum or minimum temperature of the inlet fluid [41].

Ground thermal properties

Thermal properties influence the energy distribution through the soil, the heat extraction capacity of the structure, and the type of system to implement. Thus, the initial step in designing an energy pile is to define the thermal parameters of the study site through laboratory or field tests. Because conduction is the predominant mechanism for heat transfer within the ground, the main soil thermal properties to determine are the thermal conductivity (λ) and specific heat capacity (c_s) (Fig. 6). Although the most reliable method for determining this information is based on the results obtained from an in-situ test called Thermal Response Test (TRT), this method can be costly and time consuming. Therefore, laboratory techniques are preferred for small projects. More details are explained in Sect. 6.3 of this chapter.

Fig. 5 Soil temperature variation with depth, Puerto Vallarta, Jalisco (Mexico)



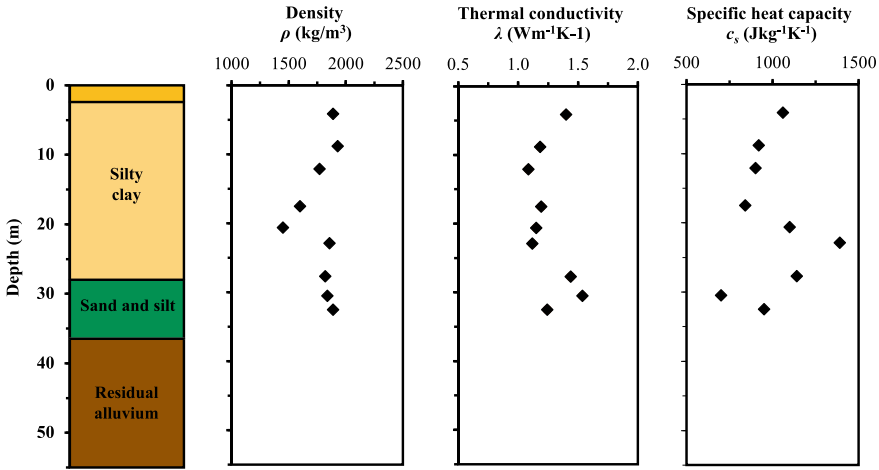


Fig. 6 Stratigraphy and thermal properties of the soil, Puerto Vallarta, Jalisco (Mexico)

Temperature limits

In the design of energy piles, a minimum and/or maximum fluid temperature restriction is usually imposed. There are several factors to consider when choosing the temperature limits necessary to achieve optimum system efficiency. Kavanaugh [65] recommends that the upper temperature limit of the fluid entering the heat pump be equal to 11–19 °C above the undisturbed soil temperature and the lower limit equal to 6–8 °C below the undisturbed ground temperature. In addition, the specifications set by the heat pump manufacturer should be considered.

Loads: imbalanced or balanced

Thermal load distributions influence the amount of heat rejection/extraction from energy geostructures because the continuous use of systems with imbalance loads can affect the thermal conditions of the ground in the long term. For example, in cooling dominated climates, there may be more heat extracted than rejected. Figure 7 shows the thermal loads of a typical residential building located in Mexico City (Mexico). In this case, the maximum thermal load was estimated at 22.8 kW, with an annual average of 2.1 kW [54]. Since the thermal loads required by the building are exclusively for heating, the operation of the energy piles may cause long-term over-cooling of the ground. The above can be solved by increasing the element length or implementing a hybrid system.

5.3.3 Energy Pile Sizing

There are some standards and design manuals related to the sizing of energy piles. Standards usually include simplified data or rule of thumbs, whereas manuals propose

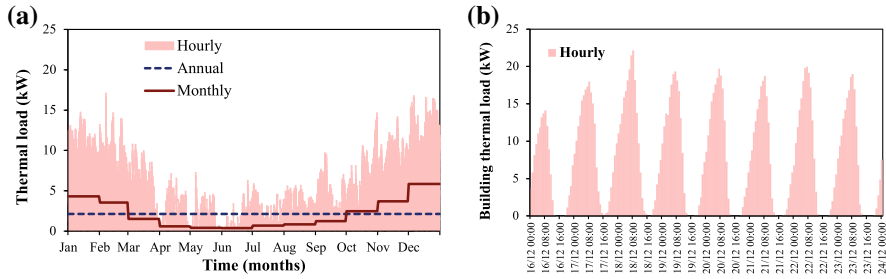


Fig. 7 Hourly thermal loads of the project *Residence C73* in Mexico City (Mexico) for: **a** one year of operation and **b** the week of December 16 to December 24

procedures that are more complex. In general, simplified methods are only recommended for small-scale projects, as they present some computational limitations. These methods have been implemented mainly in Austria, Germany, Switzerland, and the United Kingdom [66].

The International Ground Source Heat Pump Association (IGSHPA) [67] recommends following the American Society of Heating, Refrigerating and Air-Conditioning Engineers (ASHRAE) sizing manual as it is one of the simplest approaches to designing heat exchangers. This sizing method, originally proposed for borehole heat exchangers, estimates the total length of energy piles required to supply the thermal demand of a building. Kavanaugh and Rafferty [68] propose that the total pile length for heating (L_c) and cooling (L_h) be calculated as:

$$L_c = \frac{q_a R_{ga} + q_{m,c} R_{gm} + q_{h,c} R_{gd} + q_{h,c} R_b}{T_g - \frac{(T_{wi} + T_{wo})}{2} - T_p} \quad (19)$$

$$L_h = \frac{q_a R_{ga} + q_{m,h} R_{gm} + q_{h,h} R_{gd} + q_{h,h} R_b}{T_g - \frac{(T_{wi} + T_{wo})}{2} - T_p} \quad (20)$$

where q_a is the net annual average heat transfer to the ground, $q_{m,c}$ and $q_{m,h}$ are the average monthly ground loads during the design month in cooling and heating, $q_{h,c}$ and $q_{h,h}$ are the peak ground loads in cooling and heating, R_{ga} , R_{gm} , R_{gd} are the effective thermal resistances of the ground for the annual, monthly, and daily pulses, R_b is the resistance of the energy pile, T_g is the undisturbed ground temperature, T_{wi} , T_{wo} are the design heat pump inlet and outlet fluid temperatures, and T_p is the temperature penalty for the interference of adjacent boreholes/energy piles. ASHRAE [69] recommends that heat transfer be evaluated at worst ground load conditions, represented by three successive pulses of heat transfer with durations of 10 years, 1 month, and 4 h. The thermal resistances of the soil associated with these loads are calculated using the infinite cylindrical surface source model (Table 2) as:

$$R_{ga} = \frac{G_{(t_3-t_0)} + G_{(t_3-t_1)}}{2\pi\lambda_g} \quad (21)$$

$$R_{gm} = \frac{G_{(t_3-t_1)} + G_{(t_3-t_2)}}{2\pi\lambda_g} \quad (22)$$

$$R_{gd} = \frac{G_{(t_3-t_2)}}{2\pi\lambda_g} \quad (23)$$

where $G_{(ti-tj)}$ is the g -function evaluated for a period corresponding to $(t_i - t_j)$ where $t_0 = 0$ and λ_g is the effective ground thermal conductivity. The thermal resistance of the pile (R_b) can be estimated using the method proposed by Claesson and Javed [64]:

$$R_b = \frac{1}{N \cdot 2\pi\lambda_b} \cdot \left[\ln\left(\frac{r_b^b}{N \cdot r_p \cdot r_c^{N-1}}\right) + \sigma \cdot \ln\left(\frac{r_b^b}{N \cdot r_p \cdot r_c^{N-1}}\right) \right] \quad (24)$$

where N is the number of heat exchanger pipes, λ_b is the thermal conductivity of the energy pile, r_b is the radius of the pile, and r_p is the outer radius of the pipes.

When there is more than one pile, there is thermal interference between adjacent elements. To account for this effect, ASHRAE [69] proposes to include a temperature penalty (T_p) that calculates the amount of heat accumulated at the site using the infinite line source model.

5.4 Mechanical Performed-Based Design

Eurocodes divide the safety verification of conventional pile-based foundations into ultimate and serviceability limit states. The ultimate limit states are related to the structure's safety, whereas the serviceability limit states refer to its performance. Based on these considerations, Rotta-Loria et al. [70] developed a design methodology that integrates the effect of temperature changes on the mechanical response of energy piles. The main aspects of this procedure are described below.

5.4.1 Types of Actions and Design Intensities

Actions are classified according to their variation in time into three types: permanent G_k , variable Q_k , and accidental A . Permanent actions act continuously on the structures, and their intensity does not vary with time. On the other hand, accidental actions occur sporadically during short periods and usually have significant magnitudes. Variable actions affect structures with intensities that change significantly over time and have four typical values (Fig. 8) [71]:

- Characteristic value (Q_k). It represents the maximum intensity that will occur during the service life of the structure.

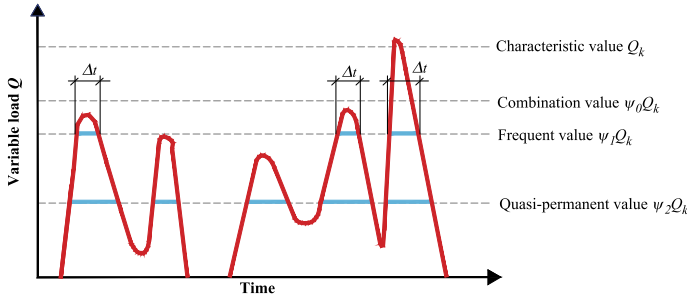


Fig. 8 Classification of variable actions according to their frequency (adapted from [71])

- Combination value ($\psi_0 Q_k$). It refers to the reduced probability that the most unfavorable values of the analyzed loads occur simultaneously.
- Frequent value ($\psi_1 Q_k$). It is applied to evaluate failure limit states, including accidental actions and reversible limit states (deflections).
- Quasi-permanent value ($\psi_2 Q_k$). It corresponds to the maximum probable value in the time span in which an accidental action or more than one variable action may occur.

Thermal loads applied to energy piles can be considered as variable, indirect, free, and static actions [70]. The above is based on the classification described in the Eurocodes for thermal actions applied to buildings and bridges.

5.4.2 Load and Combination Factors for Energy Pile Design

The effects of all actions must be affected by their respective load factor ($\gamma_{G,i}$ or $\gamma_{Q,i}$). This numerical value will depend on the situation being analyzed, as shown below:

- The unfavorable permanent loads are increased by 10% ($\gamma_G = 1.1$) and the favorable ones are reduced by 10% ($\gamma_G = 0.9$).
- A factor $\gamma_Q = 1.5$ corresponds to the unfavorable variable loads and the favorable ones are neglected $\gamma_Q = 0$.

The design of an energy pile requires defining the characteristic value of the expected temperature change in the structural element. Several methods have been proposed in the literature to calculate the representative temperature change based on thermal loads [72, 73]. The frequent and quasi-permanent values of the temperature change can be obtained from the characteristic value using the combination factors proposed by Rotta-Loria et al. [70]. For energy piles, the authors suggest the following values: $\psi_0 = 0.6$, $\psi_1 = 0.5$ and $\psi_2 = 0.5$.

5.4.3 Ultimate and Serviceability Limit States

Rotta-Loria et al. [70] recommend that the design of energy piles be performed with “Design approach 1—Combination 1”, which represents the worst-case condition proposed by the Eurocodes. Thus, in the review by the ultimate limit state, subjected only to permanent and variable loads, the following inequality must be satisfied:

$$\Sigma \gamma_{G,j} G_{k,j} + \gamma_{Q,1} Q_{k,1} + \Sigma \gamma_{Q,i} \psi_{0,i} Q_{k,i} < R_d \quad (25)$$

where $\gamma_{j,i}$ are the partial factors of the (j th and i th, respectively) actions or actions effects, $G_{k,j}$ represent the permanent loads, $Q_{k,1}$ is the dominant variable load, ψ_i are combination factors, $Q_{k,i}$ are the accompanying variable loads, and R_d is the design value of the resistance. For the serviceability limit state, the design effects of the E_d actions must be less than or equal to the corresponding limit value of this effect C_d :

$$E_d < C_d \quad (26)$$

6 Site Investigation for Energy Pile Design

6.1 Design Stages

The design of energy piles involves determining the amount of heating and cooling the system can supply to the building, besides ensuring that no limit state is exceeded for the effects of thermo-mechanical actions. Therefore, it is important to ensure that each design stage, which has a different process and level of detail, is met. In the planning stage, simplified methods are often used to estimate the energy output of the project. In contrast, in the conceptual design phase, extensive research is conducted on the thermal properties determined from the literature for use in energy analysis. Finally, during detailed design stage, in-situ tests are performed to obtain soil and concrete parameters in real field conditions [74].

The efficiency of the energy piles depends significantly on the system design parameters and thermal demand. In addition, the sensitivity of the geothermal system design to thermal properties is affected by the balance between heat and cooling demands [74]. In balanced systems, the influence of thermal properties on the heat exchange rate is minimal resulting in high efficiency over long-term is obtained. However, in unbalanced systems, where the thermal loads required by the building are exclusively heating or cooling, the heat exchange rate gradually decreases over time [75].

6.2 Design Parameters

The parameters required for the design of energy piles can be classified into two types: energy output and geotechnical (Table 3). The parameters for energy output include the thermal and hydraulic properties of the materials. For example, soil temperature influences the choice of pipe configuration. In cold climate regions (soil temperature of about 5 °C), it is more feasible to use systems with less length of heat exchange pipes, as the ground temperature will eventually drop below 0 °C [66]. Groundwater flow is also an important parameter because it can enhance heat transfer by thermal convection. However, seasonal systems are not recommended in the presence of groundwater flow due to heat energy dissemination resulting from flow effects [76].

For geotechnical and structural design, the parameters employed in conventional analyses such as strength, stiffness, and pore-water conditions are considered. In this case, the concrete coefficient of thermal expansion is also used to estimate the various variables that influence the interaction in energy pile groups [77].

6.3 Determination of Design Parameters

The main thermal properties of soil are the specific heat capacity c_s , thermal conductivity λ , and thermal diffusivity α . These are temperature dependent and can be estimated based on the different soil phase components [78–81]. The measurement of the thermal conductivity λ in soils and rocks can be performed with laboratory tests or in situ tests (Fig. 9). Laboratory tests allow obtaining specific values of the material thermal properties. Among the main advantages of these tests are their low costs, speed, and the possibility of controlling the boundary conditions of the soil [82]. However, they require the extraction, transport, and proper handling of undisturbed samples. On the other hand, in situ tests allow obtaining average values of λ in real field conditions. Their main disadvantage is the high costs of implementation and the long time required for their execution [83]. A detailed summary of the different techniques to measure the thermal properties of the soil required for the design of energy geostructures can be consulted in [84].

Both laboratory and in situ tests can be classified into two categories: stationary and transient. In stationary methods, the soil sample remains at a constant temperature while it is subjected to a thermal gradient and the heat flow through it is stabilized [85]. In transient methods the temperature of the soil sample varies with time. In general, they are more versatile than stationary ones and their execution is simpler. A list of various test methods developed for the determination of thermal conductivity is presented in Table 4. A detailed summary of these can be found in [86].

In the case of complex projects, the value of the thermal conductivity λ can be determined from Thermal Response Tests (TRT). These tests consist of injecting a specific amount of heat energy into the ground at a constant rate and monitoring the temperature changes produced (Fig. 10) [87]. Thus, a fluid (usually water) is

Table 3 Design parameters [74]

Design parameter	Required for	Comments
Soil thermal conductivity	Energy output	An average value is used in most design approaches, although real conditions are likely to be anisotropic and heterogeneous
Soil specific heat capacity	Energy output	–
Undisturbed ground temperature	Energy output	Average value, or preferably a profile with depth
Groundwater flow rate (Darcy velocity)	Energy output	As a minimum, an indication is required of whether significant groundwater flow is to be expected at the site
Concrete thermal conductivity	Energy output	Often included within the thermal resistance parameter
Concrete specific heat	Energy output	For storage of heat within the concrete
Thermal resistance of heat exchanger	Energy output	A lumped parameter that includes the thermal properties and geometry of the heat exchanger
Soil strength	Geotechnical design	In total or effective stress terms as appropriate; it should include an estimate of whether likely to be significantly temperature dependent
Soil stiffness	Geotechnical design	For serviceability considerations
In situ stresses (K_0) and pore-water regime	Geotechnical design	‘Apparent’ pre-consolidation pressure can be affected by temperature
Stress history	Geotechnical design	–
Over-consolidation ratio (OCR)	Geotechnical design	Determines the nature of the thermo-elastic (or thermoplastic) response
Concrete coefficient of thermal expansion	Geotechnical design	To determine the potential expansion of the geostructure
Soil coefficient of thermal expansion	Geotechnical design	Expansion of soil relative to concrete may be important for soil structure interactions
Concrete limiting stress	Structural design	Additional stresses may develop owing to restraint of the geostructure as it tries to expand on heating

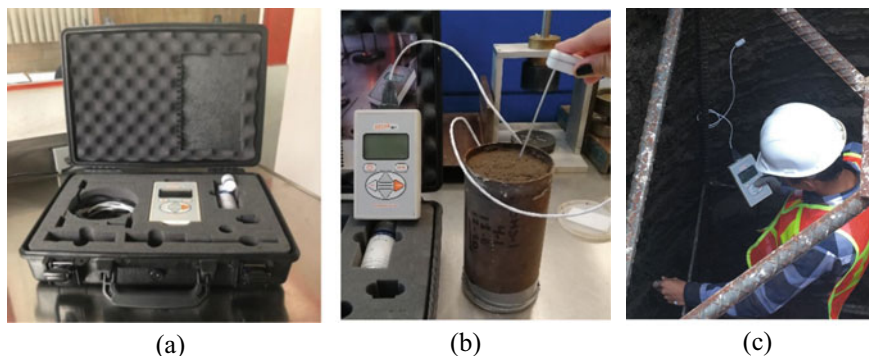


Fig. 9 Needle probe method: **a** Equipment KD2 Pro, **b** Laboratory tests (IIUNAM, Mexico) and, **c** in situ tests (Mexico City, Mexico)

Table 4 Tests for the determination of the thermal conductivity of soils

Type of test	Test
Stationary	Guarded hot-plate apparatus [91]
	Cylindrical configuration [92]
	In situ sphere meter [93]
	Heat flow meter apparatus [94, 95]
Transient	Needle probe method [96, 97]
	Periodic temperature waves [98]
	Thermal shock method [99]
	Thermal Response Test [87]

circulated through the pipes installed in the heat exchanger for a period of several days, which is calculated according to the dimensions of the heat exchanger. Finally, the data obtained are fitted to an analytical heat transfer model to determine the thermal conductivity of the soil and the thermal resistance of the heat exchanger R_b [88]. Several studies indicate that laboratory methods are more conservative and provide lower λ values than TRT tests [84, 89, 90].

7 Construction Recommendations for Energy Piles

7.1 Materials

The primary circuit can be made of high-density polyethylene (HDPE) or cross-linked polyethylene (PEX) and must meet the specifications presented in Table 5.

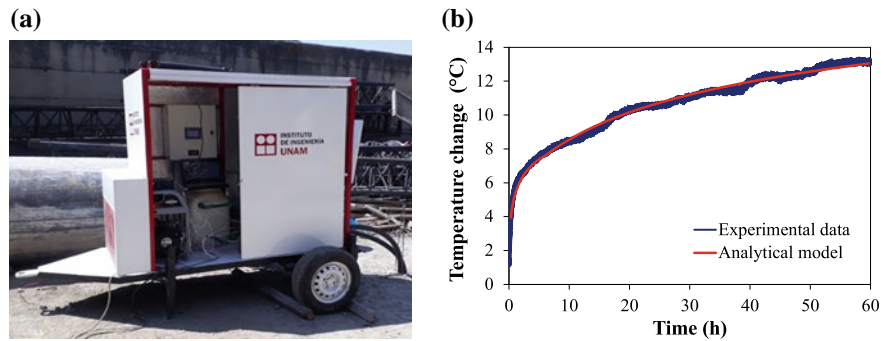


Fig. 10 Thermal Response Test (TRT) in State of Mexico (Mexico): **a** Mobile equipment TRT-IIUNAM and **b** Variation with time of the measured temperature

Table 5 Specifications for the primary circuit [67]

Type	Comments	References
High-density polyethylene (HDPE)	Outer diameter and inner diameter, wall thickness and their respective tolerances	[100, 101]
	High density polyethylene (HDPE) should be PE3408/3608 or PE4710, with Hydrostatic Design Basis of 1600 psi (11.03 MPa) at 73°F (23 °C)	[102, 103]
	All pipe and heat fused materials shall be manufactured from virgin polyethylene extrusion compound material	[104]
	Diameters, wall thicknesses and respective tolerances of the fittings	[105–107]
Cross-linked polyethylene (PEX)	Pipes requirements and dimensions	[104, 108, 109]
	Only polymer electro-fusion fittings or cold expansion compression-sleeve metal fittings are allowed	[107, 110]
	Cross-linked polyethylene (PEX) must be high-density PEX 1006 or PEX 1008 manufactured using the high-pressure peroxide method with a minimum cross-linking degree of 75%	[108, 111]

7.2 Pipes Features and Bending

According to the IGSHPA [67], the acceptable methods for joining buried pipes are heat fusion and stab-type fittings. High-density polyethylene pipes (HDPE) can be joined by butt, socket, sidewall, or electro-fusion, following the manufacturer's specifications. Polyethylene fusion transition fittings with threads should be used to adapt to copper. Conversely, polyethylene fusion transition fittings with threads or barbs should be used to fit high-strength duty hose. It is important to note that all mechanical connections should be accessible.

Cross-linked polyethylene (PEX) tubing shall not be butt-fused or socket-fused to fittings. In this case, polymer electro-fusion and cold expansion compression sleeve fittings may be used with PEX tubing when installed following the manufacturer's published procedures.

7.3 Pipes Fixing

The pipes embedded in the concrete must be fixed using a temporary or definitive rigid system (e.g., profiles, pipes, or pile reinforcement) as long as it allows the positioning specified in the design. The minimum recommended separation between pipes is 15 cm [59]. Therefore, the maximum number of loops depends on the diameter of the pile. Following the above criteria, Table 6 specifies the recommended number of loops according to the pile size.

When the element used as a positioning system has a structural function (i.e., pile reinforcement), the distance between the longitudinal reinforcements and the pipes should be at minimum $4D_{max}$, being D_{max} the maximum size of the concrete aggregate. Pipes should be supported transversely to avoid excessive strains. The maximum recommended spacings are 1 m for metal ties and 50 cm for plastic ties. In addition, a minimum spacing of 25 cm is recommended between the reinforcement base and the loop bottom. In the case of piles with two or more loops, a minimum distance of 20 cm is recommended between the reinforcement beginning and the loops located at the pile head [59].

Table 6 Maximum number of loops as a function of pile diameter [59]

Pile diameter	Number of loops
<40 cm	1
40 to 60 cm	2
60 to 80 cm	3
80 to 100 cm	4
>100 cm	4 + 1 additional loop for each 20 cm increment

7.4 *Installation*

Prior to installation, it is important to perform purge and pressure tests on the embedded pipes to determine the presence of possible leaks or obstructions. First, each supply circuit should be purged by circulating water in both directions at a minimum velocity of 0.61 m/s, maintaining the flow for a minimum of 15 min in each direction to remove all debris and air from the piping. Pressure tests should be performed in accordance with ASTM F2164 [112]. The pressure should be kept for at least one hour after stabilization. At the end of the above tests, each circuit should remain filled with water at a minimum pressure of 400 kPa until the final connection to the secondary circuit [59].

Pressure tests should be performed at the following stages of construction: (1) After assembly of each circuit, including connections to the borehole and after casting of the structure, and (2) After completing the installation of the entire heat exchange system and before connecting it to the secondary system.

For the pile construction (Fig. 11), typically, a borehole is first drilled from the natural ground, with the diameter and depth proposed in the project. Next, the material at the bottom of the excavation is cleaned. Purge and pressure tests are performed. Then, the reinforcing steel is installed, previously prepared with the heat exchanger pipe. Finally, the concrete is placed with the help of a “Tremie” pipe to avoid contaminating or segregating the concrete. Nevertheless, the construction procedure in energy piles may vary depending on the case.

7.5 *Quality Control*

CFMS-SYNTEC-SYNTEC-SOFFONS-FNTP [59] provides a detailed quality control procedure for the different phases of energy geostructures construction, which is described below:

- Pipeline arrival: Visual inspection.
- After fixing the pipes to the temporary/definitive rigid system: Pressure test with a minimum pressure of 400 kPa. If the test fails, it is necessary to reinstall the pipes. Pressure is maintained while moving the pipes to the installation site.
- Installation: During installation, continuous visual inspection is required to rule out scratches and strains. Pipes should be under rated pressure during this stage.
- After installation: A pressure test must be performed after casting, with the same pressure applied during attachment to the reinforcement. If the pressure drops more than 10 kPa, the pipe should be repaired. If this is not possible, the loop should be noted as lost, and the horizontal connections should be adapted accordingly.



Fig. 11 Construction process of an energy pile in Mexico City (Mexico)

- After the cut-off: A pressure test is carried out which must meet the same requirements as the check carried out after installation, i.e., a pressure drop of more than 10 kPa means that the loop is lost.
- After pipework: All pipes are under pressure and any items showing a pressure drop should be repaired if possible or noted as lost. Both discharge and pressure testing should be performed prior to delivery of the system to the customer.

References

1. García A, Martínez I (2012) Estado actual de desarrollo de las Bombas de Calor Geotérmico. *Geotermia* 25(2):58–68
2. Lee S, Park S, Ahn D, Choi H (2022) Thermal performance of novel cast-in-place energy piles equipped with multipurpose steel pipe heat exchangers (SPHXs). *Geothermics* 102:102389
3. Cherati DY, Ghasemi-Fare O (2021) Practical approaches for implementation of energy piles in Iran based on the lessons learned from the developed countries experiences. *Renew Sustain Energy Rev* 140:110748
4. Brandl H (2013) Thermo-active ground-source structures for heating and cooling. *Procedia Eng* 57:9–18
5. Brandl H (2006) Energy foundations and other thermo-active ground structures. *Géotechnique* 56(2):81–122

6. Asociación Técnica Española de Climatización y Refrigeración (ATECYR) (2012) Guía Técnica de Diseño de Sistemas de Intercambio Geotérmico de Circuito Cerrado. Instituto para la Diversificación y Ahorro de la Energía, Madrid
7. Suryatriyastuti ME, Mroueh H, Burlon S (2012) Understanding the temperature-induced mechanical behaviour of energy pile foundations. *Renew Sustain Energy Rev* 16(5):3344–3354
8. De Moel M, Bach PM, Bouazza A, Singh RM, Sun JO (2010) Technological advances and applications of geothermal energy pile foundations and their feasibility in Australia. *Renew Sustain Energy Rev* 14(9):2683–2696
9. Sanner B (2001) Shallow geothermal energy. *Geo-Heat Center Bull* 22(2):19–25
10. Kovačević MS, Bačić M, Arapov I (2013) Possibilities of underground engineering for the use of shallow geothermal energy. *Gradevinar* 64(12):1019–1028
11. Florides G, Kalogirou S (2007) Ground heat exchangers—a review of systems, models and applications. *Renew Energy* 32(15):2461–2478
12. Aresti L, Christodoulides P, Florides G (2018) A review of the design aspects of ground heat exchangers. *Renew Sustain Energy Rev* 92:757–773
13. Cui P, Man Y, Fang Z (2015) Geothermal heat pumps. In: Yan J (ed) *Handbook of clean energy systems*. Wiley, pp 1–22
14. Loveridge F, Powrie W (2013) Temperature response functions (G-functions) for single pile heat exchangers. *Energy* 57:554–564
15. Mimouni T (2014) Thermomechanical Characterization of Energy Geostructures with Emphasis on Energy Piles. PhD thesis, Ecole Polytechnique Federale de Lausanne
16. Sekaine K, Ooka R, Yokoi M, Shiba Y, Hwang S (2007) Development of a ground source heat pump system with Ground heat exchanger utilizing the cast-in-place concrete pile foundations of a building. *ASHRAE Trans* 113:558–566
17. Soga K, Rui Y (2016) Energy geostructures. In: Rees SJ (ed) *Advances in ground-source heat pump systems*. Woodhead Publishing, pp 185–221
18. Park S, Sung C, Jung K, Sohn B, Chauchois A, Choi H (2015) Constructability and heat exchange efficiency of large diameter cast-in-place energy piles with various configurations of heat exchange pipe. *Appl Therm Eng* 90:1061–1071
19. Carotenuto A, Marotta P, Massarotti N, Mauro A, Normino G (2017) Energy piles for ground source heat pump applications: comparison of heat transfer performance for different design and operating parameters. *Appl Therm Eng* 124:1492–1504
20. Laloui L, Di Donna A (2011) Understanding the behaviour of energy geo-structures. *Proc ICE-Civ Eng* 164:184–191
21. Adam D, Markiewicz R (2009) Energy from earth-coupled structures, foundations, tunnels and sewers. *Géotechnique* 59(3):229–236
22. Pahud D, Hubbuch M (2007) Measured thermal performances of the energy pile system of the dock midfield at Zürich Airport. In: *Proceedings European geothermal congress, unterhaching, Germany, 30 May–1 June 2007*
23. Laloui L, Nuth M, Vulliet L (2006) Experimental and numerical investigations of the behaviour of a heat exchanger pile. *Int J Numer Anal Meth Geomech* 30(8):763–781
24. Mimouni T, Laloui L (2015) Behaviour of a group of energy piles. *Can Geotech J* 52(12):1913–1929
25. Fisch MN, Himmler R (2005) International solar centre, berlin—a comprehensive energy design. In: *Proceedings of the fifth international conference for enhanced building operations, Pittsburgh, Pennsylvania, 11–13 October 2005*
26. Lennon DJ, Watt E, Suckling TP (2008) Energy piles in Scotland. In: Van Impe P (ed) *Van Impe WF. Deep foundations on bored and auger piles-BAP V*, CRC Press, pp 361–368
27. Bourne-Webb PJ, Amatya B, Soga K, Amis T, Davidson C, Payne P (2009) Energy pile test at Lambeth College, London: geotechnical and thermodynamic aspects of pile response to heat cycles. *Géotechnique* 59(3):237–248
28. Laloui L, Rotta-Loria A (2019) Analysis and design of energy geostructures: theoretical essentials and practical application. Academic Press

29. Abdelaziz SL, Olgun CG, Martin JR (2011) Design and operational considerations of geothermal energy piles. In: *Geo-Frontiers 2011. Advances in geotechnical engineering*, Dallas, Texas, 13–16 March 2011
30. Chiasson AD, Rees SJ, Spitler JD (2000) A preliminary assessment of the effects of groundwater flow on closed-loop ground source heat pump systems. *ASHRAE Trans* 106(1):DA-00-13-5(4365)
31. Li M, Lai AC (2015) Review of analytical models for heat transfer by vertical ground heat exchangers (GHEs): a perspective of time and space scales. *Appl Energy* 151:178–191
32. Li M, Zhu K, Fang Z (2016) Analytical methods for thermal analysis of vertical ground heat exchangers. In: Rees SJ (ed) *Advances in ground-source heat pump systems*. Woodhead Publishing, pp 157–183
33. Freitas R (2014) Thermal and thermal-mechanical analysis of thermo-active pile foundations civil engineering. MSc thesis, Instituto Superior Técnico de Lisboa
34. American Society of Heating, Refrigerating and Air-Conditioning Engineers (ASHRAE) (2011) *ASHRAE handbook: HVAC applications*. ASHRAE, Atlanta, GA
35. Loveridge F (2012) The thermal performance of foundation piles used as heat exchangers in ground energy systems. PhD thesis, University of Southampton
36. Jaeger JC, Carslaw HS (1959) *Conduction of heat in solids*. Clarendon P Oxford, UK
37. Zeng H, Diao N, Fang Z (2003) Heat transfer analysis of boreholes in vertical ground heat exchangers. *Int J Heat Mass Transf* 46(23):4467–4481
38. Ingersoll LR, Zabel OJ, Ingersoll AC (1954) *Heat conduction with engineering, geological, and other applications*. University of Wisconsin Press, Madison, Wisconsin
39. Diao N, Li Q, Fang Z (2004) Heat transfer in ground heat exchangers with groundwater advection. *Int J Therm Sci* 43(12):1203–1211
40. Ozisik MN (1993) *Heat conduction*. Wiley, New York
41. Spitler JD, Bernier M (2016) Vertical borehole ground heat exchanger design methods. In: Rees SJ (ed) *Advances in ground-source heat pump systems*. Woodhead Publishing, pp 29–61
42. Eskilson P (1987) *Thermal analysis of heat extraction boreholes*. PhD thesis, Sweden: University of Lund
43. Yavuzturk C, Spitler JD, Rees SJ (1999) A transient two-dimensional finite volume model for the simulation of vertical U-tube ground heat exchangers. *ASHRAE Trans* 105(2):465–474
44. He M, Rees S, Shao L (2011) Simulation of a domestic ground source heat pump system using a three-dimensional numerical borehole heat exchanger model. *J Build Perform Simul* 4(2):141–155
45. Lee CK, Lam HN (2013) A simplified model of energy pile for ground-source heat pump systems. *Energy* 55:838–845
46. Gashti EHN, Uotinen VM, Kujala K (2014) Numerical modelling of thermal regimes in steel energy pile foundations: a case study. *Energy Build* 69:165–174
47. Dupray F, Laloui L, Kazangba A (2014) Numerical analysis of seasonal heat storage in an energy pile foundation. *Comput Geotech* 55:67–77
48. Laloui L, Moreni M, Fromentin A, Pahud D, Steinmann G (1999) Heat exchanger pile: effect of the thermal solicitations on its mechanical properties. *Bull D'hydrogéologie* 17:331–338
49. Bourne-Webb PJ, Soga K, Amatya B (2013) A framework for understanding energy pile behaviour. *Geotech Eng* 166(GE2):170–177
50. Amatya BL, Soga K, Bourne-Webb PJ, Amis T, Laloui L (2012) Thermo-mechanical behaviour of energy piles. *Géotechnique* 62(6):503–519
51. Murphy KD, McCartney JS, Henry KS (2015) Evaluation of thermo-mechanical and thermal behavior of full-scale energy foundations. *Acta Geotech* 10(2):179–195
52. Bourne-Webb PJ, Burlon S, Javed S, Kürten S, Loveridge F (2016) Analysis and design methods for energy geostructures. *Renew Sustain Energy Rev* 65:402–419
53. Makasis N, Narsilio GA, Bidarmaghz A (2018) A machine learning approach to energy pile design. *Comput Geotech* 97:189–203

54. López-Acosta NP, Barba-Galdámez DF (2022) Diseño térmico preliminar del primer proyecto de pilas de energía en México. In: López-Acosta NP, Martínez-Hernández E (eds) 5° Simposio internacional de cimentaciones profundas, sociedad mexicana de ingeniería geotécnica, México, pp 71–77
55. Bourne-Webb P, Pereira J-M, Bowers G, Mimouni T, Loveridge F, Burlon S, Olgun CG, McCartney JS, Sutman M (2014) Design tools for thermoactive geotechnical systems. *DFI J: J Deep Found Inst* 8(2):121–129
56. Verein Deutscher Ingenieure (VDI) (2001) 4640. Part 2. Thermal use of the underground—ground source heat pump systems
57. Société suisse des Ingénieurs et des Architectes (SIA) (2005). Utilisation de la chaleur du sol par des ouvrages de fondation et de soutènement en béton. Guide pour la conception, la réalisation et la maintenance. Zurich, Switzerland
58. Ground Source Heat Pump Association (GSHPA) (2012) Thermal pile design, installation and materials standards. Ground Source Heat Pump Association, Milton Keynes, UK
59. CFMS-SYNTEC-SOFFONS-FNTP (2017) Recommandations pour la conception, le dimensionnement et la mise en œuvre des géostructures thermiques. *Rev Fr Geotech* 149:1–120
60. Kavanaugh S (1991) Ground and water source heat pumps. A manual for the design and installation of ground-coupled, ground water and lake water heating and cooling systems in southern climates. University of Alabama, Tuscaloosa, AL
61. Kavanaugh S (1995) A decision method for commercial ground-coupled heat pumps (No. CONF-950624). American Society of Heating, Refrigerating and Air-Conditioning Engineers, Inc., Atlanta, Georgia
62. Cullin JR, Spitler JD (2011) A computationally efficient hybrid time step methodology for simulation of ground heat exchangers. *Geothermics* 40(2):144–156
63. Javed S, Spitler JD (2016) Calculation of borehole thermal resistance. In: Rees SJ (ed) *Advances in ground-source heat pump systems*. Woodhead Publishing, pp 63–95
64. Claesson J, Javed S (2020) Explicit multipole formula for the local thermal resistance in an energy pile—the line-source approximation. *Energies* 13(20):5445
65. Kavanaugh S (2008) A 12-step method for closed-loop ground heat-pump design source. *ASHRAE Trans* 114(2):328–337
66. Fadejev J, Simson R, Kurnitski J, Haghighat F (2017) A review on energy piles design, sizing and modelling. *Energy* 122:390–407
67. International Ground Source Heat Pump Association (IGSHPA) (2009) Ground source heat pump residential and light commercial: design and installation guide. Oklahoma State University, Oklahoma, USA
68. Kavanaugh SP, Rafferty KD (2014) Geothermal heating and cooling: design of ground-source heat pump systems. ASHRAE, Atlanta, GA
69. American Society of Heating, Refrigerating and Air-Conditioning Engineers (ASHRAE) (2015) *ASHRAE Handbook e Applications*. ASHRAE, Atlanta, GA
70. Rotta-Loria AF, Bocco M, Garbellini C, Muttoni A, Laloui L (2020) The role of thermal loads in the performance-based design of energy piles. *Geomech Energy Environ* 21:100153
71. Gulvanessian H (2001) EN1990 Eurocode-basis of structural design. *Proc ICE-Civ Eng* 144(6):8–13
72. Abdelaziz SL, Ozudogru TY (2016) Selection of the design temperature change for energy piles. *Appl Therm Eng* 107:1036–1045
73. Song H, Pei H, Zhou C, Zou D, Cui C (2022) Calculation of the representative temperature change for the thermomechanical design of energy piles. *Geomech Energy Environ* 29:100264
74. Loveridge F, Low J, Powrie W (2017) Site investigation for energy geostructures. *Q J Eng GeolHydrogeol* 50(2):158–168
75. Olgun CG, Ozudogru TY, Abdelaziz SL, Senol A (2015) Long-term performance of heat exchanger piles. *Acta Geotech* 10(5):553–569
76. Gashiti EHN, Malaska M, Kujala K (2015) Analysis of thermo-active pile structures and their performance under groundwater flow conditions. *Energy Build* 105:1–8

77. Rotta Loria AF, Laloui L (2017) The equivalent pier method for energy pile groups. *Géotechnique* 67(8):691–702
78. Dong Y, McCartney JS, Lu N (2015) Critical review of thermal conductivity models for unsaturated soils. *Geotech Geol Eng* 33(2):207–221
79. Jia GS, Tao ZY, Meng XZ, Ma CF, Chai JC, Jin LW (2019) Review of effective thermal conductivity models of rock-soil for geothermal energy applications. *Geothermics* 77:1–11
80. López-Acosta NP, Zaragoza-Cardiel AI, Barba-Galdámez DF (2021) Determination of thermal conductivity properties of coastal soils for GSHPs and energy geostructures applications in Mexico. *Energies* 14:5479
81. López-Acosta NP, Portillo-Arreguín DM, Barba-Galdámez DF, Singh RM (2022) Thermal properties of soft clayey soils from the former Lake Texcoco in Mexico. *Geomechanics for Energy and the Environment*: 100376
82. Barry-Macaulay D, Bouazza A, Singh RM, Wang B, Ranjith PG (2013) Thermal conductivity of soils and rocks from the Melbourne (Australia) region. *Eng Geol* 164:131–138
83. Akrouch GA, Briaud J-L, Sanchez M, Yilmaz R (2016) Thermal cone test to determine soil thermal properties. *J Geotech Geoenviron Eng* 142(3):04015085
84. Vieira A, Alberdi-Pagola M, Christodoulides P, Javed S, Loveridge F, Nguyen F et al (2017) Characterisation of ground thermal and thermo-mechanical behaviour for shallow geothermal energy applications. *Energies* 10(12):2044
85. Abuel-Naga H, Bergado D, Bouazza A, Pender M (2009) Thermal conductivity of soft Bangkok clay from laboratory and field measurements. *Eng Geol* 105:211–219
86. Farouki O (1981) Thermal properties of soils. CRREL Monograph 81-1. Cold Regions Research and Engineering Laboratory, Hanover, NH
87. Franco A, Conti P (2020) Clearing a path for ground heat exchange systems: a review on thermal response test (TRT) methods and a geotechnical routine test for estimating soil thermal properties. *Energies* 13(11):2965
88. IEA ECES (2013) Annex 21 thermal response test. Final report
89. Loveridge FA, Brettmann T, Olgun CG, Powrie W (2014) Assessing the applicability of thermal response testing to energy piles. In: Global perspectives on the sustainable execution of foundations works, Stockholm, Sweden, 21–23 May 2014
90. Low JE, Loveridge FA, Powrie W, Nicholson D (2015) A comparison of laboratory and in situ methods to determine soil thermal conductivity for energy foundations and other ground heat exchanger applications. *Acta Geotech* 10(2):209–218
91. American Society for Testing and Materials (ASTM) (2016) Standard test method for steady-state heat flux measurements and thermal transmission properties by means of the guarded-hot-plate apparatus. ASTM C177-13. ASTM International, West Conshohocken, PA
92. Kersten MS (1949) Laboratory research for the determination of the thermal properties of soils. ACFEL Technical Rep. 23. AD712516. Engineering Experiment Station, University of Minnesota
93. Mochlinski K (1964) Some industrial measurements of thermal properties of soil. International study group on soils, lectures at meeting in Cambridge, international study group on Soils, Cambridge
94. American Society for Testing and Materials (ASTM) (2015) Standard test method for steady-state thermal transmission properties by means of the heat flow meter apparatus. ASTM C518-15. ASTM International, West Conshohocken, PA
95. Scott RF (1969) The freezing process and mechanics of frozen ground. CRREL Monograph II-D1. Cold Regions Research and Engineering Laboratory, Hanover, NH
96. American Society for Testing and Materials (ASTM) (2016) Standard test method for determination of thermal conductivity of soil and soft rock by thermal needle probe procedure. ASTM D5334-14. ASTM International, West Conshohocken, PA
97. De Vries DA, Peck AJ (1958) On the cylindrical probe method of measuring thermal conductivity with special reference to soils. *Austr J Phys* 11:409–423
98. Hoekstra P, Delaney A, Atkins R (1973) Measuring the thermal properties of cylindrical specimens by the use of sinusoidal temperature waves. CRREL Technical Report 244, AD770425. Cold Regions Research and Engineering Laboratory, Hanover, NH

99. Shannon WL, Wells WA (1947) Tests for thermal diffusivity of granular materials. *Proc ASCE* 47:1044–1055
100. American Society for Testing and Materials (ASTM) (2016) Standard specification for polyethylene (PE) plastic pipe (DR-PR) based on controlled outside diameter. ASTM D3035-15. ASTM International, West Conshohocken, PA
101. American Society for Testing and Materials (ASTM) (2013) Standard specification for polyethylene (PE) plastic pipe (DRPR) based on outside diameter. ASTM F714-13. ASTM International, West Conshohocken, PA
102. American Society for Testing and Materials (ASTM) (2014) Standard specification for polyethylene plastics pipe and fittings materials. ASTM D3350-14. ASTM International, West Conshohocken, PA
103. American Society for Testing and Materials (ASTM) (2013) Standard test method for obtaining hydrostatic design basis for thermoplastic pipe materials or pressure design basis for thermoplastic pipe products. ASTM D2837-13. ASTM International, West Conshohocken, PA
104. American Society for Testing and Materials (ASTM) (2013) Standard specification for polyethylene (PE) gas pressure pipe. Tubing, and fittings. ASTM D2513–13. ASTM International, West Conshohocken, PA
105. American Society for Testing and Materials (ASTM) (2016) Standard specification for butt heat fusion polyethylene (PE) plastic fittings for polyethylene (PE) plastic pipe and tubing. ASTM D3261-16. ASTM International, West Conshohocken, PA
106. American Society for Testing and Materials (ASTM) (2013) Standard test method for obtaining hydrostatic design basis for thermoplastic pipe materials or pressure design basis for thermoplastic pipe products. ASTM D2683-13. ASTM International, West Conshohocken, PA
107. American Society for Testing and Materials (ASTM) (2016) Standard specification for electrofusion type polyethylene fittings for outside diameter controlled polyethylene and crosslinked polyethylene (PEX) pipe and tubing. ASTM F1055-16. ASTM International, West Conshohocken, PA
108. American Society for Testing and Materials (ASTM) (2020) Standard specification for crosslinked polyethylene (PEX) tubing. ASTM F876-20. ASTM International, West Conshohocken, PA
109. American Society for Testing and Materials (ASTM) (2020) Standard specification for crosslinked polyethylene (PEX) hot- and cold-water distribution systems. ASTM F877-20. ASTM International, West Conshohocken, PA
110. American Society for Testing and Materials (ASTM) (2019) Standard specification for cold-expansion fittings with metal compression-sleeves for crosslinked polyethylene (PEX) pipe and SDR9 polyethylene of raised temperature (PE-RT) pipe. ASTM F2080-19. ASTM International, West Conshohocken, PA
111. American Society for Testing and Materials (ASTM) (2016) Standard test methods for determination of gel content and swell ratio of crosslinked ethylene plastics. ASTM F2765-16. ASTM International, West Conshohocken, PA
112. American Society for Testing and Materials (ASTM) (2021) Standard practice for field leak testing of polyethylene (PE) and crosslinked polyethylene (PEX) pressure piping systems using hydrostatic pressure. ASTM F2164-21. ASTM International, West Conshohocken, PA

Multiparametric Evaluation of Electrical, Biogas and Natural Gas Geothermal Source Heat Pumps



Cristina Sáez Blázquez, David Borge-Diez, Ignacio Martín Nieto, Arturo Farfán Martín, and Diego González-Aguilera

Abstract The use of low-impact energy sources is gradually growing with the aim of reducing greenhouse gases emission and air pollution. The alternatives offered by geothermal systems are one of the key solutions for a future renewable development, enabling the electrification of heating systems and the use of biofuels. This research addresses an overview of geothermal heating systems using ground source heat pumps in different European countries. Besides the traditional electrical heat pumps, gas engine heat pumps aided by natural gas or biogas are analysed in three areas. From a previous research, the technical parameters defining the geothermal system are used here to evaluate the most appropriate system in each scenario. The evaluation of different influential factors (operational costs, initial investment, environmental impact, and availability) allows defining the most recommendable systems for each area. Results of this multi-parametric study show that gas engine heat pumps aided by biogas could mean an excellent solution in all countries, also contributing to the management of waste and polluting substances. If biogas systems were not available, the electrical heat pump would be the first option for areas 1 and 3 (Italy and Sweden) but not for area 2 (United Kingdom), where natural gas is preferred.

Keywords Geothermal energy · Ground source heat pumps · Electrical heat pumps · Gas engine heat pumps · Natural gas · Biogas

C. S. Blázquez · D. Borge-Diez (✉) · A. F. Martín
Department of Electric, System and Automatic Engineering, Universidad de León, León, Spain
e-mail: david.borge@unileon.es

I. M. Nieto · D. González-Aguilera
Department of Cartographic and Land Engineering, University of Salamanca, Higher Polytechnic School of Avila, Avila, Spain

Nomenclature

Acronyms

GSHP	Ground source heat pump
GEHP	Gas engine heat pump
EHP	Electric heat pump
HP	Heat pump
DHW	Domestic hot water
COP	Coefficient of performance
nZEB	Nearly zero energy building
D _L	Total drilling length
COP _R	System real COP
E _C	Annual electricity consumption
G _C	Annual gas consumption
IEA	International Energy Agency
IRENA	International Renewable Energy Agency
IDAE	Institute for the Diversification and Energy Saving
HCV	Higher calorific value

1 Introduction

It is internationally recognised by the Paris Agreement [1] that global greenhouse gases emissions require to be urgently reduced to prevent hazardous climate change. Within these gases, human activity is mainly linked to the production of CO₂, and, in most European countries, around one third of CO₂ emissions are related to heat technologies (specially space heating in public and private buildings) [2]. In this context, renewable energy technologies are viewed as a potential mitigation option for fighting against climate change through the reduction of greenhouse gases emission [3, 4]. One promising potential source for heating and cooling with low CO₂ emissions is the shallow geothermal energy, and, in particular, the ground source heat pump (GSHP) systems [5–7]. GSHP technologies are one of the most common geothermal applications within the renewable sources that are able to supply the user's energy needs. These systems are characterized by extracting the earth's interior heat from the subsurface at low depth, (reason why they are called “shallow resources”) and using it for space and domestic hot water (DHW) heating [8, 9]. The number of GSHP systems is increasingly worldwide, being especially important in the European Countries. Nowadays, these technologies contribute to achieve the low carbon emission targets set by cities and countries [10].

A GSHP system is mainly constituted by two modules: the heat source, commonly a borehole heat exchanger and the heat pump. The heat exchanger allows the extraction of the energy stored beneath the surface through the use of a working fluid, and the heat pump increases the temperature of the fluid, whose temperature is often too low for direct use. For the operation of the heat pump, auxiliary energy is required, typically in the form of electricity. In this regard, although electricity driven heat pumps (EHP) are, by far, the most frequent model, gas engine heat pumps (GEHP) are also possible.

Geothermal heat pumps are characterized by low operating costs, reliable operation, absence of greenhouse gases direct emissions and low need for maintenance [11]. The efficiency of these devices is usually expressed by the coefficient of performance (COP) which relates the thermal energy produced and the energy consumed. EHPs commonly achieve COPs of around 4–4.5, whereas the COP of GEHPs is of about 1.5–1.6. These last models are, however, capable of recovering around 80% of the heat generated during the heat pump operation. In this context, there are two main factors that will influence the selection of one or another heat pump model: operational costs and CO₂ emissions. Operational costs are directly influenced by the electricity and gas price in the location of the future system. CO₂ emissions derive from the nature and properties of the gas used as auxiliary energy (when using GEHPs) or from the electricity mix of the location (if EHPs are chosen). It is therefore recommendable to perform an exhaustive analysis of the global GSHP system considering the factors commented above. This analysis will allow the selection of the most suitable heat pump device for each particular system.

With the aim of addressing the importance of installing the most appropriate GSHP system, this research starts from the technical results of one of the author's previous work [12] focused on the calculation of three different GSHP systems (EHP and GEHPs supplied by natural gas and biogas) in three different locations. From the results of the mentioned work, the strength of the present research will be the determination of the most suitable heat pump model in each location from the economic and environmental points of view. To this effect, the energy mix of each place will require to be thoroughly analysed. As can be observed in the following sections, the manuscript firstly studies the energy characteristics of each location to subsequently include the results derived from the use of each heat pump model and the final discussion and conclusion sections.

It is crucial to highlight that this work is in the context of complying with the European Regulations. The Clean energy for all Europeans package aims to balance the decisions at EU, national and local level and lead the clean energy transition. In the fight against climate change, EU has set ambitious energy targets for 2030 but also a long-term climate neutrality strategy for 2050. The package is based on the principle of “energy efficiency first” which set the target to be almost one third more efficient (at least 32.5% in our energy use by 2030) making special emphasis to the building sector. Buildings are the largest energy consumers, accounting for 40% of final energy consumption and 36% of greenhouse gas emissions in Europe. One additional target of this agreement is the use of at least 32% renewables in energy consumption by 2030 [13]. Within this frame of decarbonisation, it is important

to remark the role of geothermal heat pumps, meaning an excellent solution for simultaneously heating and cooling purposes. Since the use of fossil energy sources, such as the natural gas, makes it impossible to get a zero emissions heating system, low enthalpy geothermal resources will constitute one of the most fundamental tools in the Europeans ambitions, especially those using clean sources as the ones presented in this research (biogas or electricity from renewables).

Regarding the use of biogas, interest in the technology of this gas is increasing around the world as a result of the constant search of renewable production, reuse of materials and reduction or elimination of harmful emissions. This local biofuel is also a solution for additional problems such as the reuse of purines or the ground and water pollution. However, despite its high potential, the use of biogas is not widespread in the European countries [14, 15]. Thus, the use of GEHP with biogas would have a double positive effect; contributing to the achievement of the European energy strategies and promoting an extended use of biogas.

2 Research Scope

As already mentioned, the basis of this work is the technical design presented in a previous research [12] for three different alternatives of GSHP systems in three different scenarios. The starting data and the principal scope of this work are shown below.

Three areas representative of the common climates in Europe (warm, medium and cold) were selected to design each GSHP system to cover the heating demand of a building under the structural conditions. In this way, the starting point of the previous study was a building of 173.38 m² and 6.25 m of height planned to be installed in the localities of *Ancona*, Italy (area 1, representative of the warm climate), *Edinburgh*, Scotland (area 2, representative of the medium climate) and *Karlstad*, Sweden (area 3, representative of the cold climate).

Before describing the technical parameters obtained from the mentioned published research, it is important to highlight the principal characteristics of the energy mix in each of the scenarios under study.

- Italy

In the case of Italy, the electricity production through fossil sources is considerably high. Although the Italian energy mix includes renewable generation, the nuclear energy production was abandoned in 1987. This country has stated notable strategies with the aim of reducing the environmental impact, ensuring the energy supply and a progressive economic impulse.

- United Kingdom

The electricity generation of this country has been traditionally dominated by coal and gas plants although the production of renewable and nuclear plants is on the rise. United Kingdom has become aware of the importance of reducing the consumption

of fossil sources, in this way; it has established crucial goals to reduce the emissions, setting a nearly zero purpose by the year 2050. This country highlights because of the fossil transformation and the increase of wind (in offshore plants) and solar PV production. It is also expected a considerable growth of these renewable energies by 2030. It must be also mentioned that this country left the EU at the beginning of 2020.

- Sweden

Sweden is on the top in achieving an energy mix based on non-fossil sources. With these strategies in mind, this country pretends to eliminate the carbon use by 2045. These purposes are already noticeable with only analysing its large renewable and nuclear electricity production. Regarding the heating/cooling sector, bioenergy district heating systems and electric heat pumps are one of the most widespread solutions. Within the ambitious target of Sweden are achieving total electricity generation by renewables in 2040 and reducing the emissions derived of transport by 70% in the near future.

In the following Fig. 1 it is possible to observe the evolution of the electricity production for each of the countries under study (1990–2018).

More information about the electricity generation of each country is provided in Table 1, which includes the GWh generated by each energy source in 2018.

Once known the energy sources dominating the electricity field of each scenario, for the development of this research is also necessary to consider the technical parameters of each EHP and GEHP systems defined in the previous work [12]. These data are summarized in the following Table 2 for each of the areas considered in the study.

The parameters shown in Table 2 for the GEHPs are identical whether the heat pump works with natural gas or biogas. This fact is because the heat pump COP is exclusively a function of the thermodynamic side of the cycle, meaning that the use of energy consumption to generate a unity of heat is identical for both gases (but not the volumetric gas use which is higher for the biogas that has also a lower higher calorific value).

Once defined the initial information about each of the countries under study, the following paragraphs address the description of the specific scope of the work. The original study, on which this research is based, was focused on defining the geothermal design of each heat pump model in each location and, from this point, analysing if these scenarios met the Nearly Zero Energy Building (nZEB) regulation and the “Clean energy for all Europeans” package [13]. The present research intends to go a step further and to determine the most recommendable GSHP system in each scenario by attending to economic, technical and environmental factors. The particular conditions relating to the characteristics of the energy mix in each location and the technical availability of each heat pump system will be decisive when selecting one or another model. For the achievement of the aforementioned objective, the following steps are required:

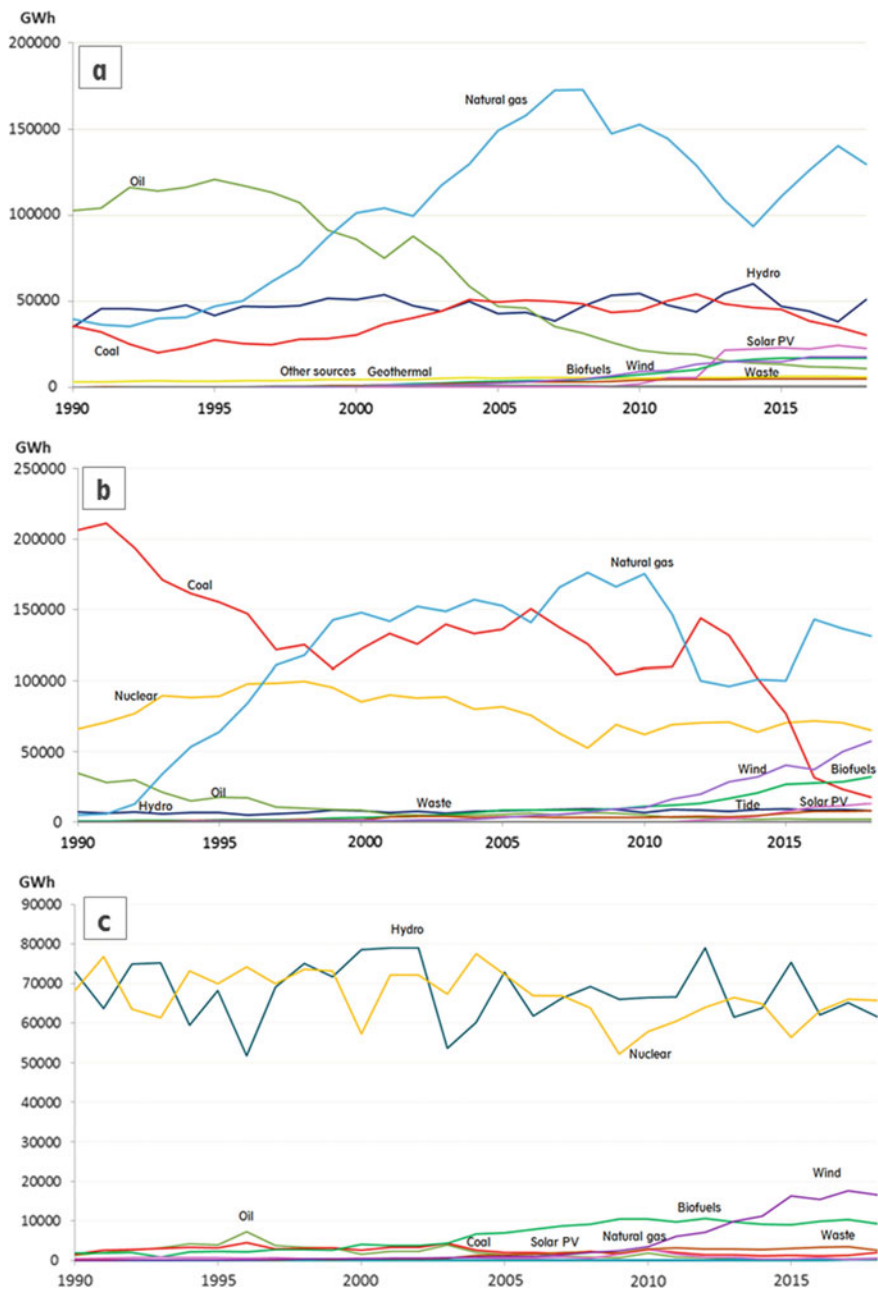


Fig. 1 Electricity generation by source in the period 1990–2018, **a** Italy, **b** United Kingdom, **c** Sweden [16]

Table 1 Origin of the global electricity generated in each area for the year 2018 [16]

Source	Electricity [GWh]		
	Italy	United Kingdom	Sweden
Coal	30,542	17,570	2035
Oil	10,762	1682	379
Natural Gas	129,743	131,482	564
Biofuels	16,858	32,086	9338
Waste	4806	8023	2539
Nuclear	–	65,064	65,801
Hydro	50,925	7963	61,606
Geothermal	6080	–	–
Solar PV	22,653	12,922	404
Wind	17,492	57,116	16,623
Tide	–	8	–
Municipal waste	4721	7130	2506
Waste (renewable)	2360	3564	1303
Other sources ^a	721	–	–

^a It includes the generation from chemical heat and other sources

Table 2 Principal parameters of the EHP and GEHP systems for each area. D_L = total drilling length, COP_R = system real COP and E_C = annual electricity consumption and G_C = annual gas consumption

	Italy	United Kingdom	Sweden
EHP	$D_L = 227$ m $COP_R = 5.17$ $E_C = 7,560.54$ kWh/year	$D_L = 446$ m $COP_R = 5.05$ $E_C = 14,206.34$ kWh/year	$D_L = 376$ m $COP_R = 4.98$ $E_C = 17,847.79$ kWh/year
GEHP	$D_L = 114$ m $COP_R = 1.57$ $G_C = 27,386.50$ kWh/year	$D_L = 199$ m $COP_R = 1.48$ $G_C = 53,321.75$ kWh/year	$D_L = 173$ m $COP_R = 1.48$ $G_C = 66,060.95$ kWh/year

- Evaluation of the specific conditions that dominate the energy mix in each of the areas under study. With that aim, official data will be taken from the International Energy Agency [16] and Eurostat [17], so the principal economic and environmental indicators of each country will be established. This stage will allow determining two essential factors for each location: price per kWh of electricity, natural gas or biogas (€/kWh) and kilograms of CO_2 per kWh of electricity, natural gas and biogas (kg- CO_2 /kWh).
- Determination of the principal costs (initial investment and operational costs) and greenhouse gases emissions associated to the operation of each GSHP model in each scenario.

- Analysis and evaluation of all the results obtained in the previous step with the aim of deducing the most recommendable choice for each scenario. In this evaluation four principal factors will be considered: overall process economy, initial investment, environmental impact and technical availability.

3 Practical Procedure

3.1 Economic Evaluation

As mentioned above, the basis of this subsection falls on the economic information available at official institutions as Eurostat or the International Energy Agency (IEA). These two organizations collect and disseminate different energy statistics (energy prices, measures of energy efficiency, etc.) of over 150 countries. This section is divided into three subsections addressing each of the energy sources constituting the present research.

3.1.1 Energy Source: Electricity

Eurostat database allows consulting the electricity prices in each of the three areas for the period 2008–2018. In this way, Table 3 includes, for the last year available (2018) the average national price in Euro per kWh in each location as well as the annual costs associated to the use of the EHP systems.

The information provided in the previous Table 3 would be only acceptable when referring to the cost of the EHP in the first year of the system operation in each area. With the aim of analysing the accumulated cost during the useful life of these systems (commonly around 30 years), it is desirable to estimate the evolution of the electricity prices in the coming years.

Considering that the useful life of these systems is around 30 years, for analysing the final costs accumulated in that period it is also necessary to estimate how the cost of the electricity will evolve. Electricity price forecasting is one of the key issues of the current electricity market. The estimation of this parameter is not simple since it does not follow a linear pattern and depends on a large number of factors. It is characterized by complex variables such as nonlinearity, non-stationarity and multiple seasonality.

Table 3 Annual costs derived from the use of the EHP systems in each scenario

	Italy	United Kingdom	Sweden
Price per kWh [€]	0.2067	0.1887	0.1891
Annual electricity use [kWh]	7,560.54	14,206.34	17,847.79
Annual electricity cost [€]	1,562.76	2,680.74	3,375.0.17

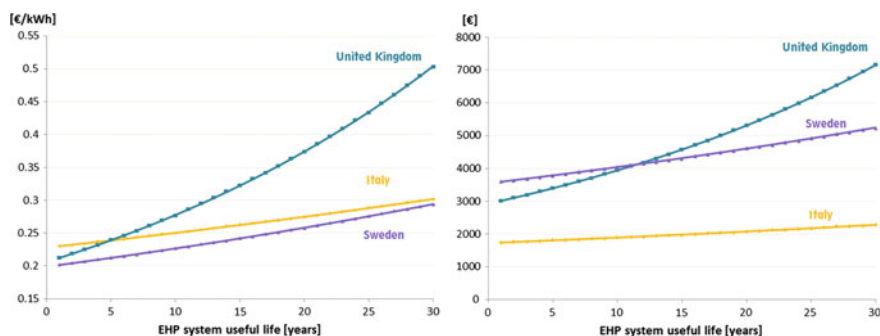


Fig. 2 Evolution of the electricity price (on the left) and annual operational cost (on the right) during the useful life of the EHP system in each area

There are numerous previous research works focused on predicting electricity price signal through different prediction models and functional methods [18–21].

The aim of the present study thoroughly differs from developing a new procedure for electricity price forecasting, but an indicator of this evolution is required. With this purpose, following an analytical extension method, the evolution of the electricity rate has been analysed for the period 2008–2018 in each country. In this way, the average rate deduced from this period will be applied to the corresponding 30 years of each system useful life. Based on the electricity price evolution, the annual costs derived from the consumption of the EHP system in each area can be also established. Figure 2 graphically shows both the electricity price and the annual costs for each scenario during the system useful life.

3.1.2 Energy Source: Natural Gas

Turning back to Eurostat database and following an analogous procedure, the natural gas prices in each of the three areas for the last year available (2018) were consulted and are shown in Table 4. This Table 4 also includes the annual costs associated to the use of the GEHP systems by using natural gas.

As in the electricity assumption, data from the previous Table 4 would be only acceptable when referring to the cost of the GEHP aided by natural gas in the first operational year of each scenario. In this case, it is again required to analyse the

Table 4 Annual costs derived from the use of the GEHP systems aided by natural gas in each scenario

	Italy	United Kingdom	Sweden
Price per kWh [€]	0.0714	0.0465	0.1153
Annual natural gas use [kWh]	27,386.50	53,321.75	66,060.95
Annual natural gas cost [€]	1,955.40	2,479.46	7,616.83

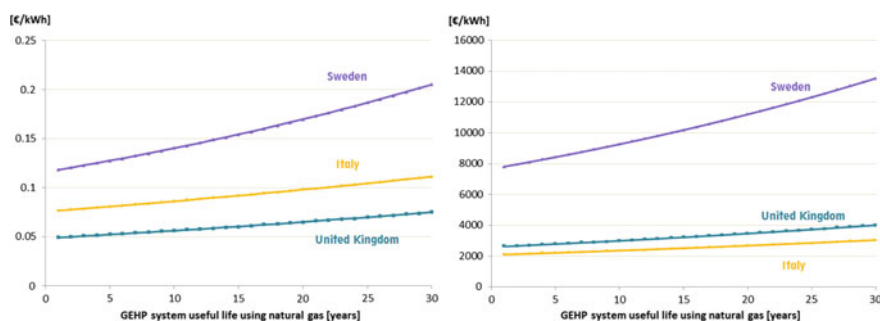


Fig. 3 Evolution of the natural gas price (on the left) and annual operational cost (on the right) during the useful life of the GEHP system aided by natural gas in each scenario

evolution of the natural gas cost during the system useful life (30 years). To this end, an analytical extension procedure was also applied to deduce the natural gas average rate during the period 2008–2018 (period in which data are available) in each country. The specific rate obtained for each country is then applied to the corresponding 30 years of operational period. The annual costs associated to the natural gas consumption of each GEHP system are also established and included in Fig. 3.

3.1.3 Energy Source: Biogas

The last assumption refers to the GEHP systems aided by biogas. Biogas is a versatile energy source, linked to a reduction of greenhouse gas emissions, an efficient use of waste and generation of valuable fertilizer [22, 23]. A biogas system usually consists of several processes of biological origin and energy conversion stages [24]. These systems are frequently divided into four main steps (feedstock supply, biogas generation, utilization of digested residue and utilization of biogas) that finally allow the use of biogas as biofuel or for generation in heat and power units.

When performing the economic evaluation intended in this work, specific biogas prices (in terms of €/energy unit) are not available in the published literature. Biogas installations can be based on feedstock from different nature such as industrial and municipal organic waste, animal waste, sewage or products coming from agricultural activities or renewable raw materials/energy crops. The total production cost is influenced by a series of factors, including here the associated transport costs, which can be decisive for the future biogas use. In this way, final prices of this gas also depend on the particular properties of the biogas originated in the plant or external factors such as government support and incentives.

For all the mentioned above, it is almost impossible to set a biogas price for a certain location. According to the International Renewable Energy Agency (IRENA), the estimated costs of bio-methane range from 0.0405 to 0.1292 €/kWh [25]. Within

Table 5 Annual costs derived from the use of the GEHP systems aided by biogas in each scenario

	Italy	United Kingdom	Sweden
Price per kWh [€]	0.0263	0.0169	0.0405
Annual natural gas use [kWh]	27,386.50	53,321.75	66,060.95
Annual natural gas cost [€]	720.26	901.14	2,675.47

this range, biogas prices in the different European countries will vary depending on the particular renewable energy policies.

Since no specific information for each of the areas under study has been found, for the objective of this section, an approximate biogas price (€/kWh) has been set for each of these locations. This index has been established from the available information of previous studies which also derives from a deep energy analysis of the locations.

- Area 1 (Italy) leads the production of biogas in Europe, being the number 2 with the largest number of plants. In the last years, Italy has had a high Feed-in Tariff which stimulated a lot the biogas market. Depending on the plant's capacity or the nature of the feedstock, different tariffs are applied so prices of biogas fluctuate in a high way [26].
- Area 2 (United Kingdom), the number of new biogas plants has increased rapidly since 2005, and is predicted to keep on rising. In the UK, financial support systems are available for anaerobic digestion operators. These tariffs also vary in function of the total installed capacity, so an average price has also been estimated.
- Area 3 (Sweden), the production of biogas has been slowly climbing for several years due to the difficulties in showing a reasonable profit for new biogas plants. This country has no Feed-in Tariffs, but instead uses other support systems principally focused on increasing the use of bio-methane as automotive fuel [27].

Considering the above mentioned price range and the characteristics of the biogas production in each country, the following Table 5 shows the costs derived from the use of the GEHP systems aided by biogas.

From the information of Table 5, the evolution of the biogas prices during the useful life of the installation was also established. There is again a lack of information about it, so that the trend estimated for the natural gas price in each location has been applied to the corresponding biogas price of each scenario.

3.2 Environmental Footprint

Another factor to be evaluated in this research refers to the environmental field. The greenhouse gas emissions generated by the energy sources feeding the EHP and GEHP systems are mainly carbon dioxide (CO₂), so this section is focused on the estimation of this kind of emissions.

3.2.1 Energy Source: Electricity

The generation of electricity (providing a non-renewable origin) implies the emission into the atmosphere of a series of polluting compounds. As already mentioned, this study only considers the CO₂ emissions although other contaminating gases (NO_x, CO...) are also generated but in a considerably lower amount, depending on the primary energy source.

The analysis of the CO₂ emissions derived from the use of electricity as an energy supply is not an easily estimated parameter. Emission factors highly fluctuate and depend on the electricity origin. Since final conversion factors have not been found in the countries contemplated in this study, the calculation of the amount of CO₂ per kWh of final electricity generated has been carried out based on the total CO₂ gases emitted in each area and its electricity production (origin and magnitude) in the same period of time.

The final CO₂ emission intensity factors included in Table 6 derive from the implementation of the following steps:

- Deduction for each area of a series of energy information from the IEA: global CO₂ emissions from electricity and heat (MT), total electricity and heat generation (GWh) and heat and electricity generation from non-renewable sources.
- From the above information, the total emissions generated by electricity and large-scale heating needed to be separated. The production of electricity from fossil fuels (those that contribute to these emissions), is given in the form of electrical energy. In this way, a performance factor in that transformation of 0.4 was considered to evaluate the thermal energy used, and to be able to establish a proportion which determines the electrical contribution to the total emissions of the data.
- Quantification of the amount of CO₂ emissions produced by electricity generation and determination of a preliminary CO₂ emission intensity factor.
- The emission factor previously calculated would be applicable if all of the electricity used by the EHP came from fossil sources (non-renewable generation plants). However, that electricity could also come from a renewable source. For this reason, the emission factor must be recalculated by considering the percentage of renewable electricity production for the country in question.

Table 6 Electricity CO₂ emissions in each area and global, 2018

	Italy	United Kingdom	Sweden
CO ₂ emissions from electricity [MT]	89.82	77.28	4.12
Electricity and heat (from non-renewable sources) [GWh]	427,617.50	376,835.00	7,445.00
CO ₂ emission intensity [kg/kWh]	0.3091	0.2467	0.0259
CO ₂ annual emissions [kg]	2,336.96	3,504.70	192.83

Table 7 Natural gas CO₂ emissions in each area

	Italy	United Kingdom	Sweden
CO ₂ emission intensity [kg/kWh]	0.2520	0.2520	0.2520
CO ₂ annual emissions [kg]	6,901.40	13,437.08	16,647.36

- Establishment of the global conversion factor (CO₂ emission intensity) for each location and calculation of the CO₂ emissions associated to the operation of the EHP system in each area.

3.2.2 Energy Source: Natural Gas

Natural gas is the fossil fuel with the lowest environmental impact of all the commonly used. In terms of CO₂ emissions, due to the high proportion of hydrogen-carbon in the molecules of this gas, its emissions are 40–50 and 25–30% lower than those of coal and fuel oil respectively. In this research, it is assumed that the natural gas feeding the GEHPs was preliminary subjected to the corresponding purification processes, so the greenhouse gas emissions will be mainly CO₂ gases.

The determination of the natural gas CO₂ emissions is highly simplified in relation to the previous electricity energy source. In contrast to the variable electricity origin, natural gas is naturally produced and its composition is almost the same regardless of its specific origin. CO₂ emissions will generally take place mainly when using the gas and, to a lesser extent, during its extraction or transportation [28, 29]. This research establishes an equal natural gas composition for all the countries, consisting of 99% methane and 1% of other components, mainly CO₂. Considering these facts, and given that the GEHPs suggested here are identical for all the areas under study, the global natural gas conversion factor (kg-CO₂ per kWh of natural gas) will be also the same in each scenario.

The source of the energy data required in this section comes from the IDAE, in particular from its report on calorific powers of fuels based on EUROSTAT and the IEA. According to this database, the higher calorific value (HCV) of the natural gas is set to 9,667 kcal/Nm³ (11.23 kWh/Nm³) and the CO₂ emission intensity to 0.252 kg-CO₂ per kWh of final energy [30]. Thus, the above factor will be extended to all countries (since equal natural gas conditions have been set) and used in further calculations included in Table 7.

3.2.3 Energy Source: Biogas

Provided that possible contaminants constituting biogas are eliminated, the emissions derived from this gas are limited to CO₂. Depending on its origin, biogas is usually characterized by 50–75% of methane, being the rest mainly CO₂. In the process of the methane's combustion, CO₂ is also produced. However, these emissions are commonly considered null since they are framed within the short carbon cycle. The

reason of the above is that the CO_2 produced both in the generation of the gas and in the methane's combustion, is the same that would be naturally produced by the waste biological degradation. Thus, biogas is usually considered as a renewable energy with zero CO_2 emissions.

This research estimates the CO_2 emissions derived from the use of biogas based on its chemical composition and the natural gas composition and emissions. According to IDAE [30], the biogas type composition (standard for all the countries) is 53.5% methane and 46.5% CO_2 and the HCV is $5,200 \text{ kcal/Nm}^3$ (6.04 kWh/Nm^3). From the normal natural gas composition (99% methane and 1% CO_2) and its HCV, the following statements are applied to estimate the biogas CO_2 emission factor:

- 0.058 kg of methane and 0.0016 kg of CO_2 are burned per 1 kWh of natural gas. From the natural gas emission factor, it is known the amount of CO_2 (0.0016 kg) contributing to the emissions and it is easily determinable that the methane is responsible for the remaining amount of CO_2 (0.2504 kg).
- Regarding the biogas, 0.065 kg of methane and 0.1411 kg of CO_2 react. When using this gas, the same amount of CO_2 is produced by the methane. This amount added to the previous 0.1411 kg would mean a global emission factor of $0.3915 \text{ kg-CO}_2/\text{kWh}$ of biogas.

The above calculated factor could be applied to all the areas under study since identical composition and conditions of generation are considered here. However, for the reasons already described, assuming a closed carbon cycle, the annual CO_2 emissions from the use of the GEHP aided by biogas are estimated as zero in each scenario.

4 Discussion

The final objective of all the calculations presented in the previous sections is to define the most appropriate energy source to supply the needs of the geothermal heat pump system in each place. The discussion section is focused on addressing the mentioned objective from different points of view: the process economy, the initial investment, the environmental impact and the availability of the system.

4.1 Overall Process Economy

Through the first economic evaluation of each of the HP solutions proposed for each location, it is possible to compare the total outlay required as a result of the EHP or GEHP operation during the established 30 years of useful life. Thus, in the following Fig. 4, it is possible to analyse, in a graphical way, the accumulated outlay in the last operational year of each solution in each area.

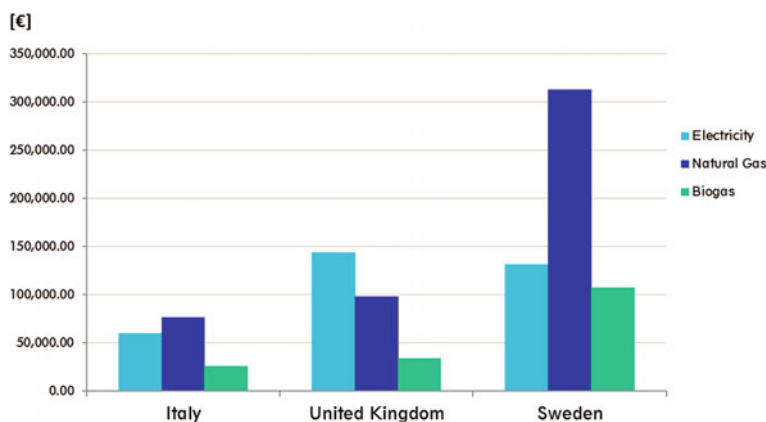


Fig. 4 Accumulated outlay in the year 30 depending on the solution adopted in each HP scenario

Figure 4 allows deducing that GEHP system aided by biogas is, undoubtedly, the most economical option in all the areas under study. Regarding the other two energy sources, EHP constitutes a more suitable alternative in areas 1 and 3 compared to GEHP aided by natural gas.

4.2 Initial Investment

The second factor discussed here is the initial investment required in the installation of each heat pump system. For the determination of this value, the heat pump equipment, the well field and the corresponding geothermal components have been considered. The space distribution system has not been included here since it is almost the same for the three assumptions of each scenario. Tables 8, 9 and 10 show all the mentioned information for the three study areas. Prices are based on the commercial catalogues of “Enertres” and “ALB” [31, 32] and a global drilling cost of 40 € per lineal meter has been assumed.

It must be mentioned that, when estimating the price of the GEHPs, no precise information has been found. The cost of this equipment has been estimated as 25–35% higher than that of the EHP, due to the greater complexity of the gas device (starter

Table 8 Comparative initial investment based on the HP model used in area 1

	EHP	GEHP (natural gas)	GEHP (biogas)
Heat pump system [€]	17,079.00	22,202.70	24,422.97
Drillings [€]	9,080.00	4,560.00	4,560.00
Geothermal components [€]	2,878.60	1439.30	1439.30
Total initial investment [€]	29,037.60	28,162.00	30,422.27

Table 9 Comparative initial investment based on the HP model used in area 2

	EHP	GEHP (natural gas)	GEHP (biogas)
Heat pump system [€]	21,986.00	28,581.80	31,439.98
Drillings [€]	17,840.00	7,960.00	7,960.00
Geothermal components [€]	5,121.50	2,101.50	2,101.50
Total initial investment [€]	44,947.50	38,643.30	41,501.48

Table 10 Comparative initial investment based on the HP model used in area 3

	EHP	GEHP (natural gas)	GEHP (biogas)
Heat pump system [€]	21,986.00	28,581.80	31,439.98
Drillings [€]	15,040.00	6,920.00	6,920.00
Geothermal components [€]	4,102.70	1,984.70	1,984.70
Total initial investment [€]	41,128.70	37,486.50	40,344.68

and combustion engine, residual heat exchanger...). For the biogas equipment, it will possibly require some additional filtering system to operate with the higher content of CO₂ of this fuel in relation to the natural gas one. Considering this fact, the price of the GEHP aided by biogas has been overestimated in 10% in relation to the natural gas device.

As can be observed in the above Tables, for all the scenarios, when using GEHP aided by natural gas, the initial investment can be slightly reduced. However, initial investments are quite similar among the three systems of each area.

In a general way, it can be assumed that the drilling length required for the EHP is approximately twice the length of the GEHP. This means a reduction in the drilling costs but also in the geothermal material (heat exchangers, grouting material, working fluid...). Despite this reduction, the global investment is then compensated by the higher prices of the GEHP devices.

4.3 Environmental Impact

In relation to the environmental impact derived from the use of each HP solution, Fig. 5 shows the total CO₂ emissions generated at the end of the useful life period in each area.

From the graph of Fig. 5, it is easily observable that the highest amount of CO₂ emissions derive from the use of the GEHP aided by natural gas. The implementation of the biogas solution has a zero environmental impact since the assumption of the closed carbon cycle was considered. It must be also mentioned that the use of this biofuel also contributes to the management of organic matter, purines and other types of wastes and polluting phenomena.

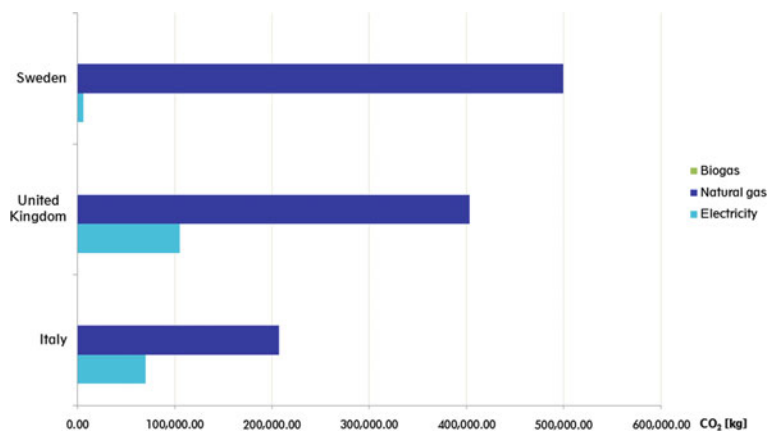


Fig. 5 Accumulated CO₂ emissions in the year 30 depending on the solution adopted in each scenario

In the three study cases, the high rate of electricity renewable generation makes the EHP a more appropriate alternative than the natural gas option. But it is remarkable that EHP system is especially recommendable in area 3. In this country (Sweden), almost all the electricity production comes from green and nuclear energy so the CO₂ electricity emission factor is considerably low.

4.4 System Availability

One final aspect to be considered is the current availability of the different heat pump models that have been analysed in this research. Within the market of EHPs, numerous manufacturers and models can be found and a wide range of powers and technologies are available.

Regarding the GEHPs, the number of manufacturers focused on the development of these devices is comparatively lower as well as the different ranges of power. This fact inevitably results in a notable increase of the prices of these systems. In addition, existing models are usually designed to operate with natural gas or liquefied petroleum gases and not for biogas. When using biogas, an added challenge is that its use is linked to the availability of generating plants in the surrounding area where the system pretends to be installed. Depending on the waste used as the primary source, the generation of biogas will be more or less viable.

4.5 Global Discussion

As already mentioned in the previous sections, the final purpose of this study is to finally evaluate (from all the factors considered in the previous sections) the most recommendable HP system for location. With that aim, a numeric value has been given to each model depending on the suitability of the model according to the factor taken into account. In this way, the most appropriate HP system according to the specific factor is given the maximum score and so on. Figure 6 graphically shows the final evaluation of each geothermal system for each area.

In this way, Fig. 6 allows to make a reasonable and approximate estimation of which system is the most recommendable in each location. In general terms, and leaving aside the availability issues, GEHP systems would constitute the most optimal option among all the countries included in the study. However, since nowadays the implementation of these installations is highly linked to the existence of close biogas plants and specific heat pump devices, it is desirable to compare the two solutions that are currently feasible.

- In Italy, the first area of the study, EHP should be the selected option for a GSHP system. Although the initial investment of the GEHP with natural gas is lower, the environmental impact, and operational costs are more favourable for the electricity assumption.
- In area 2 (U.K.), the environmental impact is lower for the EHP but the economic aspect makes the GEHP aided by natural gas the most appropriate alternative.
- Finally, in Sweden (area 3), the EHP is again the most suitable option. However, if both systems were available, the selection of one or another system would have the same effect on the compendium of the economic and environmental factors. This selection will depend on the importance given to each of the mentioned variables.

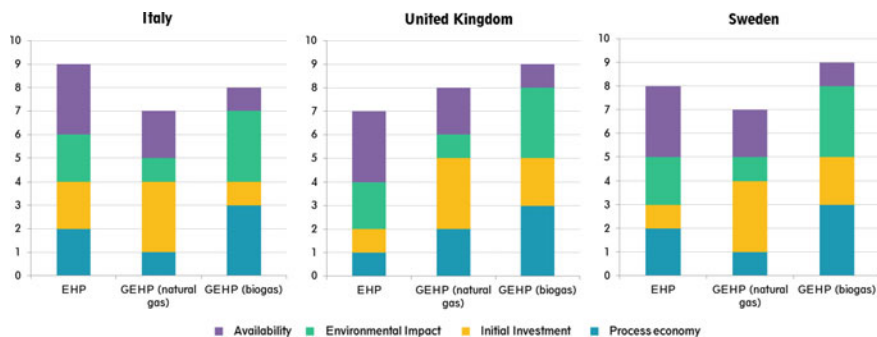


Fig. 6 Final evaluation of each system according to the factors discussed before

5 Conclusions

This research addresses a thorough analysis of the conventional geothermal heat pumps (electrically operated) and the less usual gas engine heat pumps (aided by natural gas and biogas). In general terms, and independently of the area where the geothermal systems aims to be installed, EHPs are characterized by high COPs (4–4.5), engine performances of around 90% and reduced electricity use. Meanwhile GEHPs usually achieve COPs of 1.5–1.6, need a refrigeration system and the engine performance is of only around 30%. Despite these facts, gas systems are less sensitive to the working fluid temperature due to the reuse of the residual heat.

This work is therefore concluded, stating that, for choosing one or another EHP or GEHP with natural gas or biogas is highly advisable to analyse the particular conditions of the energy mix of the area. It is also remarkable that biogas could mean an excellent alternative as the energy source of GEHP systems. This underused biofuel could aid the geothermal system being at the same time a solution for the management of fermentation waste and ground/water pollution. The feasibility of implementation of GEHP systems makes biogas a solution to be worldwide reproduced and used in heating and cooling purposes.

Acknowledgements Authors want to thank the Higher Polytechnic School of Avila, University of Salamanca (Department of Cartographic and Land Engineering), for providing their facilities in the experimental stages carried out in this research.

References

1. United Nations Framework Convention on Climate Change, (2015). Adoption of the Paris Agreement, 21st Conference of the Parties. United Nations, Paris. <https://unfccc.int/process-and-meetings/the-paris-agreement/the-paris-agreement>, Accessed 2 Sep 2018
2. DECC, Department for Energy and Climate Change, 2012. Emissions from heat: statistical summary. https://assets.publishing.service.gov.uk/government/uploads/system/uploads/attachment_data/file/140095/4093-emissions-heat-statistical-summary.pdf, Accessed 15 Jun 2018
3. Turner JA (1999) A realizable renewable energy future. *Science* 285(5428):687–688
4. Bromley CJ, Mongillo M, Hiriart G, Goldstein B, Bertani R, Huenges E, Ragnarsson A, Tester J, Muraoka H, Zui V (2010) Contribution of geothermal energy to climate change mitigation: the IPCC renewable energy report. In: Proceedings of the world geothermal congress, Bali, 25–30 April 2010, pp 25–29
5. Fridleifsson IB, Bertani R, Huenges E, Lund JW, Ragnarsson A, Rybach L (2008) The possible role and contribution of geothermal energy to the mitigation of climate change. IPCC Geothermal, Lübeck, Germany, pp 59–80
6. Hähnlein S, Molina-Giraldo N, Blum P, Bayer P, Grathwohl P (2010) Spread of cold plumes in groundwater with geothermal pipes. *Groundwater* [in German] 15:123–133
7. Rybach L (2005) The advance of geothermal heat pumps world-wide. *IEA Heat Pump Centre Newslett* 23:13–18
8. Curtis R, Lund J, Sanner B, Rybach L, Hellström G (2005) Ground source heat pumps—geothermal energy for anyone, anywhere: current worldwide activity. In: World geothermal congress, pp 24–9

9. Rybach L, Sanner B (2000) Ground-source heat pump systems—the European experience. *GHC Bull* 21:16–26
10. Forsén M (2011) The European market for heat pumps: heat pump outlook 2011. In: 4th EHPA European heat pump forum
11. Colangelo G, Romano D, De Risi A, Starace G, Laforgia D (2012) A tool in Matlab and Simulink for the simulation of geothermal heat pumps. *Thermotechnics* [In Italian] 4:63–72
12. Blázquez CS et al (2019) Technical optimization of the energy supply in geothermal heat pumps. *Geothermics* 81:133–142
13. European Commission (2019) Clean energy for all Europeans package
14. Pazera A et al (2015) Biogas in Europe: food and beverage (FAB) waste potential for biogas production. *Energy Fuels* 29.7:4011–4021
15. Alhassan KA, Abdullahi BT, Manjur Shah M (2019) A review on biogas production as the alternative source of fuel. *J Appl Adv Res* 4.2:61–65
16. International Energy Agency (IEA). <https://www.iea.org/>. Accessed 2019
17. European Statistics Office, “EUROSTAT”, <http://ec.europa.eu/eurostat/web/main/home>. Accessed 2019
18. Yang Z, CE L, Lian L (2017) Electricity price forecasting by a hybrid model, combining wavelet transform, ARMA and kernel-based extreme learning machine methods. *Appl Energy* 190:291–305
19. Vilar J, Aneiros G, Raña P (2018) Prediction intervals for electricity demand and price using functional data. *Int J Electr Power Energy Syst* 96:457–472
20. Yang Z, Ce Li, Lian Li (2017) Electricity price forecasting by a hybrid model, combining wavelet transform, ARMA and kernel-based extreme learning machine methods. *Appl Energy* 190:291–305
21. Shao Z et al (2017) A new electricity price prediction strategy using mutual information-based SVM-RFE classification. *Renew Sustain Energy Rev* 70:330–341
22. Hijazi O et al (2016) Review of life cycle assessment for biogas production in Europe. *Renew Sustain Energy Rev* 54:1291–1300
23. Kang JY, Kim TS, Hur KB (2014) Economic evaluation of biogas and natural gas co-firing in gas turbine combined heat and power systems. *Appl Thermal Eng* 70.1:723–731
24. Hartmann JK (2006) Life-cycle-assessment of industrial scale biogas plants. Diss. Niedersächsische Staats-und Universitätsbibliothek Göttingen
25. IRENA, International and Renewable Energy Agency (2014) Global bioenergy supply and demand projections, a working study for Remap 2030
26. Torrijos M (2016) State of development of biogas production in Europe. *Procedia Environ Sci* 35:881–889
27. International Energy Agency (IEA), task 37 Country Report Summaries (2019)
28. Gold T (1985) The origin of natural gas and petroleum, and the prognosis for future supplies. *Annual Review of Energy* 10(1):53–77
29. Hu G et al (2008) Preliminary study on the origin identification of natural gas by the parameters of light hydrocarbon. *Sci China Ser D: Earth Sci* 51.1:131–139
30. Institute for the Diversification and Energy Save (2014) “IDAE”, CO₂ emission factors and coefficients to convert the primary energy of different energy sources in the Spanish building sector
31. ALB SISTEMAS, Price list, Geothermal Systems [Spanish Company] (2019). <https://www.alb.es/>. Accessed 2019
32. ENERTRES, Price list, heat pump, [Spanish Company] (2018). <https://enertres.com/>. Accessed 2019

Transient Thermal-Resistance-Capacitance Model for U-Tube Ground Heat Exchanger



Quan Liao and Wenzhi Cui

Abstract In a GSHP system, one of the most important components is the ground-coupled heat exchanger through which the thermal energy is exchanged between heat carrier fluid (i.e., water or water-antifreeze fluid) and soil. Since the ground heat exchanger is responsible for a major part of the initial cost of GSHP system and the efficiency of this system depends on the performance of ground heat exchanger, a careful design of ground heat exchanger is crucial for a successful application of GSHP system. Although the simplified analytical model or 3D numerical model for single U-tube ground heat exchanger has been proposed in the past several decades, the transient thermal-resistance-capacitance model of ground heat exchanger has become more popular due to the high numerical precision and low computational demand. This chapter will discuss the above-mentioned transient thermal-resistance-capacitance model for the typical single U-tube ground heat exchanger, the corresponding thermal resistance network within a borehole, and how to determine the specific thermal resistances for different thermal resistance networks with a borehole.

Keywords Ground heat exchanger · Thermal resistance network · Borehole thermal resistance · Transient thermal-resistance-capacitance model

1 Introduction

In this chapter, typical thermal resistance network models, i.e., three-thermal-resistance model and four-thermal-resistance model, within a borehole will be described in the first section. Then, the methods to determine the specific thermal resistances for different thermal resistance networks within a borehole are proposed in the second section. Finally, an improved transient thermal-resistance-capacitance model (TRCM) is established and CFD validated in the last section.

Q. Liao · W. Cui (✉)

School of Energy and Power Engineering, Chongqing University, Chongqing 400030, China
e-mail: wzcui@cqu.edu.cn

Q. Liao

e-mail: Quanliao@cqu.edu.cn

© The Author(s), under exclusive license to Springer Nature Switzerland AG 2023

D. Borge-Diez and E. Rosales-Asensio (eds.), *Geothermal Heat Pump Systems*,
Green Energy and Technology, https://doi.org/10.1007/978-3-031-24524-4_5

1.1 Thermal Resistance Network Within a Borehole

Since the length of single U-tube borehole heat exchanger is relatively big in the vertical direction than that in the horizontal direction, the whole heat exchanger could be simplified as different horizontal slices which are piled up in vertical direction if the end of U-tube borehole heat exchanger could be ignored. Therefore, one could focus on the heat transfer process of horizontal slice with unit length, then the heat transfer performance of single U-tube borehole heat exchanger could be obtained.

According to the heat transfer process within borehole in the horizontal direction of a single U-tube borehole heat exchanger, the heat transfer between pipes, grout and ground material is relatively complicated due to the non-conformal position of pipes and composite material within borehole. Since the fully discretized Computational Fluid Dynamics (i.e., CFD) model within borehole will lead to extensive computation times and a substantial effort in terms of pre-processing work, and the simplified analytical model (i.e., the line source or cylinder source model) cannot provide the detailed quantitative amount of heat between pipes, grout and ground material during the heat transfer process, the concepts of thermal resistance between pipes and borehole wall were proposed in the past decades, and the so-called thermal resistance model within the borehole has been established to describe the heat transfer process and provide the enough information to analyze the heat transfer within borehole. Therefore, the balance of calculation precision and computation time could be reached for the heat transfer analysis of a single U-tube borehole heat exchanger.

1.1.1 Three-Thermal-Resistance Model

As far as the thermal resistance model was concerned, there are two kinds of the so-called three-thermal-resistance model to describe the heat transfer process within a borehole, as shown in Figs. 1 (i.e., Model A) and 2 (i.e., Model B). The Model A is usually adopted in the literature, however, from the point view of heat transfer process in the borehole, if the pipe conduction and carrier fluid convection heat transfer of inner side of pipes are taken into account, the detailed thermal resistance model could be obtained as the same as the Model B in Fig. 2 [1].

Under the condition of uniform thermal properties and symmetrical geometry within borehole, the following relationships could be obtained based on the law of conservation of energy for the three-thermal-resistance model as shown in Fig. 1.

$$q_1 = \frac{T_{f1} - T_b}{R_{f1-b}} + \frac{T_{f1} - T_{f2}}{R_{f1-f2}} \quad (1)$$

$$q_2 = \frac{T_{f2} - T_b}{R_{f2-b}} + \frac{T_{f2} - T_{f1}}{R_{f1-f2}} \quad (2)$$

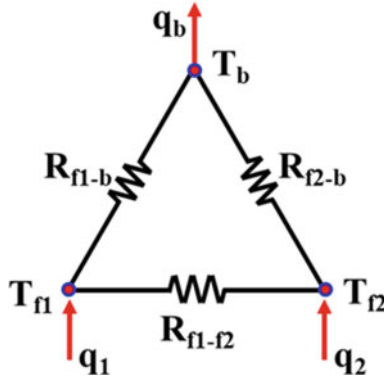


Fig. 1 Three-thermal-resistance network within a borehole (Model A)

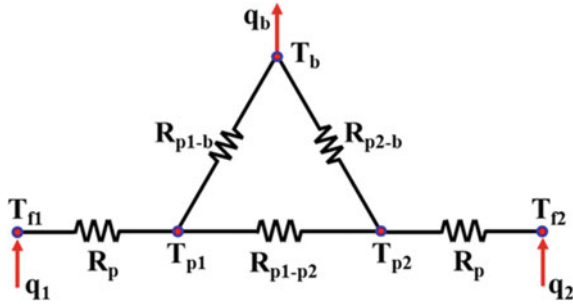


Fig. 2 Three-thermal-resistance network within a borehole (Model B)

where, T_b is the average temperature of borehole; T_{f1} and T_{f2} are the temperatures of carrier fluid at inlet and outlet pipes, respectively.

Based on the Eqs. (1) and (2), the thermal resistances of R_{f1-b} and R_{f1-f2} in Fig. 1 could be evaluated as follows.

$$R_{f1-b} = R_{f2-b} = \frac{T_{f1} + T_{f2} - 2T_b}{q_1 + q_2} \quad (3)$$

$$R_{f1-f2} = \frac{2(T_{f1} - T_{f2})}{q_1 - q_2 - \frac{T_{f1} - T_{f2}}{R_{f1-b}}} \quad (4)$$

According to the definitions of total internal thermal resistance (i.e., R_a) and the borehole thermal resistance (i.e., R_b) [4], the following evaluation equations could be obtained for R_b and R_a , respectively, based on the three-thermal-resistance network of Model A.

$$R_b = R_{f1-b} // R_{f2-b} = \frac{1}{2} R_{f1-b} \quad (5)$$

$$R_a = R_{f1-f2} / (R_{f1-b} + R_{f2-b}) \quad (6)$$

Therefore, the borehole thermal resistance and the total internal thermal resistance between two pipes could be evaluated as follows:

$$R_b = \frac{T_{f1} + T_{f2} - 2T_b}{2(q_1 + q_2)} \quad (7)$$

$$R_a = \frac{R_{f1-f2} * (R_{f1-b} + R_{f2-b})}{R_{f1-f2} + R_{f1-b} + R_{f2-b}} = \frac{R_{f1-f2} * 4R_b}{R_{f1-f2} + 4R_b} \quad (8)$$

where, R_{f1-f2} is the direct thermal resistance between two temperatures of carrier fluid as shown in Fig. 1, and R_b is the so-called borehole thermal resistance which is defined between the two temperatures of carrier fluid and borehole wall.

Rearrange the equation of the total internal thermal resistance R_a , i.e. Eq. (8), the following direct thermal resistance between two temperatures of carrier fluid, i.e. R_{f1-f2} , could be obtained as follows:

$$R_{f1-f2} = \frac{4R_b * R_a}{4R_b - R_a} \quad (9)$$

If the thermal resistances of convection heat transfer of carrier fluid and conduction heat transfer of pipes are taken into account in the thermal resistance network, the so-called three-thermal-resistance network of Model B could be obtained, as shown in Fig. 2 [1].

Based on the law of conservation of energy as shown in Fig. 2, the following relationships could be obtained.

$$q_1 = \frac{T_{f1} - T_{p1}}{R_p} = \frac{T_{p1} - T_b}{R_{p1-b}} + \frac{T_{p1} - T_{p2}}{R_{p1-p2}} \quad (10)$$

$$q_2 = \frac{T_{f2} - T_{p2}}{R_p} = \frac{T_{p2} - T_b}{R_{p2-b}} + \frac{T_{p2} - T_{p1}}{R_{p1-p2}} \quad (11)$$

where, T_{p1} and T_{p2} are the average temperature of outer diameter for inlet and outlet pipes, respectively.

Based on the Eqs. (10) and (11), the thermal resistances of R_{p1-b} and R_{p1-p2} in Fig. 2 could be evaluated as follows.

$$R_{p1-b} = R_{p2-b} = \frac{T_{p1} + T_{p2} - 2T_b}{q_1 + q_2} \quad (12)$$

$$R_{p1-p2} = \frac{2(T_{p1} - T_{p2})}{q_1 - q_2 - \frac{T_{p1} - T_{p2}}{R_{p1-b}}} \quad (13)$$

The thermal resistance of R_p , as shown in Fig. 2, includes two parts, i.e., the convection heat transfer thermal resistance of inner side of pipe and the conduction thermal resistance of pipe, which is defined as follows:

$$R_p = \frac{1}{\pi d_{pi} h_{pi}} + \frac{\ln\left(\frac{d_{po}}{d_{pi}}\right)}{2\pi k_p} \quad (14)$$

where, d_{pi} and d_{po} are the inner and outer diameters of pipe, respectively, h_{pi} is the convection heat transfer coefficient of inner side of pipe, and k_p is the thermal conductivity of pipe material.

According to the definitions of total internal thermal resistance (i.e., R_a) and the borehole thermal resistance (i.e., R_b), the following equations could be obtained based on the thermal resistance network as shown in Fig. 2.

$$R_b = (R_p + R_{p1-b}) / (R_p + R_{p2-b}) = \frac{1}{2}(R_p + R_{p1-b}) \quad (15)$$

$$R_a = 2R_p + R_{p1-p2} / (R_{p1-b} + R_{p2-b}) \quad (16)$$

Therefore, the evaluation formula for R_a and R_b in Model B could be obtained as follows:

$$R_b = \frac{1}{2} \left(R_p + \frac{T_{p1} + T_{p2} - 2T_b}{q_1 + q_2} \right) \quad (17)$$

$$R_a = 2R_p + \frac{R_{p1-p2} * (4R_b - 2R_p)}{R_{p1-p2} + 4R_b - 2R_p} \quad (18)$$

And the thermal resistance of R_{p1-p2} could be evaluated by the following equation.

$$R_{p1-p2} = \frac{2(R_a - 2R_p)(2R_b - R_p)}{4R_b - R_a} \quad (19)$$

Compare the Model A in Fig. 1 with the Model B in Fig. 2, one could find that if the R_p is neglected in Fig. 2, the Model B will be evolved into the Model A.

1.1.2 Four-Thermal-Resistance Model

In the above three-thermal-resistance network model (i.e., Model A in Fig. 1 or Model B in Fig. 2), the non-uniform temperature along the outer diameter of pipe is not taken into account, i.e., the uniform temperature of outer diameter of pipe is assumed, because the conductive thermal resistance and convective thermal resistance inside the pipe are assumed as constants, respectively. Furthermore, the temperature of borehole wall is assumed as constant in the three thermal resistance network models

[3]. As shown in Eq. (19), the so-called negative thermal resistance phenomena could be observed for the thermal resistance of R_{p1-p2} when the denominator is less than zero, i.e., the value of term of $4R_b - R_a$ is negative. On the one hand, the closer of pipes to the borehole wall, the smaller of borehole thermal resistance (i.e., R_b), the greater of internal thermal resistance (i.e., R_a), it is easier to make the value of $4R_b - R_a$ be less than zero; on the other hand, the greater of thermal conductivity for grout material, the smaller of borehole thermal resistance R_b and the internal thermal resistance R_a , then, the negative value of $4R_b - R_a$ could be satisfied as well. Since the value of borehole thermal resistance R_b and internal thermal resistance R_a are always positive, the sign of term of $4R_b - R_a$ will decide the sign of the thermal resistance R_{p1-p2} , as shown in Eq. (19). This is the reason that the negative thermal resistance phenomena is usually observed when the position of pipes are closer to the borehole wall or the thermal conductivity of grout material is greater than that of the ground material [3].

In the real industrial application, the temperature distribution along the outer diameter of pipes and borehole wall can not be uniform, it will be somewhat symmetrical distribution along the symmetrical line of pipes or between two pipes, as shown in Fig. 3. Although the temperatures of pipes are not uniform, the temperature difference for each pipe is relatively smaller than that of the borehole wall. Therefore, if the assumptions of uniform wall temperature for the pipes are still held and the non-uniform temperature distribution along the borehole wall is taken into account, the so-called four thermal resistance network model is proposed as shown in Fig. 4 [3].

Based on the law of conservation of energy, the following equations could be obtained for the four-thermal-resistance network within a borehole.

$$q_1 = \frac{T_{p1} - T_{b1}}{R_{p1-b1}} + \frac{T_{p1} - T_{p2}}{R_{p1-p2}^*} \quad (20)$$

$$q_2 = \frac{T_{p2} - T_{b2}}{R_{p2-b2}} + \frac{T_{p2} - T_{p1}}{R_{p1-p2}^*} \quad (21)$$

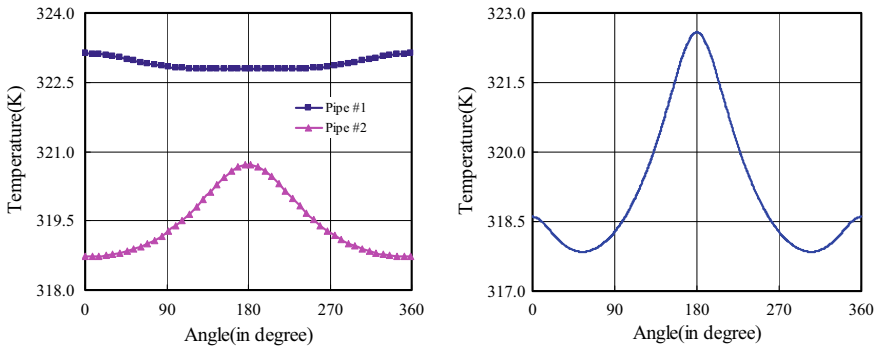


Fig. 3 Temperature distribution of pips and borehole wall

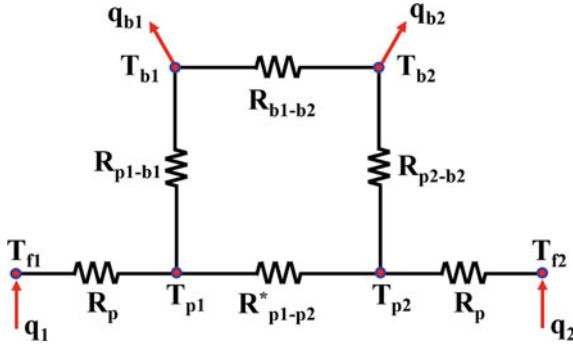


Fig. 4 Four-thermal-resistance network within a borehole

Using the Eqs. (20) and (21), the thermal resistances of R_{p1-b1} and R_{p1-p2}^* could be evaluated by the following equations.

$$R_{p1-b1} = R_{p2-b2} = \frac{T_{p1} + T_{p2} - (T_{b1} + T_{b2})}{q_1 + q_2} \quad (22)$$

$$R_{p1-p2}^* = \frac{T_{p1} - T_{p2}}{q_1 - \frac{T_{p1} - T_{b1}}{R_{p1-b1}}} = \frac{T_{p2} - T_{p1}}{q_2 - \frac{T_{p2} - T_{b2}}{R_{p2-b2}}} = \frac{2(T_{p1} - T_{p2})}{q_1 - q_2 - \frac{(T_{p1} - T_{p2}) - (T_{b1} - T_{b2})}{R_{p1-b1}}} \quad (23)$$

Based on the law of conservation of energy in Fig. 4, the thermal resistance of R_{b1-b2} could be evaluated as follows.

$$R_{b1-b2} = \frac{2(T_{b2} - T_{b1})}{q_{b1} - q_{b2} - \frac{(T_{p1} - T_{p2}) - (T_{b1} - T_{b2})}{R_{p1-b1}}} \quad (24)$$

According to the definitions of R_a and R_b , the following equations could be obtained.

$$R_b = (R_p + R_{p1-b1}) / (R_p + R_{p2-b2}) = \frac{1}{2}(R_p + R_{p1-b1}) \quad (25)$$

$$R_a = 2R_p + R_{p1-p2}^* / (R_{p1-b1} + R_{b1-b2} + R_{p2-b2}) \quad (26)$$

Therefore, the thermal resistances of R_a and R_b in the four thermal resistance network model could be evaluated as follows.

$$R_b = \frac{1}{2}(R_p + R_{p1-b1}) \quad (27)$$

$$R_a = 2R_p + \frac{R_{p1-p2}^* (2R_{p1-b1} + R_{b1-b2})}{R_{p1-p2}^* + 2R_{p1-b1} + R_{b1-b2}} \quad (28)$$

And the direct thermal resistance of R_{p1-p2}^* in Fig. 4 could be evaluated by the following equation.

$$R_{p1-p2}^* = \frac{(R_a - 2R_p) * (4R_b - 2R_p + R_{b1-b2})}{4R_b - R_a + R_{b1-b2}} \quad (29)$$

Based on the above four-thermal-resistance network within a borehole in Fig. 4, it could be seen that the results of R_a and R_b are as the same as the three thermal resistance network, i.e., Model A and Model B. As far as the four-thermal-resistance network was concerned, the evaluation formula of R_b is the same as that of three-thermal-resistance of Model A and Model B. However, it should be emphasized that the evaluation formula of R_a in four-thermal-resistance model is different than that of the three-thermal-resistance of Model A or Model B.

1.2 How to Determine the Specific Thermal Resistances

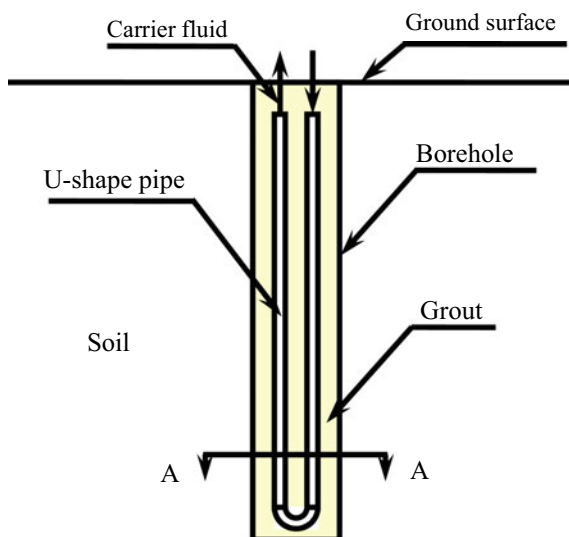
Based on the above mentioned either three-thermal-resistance network model or four-thermal-resistance network model within a borehole, it is necessary to determine the values of each thermal resistance corresponding to the different thermal resistance network model for specific thermal properties and geometrical parameters of a single U-tube ground heat exchanger. Due to the nonconformal geometry of borehole, the heat transfer process between the pipes, grout material and soil are very complicated, and it is impossible to find the analytical solution for a specific single U-tube ground heat exchanger. Therefore, the numerical simulation is adopted to analyze the heat transfer process within borehole, and the corresponding amount of heat transferred between pipes and borehole wall could be evaluated and so do the average temperatures of outer wall temperature of pipes and borehole. In this section, the CFD method will be introduced to obtain the above-mentioned parameters in order to determine all the thermal resistances for different thermal resistance network model within a borehole.

1.2.1 Dimensionless Parameters and Borehole Thermal Resistance

For a typical single U-tube ground heat exchanger (as shown in Fig. 5), a U-shape pipe is vertically and symmetrically inserted in a borehole and the gap between pipes and borehole wall is filled by grout material. A heat carrier fluid is circulated in the U-shape pipe and heat is exchanged between carrier fluid and soil through pipes and grout within the borehole [1].

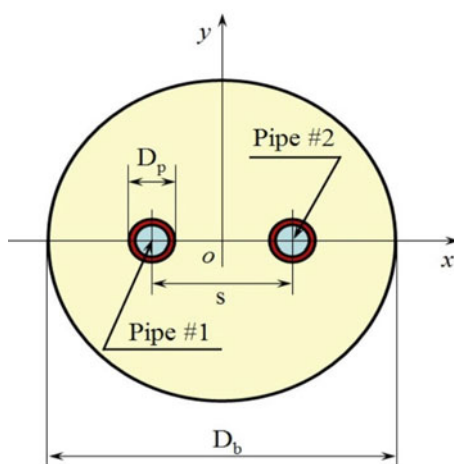
Since the borehole thermal resistance, which is defined as the thermal resistance between the outside diameter of pipes and borehole wall for a unit length of ground

Fig. 5 Schematic diagram of a typical single U-tube ground heat exchanger



heat exchanger, plays a dominant role to size the ground heat exchanger, some analytical and numerical models were proposed to estimate it based on the 2D heat conduction problem with different geometry parameters and thermal properties of soil and grout, as shown in Fig. 6. The geometry parameters of the single U-tube ground heat exchanger could be described by borehole diameter, D_b , outer diameter of pipe, D_p , and shank spacing, S . The thermal conductivities of soil and grout are k_s and k_g , respectively; therefore, four dimensionless variables of ground heat exchanger could be defined as follows:

Fig. 6 Schematic diagram of A-A cross-section view in Fig. 5



$$\theta_1 = \frac{S}{D_b} \quad (30)$$

$$\theta_2 = \frac{D_b}{D_p} \quad (31)$$

$$\theta_3 = \frac{D_p}{2S} = \frac{1}{2\theta_1 \cdot \theta_2} \quad (32)$$

$$\sigma = \frac{k_g - k_s}{k_g + k_s} \quad (33)$$

Shonder and Beck [4] simplified the complicated geometry parameters of the ground heat exchanger and treated U-shape pipes as a single coaxial pipe with an equivalent diameter that has the same cross section area as those of the U-shape pipes. Therefore, the complex geometry of borehole is represented as a coaxial pipe, and the borehole thermal resistance was given as:

$$R_b = \frac{1}{2\pi \cdot k_g} \ln\left(\frac{\theta_2}{\sqrt{n}}\right) \quad (34)$$

where, n is the number of pipes within the borehole, k_g is the thermal conductivity of grout material. Since this simple model neglects the thermal interference between the pipes, the borehole thermal resistance of Eq. (34) is not the function of shank spacing, i.e., S .

Sharqawy et al. [5] developed a 2D numerical model that assumes steady-state heat conduction within the borehole. The different geometry of the U-tube ground heat exchanger and the thermal property of grout were considered in the simulations. After numerous simulations were performed, a best-fit correlation was obtained for the borehole thermal resistance (i.e., R_b) as follows:

$$R_b = \frac{1}{2\pi \cdot k_g} [-1.49 \cdot \theta_1 + 0.656 \ln(\theta_2) + 0.436] \quad (35)$$

Although Sharqawy claimed that the accuracy of Eq. (35) to estimate the borehole thermal resistance is better than other available formulas in the literature, Lamarche et al. [2] pointed out the boundary conditions (i.e., uniform temperature distributions for the borehole wall and outside diameter of pipes, respectively) adopted in the 2D model by Sharqawy is not consistent with the real physical situation. An improved 2D numerical model was developed and solved by using COMSOLTM finite element software. This improved 2D model considers the soil surrounding the borehole region, and the distance between the inner and outer soil surface is much greater than the diameter of borehole. Since the isothermal boundary conditions are imposed at the outside diameter of pipes and soil outer surface, there is no more constrain for the temperature distribution along the perimeter of borehole and the

non-uniform temperature distribution on the borehole was observed. After comprehensive comparisons of borehole thermal resistance between the existing formulas and numerical simulation data, Lamarche concluded the equation proposed by Bennet et al. [6] gives the best estimation for the borehole thermal resistance, and the root mean square error between the simulation data and the Bennet formula is less than 0.003. The equation of borehole thermal resistance proposed by Bennet et al. is as follows:

$$R_b = \frac{1}{4\pi \cdot k_g} \left[\ln \left(\frac{\theta_2}{2\theta_1(1 - \theta_1^4)^\sigma} \right) - \frac{\theta_3^2 \cdot \left(1 - \frac{4\sigma \cdot \theta_1^4}{1 - \theta_1^4}\right)^2}{1 + \theta_3^2 \cdot \left(1 + \frac{16\sigma \cdot \theta_1^4}{(1 - \theta_1^4)^2}\right)} \right] \quad (36)$$

where, all the dimensionless parameters are defined in Eqs. (30)–(33), k_g and k_s are thermal conductivities of grout and soil, respectively.

Although the improved 2D model by Lamarche et al. considered the non-uniform temperature distribution on the borehole wall, the isothermal boundary conditions are still imposed at the outside diameter of pipes. Unfortunately, in a real physical situation using a ground heat exchanger, not only is the temperature distribution at the borehole wall non-uniform, but also that at outside diameter of the pipes is non-uniform. All these angular variations of temperature at the borehole wall and outside diameter of the pipes are due to the symmetrical arrangement of pipes, temperature differences of carrier fluid between pipes, and the thermal conductivities of pipe, grout, and soil. In order to consider the influence of non-uniform temperature at the outside diameter of pipes to the borehole thermal resistance, the thickness of pipes are taken into account by a new 2D numerical model in this chapter, and the third kind of boundary conditions (i.e., the temperature of carrier fluid and heat transfer coefficient are given) are imposed at the inner diameter of pipes.

After systematically selecting dimensionless geometrical variables and thermal properties of grout and soil in a ground heat exchanger, the new 2D numerical model was solved by Fluent 6.3.26 software and the borehole thermal resistances could be obtained based on the average temperatures of outside diameter of pipes and average temperature of borehole wall. Eventually, a new best-fit correlation for the borehole thermal resistance is proposed by using the Nelder Mead method [7] and comprehensive comparisons between the proposed correlation and the available formulas in the literature are presented in this section.

1.2.2 Heat Transfer Simulation Within Borehole

In order to consider the non-uniform temperature distributions at the borehole wall and outside diameter of pipes, a 2D numerical model consisting of soil, grout, and thickness of pipes were developed. The geometrical configuration and meshes of this new model are presented in Fig. 7.

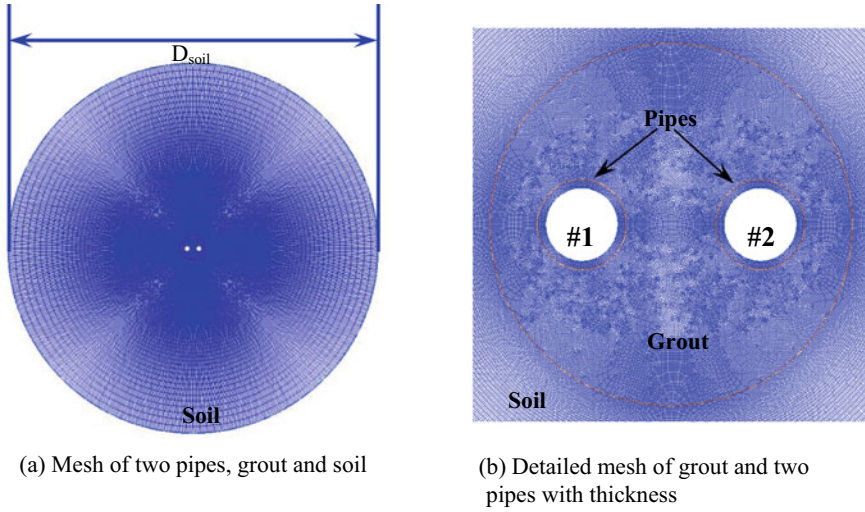


Fig. 7 Computational domain and meshes in a new 2D model

The diameter of computational domain (D_{soil}), diameter of borehole (D_b), outer diameter of pipes (D_p), shank spacing (S), thickness of pipes (δ), and thermal conductivity of pipes (k_p) in the numerical model are given in Table 1. In a real U-tube, since the minimum bending diameter is 1.5 times of outer diameter of pipe, the range of shank spacing is between $1.5D_p$ and $D_b - D_p$.

In order to solve the above 2D heat conduction problem, some assumptions have to be made as follows:

1. Steady-state 2D heat conduction is assumed for this numerical model;
2. The materials (including soil, grout and pipes) are homogenous and all the thermal properties are independent of temperature;

Under the above assumptions, the governing equation of 2D steady-state heat conduction in a Cartesian x - y coordinate system could be written as:

$$\frac{\partial^2 T}{\partial x^2} + \frac{\partial^2 T}{\partial y^2} = 0 \quad (37)$$

The boundary conditions for the above governing equation are as follows: constant temperature is imposed at the outer boundary of computational domain and the

Table 1 Range of parameters in present 2D numerical model

$D_{soil}(m)$	$D_b(m)$	$D_p(m)$	$S(m)$	$\delta(m)$	$k_p(W/m-K)$
4.0	0.13–0.2	0.025–0.065	$1.5D_p - (D_b - D_p)$	0.003	0.44

third kind of boundary condition (i.e., the carrier fluid temperature and heat transfer coefficient are given) is imposed at the inner diameter of #1 and #2 pipe surfaces.

The four-thermal-resistance network model is adopted to evaluate the borehole thermal resistance, i.e., R_b . As shown in Fig. 4, due to the symmetrical arrangement of borehole, the thermal resistance R_{lb} is equal to R_{2b} and the borehole thermal resistance could be written as:

$$R_b = \frac{R_{1b}}{2} = \frac{R_{2b}}{2} = \frac{(T_{p1} + T_{p2}) - (T_{b1} + T_{b2})}{2 \cdot (q_1 + q_2)} \quad (38)$$

$$R_{12} = \frac{2(T_{p1} - T_{p2})}{q_1 - q_2 - [(T_{p1} - T_{p2}) - (T_{b1} - T_{b2})]/R_{b1}} \quad (39)$$

$$R_{b12} = \frac{2(T_{p1} - T_{p2})}{q_{b1} - q_{b2} + [(T_{p1} - T_{p2}) - (T_{b1} - T_{b2})]/R_{b1}} \quad (40)$$

where, T_{p1} and T_{p2} are the average temperatures at outer diameter of pipe #1 and pipe #2, respectively; T_{b1} and T_{b2} are the average temperatures with half perimeter of borehole wall surface, as shown in Fig. 6. The symbols of q_1 and q_2 are the rate of heat transfer from pipe #1 and pipe #2, respectively. The q_{b1} and q_{b2} are the rate of heat transfer from half perimeter of borehole wall surface, respectively.

1.2.3 Correlations of Thermal Resistance Within Borehole

The simulations of new 2D model for a ground heat exchanger were systematically carried out for the different combinations of dimensionless parameters of θ_1 , θ_2 and σ . At end of each simulation, the borehole thermal resistance, i.e., R_b , could be obtained by using Eq. (38). In this section, 744 numerical simulations were systematically conducted and all the data of R_b , θ_1 , θ_2 and σ were collected. The Nealder Mead method was adopted to obtain the relationship between these primary simulation data sets of R_b , θ_1 , θ_2 and σ . Eventually, a best-fit correlation for the borehole thermal resistance, i.e., R_b , is obtained.

$$R_b = \frac{1}{2\pi\lambda_g} \left[-0.50125 \ln(\theta_1) + 0.51248 \ln(\theta_2) + 0.51057\sigma \cdot \ln\left(\frac{1}{1-\theta_1^4}\right) - 0.36925 \right] \quad (41)$$

$$R_{12} = \frac{1}{\lambda_g} (0.030455 \cdot \theta_2 + 0.0020030 \cdot \sigma^2 + 0.0065003 \cdot \sigma - 0.026484) e^{(0.10664\sigma + 4.7420)\theta_1} \quad (42)$$

$$R_{b12} = \frac{1}{\lambda_g} \left(\frac{0.25920 \cdot \sigma + 0.94137}{-\frac{0.25161 \cdot \sigma + 0.79423}{\ln(\theta_2)}} \right) e^{\left(0.18494 \cdot \sigma - 0.93402 + \frac{1.7547 - 0.16530 \cdot \sigma}{\ln(\theta_2)}\right) \frac{1}{\theta_1}} \quad (43)$$

For all these 744 simulation data sets, the relative error range of correlations for pipe-to-borehole thermal resistance (i.e., R_b), pipe-to-pipe thermal interference resistance (i.e., R_{12}) and borehole-to-borehole thermal resistance (i.e., R_{b12}) are from -1.7 to 3.08% , from -6.68 to 7.29% and from -14.5 to 11.4% , respectively. The root mean square errors for these three thermal resistance correlations are $3.06\text{E}-4$, $1.66\text{E}-2$ and $1.39\text{E}-2$, respectively. Therefore, the Eqs. (41)–(43) are relatively accurate enough to estimate the pipe-to-borehole thermal resistance, pipe-to-pipe thermal interference resistance and borehole-to-borehole thermal resistance within the range of dimensionless parameters $-0.214 \leq \theta_1 \leq 0.85$, $2.5 \leq \theta_2 \leq 7.0$ and $-0.2 \leq \sigma \leq 0.6$.

1.2.4 Comparison of Borehole Thermal Resistance Between Correlations

To show the differences between the present correlation and available formulas to estimate the borehole thermal resistance, the comparisons between present correlation, Bennet equation, i.e., Eq. (36), and Sharqawy formula, i.e., Eq. (35), are presented with different combinations of dimensionless parameters θ_1 , θ_2 and σ , as shown in Figs. 8 and 9.

As shown in Figs. 8 and 9, the relationships between $2\pi \cdot k_g \cdot R_b$ and σ are presented at the condition of $\theta_2 = 4$, $\theta_1 = 0.375$ or $\theta_1 = 0.7$. Since the correlation of Sharqawy is not the function of σ , the dimensionless thermal resistance of Eq. (35) is independent of thermal conductivity of soil. Comparing Figs. 10 and 11, one could find the differences of $2\pi \cdot k_g \cdot R_b$ between the present correlation, and Eq. (36) decreases as the dimensionless parameters θ_1 and σ increase. This could be explained as follows. On the one hand, with the increase of θ_1 , the distance between two pipes increases for a given borehole diameter, and the influence of temperature differences between two

Fig. 8 Comparisons of dimensionless borehole thermal resistance at $\theta_1 = 0.375$ and $\theta_2 = 4$ when σ is between -0.2 and 0.6

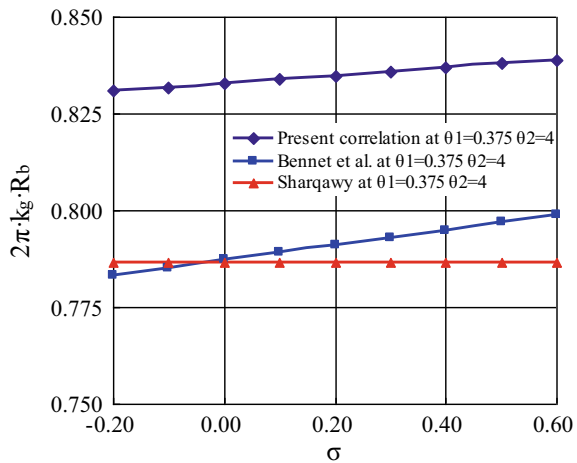
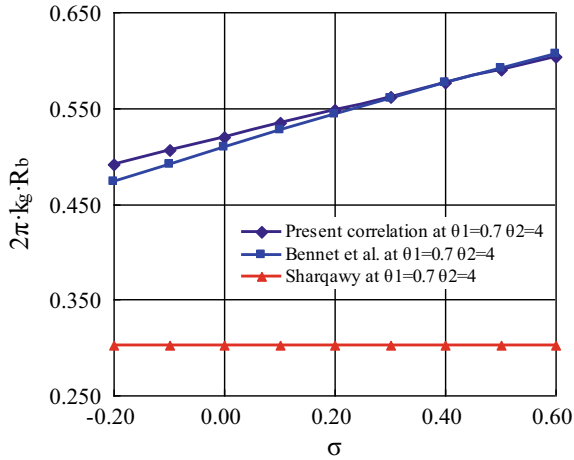


Fig. 9 Comparisons of dimensionless borehole thermal resistance at $\theta_1 = 0.7$ and $\theta_2 = 4$ when σ is between -0.2 and 0.6



carrier fluids in pipes to the non-uniform temperature distribution at outside diameter of pipes decreases. Therefore, the temperature distributions at the outside diameter of pipes become more uniform, and the differences between the third kind of boundary condition in the present model and isothermal boundary condition in Lamarche’s model get decreased. On the other hand, as σ increases, the thermal conductivity of soil decreases for a given grout thermal conductivity and the total rate of heat transfer from borehole wall to soil decreases. Therefore, the temperature distributions at the outside diameter of pipes become uniform and the difference of boundary condition between the present model and Lamarche’s model gets decreased.

In Figs. 10 and 11, the relationships between $2\pi \cdot k_g \cdot R_b$ and θ_1 are presented at the condition of $\sigma = 0.1$, $\theta_2 = 3.5$ or $\theta_2 = 7.0$. From these two figures, it could be seen that these three correlations have the similar trend as θ_1 increases, i.e., the dimensionless

Fig. 10 Comparisons of dimensionless borehole thermal resistance at $\sigma = 0.1$ and $\theta_2 = 3.5$ when θ_1 is between 0.43 and 0.7

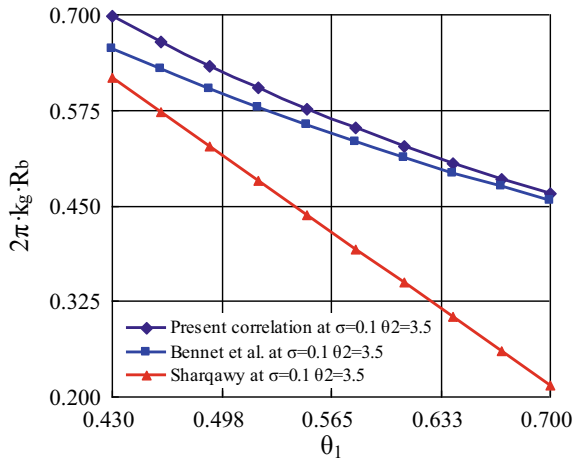
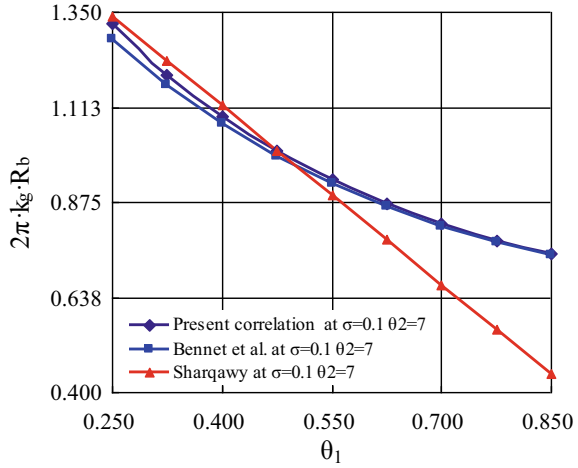


Fig. 11 Comparisons of dimensionless borehole thermal resistance at $\sigma = 0.1$ and $\theta_2 = 7.0$ when θ_1 is between 0.25 and 0.85



borehole thermal resistance of these three correlations decreases with an increase of θ_1 ; however, the differences between the present correlation (or Bennet equation) and the Sharqawy formula increase as θ_1 increases because the non-uniform temperature distribution at both outside diameter of pipes and borehole become worse as the dimensionless parameter θ_1 increases. On the other hand, the change of differences between the present correlation and the Bennet equation in Figs. 10 and 11 decreases in terms of $2\pi \cdot k_g \cdot R_b$ when θ_1 or θ_2 increases. The same reasons adopted in Figs. 8 and 9 could be explained for the changes of $2\pi \cdot k_g \cdot R_b$ v.s. θ_1 in Figs. 10 and 11.

As shown in Figs. 12 and 13, the relationships between $2\pi \cdot k_g \cdot R_b$ and θ_2 are presented at the condition of $\theta_1 = 0.5$, $\sigma = -0.2$ or $\sigma = 0.6$. From these two figures, one could clearly see these three correlations have the similar trend of $2\pi \cdot k_g \cdot R_b$ v.s. θ_2 at the different values of σ when θ_2 increases, i.e., the dimensionless borehole thermal resistance gradually increases for a given σ ; however, comparing these two figures, the influence of σ to the value of $2\pi \cdot k_g \cdot R_b$ is much smaller than that of θ_2 . On the other hand, it clearly shows the value of $2\pi \cdot k_g \cdot R_b$ in the present correlation is always higher than that of the Bennet equation and/or Sharqawy formula due to the difference in boundary conditions at the outside diameter of pipes and the borehole for these three models.

1.3 How to Establish the Transient Thermal-Resistance-Capacitance Model

At present there exist three kinds of model to describe the transient heat transfer process for the ground heat exchanger, i.e., analytical model (i.e., line or cylindrical source model), numerical model (i.e., 3D finite volume or finite element model) and thermal-resistance-capacitance model (TRCM) [8–13]. Since the analytical model

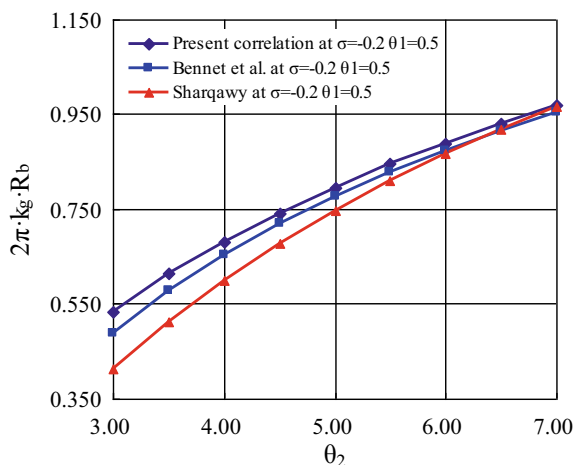


Fig. 12 Comparisons of dimensionless borehole thermal resistance at $\sigma = -0.2$ and $\theta_1 = 0.5$ when θ_2 is between 3.0 and 7.0

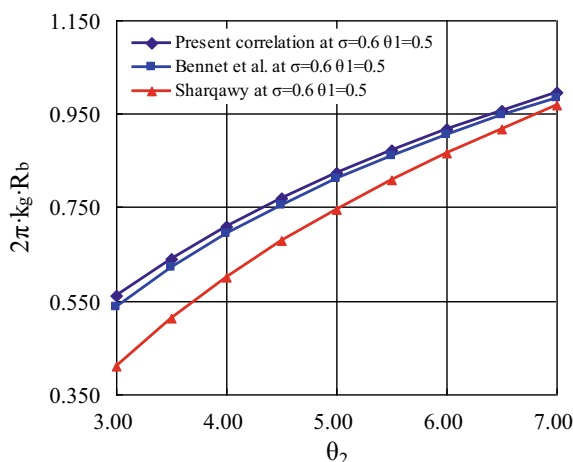


Fig. 13 Comparisons of dimensionless borehole thermal resistance at $\sigma = 0.6$ and $\theta_1 = 0.5$ when θ_2 is between 3.0 and 7.0

ignores the details of the complicated geometry of the U-tube within a borehole and the differences in thermal properties of the backfilled grout and surrounding soil, it is usually not suitable to evaluate the performance of ground heat exchanger in a short-term transient heat transfer process, and this is the reason that about 10 h data from the beginning time should be discarded to interpret the Thermal Responses Test (TRT) data by using the line source or cylindrical source model [14, 15]. Although all these disadvantages of analytical models could be overcome by the 3D numerical model,

the shortcomings become the dominant barrier in the real application of 3D numerical model for ground heat exchanger such as substantial effort to establish 3D model and large computational demand to mesh and solve the model. Since the lumped parameter method is adopted in the TRCM of ground heat exchanger, some advantages could be obtained such as less time-consuming to solve, relatively high accurate results and easy to establish the parameter-based model, and several TRCMs [16, 17] were proposed in recent years based on the different thermal-resistance-capacitance networks to describe the heat transfer process within a borehole. For a conventional TRCM of vertical single U-tube ground heat exchanger, which is based on three-thermal-resistance-capacitance network within the borehole, a uniform temperature distribution is assumed along the perimeter of borehole to simplify the heat transfer process between tubes, grout and surrounding soil in the horizontal plane. Unfortunately, this assumption of uniform temperature might lead to a negative heat flux between downward and upward tubes (i.e., the heat flows from the lower temperature region around cold tube to the higher temperature region around hot tube) under certain geometrical conditions for the three-thermal-resistance-capacitance network within the borehole [2, 18, 19], which is physically not possible and incorrect due to the negative thermal resistance [19, 20]. As a matter of fact, the temperature distribution along the perimeter of borehole cannot be uniform on each horizontal plane because the temperature difference always exists for the carrier fluid between downward and upward tubes of the ground heat exchanger with cooling/heating work mode. The magnitude of temperature difference along the perimeter of borehole depends on the temperature of carrier fluid, the thermal properties of tube, grout and soil, and it actually presents a kind of symmetrical distribution along the perimeter of borehole due to the symmetrical arrangement in a typical vertical single U-tube ground heat exchanger with uniform and constant thermal properties.

In this section, a four-thermal-resistance-capacitance network is adopted to describe the horizontal heat transfer process within a borehole for vertical single U-tube ground heat exchanger, in which the borehole perimeter is divided into two equal parts along the symmetrical line and the effect of non-uniform temperature distribution along borehole perimeter could be taken into account [3]. Based on this four-thermal-resistance-capacitance network, the fluid flow and heat transfer in horizontal/vertical direction and the thermal capacitances of carrier fluid, tube, grout and surrounding soil are all considered to analyse the transient heat transfer process of ground heat exchanger, and then an improved TRCM could be developed and solved for a vertical single U-tube ground heat exchanger. The comprehensive comparisons between the proposed TRCM with four-thermal-resistance-capacitance network, conventional TRCM with three-thermal-resistance-capacitance network and 3D finite volume CFD model by using Fluent software have been conducted. Based on the benchmark results of 3D finite volume CFD model, it shows that the results of the proposed TRCM are very consistent with those of 3D finite volume CFD model and this TRCM has relatively higher accuracy than the conventional TRCM, especially in the beginning short period of time for transient heat transfer process. Since the proposed TRCM is much easier, simpler and less time-consuming to solve than the 3D finite volume CFD model and the accuracy of numerical results

are good enough for the ground heat exchanger in the real industrial applications, it is possible and feasible to adopt this improved TRCM for the design, optimization and operation monitoring of ground heat exchanger, data interpretation of TRT and other real industrial applications in which the model of vertical single U-tube ground heat exchanger is required.

1.3.1 Conventional TRCM for Ground Heat Exchanger

As far as the conventional TRCM of vertical single U-tube ground heat exchanger was concerned, a uniform temperature distribution is assumed along the perimeter of borehole (i.e., $T_{b,1}$ is equal to $T_{b,2}$ as shown in Fig. 4) and a three-thermal-resistance-capacitance network is adopted to describe the heat transfer process within a borehole. Therefore, the horizontal heat transfer process within the borehole could mainly depend on the three thermal resistances and two equal thermal capacitances as shown in Fig. 15, where R_{b1} and R_{b2} are the two equal thermal resistances between outer surface of tubes and borehole wall per unit depth, R_{p12} is the thermal resistance between two outer surface of tubes per unit depth, and C_g is the half thermal capacitance of grout material with unit depth due to the symmetrical structure and uniform thermal properties.

All the thermal resistances (i.e., R_{b1} , R_{b2} and R_{p12} as shown in Fig. 15) could be determined through the following equations [5].

$$R_b = \frac{1}{2\pi k_g} [-1.49\theta_1 + 0.656\ln(\theta_2) + 0.436] \quad (44)$$

$$R_a = \frac{1}{\pi k_g} \left[\ln \left(\frac{2\theta_2(\theta_1^{-2} + 1)^\sigma}{\theta_1^{-1}(\theta_1^{-2} - 1)^\sigma} \right) - \frac{\theta_3^2 \left(1 + \frac{4\sigma\theta_1^{-2}}{\theta_1^{-4} - 1} \right)^2}{4 - \theta_3^2 + \frac{8\sigma\theta_1^{-2}\theta_3^2(\theta_1^{-4} + 1)}{(\theta_1^{-4} - 1)^2}} \right] \quad (45)$$

$$R_{p12} = \frac{4R_b R_a}{4R_b - R_a} \quad (46)$$

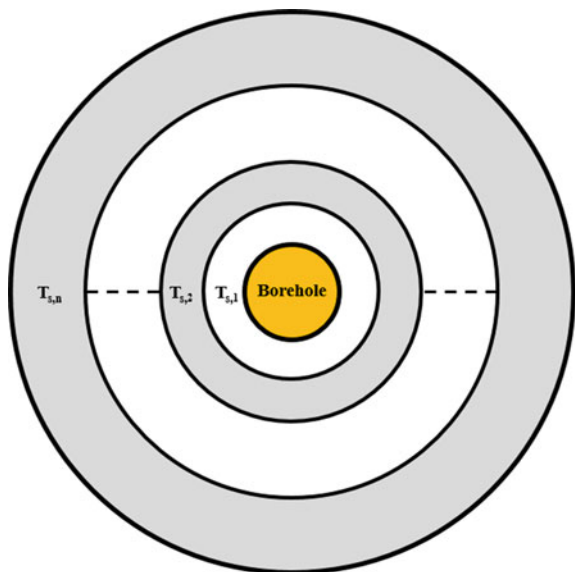
$$R_{b1} = R_{b2} = 2R_b \quad (47)$$

where, the dimensionless parameters (i.e., θ_1 , θ_2 , θ_3 and σ) are defined as the same as before.

Due to the cylindrical structure of ground heat exchanger and the assumed uniform temperature along the perimeter of borehole, the horizontal heat transfer process of soil region could be easily simplified as serial thermal-resistance-capacitance network by adjacent concentric soil layers with different radius, as shown in Fig. 14.

If the temperature and velocity gradients of carrier fluid within downward and upward tubes are neglected at each horizontal plane, the average temperature

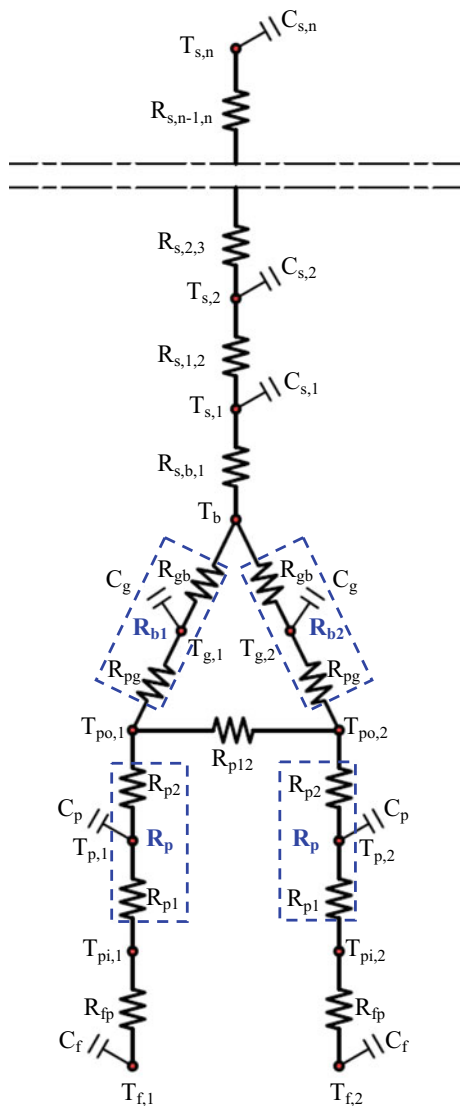
Fig. 14 Horizontal thermal-resistance-capacitance network for the soil region in a conventional TRCM of ground heat exchanger



and velocity of carrier fluid would be adopted, and the three-thermal-resistance-capacitance series network for unit depth of ground heat exchanger could be obtained at each horizontal plane, as shown in Fig. 15, based on the three-thermal-resistance-capacitance network within a borehole (i.e., as shown in Fig. 2) and serial thermal-resistance-capacitance network in soil region (i.e., as shown in Fig. 14). Since the average temperature has been used for carrier fluid, the location of corresponding thermal capacitance is assigned at the same place as that of carrier fluid temperature. In order to determine the specific locations of thermal capacitance for tube, grout and soil, the method of equivalent mass center described in Bauer et al. [21] is adopted in this section. Therefore, the thermal resistance between the outer and inner surface of tube or between the outer surface of tube and borehole wall (i.e., R_{b1} or R_{b2} as shown in Fig. 15) could be divided into two portions. As shown in dashed rectangle region in Fig. 15, the summation of R_{p1} and R_{p2} is the thermal resistance (i.e., R_p) between outer and inner surface of tube that could be evaluated by the classical thermal resistance formula of cylindrical wall, the summation of R_{pg} and R_{gb} is the thermal resistance (i.e., R_{b1} or R_{b2}) between outer surface of tube and borehole, and the locations of thermal capacitance (or temperature) for tube and grout material could be assigned at the connection point of these two portions of thermal resistance, respectively. The R_{fp} is the thermal resistance of convection heat transfer between the carrier fluid and inner surface of tube with unit depth, which could be evaluated by the Dittus-Boelter equation [22].

Once the horizontal transient heat transfer process for unit depth of ground heat exchanger is described by the three-thermal-resistance-capacitance series network as shown in Fig. 15, all these horizontal networks could be piled up to describe the transient heat transfer process of ground heat exchanger according to the flow

Fig. 15 Three-thermal-resistance-capacitance series network for unit depth of ground heat exchanger at horizontal plane



direction of carrier fluid and the vertical heat conduction of tube, grout and soil, and then the so-called conventional TRCM is obtained as shown in Fig. 16, in which the thermal capacitances of all components (including carrier fluid, tube, grout and soil) and the horizontal or vertical heat conduction are all taken into account.

As shown in Fig. 16, the heat transport relationships between the equal depth δz of layer $i - 1$, i and $i + 1$ are clearly presented. Take the i th layer of ground heat exchanger as an example, the equations of transient heat transfer could be obtained by using the conservation law of energy.

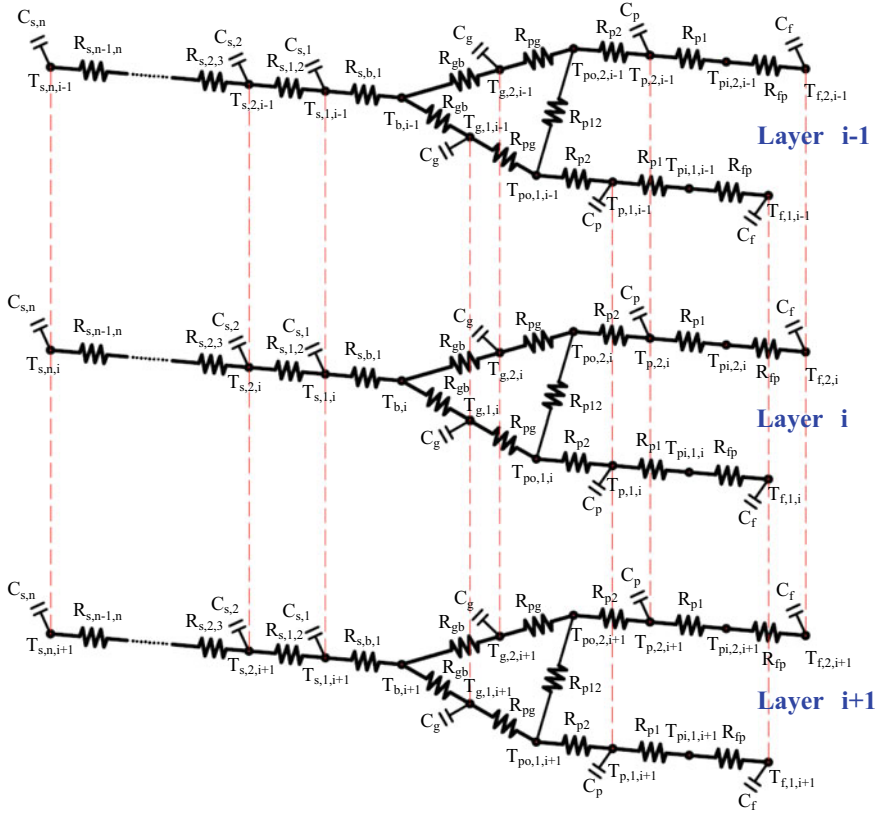


Fig. 16 Schematic diagram of conventional TRCM for vertical single U-tube ground heat exchanger

(a) **Heat transfer of the carrier fluid:**

$$\delta z C_f \frac{\partial T_{f,1,i}}{\partial \tau} + \frac{T_{f,1,i} - T_{pi,1,i}}{R_{fp} \delta z^{-1}} + \frac{2T_{f,1,i} - T_{f,1,i-1} - T_{f,1,i+1}}{\delta z k_{fluid}^{-1} A_{fluid}^{-1}} + m_f C_{p,f} (T_{f,1,i} - T_{f,1,i-1}) = 0 \quad (48)$$

$$\delta z C_f \frac{\partial T_{f,2,i}}{\partial \tau} + \frac{T_{f,2,i} - T_{pi,2,i}}{R_{fp} \delta z^{-1}} + \frac{2T_{f,2,i} - T_{f,2,i-1} - T_{f,2,i+1}}{\delta z k_{fluid}^{-1} A_{fluid}^{-1}} + m_f C_{p,f} (T_{f,2,i} - T_{f,2,i+1}) = 0 \quad (49)$$

where, C_f is the thermal capacitance for unit depth of carrier fluid, δz is the vertical interval between two adjacent layers, R_{fp} is the thermal resistance between carrier fluid and inner surface of tube, A_{fluid} is the cross section area of carrier fluid inside

the tube, k_{fluid} is the thermal conductivity of carrier fluid, m_f is the mass flow rate of the carrier fluid and $C_{p,f}$ is the specific thermal capacitance of carrier fluid.

(b) **Heat conduction of tubes:**

$$\frac{T_{pi,1,i} - T_{f,1,i}}{R_{fp}\delta z^{-1}} + \frac{T_{pi,1,i} - T_{p,1,i}}{R_{p1}\delta z^{-1}} = 0 \quad (50)$$

$$\frac{T_{pi,2,i} - T_{f,2,i}}{R_{fp}\delta z^{-1}} + \frac{T_{pi,2,i} - T_{p,2,i}}{R_{p1}\delta z^{-1}} = 0 \quad (51)$$

$$\delta z C_p \frac{\partial T_{p,1,i}}{\partial \tau} + \frac{T_{p,1,i} - T_{pi,1,i}}{R_{p1}\delta z^{-1}} + \frac{T_{p,1,i} - T_{po,1,i}}{R_{p2}\delta z^{-1}} + \frac{2T_{p,1,i} - T_{p,1,i-1} - T_{p,1,i+1}}{\delta z k_{tube}^{-1} A_{tube}^{-1}} = 0 \quad (52)$$

$$\delta z C_p \frac{\partial T_{p,2,i}}{\partial \tau} + \frac{T_{p,2,i} - T_{pi,2,i}}{R_{p1}\delta z^{-1}} + \frac{T_{p,2,i} - T_{po,2,i}}{R_{p2}\delta z^{-1}} + \frac{2T_{p,2,i} - T_{p,2,i-1} - T_{p,2,i+1}}{\delta z k_{tube}^{-1} A_{tube}^{-1}} = 0 \quad (53)$$

$$\frac{T_{po,1,i} - T_{p,1,i}}{R_{p2}\delta z^{-1}} + \frac{T_{po,1,i} - T_{g,1,i}}{R_{pg}\delta z^{-1}} + \frac{T_{po,1,i} - T_{po,2,i}}{R_{p12}\delta z^{-1}} = 0 \quad (54)$$

$$\frac{T_{po,2,i} - T_{p,2,i}}{R_{p2}\delta z^{-1}} + \frac{T_{po,2,i} - T_{g,2,i}}{R_{pg}\delta z^{-1}} + \frac{T_{po,2,i} - T_{po,1,i}}{R_{p12}\delta z^{-1}} = 0 \quad (55)$$

where, C_p is the thermal capacitance for unit depth of tube, k_{tube} is the thermal conductivity of tube and A_{tube} is the cross section area of tube.

(c) **Heat conduction of grout:**

$$\delta z C_g \frac{\partial T_{g,1,i}}{\partial \tau} + \frac{T_{g,1,i} - T_{po,1,i}}{R_{pg}\delta z^{-1}} + \frac{T_{g,1,i} - T_{b,i}}{R_{gb}\delta z^{-1}} + \frac{2T_{g,1,i} - T_{g,1,i-1} - T_{g,1,i+1}}{\delta z k_{grout}^{-1} A_{grout}^{-1}} = 0 \quad (56)$$

$$\delta z C_g \frac{\partial T_{g,2,i}}{\partial \tau} + \frac{T_{g,2,i} - T_{po,2,i}}{R_{pg}\delta z^{-1}} + \frac{T_{g,2,i} - T_{b,i}}{R_{gb}\delta z^{-1}} + \frac{2T_{g,2,i} - T_{g,2,i-1} - T_{g,2,i+1}}{\delta z k_{grout}^{-1} A_{grout}^{-1}} = 0 \quad (57)$$

$$\frac{T_{b,i} - T_{g,1,i}}{R_{gb}\delta z^{-1}} + \frac{T_{b,i} - T_{g,2,i}}{R_{gb}\delta z^{-1}} + \frac{T_{b,i} - T_{s,1,i}}{R_{s,b,1}\delta z^{-1}} = 0 \quad (58)$$

where, C_g is the half thermal capacitance for unit depth of grout material along the depth of borehole, k_{grout} is the thermal conductivity of grout and A_{grout} is the horizontal cross section area of grout within borehole.

(d) **Heat conduction of soil:**

Since the soil has cylindrical structure in the ground heat exchanger, the soil region could be divided into adjacent different concentric layers in radial direction, and then the heat conduction of each adjacent soil layer could be described as follows.

(i) The first layer of soil in radial direction ($j = 1$)

$$\delta z C_{s,1} \frac{\partial T_{s,1,i}}{\partial \tau} + \frac{T_{s,1,i} - T_{b,i}}{R_{s,b,1} \delta z^{-1}} + \frac{T_{s,1,i} - T_{s,2,i}}{R_{s,1,2} \delta z^{-1}} + \frac{2T_{s,1,i} - T_{s,1,i-1} - T_{s,1,i+1}}{\delta z k_{soil}^{-1} A_{s,1}^{-1}} = 0 \quad (59)$$

where, $C_{s,1}$ is the thermal capacitance of first layer soil with unit depth, k_{soil} is the thermal conductivity of soil and $A_{s,1}$ is the horizontal cross section area of the first soil layer in radial direction.

(ii) Other layers of soil in radial direction ($2 \leq j < n$)

$$\delta z C_{s,j} \frac{\partial T_{s,j,i}}{\partial \tau} + \frac{T_{s,j,i} - T_{s,j-1,i}}{R_{s,j-1,j} \delta z^{-1}} + \frac{T_{s,j,i} - T_{s,j+1,i}}{R_{s,j,j+1} \delta z^{-1}} + \frac{2T_{s,j,i} - T_{s,j,i-1} - T_{s,j,i+1}}{\delta z k_{soil}^{-1} A_{s,j}^{-1}} = 0 \quad (60)$$

where, $C_{s,j}$ is the thermal capacitance of the j th layer soil with unit depth, $R_{s,j-1,j}$ is the thermal resistance between the $j - 1$ th soil and the j th soil in radial direction, and $A_{s,j}$ is the horizontal cross section area of the j th soil layer.

Since the constant temperature boundary condition is imposed on the radial outer surface of soil, the temperature of outermost layer of soil (i.e., $j = n$) could be directly determined by the given constant temperature.

1.3.2 Improved TRCM for Ground Heat Exchanger

Although the assumption of uniform temperature of borehole will simplify the heat transfer process within borehole, it is not consistent with the real temperature distribution of borehole for ground heat exchanger and it will bring corresponding error for the conventional TRCM, i.e., the model of ground heat exchanger based on three-thermal-resistance-capacitance network within a borehole. In order to take into account the effect of non-uniform temperature distribution of borehole perimeter in the improved TRCM for ground heat exchanger, the borehole perimeter is divided into two equal parts along the symmetrical line and the average temperatures of each half borehole perimeter are adopted to analyse the heat transfer process within a borehole, i.e., $T_{b,1}$ is no longer equal to $T_{b,2}$ as shown in Fig. 17. Therefore, the horizontal heat transfer process within the borehole could be described by the so-called four-thermal-resistance-capacitance network as shown in Fig. 17, where the R_{b1} and R_{b2} are the two equal thermal resistances between outer surface of tube and borehole wall due to the symmetrical structure and uniform thermal properties

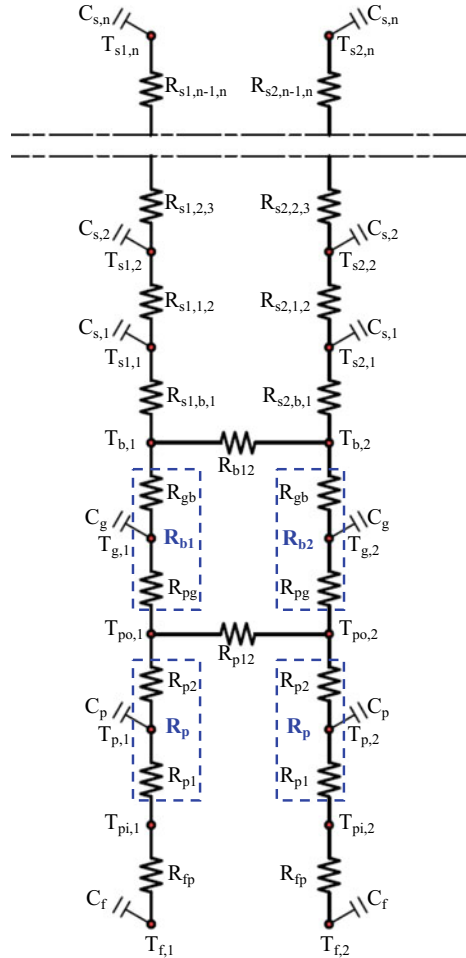
of grout, R_{p12} is the thermal resistance between two outer surface of tubes, R_{b12} is the thermal resistance between two equal half-length perimeter of borehole, and C_g is the half thermal capacitance of grout material which is defined as the same in three-thermal-resistance-capacitance network as shown in Fig. 15.

All the thermal resistances (i.e., R_{b1} , R_{b2} and R_{p12} , R_{b12} as shown in Fig. 17) could be determined through the following equations [21].

$$R_b = \frac{-501.25 \ln(\theta_1) + 512.48 \ln(\theta_2) + 510.57 \sigma \ln\left(\frac{1}{1-\theta_1^4}\right) - 369.25}{1000 \cdot 2\pi k_g} \quad (61)$$

$$R_{p12} = \frac{(30.455\theta_2 + 2.0030\sigma^2 + 6.5003\sigma - 26.484)e^{(0.10664\sigma + 4.7420)\theta_1}}{1000 \cdot k_g} \quad (62)$$

Fig. 17 Four-thermal-resistance-capacitance series network for unit depth of ground heat exchanger at horizontal plane



$$R_{b12} = \frac{\left[25.920\sigma + 941.37 - \frac{251.61\sigma + 794.23}{\ln(\theta_2)} \right] e^{\left[0.18494\sigma - 0.93402 + \frac{1.7547 - 0.1653\sigma}{\ln(\theta_2)} \right] \frac{1}{\theta_1}}}{1000 \cdot k_g} \quad (63)$$

$$R_{b1} = R_{b2} = 2R_b \quad (64)$$

where, all the dimensionless parameters (i.e., θ_1 , θ_2 and σ) are defined as the same in the Eqs. (30)–(33).

Since there exist two different temperatures along the borehole perimeter, the soil region, which has cylindrical structure and surrounds the borehole, could be discretized to adjacent concentric layers with different radius and each layer has two equal parts along the symmetrical line, as shown in Fig. 17.

If the average temperature and velocity are adopted for the carrier fluid and the heat conduction is neglected between two symmetrical half soil annulus with same radius on horizontal plane, the four-thermal-resistance-capacitance series network could be established to describe the horizontal heat transfer process of vertical single U-tube ground heat exchanger, as shown in Fig. 17. The locations of thermal capacitance (or temperature) for tube, grout material and soil could be all determined by the same method as those in three-thermal-resistance-capacitance series network, i.e., the conventional TRCM of vertical single U-tube ground heat exchanger.

Similar to the conventional TRCM of vertical single U-tube ground heat exchanger, all the horizontal four-thermal-resistance-capacitance networks could be piled up according to the flow direction of carrier fluid and the vertical heat conduction of tube, grout and soil. Therefore, the improved TRCM (i.e., the four-thermal-resistance-capacitance model) could be established to describe the transient heat transfer process of vertical single U-tube ground heat exchanger, as shown in Fig. 18, in which the effect of non-uniform temperature distribution of borehole perimeter could be taken into account, as well as the thermal capacitances of all components (including carrier fluid, tube, grout and soil) and the horizontal or vertical heat conduction.

Based on the conservation law of energy, the heat transport equations between carrier fluid, tube, grout material and soil could be established for the improved TRCM, respectively. Since the derivation process of these equations in the improved TRCM is similar to those of conventional TRCM, all these equations will not be redundantly repeated in this section for the vertical single U-tube ground heat exchanger.

1.3.3 CFD Model and Model Validation

Since geometric structure of vertical single U-tube ground heat exchanger is symmetrical about the centreline, the 3D finite volume CFD model could be chosen as only half of the whole ground heat exchanger to decrease the total number of meshes and

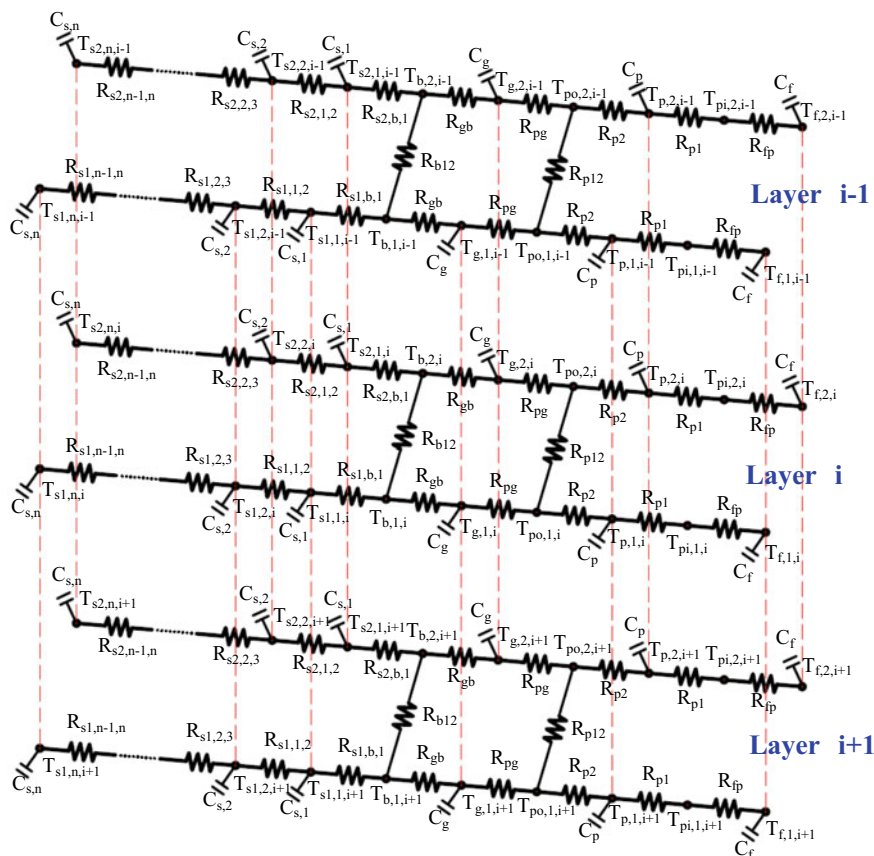


Fig. 18 Schematic diagram of improved TRCM for vertical single U-tube ground heat exchanger

reduce the solving time. The detailed geometric configuration and meshes for 3D finite volume CFD model of ground heat exchanger are shown in Fig. 19.

It is clearly shown in Fig. 19 that the fluid flow inside the tubes, heat conduction through the tube wall, heat conduction cross the grout region and heat conduction within soil region are all included in this 3D finite volume CFD model. In order to accurately describe the detailed fluid flow and heat transfer between carrier fluid and tube wall, denser grids are adopted near the tube wall and at least four grids are applied for the thickness of tube wall. Through the mesh independent tests, this CFD model is able to be used as a benchmark model which could evaluate the transient heat and mass transport of vertical single U-tube ground heat exchanger with satisfactory accuracy.

In order to validate the improved TRCM of vertical single U-tube ground heat exchanger, a fully discretized 3D finite volume CFD model by using Fluent software is established based on the method described as before. The geometric parameters

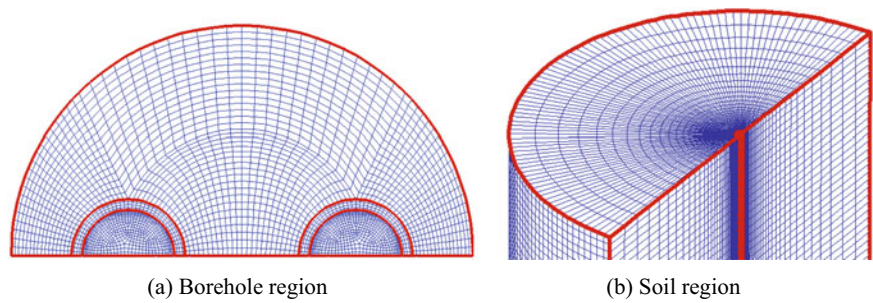


Fig. 19 Geometric configuration and meshes for 3D finite volume CFD model of vertical single U-tube ground heat exchanger

and thermal properties of this CFD model are listed in Tables 2 and 3, which are determined based on a local TRT data and field evaluation of a vertical single U-tube ground heat exchanger in Chongqing, China. The comparisons of inlet/outlet average temperature of carrier fluid between the 3D finite volume CFD model and the field experimental data are presented in Fig. 20. From this figure, it is clearly shown that the CFD simulation results have good agreement with those from the field test. Therefore, it could be reasonably believed that the presented 3D finite volume CFD model is correct and reliable, and all the simulation results based on this model are valid and they could be used as benchmark results to evaluate other models of vertical single U-tube ground heat exchanger (i.e., the conventional TRCM and the improved TRCM).

Table 2 Geometric parameters of vertical single U-tube ground heat exchanger

d_b (mm)	d_o (mm)	d_i (mm)	s (mm)	Borehole depth (m)
130	32	26	64	100

Table 3 Physical properties of ground heat exchanger

Material	Thermal conductivity k (W/(m-K))	Specific heat c_p (J/(kg-K))	Density ρ (kg/m ³)
Carrier fluid	0.60	4182	998.2
Tube	0.44	2300	950.0
Grout	2.00	840	1860.0
Soil	2.71	1645	1600.0

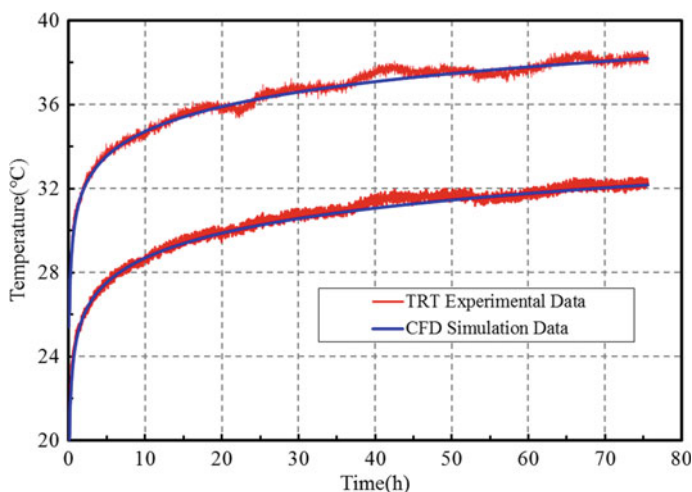


Fig. 20 Inlet/Outlet average temperature of carrier fluid between the 3D finite volume CFD simulation and TRT field experimental test

1.3.4 Comparisons and Discussion

In order to compare the above-mentioned three models of vertical single U-tube ground heat exchanger (i.e., three-thermal-resistance-capacitance model, four-thermal-resistance-capacitance model and 3D finite volume CFD model), all the geometric parameters and thermal properties listed in Tables 1 and 2 are adopted and the inlet temperature of carrier fluid is kept as constant (i.e., 35 °C), the undisturbed ground temperature (i.e., 20.0 °C) is applied as initial temperature for the ground heat exchanger including carrier fluid, tube, grout and soil, and the mass flow rate of carrier fluid (i.e., water) is kept as constant (i.e., 0.24 kg/s) for all these three models. The TRCMs are solved by programming language C and the time steps adopted to solve these three models are set to the same values. As mentioned before, since the CFD model has been validated, the simulation results of CFD model could be used as the benchmark results of transient cooling process for vertical single U-tube ground heat exchanger, and all the calculation data of conventional TRCM and the improved TRCM will be compared and evaluated with those data.

As shown in Figs. 21 and 22, the outlet average temperature of carrier fluid versus operation time are presented between the conventional TRCM (i.e., three-thermal-resistance-capacitance model), the improved TRCM (i.e., four-thermal-resistance-capacitance model) and CFD model. It could be seen in these figures that the results of the improved TRCM are more consistent with the results of CFD model than those of the conventional TRCM for the given period operation time of 48 h.

It could be also observed from Fig. 21 that there exists relatively quite big difference between the data of conventional TRCM and CFD model especially at the beginning short period of 1 h, and it seems that the temperature exists some kind

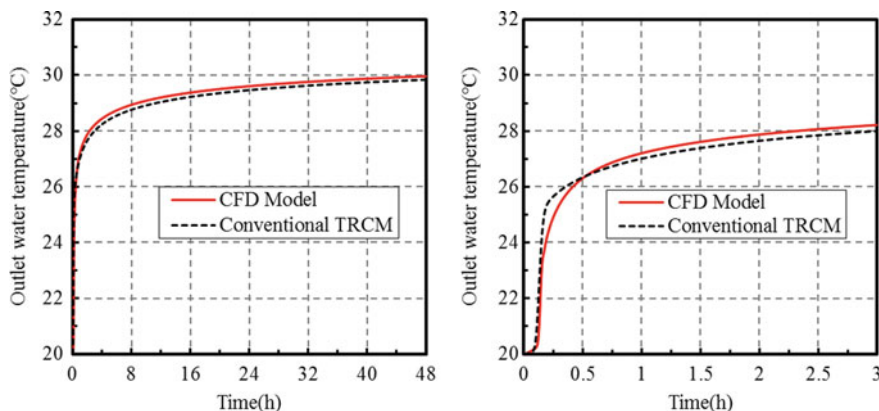


Fig. 21 Comparisons of outlet average temperature of carrier fluid versus operation time between the CFD model and the conventional TRCM

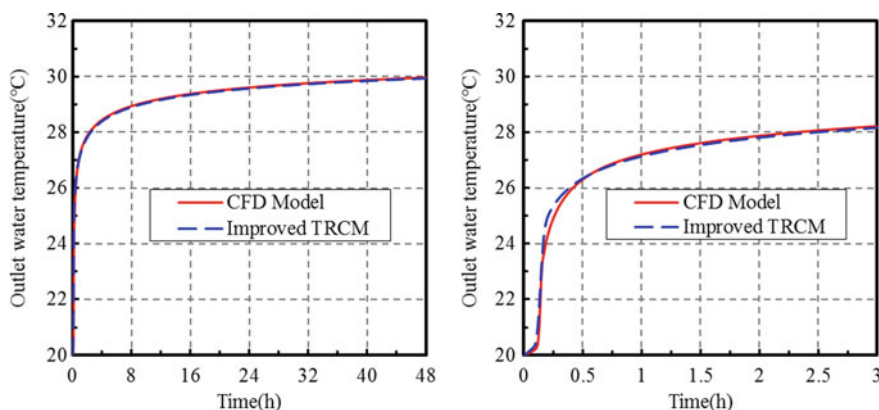


Fig. 22 Comparisons of outlet average temperature of carrier fluid versus operation time between the CFD model and the improved TRCM

of constant offset between those two models once the operation time is beyond 1 h. However, although the temperatures exist some difference between the improved TRCM and CFD model within 1 h from the starting point as shown in Fig. 22, the rest of calculation data of the improved TRCM match very well with those of CFD model. The absolute error of average temperature of carrier fluid between CFD model and the improved TRCM is less than 0.7°C when the operation time reaches up to 1 h, and it will never exceed 0.04°C when the operation time is beyond 3 h.

As shown in Fig. 23, the comparisons of outlet average temperature of carrier fluid between these three models are presented within 80 min from the beginning time. It could be clearly seen that although the calculation data of TRCMs have some difference with those of CFD model, the improved TRCM exhibits much

better performance than the conventional TRCM as compared to the benchmark CFD model.

Based on the benchmark results of CFD model, the relative errors of carrier fluid outlet average temperature versus operation time for both TRCMs are presented in Fig. 24, respectively. Since the dominant difference between the conventional TRCM and the improved TRCM is only the thermal-resistance-capacitance network within the borehole, the relative error for both models gets quickly decreased as the operation time of ground heat exchanger exceeds 1 h. Because the four-thermal-resistance-capacitance model (i.e., the improved TRCM) considers the effect of non-uniform temperature distribution along borehole perimeter, it could describe the transient heat transfer process within the borehole much better than that of three-thermal-resistance-capacitance model (i.e., the conventional TRCM), and then it has much smaller relative error than that of three-thermal-resistance-capacitance model especially at the beginning short period of operation time.

In order to further validate the advantages of the proposed improved TRCM, it is necessary to compare the temperature distribution of carrier fluid along the depth of vertical single U-tube ground heat exchanger between the conventional TRCM (i.e., three-thermal-resistance-capacitance model), the improved TRCM (i.e., four-thermal-resistance-capacitance model) and CFD model.

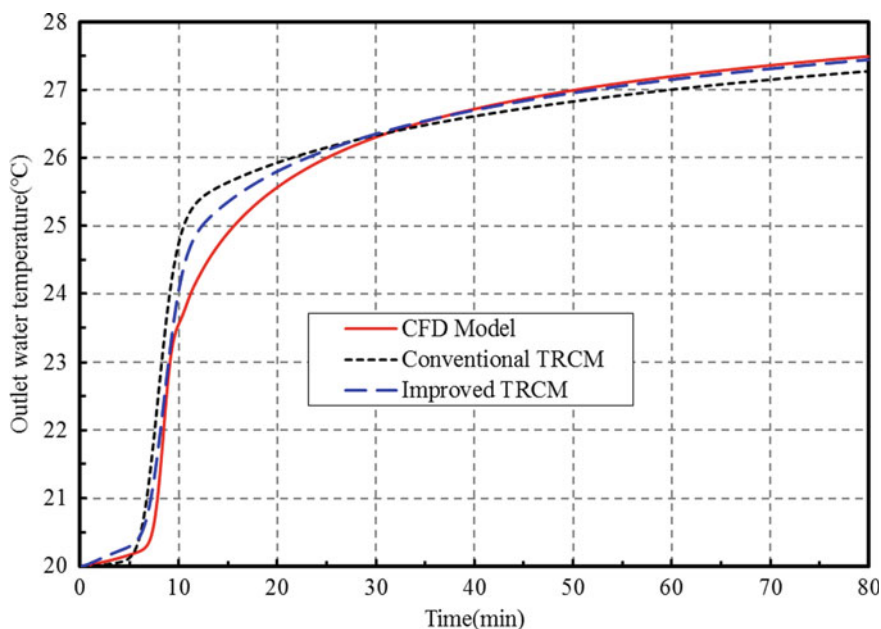


Fig. 23 Comparisons of carrier fluid outlet temperature between these three models within 80 min from the beginning time

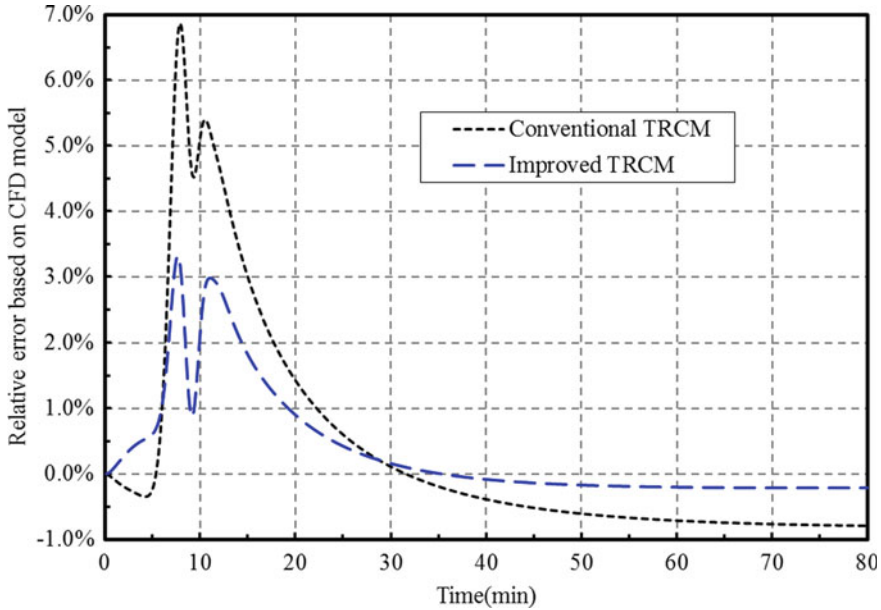


Fig. 24 Relative error of carrier fluid outlet temperature versus operation time based on the benchmark results of 3D finite volume CFD model

As shown in Figs. 25 and 26, the temperature distributions of carrier fluid along the flow direction are presented at different time for these three models of ground heat exchanger, respectively. From these two figures, it could be easily seen that the results of the improved TRCM match much better with those of CFD model than the results of conventional TRCM do, especially when the operation time is beyond 1 h. Therefore, the improved TRCM has a higher degree of accuracy than the conventional TRCM to describe the transient heat transfer process of vertical single U-tube ground heat exchanger. As compared to the conventional TRCM, since the improved TRCM does not add too many heat transport equations and the model solving time, which is much less than that of CFD model, does not get increased significantly, it could draw a conclusion that the improved TRCM has the advantages of both conventional TRCM (i.e., parameter-based modelling, easy and quick to solve) and CFD model (i.e., relatively high degree of accuracy results), and it could be adopted to describe the transient heat transfer process of vertical single U-tube ground heat exchanger and other vertical single U-tube ground heat exchanger based applications in the real engineering.

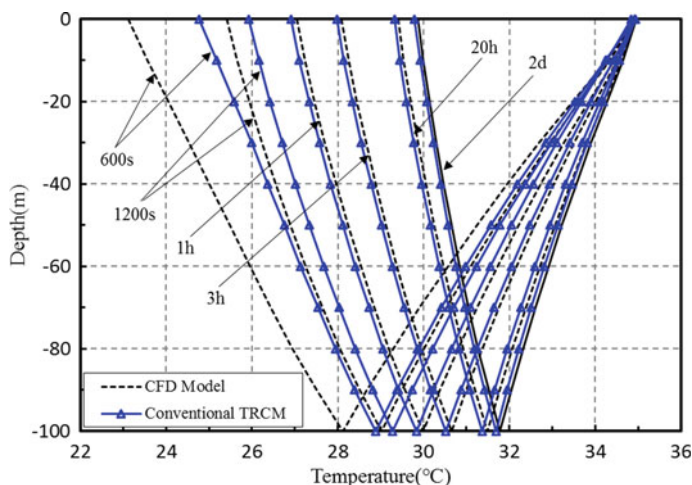


Fig. 25 Comparisons of temperature distribution of carrier fluid along the depth between the conventional TRCM and CFD model

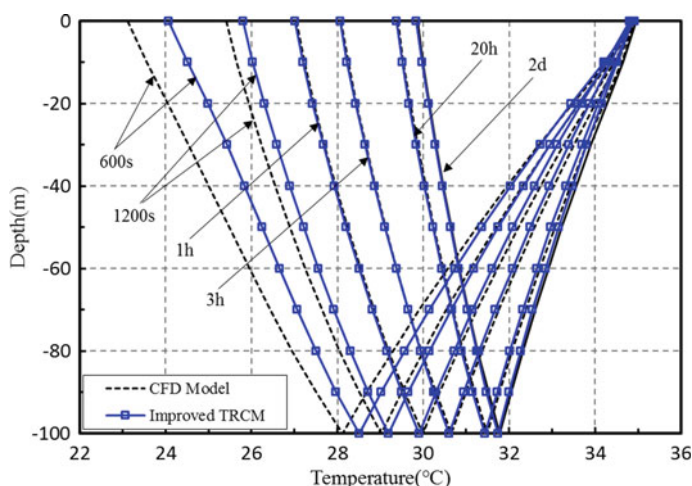


Fig. 26 Comparisons of temperature distribution of carrier fluid along the depth between the improved TRCM and CFD model

References

1. Liao Q, Zhou C, Cui W et al (2012) Effective borehole thermal resistance of a single U-tube ground heat exchanger. *Numer Heat Transf Part A Appl* 62(3):197–210
2. Lamarche L, Kaji S, Beauchamp B (2010) A review of methods to evaluate borehole thermal resistances in geothermal heat-pump systems. *Geothermics* 39(2):187–200
3. Quan L, Chao Z, Wenzhi C (2012) New correlations for thermal resistances of vertical single U-Tube ground heat exchanger. *J Thermal Sci Eng Appl* 4(3)

4. Shonder JA, Beck JV (1999) Field test of a new method for determining soil formation thermal conductivity and borehole resistance. *ASHRAE Trans* 106:843–850
5. Sharqawy MH, Mokheimer EM, Badr HM (2009) Effective pipe-to-borehole thermal resistance for vertical ground heat exchangers. *Geothermics* 38(2):271–277
6. Bennet J, Claesson J, Hellström G (1987) Multipole method to compute the conductive heat flows to and between pipes in a composite cylinder. *Notes Heat Trans* 3
7. Powell DMJ (1973) On search directions for minimization algorithms. *Math Program* 4(1)
8. Lee CK (2016) A modified three-dimensional numerical model for predicting the short-time-step performance of borehole ground heat exchangers. *Renew Energy* 87(87(Mar. Pt.1)):618–627
9. De Carli M, Tonon M, Zarrella M et al (2010) A computational capacity resistance model (CaRM) for vertical ground-coupled heat exchangers. *Renew Energy* 35(7)
10. Lamarche L (2007) A new contribution to the finite line-source model for geothermal boreholes. *Energy Build* 39(2)
11. Cui P, Yang H, Fang Z (2006) Heat transfer analysis of ground heat exchangers with inclined boreholes. *Appl Thermal Eng* 26(11–12)
12. Zeng HY, Diao NR, Fang ZH (2002) A finite line-source model for boreholes in geothermal heat exchangers. *Heat Trans Asian Res* 31(7)
13. Yavuzturk C, Spitler JD (2001) Field validation of a short time step model for vertical ground-loop heat exchangers. *ASHRAE Trans* 107(1):617–625
14. Man Y, Yang H (2010) A new model and analytical solutions for borehole and pile ground heat exchangers. *Int J Heat Mass Trans* 53(13–14)
15. Eskilson P (1987) Thermal analysis of heat extraction boreholes. University of Lund Department of Mathematical Physics and Building Technology, Sweden
16. Bauer D, Heidemann W, Müller-Steinhagen H et al (2011) Thermal resistance and capacity models for borehole heat exchangers. *Int J Energy Res* 35(4):312–320
17. Maestre IR, Gallero FJG, Gómez PÁ, Pérez-Lombard L (2015) A new RC and g-function hybrid model to simulate vertical ground heat exchangers. *Renew Energy* 78
18. Javed S, Spitler J (2017) Accuracy of borehole thermal resistance calculation methods for grouted single U-tube ground heat exchangers. *Appl Energy* 187:790–806
19. Beier RA (2011) Vertical temperature profile in ground heat exchanger during in-situ test. *Renew Energy* 36(5):1578–1587
20. Marcotte D, Pasquier P (2008) On the estimation of thermal resistance in borehole thermal conductivity test. *Renew Energy* 33(11):2407–2415
21. Bauer D, Heidemann W, Diersch J (2011) Transient 3D analysis of borehole heat exchanger modeling. *Geothermics* 40(4):250–260
22. Martin WB (1982) Heat transfer: J.P. Holman. *Int J Heat Fluid Flow* 3(1)

Technical Optimization of the Energy Supply in Geothermal Heat Pumps



Cristina Sáez Blázquez, David Borge-Diez, Ignacio Martín Nieto, Arturo Farfán Martín, and Diego González-Aguilera

Abstract There is not a widespread use of the very low enthalpy geothermal energy in a large number of countries. The reason is frequently the high initial investment these systems require. In this regard, geothermal heat pump is largely the responsible of this important outlay. This research focuses on substituting this device by the integration of a set of renewable alternatives. The ground contribution is complemented with a thermal and a power renewable module that provide the remaining energy. The model was evaluated on a real case by technical calculations of the common ground source heat pump (*GSHP*) system and the one considered here. An economic feasibility study showed notable savings in the initial investment as well as in the annual costs on the part of the suggested system. CO₂ emissions were reduced by half in comparison to the traditional geothermal plant. The model represents a general improvement in relation to the conventional GSHP system; the heat pump is removed and the total drilling length reduced. For a single family home placed the substitution of the heat pump by renewable modules achieves a reduction of 22.84% in the initial investment, 77.54% in the operational costs and CO₂ emissions are reduced 49.50%.

Keywords Geothermal heat pump · Integration · Renewable energies · Economic and environmental study

C. S. Blázquez · D. Borge-Diez (✉)

Department of Electric, System and Automatic Engineering, University of León, León, Spain

e-mail: david.borge@unileon.es

I. M. Nieto · A. F. Martín · D. González-Aguilera

Department of Cartographic and Land Engineering, University of Salamanca, Higher Polytechnic School of Avila, Hornos Caleros 50, 05003 Avila, Spain

Nomenclature

Symbols

C_T	Total thermal contribution [kJ]
C_1	Thermal contribution [kJ]
C_2	Electrical contribution [kJ]
E_g	Enthalpy gained in the geothermal borehole [kJ]
E_s	Enthalpy gained in the solar thermal panel [kJ]
E_f	Enthalpy provided by the photovoltaic panel [kJ]
E_s	Enthalpy provided by the wind generator [kJ]
E_n	Enthalpy provided by electricity network [kJ]
E_n	Enthalpy provided by the batteries [kJ]
N_b	Energy needs of the building [kJ]
f	f-Chart method value
D_1	f-Chart method factor
D_2	f-Chart method factor
E_a	Energy absorbed by the thermal solar panel [kJ]
S_c	Panel surface [m ²]
$F_r'(\tau\alpha)$	Factor calculated from the efficiency of the panel and characteristic values of each panel
R_1	Daily monthly radiation by unity of surface [kJ/m ²]
N	Number of days in the month
H_l	Monthly heat load [kJ]
E_p	Energy lost by the thermal solar panel [kJ]
$F_r'U_L$	Characteristic factor of the thermal panel losses
t_a	Monthly ambient temperature [°C]
Δt	Period of time considered [s]
K_1, K_2	Correction factors

Acronyms

<i>GSHP</i>	Ground Source Heat Pump
<i>GHG</i>	Greenhouse Gas
<i>COP</i>	Coefficient of performance
<i>GHP</i>	Geothermal Heat Pump
<i>HP</i>	Heat Pump
<i>DHW</i>	Domestic Hot Water
<i>EED</i>	Earth Energy Designer
<i>IDAE</i>	Institute of the Diversification and Energy save
<i>NPV</i>	Net Present Value.

1 Introduction

The increasing global energy demand closely related to the pivotal climate change has led to a notable growing of greenhouse gas (GHG) emissions. On this matter, there are numerous strategies with the aim of maximizing the use of renewable energies [1–6]. However, these energies are still far from being used across the board. Most of them suffer from relevant variations due to its dependence on climatic and weather conditions [7]. The economic component is another factor that negatively affects the expansion of these energy sources.

Geothermal energy and in particular low enthalpy geothermal systems are commonly used to produce Domestic Hot Water (DHW) or to warm/cool a certain space. Different from other renewable energies, they are not affected by environmental conditions, given that the earth temperature is constant from a particular depth. The main problem that complicates a generalized use of these installations is the economic issue together with the environmental restraints such as the presence of aquifers for potable use, risk of connection between different aquifers set in different depths, risk of landslides [8, 9]. The high initial investments they require mean an important impediment for a large number of users. In this regard, the main economic contributions are constituted by the set of boreholes heat exchangers and the geothermal heat pump. The number of boreholes and hence the surface of heat exchange depend on the geological characteristics of the specific area. Therefore, this first item is mostly inevitable (although it could be reduced). Geothermal heat pumps (also required in these systems) involve a high initial payment in addition to the operational costs associated to the electrical consumption. They are efficient devices whose function is increasing the temperature of the heat carrier fluid coming from the thermal exchange with the earth [10–14]. However, their high prices thoroughly raise the initial investment of the general geothermal system.

Together with the economic field, the other weakness of these systems is related to the constant dependence of external power supply for the heat pumps operation. Since these devices are electricity consumers, a certain emission of greenhouse gases is associated to their use.

Focusing on the main contributor to climate change (CO_2) geothermal heat pumps do not directly emit CO_2 gases, these emissions come from the power plants that produce the electricity. Thus, in certain locations, CO_2 emissions derived from the use of GHP systems can be considerably high if electricity is produced in high-emission power plants. Based on the literature, GHP annual CO_2 emissions were (to cover the same energy demand), for the locations of Alberta, Ontario and Nova Scotia, 6,826, 1,143 and 6,346 kg respectively [15]. These data reflect the elevated dependence on the origin of the electricity used as HPs supply.

On the other hand, the energy use of a GSHP system is directly related to the ground thermal capacity. Elevated ground thermal conductivities allow lower HP energy consumptions. Furthermore, the combination ground-heat pump is usually characterized by high COPs (usually around 4–4.5) which means reduced electricity consumptions in relation to the thermal energy provided (4 thermal unities provided/1

electricity unit used) [16]. Despite the low electricity use, heat pump operating costs must be considered. These costs are directly associated to the electricity price established in each place, being around 0.15 €/kWh for the European Union countries [17]. As already said, commercial heat pumps do not involve high electricity consumption; however, these costs could mean an important outlay in those locations where the electricity price was considerable. For this reason, the economic feasibility of a geothermal system strongly depends on the place where it is planned to be installed.

Analyzing the statements previously presented, the basis of this work lies in solving three main issues:

- CO₂ emissions associated to the heat pump operation.
- Heat pump electricity use.
- High initial investments and operational costs derived from the use of a GSHP system.

Given the reasons previously described, the present research mainly focuses on finding an appropriate alternative to deal with them. To that end, the possibility of substituting the geothermal heat pumps by other renewable solutions is considered along this work.

In this field, several research studies have been found on the literature [18, 19]. By way of example, Isafiade et al. [20] proposed a methodology for integrating renewable and non-renewable energy sources. Karunathilake et al. [21] studied the integration of renewable energy in community energy planning in Canada. Additionally, Alnifro et al. [22] tried to determine the feasibility of optimal renewable energy integration into a refinery. Thus, although the renewable energy combination has been evaluated in previous works, they mainly focus on computer simulations without implement real data of actual low enthalpy geothermal installations. Once detected this gap and the main weaknesses of the common GSHP systems, the present research proposes a new renewable energy integration whose basis is the geothermal exchange. Thus, we study the possibility of substituting the heat pump of a GSHP system by combining geothermal, solar and wind energies from a technical point of view. In particular, the new contributions of this work can be summarized as:

- Evaluation of the renewable energy integration from data implemented on a real situation.
- Design of a new geothermal alternative whose main objective is the reduction (or elimination) of the external electricity supply.
- Technical calculations of each renewable module and economic and environmental evaluations from the real parameters obtained before.

For all the above, the topic addressed in this work could mean an important boost for the traditional geothermal systems whose use is still reduced in a great number of locations.

2 Methodology

2.1 Suggested System Description

As already said, the aim of the present work is to provide an alternative to the common configuration of a very low enthalpy geothermal system. The proposed design is based on substituting the energy source of these installations (geothermal heat pumps) by a combination of different renewable energies. Basically, the difference between a traditional geothermal system and the one presented here is the way of increasing the temperature of the heat carrier fluid after coming from the thermal exchange in the boreholes. While in a conventional plant, the temperature of the fluid is increased in the geothermal heat pump, in the proposed system, the fluid gains temperature thanks to a series of renewable modules. Figure 1 graphically shows the standard workflow of a geothermal installation, indicating the additional process contemplated in the suggested solution.

The renewable module is designed to make the function of the geothermal heat pump. This system is constituted by the following items:

- Thermal solar energy
- Wind energy
- Thermal buffer tank constituted by an auxiliary electric heater
- Computerized system of data acquisition and decision making.

In this way, the main characteristics of the suggested model (summarized in Table 1) mean positive modifications in relation to the traditional GSHP system.

The operation of the mentioned module is briefly explained in Fig. 2. As described in this figure, the first step is the thermal exchange of a heat carrier fluid (mixture of

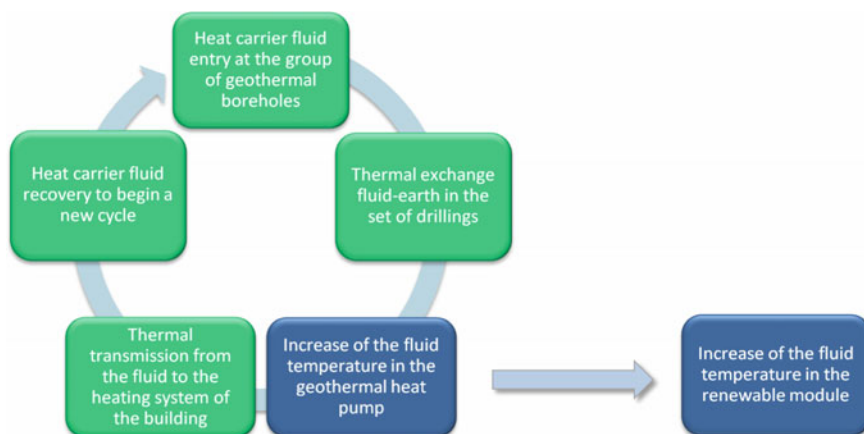


Fig. 1 Workflow of a common geothermal installation showing the different steps in the system under consideration (in blue colour)

Table 1 Principal characteristics of a traditional ground source heat pump system (GSHP) system and the model proposed in this work

Traditional GSHP system	Proposed model
High initial investment	Moderate initial investment
Quite long amortization periods	Medium amortization periods
External power supply dependence	Reduction of the external power supply dependence (It could be autonomous under ideal conditions)
Monthly costs associated electrical power consumption and system maintenance	Reduction of the monthly costs derived from the system operation and maintenance

water–glycol) in the corresponding geothermal borehole. Up to here, it corresponds to the common procedure in a geothermal installation. When the heat carrier fluid leaves the borehole, it would get in the geothermal heat pump, however, in this research; this device is replaced by the renewable module. Thus, the heat carrier fluid enters in a thermal solar panel where its temperature is increased again. In the following stage, the fluid gets in a buffer tank constituted by an electrical resistance and a set of sensors that belong to the intelligent system of data acquisition and decision making. In this tank, the automated system analyses if the fluid temperature is the one required. If the temperature is up to 40 °C, the heat carrier fluid is conducted inside the building to carry out the thermal exchange by the underfloor heating. If this temperature was <40 °C, the electrical resistance of the buffer tank would increase it until the established value. Then, the fluid would also get into the specific building. The last component of this module is made up of a solar photovoltaic panel and a wind turbine which constitute the electrical contribution. These elements provide the electrical energy required by the set of pumps responsible for the fluid movement and the electrical resistance placed in the buffer tank. If the meteorological conditions were not favorable, an external electricity contribution would be considered.

The computerized control system is the key of the whole installation. The response capacity of the proposed plant is quite slow; hence, its limited flexibility is compensated by a suitable processing of the installation and external information. The decision-making core of the computerized system is responsible for collecting a large amount of information coming from:

- Sensors from each energetic module (geothermal borehole, thermal solar panel, buffer tank).
- Sensors placed inside and outside the building.
- Weather forecasts.
- Data about the expected consumption provided by the user (personal prediction of anomalous consumptions, higher or lower, during a certain period of time).
- Data from similar installations (solar and wind systems).
- Data about the electrical supply rate with the aim of detecting the most appropriate hours if external energetic contribution was required.

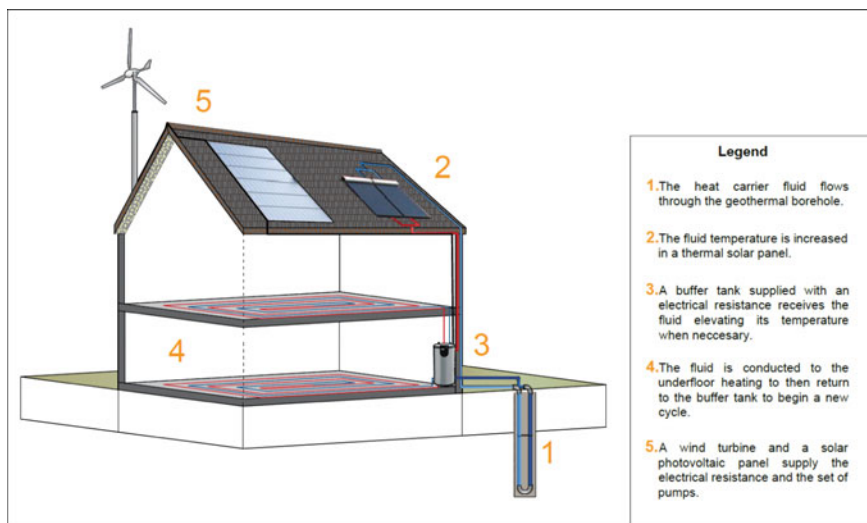


Fig. 2 Description of the renewable module proposed in the present research

With this set of information the mentioned automated system will be capable of controlling the operation and storage functions, selecting which modules get involved to efficiently cover the energy needs for an established period of time. Based on the reliability of the meteorological information (accuracy of the meteorological predictor), this period could be of 24, 48 or 72 h. If the prediction accuracy is low, the system must accumulate energy in short periods of time (24 h) in order to be prepared for unexpected variations of the energy demand. Figure 3 describes how the mentioned system is connected with each of the components of the installation, taking information from the large number of sensors distributed over the whole plant. As this Fig. 3 shows, there are two groups of sensors; one of them provides the temperature of the heat carrier fluid in each module as well as the temperature inside the building. The remaining sensors collect relevant information from the whole installation; the electrical contribution of the renewable modules (solar and wind energy), the electric rate in a certain moment, information from the user and the weather forecast. Thanks to the computerized system, the plant operates in the most efficient conditions, guaranteeing at the same time a constant energy supply to the user.

According to Fig. 3, the principal equations of the system are presented below. The total contribution of the whole installation can be expressed as:

$$C_T = C_1 + C_2 \quad (1)$$

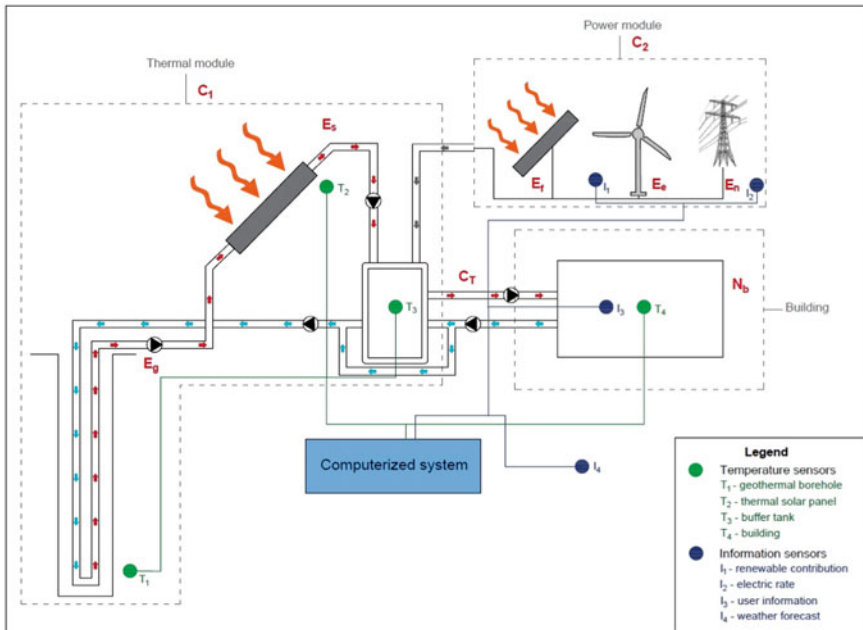


Fig. 3 Schema of the computerized system operation

where:

C_1 = Thermal contribution.

C_2 = Electrical contribution

$$C_1 = E_g + E_s \quad (2)$$

where:

E_g = Enthalpy gained in the geothermal borehole.

E_s = Enthalpy gained in the solar thermal panel

$$C_2 = E_f + E_e + E_n + E_b \quad (3)$$

where:

E_f = Enthalpy provided by the photovoltaic panel.

E_e = Enthalpy provided by the wind generator.

E_n = Enthalpy provided by electricity network.

E_b = Enthalpy provided by the batteries.

Finally, the energy needs of the building determine the total contribution required:

$$C_T = N_b \quad (4)$$

where:

N_b = Energy needs of the building.

The total quantity of energy that requires to be covered by the renewable model is derived from the energy needs (N_b) information (calculated in Sect. 3). Based on these data, the working fluid elevates its enthalpy in the geothermal borehole (E_g) and in the solar thermal panel (E_s). In the buffer tank, it continues increasing its enthalpy thanks to the thermal resistance which is in turn supplied by the wind generator and the photovoltaic panels (E_e and E_f). If additional energy was still required, the batteries system and the electricity network would be also operating. Finally, the total enthalpy gained by the fluid (C_T) must satisfy the user energy needs (N_b).

The process of decision making carried out by the computerized system is graphically described in Fig. 4.

It must be clarified from Fig. 4, that, when the fluid leaves the building, the computerized system decides if its temperature is the required (in this case it returns to the borehole) or not (the fluid needs to go across the buffer tank). The established value mentioned in this Fig. 4 will depend on the specific user needs. It usually takes a value of around 40–60 °C [23].

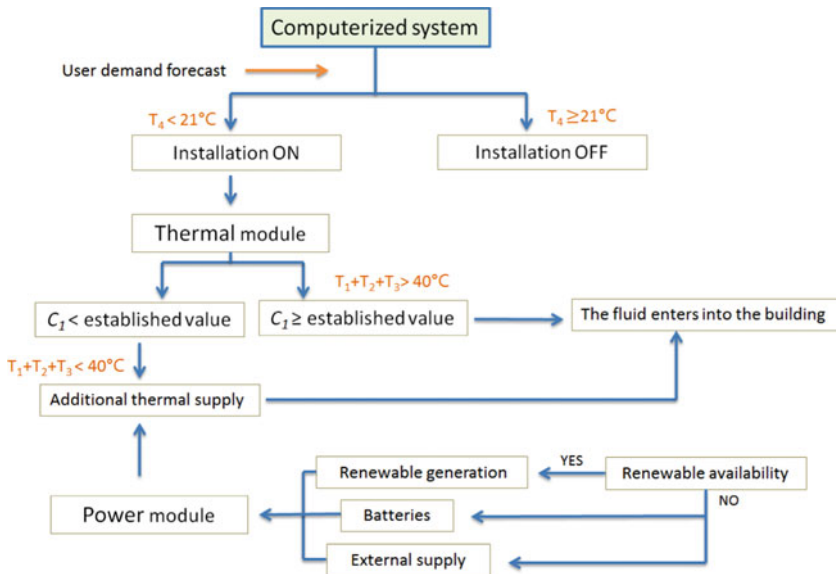


Fig. 4 Process of decision making in the computerized system

The use of electrical storage systems (batteries) in this project could be avoided if the energy was accumulated in the thermal buffer tank directly from the photovoltaic solar panel and wind generator. However, due to the limited thermal insulation of the buffer tank, the use of these elements has been preferred. These elements are intended to be used as electrical support accumulating the electrical energy generated in the renewable power module.

2.2 Workflow

With the objective of evaluating the solution previously described, this work was implemented in on a real case. The procedure followed in the present research is constituted by the following steps:

- Selection of a specific location where the suggested system will be validated and establishment of a series of initial conditions (building dimensions, energy demand, meteorological conditions...).
- Dimensioning of each of the components that constitute the plant. The geothermal borehole and the renewable section (thermal and power modules) will be calculated by the implementation of specific software and mathematical equations.
- Economic calculation and environmental analysis of the whole renewable installation. Determination of the initial investment, operational costs and GHG emissions of the suggested system.
- Economic and environmental comparison of the proposed solution and a conventional geothermal system.

3 Technical Calculation

The first step is selecting the initial conditions of the real case where the system will be implemented. The selected building is a single family home of 200 m² placed in the province of Ávila (Spain). The system is considered to only cover the demand of the building in heating mode (cooling needs are not usual in this area). Henceforth, each of the renewable components was dimensioned.

3.1 Thermal Module

3.1.1 Geothermal Energy

In the first place, the geothermal module was calculated as a common ground source heat pump system (*GSHP*). With that aim, EED (*Earth Energy Designer*) software

Table 2 Design of the geothermal system by EED software

Parameters used in EED software	
<i>Location of the building</i>	Province of Ávila (Spain)
<i>Ground geology</i>	Granitic materials
<i>Energy demand in heating mode (kWh)</i>	28,000
<i>Piping design</i>	Polyethylene double-U pipes of 32 mm in diameter
<i>Heat carrier fluid</i>	Mixture glycol/water
Results calculated by EED	
<i>Number of boreholes</i>	2
<i>Total drilling length (m)</i>	180
<i>Nominal heat pump power (kW)</i>	20.72

developed by “Blocon Software” [24–26] was used to define the most relevant parameters of this kind of systems. It constitutes an useful tool for the design of vertical heat exchangers providing (among other things) the required borehole size and layout. Entering in the software with the characteristics of the building (energy demand), ground thermal conductivity, geological properties and parameters related to the heat exchangers design (piping system, distance, material...); it automatically defines the geothermal plant. The following Table 2 collects the main data introduced in EED software and the resultant parameters of its calculation. The initial parameters collected in this Table 2 are derived from previous author’s researches on the study area (geological properties) and the main geothermal parameters (heat exchangers and heat carrier fluid). Energy demand was estimated for a standard domestic building of 200 m² placed in the mentioned study area (Ávila) [27, 28].

The above information corresponds to the usual dimensioning of a GSHP system. For the plant designed in the present research, some aspects must be reconsidered. The heat pump power required (20.72 kW) will be supplied by the renewable module described in the previous section. Regarding the number of boreholes and the drilling length, they will vary for the conditions of the suggested plant. In the case of the conventional geothermal installation, as Table 2 shows, two boreholes of 90 m are needed to supply the heat pump. The function of these boreholes is increasing the temperature of the heat carrier fluid before entering in the heat pump as well as dissipating the low temperature of the fluid when it leaves the heat pump. According to heat pump manufacturer data, the temperature of the fluid when it enters into the evaporator is 0 and −3 °C when it leaves the heat pump and returns to the set of boreholes. Additionally, EED software simulates the temperature of the fluid during the lifetime of the installation as Fig. 5 shows.

On the contrary, in the installation proposed in this research, the fluid returning to the boreholes has a higher temperature than in the conventional plant (−3 °C) where the heat pump reduces its temperature. In this second case, the ground is only required to elevate the temperature of the heat carrier fluid to a certain value before

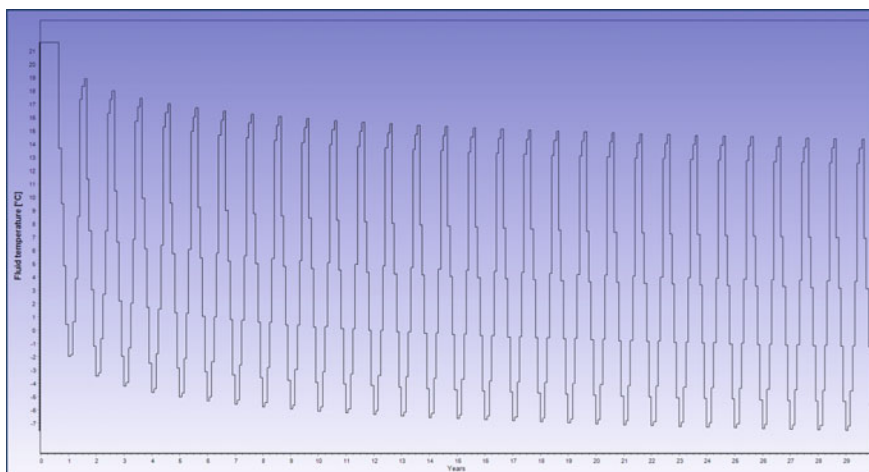


Fig. 5 Evolution of the fluid temperature in the conventional geothermal installation

getting in the solar panel. Since the conditions of the fluid are not as extreme as using a heat pump (the ground does not have to dissipate the cold of the entering fluid), the drilling length can be significantly reduced. For these reasons, only one borehole of 90 m was initially considered as the constituent of the geothermal section.

Regarding the temperature of the heat carrier fluid, for this assumption it is not possible to use the numerical simulation of EED since this software presupposes a geothermal installation constituted by a heat pump that notably decreases the outlet fluid temperature. Based on previous researches in a borehole of the study area [29], the temperature of the ground keeps constant to 14.6 °C in the depth of 20 m. Considering the standard thermal gradient of 1 °C each 33 m of depth, in the designed borehole of 90 m a temperature of around 16 °C will be easily achieved. Thus, given the conditions of the system, the heat carrier fluid will return to the borehole with a temperature of around 10–12 °C and will reach the temperature of the ground in a reasonable period of time.

3.1.2 Thermal Solar Energy

The following stage is the increase of the heat carrier fluid temperature by using the thermal solar energy. The corresponding selection of the solar module was carried out considering a series of data of the area where the system is planned to be implemented and the fact that the working fluid enters in the thermal solar panel with a temperature of 16 °C (since it comes from the geothermal borehole). Table 3 shows the main geographical and climatic information belonging to the study area.

As already mentioned, the use of the suggested installation is limited to cold months from September to May. Observing Fig. 6, it is easily perceptible how the elevation angle of the sun gets the lowest value during the winter months (priority

Table 3 Geographical and climatic data in the location of the installation [30–32]

Province	Ávila
Climatic zone	IV
Global solar radiation [MJ/m ²]	16.6 ≤ H ≤ 18.0
Latitude [°]	40.50
Altitude [m]	2279
Medium relative humidity [%]	41.00
Mean wind velocity [km/h]	21.00
Maximum temperature in summer [°C]	30.00
Minimum temperature in winter [°C]	−6.00

use of the system). A habitual practice is considering the inclination of the solar panels as the sum of 10° to the latitude of the place if the installation is specifically designed to be working in the cold months [33]. Since the latitude of the study area is 40.50°, the solar panel will be installed with an inclination angle of 50.50°. In this Fig. 6 it is also possible to observe in the solar mask that the solar radiation is not affected by surrounding constructions due to the location of the area.

Figure 7 shows how the inclination angle of the panel improves the global amount of energy received in a year comparison with the gain of a solar panel installed in a horizontal position. In addition this Figure describes the annual evolution of the ambient temperature in the study area and the temperature of the fluid gets in the solar panel (set in 16 °C since it comes from the borehole).

The characteristics of the thermal solar panel selected in function of the information presented above can be found in Table 4. This selection is based on the technical

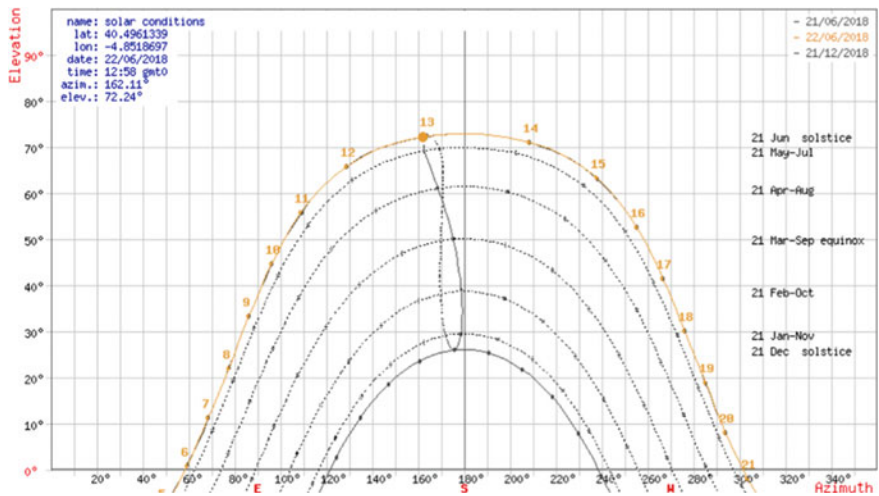


Fig. 6 Solar chart/mask of the province of Ávila from the “Sun Earth Tool” application

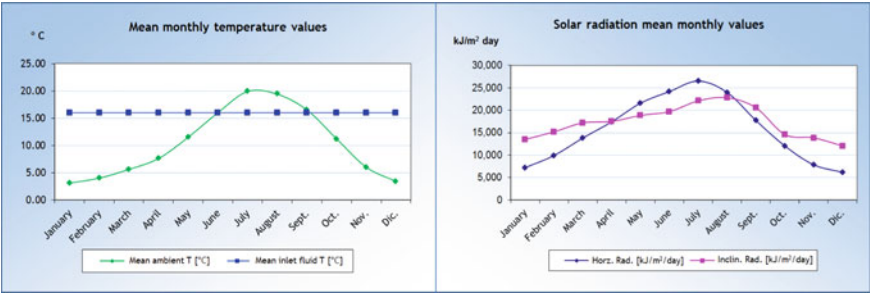


Fig. 7 Monthly ambient temperature and inlet fluid temperature (on the left). Monthly solar radiation values (on the right) [33]

and economical availability of these panels in a large number of countries. Additionally, the simplicity of installation and proved reliability motivated this decision. The design of the collector (plane panel) and the internal fluid circuits facilitates the inclusion in the geothermal fluid loop. Parameters detailed in the mentioned Table 4 correspond to the commercial solar panel selected and are provided by the corresponding manufacturer.

Finally, applying f-Chart method [35], the heat contribution of the thermal solar system was determined for the month with the highest demand. The expression used by the mentioned method can be observed in Eq. 5.

$$f = 1.029D_1 - 0.065D_2 - 0.245D_1^2 + 0.0018D_2^2 + 0.0215D_1^3 \tag{5}$$

Substituting in Eq. 5 with the values of D_1 and D_2 whose calculation is presented in Appendix A, a factor f of 0.36 was obtained. It means that in the least favourable month, the geothermal-thermal module supply the 36% of the energy demand. Since the annual demand is 28,000, 10,088 kWh are covered with the combination of these energies.

Table 4 Main information of the solar panel selected in this research

Design	Plane panel
Model	SOLARIS CP1
Surface [m ²]	2.02
Efficiency factor	0.799 ^a
Global losses coefficient [W/(m ² °C)]	3.4 ^a
Primary circuit flow [(l/h)/m ²]	50
Primary circuit specific heat [kcal/(kg °C)]	1
Panel efficiency	0.9 ^a

^aObtained according to ISO 9806 [34]

Table 5 Technical data of the photovoltaic solar kit

Design	Solar package
Model	Victron
Dimensions [mm]	1650 × 992 × 40
Power [Wp]	2250
Panel solar voltage [V]	31.4
Technology	Polycrystalline
Number of panels	9
Total kit weight [kg]	18.5

3.2 Power Module

3.2.1 Photovoltaic Solar Energy

Based on data provided by meteorological observatories, sunlight hours in the study area for the months of the installation expected use were defined [36]. Then, selecting a commercial solar kit constituted by nine photovoltaic panels, a contribution of 2,090 Wh can be obtained for the period considered in the present research (January–May, September–December). Considering 1,819 sunlight hours (applying the sun peak hour's method including information of the solar mask for the place) for the nine months of installation operation, the annual supply of this section would be of 3.80 MWh. It must be mentioned that inverters these systems usually include are not needed in this case since the electricity is directly conducted to the buffer tank. This fact will result in a significant economical saving. Table 5 shows the technical information of the solar kit selected as a part of the global suggested installation. These data are obtained from the commercial catalogue of the selected photovoltaic solar kit.

The selection of the model was made according to the availability and technical reliability of the equipment chosen. It is a standard device usually used by the common local solar installer.

3.2.2 Wind Energy

Finally, the wind module was defined by the use of a free application developed by the company “Enair Energy”. This tool allows knowing the contribution of a certain wind generator in the place where the system will be located. It is based on a method that uses the Weibull index and a series of parameters of the area in question (wind medium velocity, altitude, wind rose...). Entering in the application with the altitude and latitude and longitude coordinates of the area, it calculates (for a particular commercial model) the daily supplying of the wind resource providing at the same time the wind velocity. Figure 8 shows the software simulation of the velocities in the area where the system will be placed.

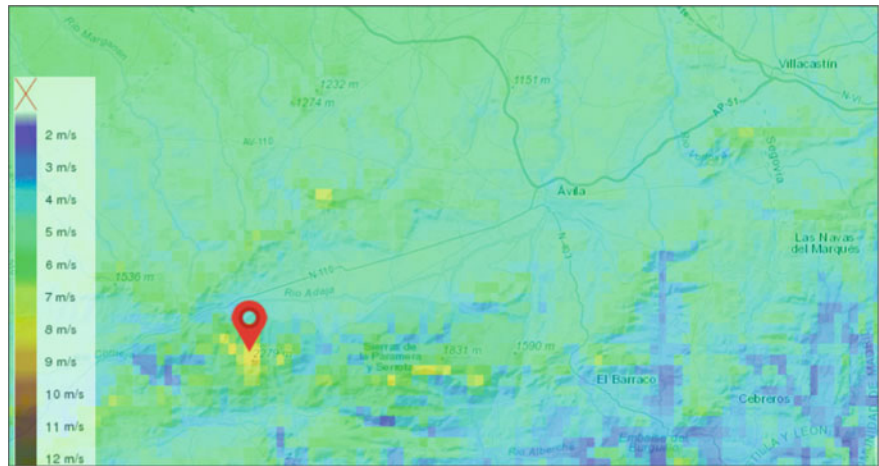


Fig. 8 Velocities distribution in the area contemplated in this research

Table 6 Technical description of the wind generator

Design	Wind generator
Model	Enair
Number of blades	3
Nominal power [W]	6000
Voltage [V]	24/48/220
Diameter [m]	4.4
Swept area [m ²]	14.5
Minimum wind speed [m/s]	2

From the output data of this tool, the annual contribution was calculated for the model of generator described in Table 6. This parameter takes the value of 8.53 MWh/year for a wind velocity of 5.9 m/s.

3.3 System Energy Contribution

By the implementation of the modules previously described, a fraction of the total demand would be covered. Thus, considering the contribution of each of these systems, the suggested installation would provide:

Total contribution = *geothermal/solar module* + *photovoltaic module*
+ *wind module* = 10.09 MWh/year + 3.80 MWh/year
+ 8.53 MWh/year = 22.42 MWh/year

Since the global energy demand reaches 28.00 MWh, the installation described in this research would be covering 80.07% of the total needs. This fact means that the remaining demand (19.93%) requires external energy supply.

4 Economic and Environmental Analysis

In order to justifying the system described throughout the present research, an economic and environmental evaluation of the conventional ground source heat pump system and the proposed installation was carried out.

4.1 Economic Analysis

The economic evaluation includes the calculation of the two main modules; initial investment and annual operational costs. This evaluation is performed on the traditional ground source heat pump system and on the one suggested in this research. In this way, the economic viability of the new model will be completely tested.

The parameters of the traditional GSHP system calculated by EED software were presented in Table 2. Based on these data, this option was economically evaluated. Thus, Table 7 shows the initial investment for the conventional geothermal installation according to the needs of the building previously described.

In order to analyse the economic viability of the system proposed in this research, its initial investment was also calculated (collected in Table 8) to compare it with the one of the conventional plant previously presented.

In addition to the initial investment of both systems, annual costs derived from the installation use must be considered. Regarding the traditional geothermal plant, these costs correspond to the heat pump electricity consumption. If the nominal power of this device was of 20.72 kW and its COP 4.5 in heating mode according to EN14511 and ISO13256 standards [39, 40], the energy consumption required by the heat pump would be of around 4.6 kW, meaning, 11,050.67 kWh per year (considering 2400 h of annual operation). In the suggested system, the demand not covered by the renewable modules (19.93% of the total demand) needs an external electricity contribution which also results in annual expenses. As already seen, the total demand was 28,000 kWh, therefore, 5,580.40 kWh must be externally provided (considering the design COP of 4.5 in heating mode). An additional characteristic of this system is that the mentioned electricity contribution can be made during the night taking advantage of more affordable rates. Table 9 presents the annual costs associated to both systems.

Table 7 Initial investment for the conventional geothermal installation

Conventional ground source heat pump system				
Element	Quantity	Unities	Unitary price (€) *	Total price (€)
Drilling	180.00	Meter	44.00	7,920.00
Geothermal heat exchanger	2.00	Unity	511.20	1,022.40
Injection tube	2.00	Unity	146.00	292.00
Guide	2.00	Unity	52.80	105.60
Assembly pack	2.00	Unity	27.20	54.40
Spacers	18.00	Unity	6.40	115.20
Grouting material	5.00	kg	0.70	3.50
Manifold	2.00	Unity	409.50	819.00
Geothermal heat pump	1.00	Unity	19,300.00	19,300.00
Heat pump accessories	–	–	–	6,553.57
Heat carrier fluid	1,050.00	Litres	4.00	4,200
Auxiliary piping	35.00	Meters	7.36	257.60
Thermal response test	1.00	Unity	4,118.36	4,118.36
Boost pump group	1.00	Unity	3,219.66	3,219.66
Total Investment				47,981.29

*Prices were taken from the commercial catalogues of Enertres and ALB systems [37, 38]

4.2 Environmental Evaluation

As described in the previous section, the electricity supply required by the suggested installation is lower in comparison to the traditional ground source heat pump system. This fact results in a reduction of the global CO₂ emissions since they are product of the electricity use. Thus, an analysis of the CO₂ emissions associated to each scenario must be made. Such evaluation can be found in Table 10.

5 Discussion

An alternative to the common ground source heat pump system has been proposed and described throughout this study. Based on technical calculations of both solutions (the common geothermal system and the one suggested) applied on the same case of study, an economic and environmental comparison was established. In Tables 7 and 8 the initial investment of each solution was thoroughly justified. Additionally, in Table 9, the annual expense associated to the use of each of the systems was also calculated. Thus, observing the mentioned data, the economic balance is clearly more favourable for the new solution presented in this research. In Fig. 9 it is easily observable the economic differences between both solutions in terms of initial investment and annual

Table 8 Initial investment for the suggested system

Suggested renewable installation				
Thermal module				
Element	Quantity	Unities	Unitary price (€)	Total price (€)
Drilling	90.00	Meter	44.00	3,960.00
Geothermal heat exchanger	1.00	Unity	511.20	511.20
Injection tube	1.00	Unity	146.00	146.00
Guide	1.00	Unity	52.80	52.80
Assembly pack	1.00	Unity	27.20	27.20
Spacers	9.00	Unity	6.40	57.60
Grouting material	2.50	kg	0.70	1.75
Manifold	1.00	Unity	409.50	409.50
Boost pump group	1.00	Unity	3,219.66	3,219.66
Heat carrier fluid	525.00	Litres	4.00	2,100.00
Auxiliary piping	50.00	Meters	7.36	368.00
Thermal response test	1.00	Unity	4,118.36	4,118.36
Buffer tank	1.00	Unity	1,088.67	1,088.67
Thermal solar panel	10.00	Unity	287.14	2,871.40
Power module				
Photovoltaic package	1.00	Unity	4,674.00	4,674.00
Wind generator	1.00	Unity	9,015.00	9015.00
Storage battery	10.00	Unity	293.90	2,939.00
Computerized system				
Core unit	1.00	Unity	1,180.25	1,180.25
Sensor	8.00	Unity	3.25	26.00
Communication system	1.00	Unity	255.10	255.10
Total Investment				37,021.49

* Prices were taken from the commercial catalogues of Enertres and ALB systems [37, 38]

Table 9 Annual expense of the traditional geothermal system and the one presented in this research

	Electricity consumption (kWh)	Rate (€/kWh)	Annual expense (€)
Conventional plant	11,050.67	0.12779 ^a	1,412.17
Suggested system	5,580.40	0.06580 ^b	317.19

^a Price of kWh in the common rate by EDP Company

^b Price of kWh in the nocturnal rate by EDP Company

Table 10 Annual CO₂ emissions of the traditional geothermal system and the one presented in this research

	Electricity consumption (kWh)	^a Conversion factor (kg CO ₂ /kWh)	Annual CO ₂ emissions (kg)
Conventional plant	11,050.67	0.399	4,409.22
Suggested system	5,580.40	0.399	2,226.58

^a Normalized values provided by the Spanish Institute of the Diversification and Energy save “IDAE” [41]

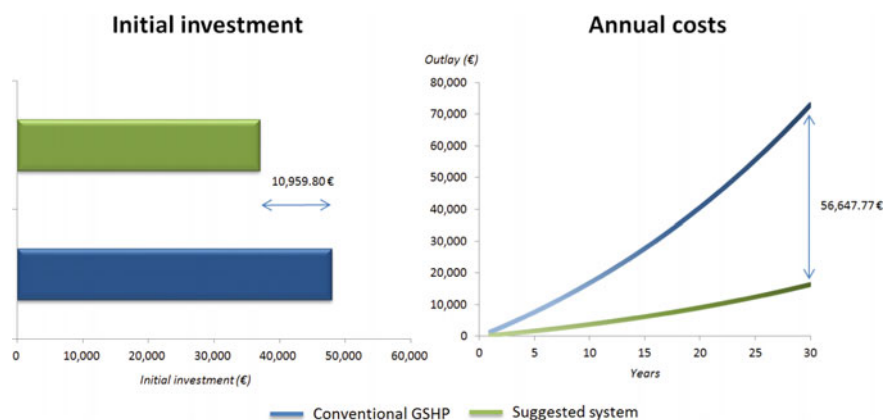
expenses. It can be seen that the initial investment of the common ground source heat pump system is 10,959.80 € higher than the investment required for the suggested solution.

Regarding the annual costs, from data of Table 9, the evolution of the costs of each system in the period of useful life was calculated. With the aim of updating the costs of each year to the real value of the moment, data are expressed in terms of the “*Net Present Value*” (NPV) using a discount rate of 1.8%. In this way, in the last year of operation (year 30), the cumulative cost for the common geothermal plant is considerably higher (56,647.77€) than the cost associated in the suggested system.

In relation to the environmental dimension, as shown in Table 10, the CO₂ emissions of the alternative presented here are half of the emissions associated to the traditional GSHP system. The CO₂ emissions difference grows during the operative phase of both systems reaching the value of 65,479.13 kg in the last year (year 30).

In connection with all the above, a series of considerations about the system suggested in this work can be addressed:

- The installation proposed as an alternative of the common GSHP system means an economic saving of around 22.84% regarding the initial investment of both solutions. Savings are possible thanks to the substitution of the geothermal heat pump

**Fig. 9** Economic comparison of the common GSHP system and the one presented in this research

and the reduction of the total drilling length. This fact will make the geothermal energy more attractive and affordable for the final user, promoting at the same time a more extensive use of renewables energies.

- Electricity annual costs of the conventional geothermal systems are considerably low in comparison with other technologies. However, the new solution reduces even more these costs, in a percentage of 77.54%, which involves an economic saving of 56,647.77€ for the global operative phase of the installation.
- The environmental side also influences the selection of the system suggested in this research. The reason of this choice derives from the reduction of the CO₂ emissions in this solution, being 49.50% lower.
- The new system still depends on an external electricity supply. However, increasing the contribution of the thermal and photovoltaic modules and wind energy, the total demand could be covered avoiding the external dependence. It would cause an increase in the initial investment but the annual expenses would disappear. The solution presented here finds equilibrium between both parameters (initial investment and annual costs) so that from the economic and environmental point of view it is more recommendable than the common GSHP.

5.1 Sensitivity Analysis

In this section, a sensitivity analysis is presented to evaluate how the different values of a set of independent variables affect the viability of the project suggested in this research. With that aim, three different variables were modified keeping constant the remaining parameters in a pessimistic, optimistic and an expected scenario.

– Electricity price

The first variable considered in this analysis is the electricity price. In the results presented in Fig. 9, a discount rate of 1.8% was applied. This rate belongs to the expected scenario. In a hypothetical optimistic scenario the discount rate estimated is of 1.5 and 2.1% for a pessimistic situation. As Fig. 10 shows, the conventional system starts being sensitive from year 15 and this sensitivity progressively grows in the remaining period considered. Regarding the suggested system, it is less sensitive to the variation of the electricity price than the conventional one. In both systems, the sensitivity is the same in any of the scenarios analyzed, optimistic and pessimistic.

– Electric rate

In this case, the electric rates showed in Table 9 belong to the expected scenario for both the conventional and the suggested systems. These rates have been reduced and increased in a percentage of 15% to respectively represent the optimistic and pessimistic scenarios. As presented in Fig. 11, the sensitivity to the variation of the electric rate is also higher in the conventional system for which the sensitivity

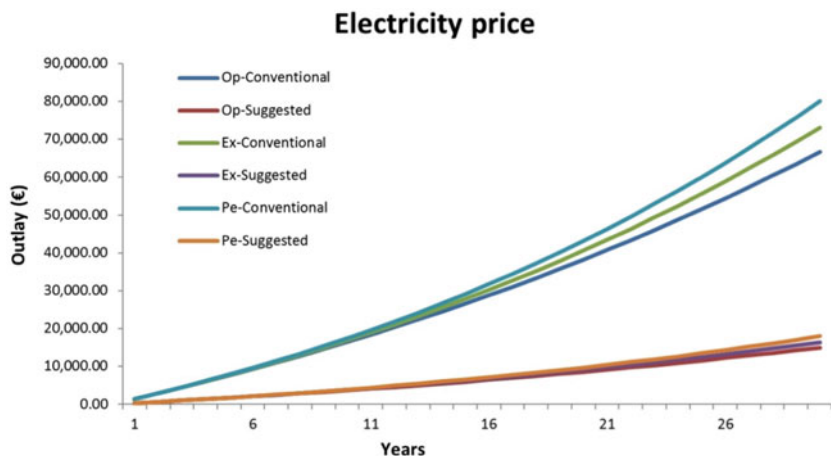


Fig. 10 Sensitivity analysis to the variation of the electricity price parameter. “Op”, optimistic scenario, “Ex”, expected scenario, “Pe”, pessimistic scenario

is the same for the optimistic and pessimistic scenario. In the case of the suggested system, it is quite sensitive to the increase of the electric rate (pessimistic scenario). However, its sensitive to the reduction of the electric rate is practically null.

– CO_2 emission factor

The last variable considered in the sensitivity analysis is the CO_2 emission factor. Observing Table 10, the expected emission factor is 0.399. As in the previous

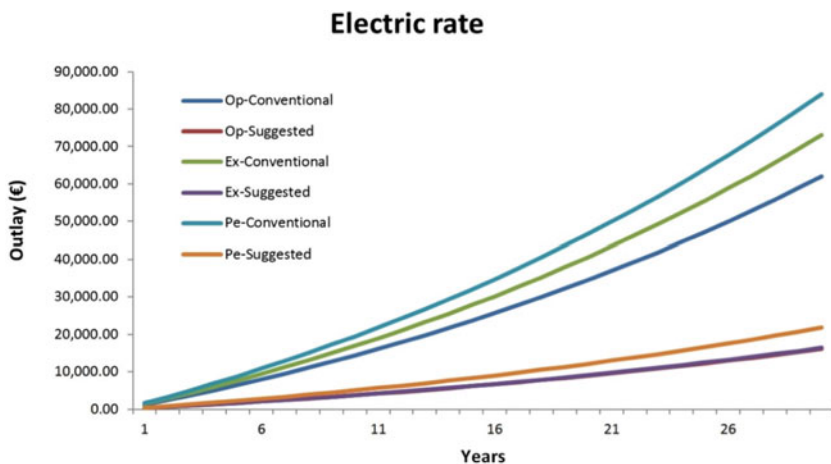


Fig. 11 Sensitivity analysis to the variation of the electric rate parameter. “Op”, optimistic scenario, “Ex”, expected scenario, “Pe”, pessimistic scenario

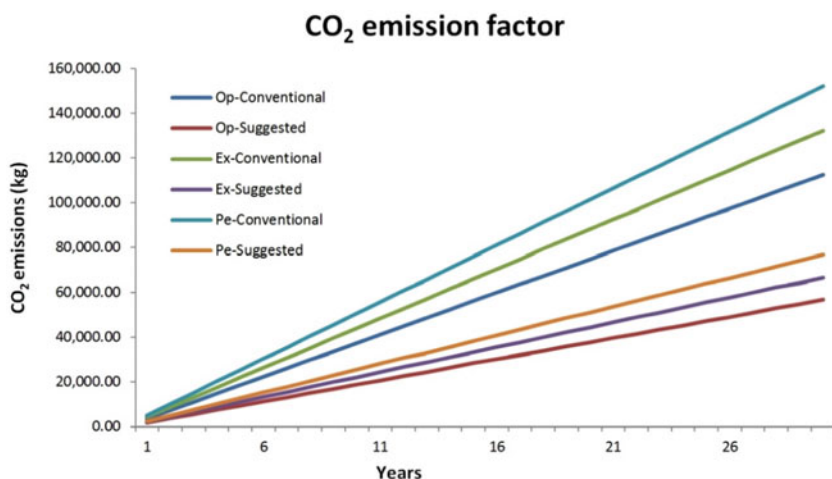


Fig. 12 Sensitivity analysis to the variation of the CO₂ emission factor. “Op”, optimistic scenario, “Ex”, expected scenario, “Pe”, pessimistic scenario

cases, optimistic and pessimistic scenarios have been also analyzed. Thus, this factor has been reduced and increased in a 15%, obtaining for the optimistic situation an emission factor of 0.339 and 0.459 for the pessimistic one. Figure 12 shows how the sensitive to the increase or reduction of the emission factor is approximately the same in both systems. However, as in the previous cases, the sensitivity of the conventional system is higher in comparison to the suggested one.

6 Conclusions

The mitigation of the climate change includes the constant search of new solutions that tend to reduce the electricity dependence increasing the use of renewable energies. The current schema of the geothermal system is frequently discarded by the general user due to the high initial outlay they demand. In this regard, it is highly recommendable to find new alternatives that promote this kind of energy. On this matter, a new schema of the common ground source heat pump system was proposed. A case of study was conducted for evaluating the viability of the new solution which considers the substitution of the geothermal heat pump by a combination of renewable modules. As seen in the methodology section, the basis of the suggested model is the computerized system of data acquisition and decision making that receives information from several sections (inputs of Fig. 13) to finally cover the energy demanded by the user (output of Fig. 13).

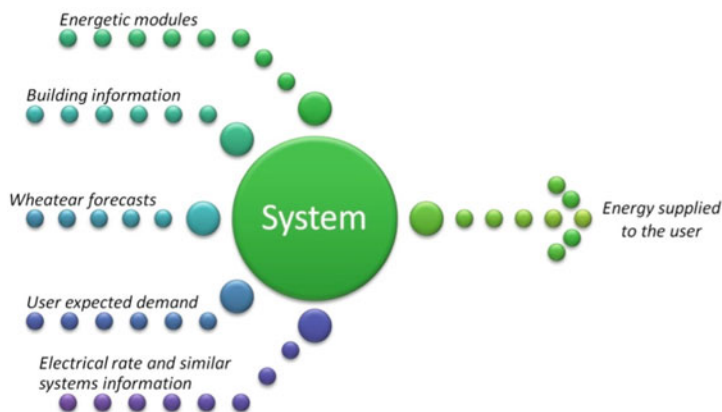


Fig. 13 Inputs and Output that constitute the computerized system of the renewable installation presented in this research

By the implementation of the proposed system, important economic savings would be achieved and the environmental side would be improved thanks to the reduction of the CO₂ emissions. The external electricity contribution is considerably reduced (not eliminated) and, additionally, the configuration of the system allows using the most economic rate of electricity supply. The model could be readily extended to alternative scenarios and areas where the contribution of each module will not be the same. Regardless, the system would still present important advantages even in the least favourable cases where the renewable contribution was considerably lower. In summary, for the single family home considered here, placed in the province of Ávila, the substitution of the heat pump by renewable modules achieves a reduction of 22.84% in the initial investment, 77.54% in the operational costs and CO₂ emissions are reduced 49.50%.

Acknowledgements Authors would like to thank the Department of Cartographic and Land Engineering of the Higher Polytechnic School of Avila, University of Salamanca, for allowing us to use their facilities and their collaboration during the experimental phase of this research. Authors also want to thank the Ministry of Education, Culture and Sport for providing a FPU Grant (Training of University Teachers Grant) to the corresponding author of this study what has made possible the realization of the present work.

Appendix A

This section describes the calculation of factors D_1 (energy absorbed by the panel) and D_2 (energy lost by the panel) required to solve Eq. 5 of f-Chart method used in the dimensioning of the thermal solar module.

- **D_1 (Energy absorbed by the panel) Calculation**

$D_1 = \text{energy absorbed by the panel } (E_a) / \text{monthly heat load } (H_l)$

$$E_a = S_c F'_r (\tau \alpha) R_1 N$$

where:

S_c = panel surface (m^2). This value is 20.2 m^2

$F'_r (\tau \alpha)$ = Dimensionless factor calculated from the efficiency of the panel and characteristic values of each panel. In this case this factor is 0.84.

R_1 = Daily Monthly Radiation by Unity of Surface (kJ/m^2). Its Value is $13,521 \text{ kJ/m}^2 \cdot \text{day}$ [32]

N = number of days in the month.

H_l = Monthly heat load in kJ. For the month with the highest demand (January), this value is $1.56 \cdot 10^6 \text{ kJ}$.

$$D_1 = (20.2 \cdot 0.84 \cdot 13,521 \cdot 31) / 1.56 \cdot 10^6 = 0.46$$

- **D_2 (Energy lost by the panel) Calculation**

$D_2 = \text{energy lost by the panel } (E_p) / \text{Monthly heat load } (H_l)$

$$E_p = S_c F'_r U_L (100 - t_a) \Delta t K_1 K_2$$

where:

S_c = panel surface (m^2). This value is 20.2 m^2 .

$F'_r U_L$ = characteristic factor of the panel losses. Its value is 3.56.

t_a = monthly ambient temperature. It is 16°C .

Δt = period of time considered (s). In this case for the whole month, it is $2,678,400 \text{ s}$.

K_1 , K_2 = Correction Factors. $K_1 = 1.02$. $K_2 = 0.97$. These Factors Correct the Orientation and the Geometry of the Panels.

H_l = Monthly heat load in J. Its value is $1.56 \cdot 10^{10}$

$$D_2 = (20.2 \cdot 3.56 \cdot (100 - 16) \cdot 2,678,400 \cdot 1.02 \cdot 0.97 / 1,56 \cdot 10^{10}) = 1.02.$$

References

1. Bartolucci L, Cordiner S, Mulone V, Rocco V, Rossi JL (2018) Hybrid renewable energy systems for renewable integration in microgrids: influence of sizing on performance. *Energy* 152:744–758
2. Fikiin K, Stankov B (2015) Integration of renewable energy in refrigerated warehouses. *Handbook Res Adv Appl Refri Syst Technol* 28:803–853
3. Bassetti MC, Consoli D, Manente G, Lazzaretto A (2018) Design and off-design models of a hybrid geothermal-solar power plant enhanced by a thermal storage. *Renew Energy* 128(Part B):460–472
4. Ciani Bassetti M, Consoli D, Manente G, Lazzaretto A (2018) Design and off-design models of a hybrid geothermal-solar power plant enhanced by a thermal storage. *Renew Energy* 128:460–472
5. Jacobson MZ, Cameron MA, Hennessy EM, Petkov I, Meyer CB, Gambhir TK, Maki AT, Pflieger K, Clonts H, McEvoy AL, Miccioli ML, von Krauland A-K, Fang RW, Delucchi MA (2018) 100% clean and renewable Wind, Water, and Sunlight (WWS) all-sector energy roadmaps for 53 towns and cities in North America. *Sustain Cities Soc* 42:22–37
6. Guo S, Liu Q, Sun J, Jin H (2018) A review on the utilization of hybrid renewable energy (Review). *Renew Sustain Energy Rev* 91:1121–1147
7. Nanaki EA, Xydis GA (2018) Deployment of renewable energy systems: barriers, challenges, and opportunities. *Adv Renew Energ Power Technol* 2:207–229
8. Instituto para la Diversificación y Ahorro de la Energía “IDAE” (2012) Diseño de sistemas de intercambio geotérmico de circuito cerrado. Ministerio de Industria, Turismo y Comercio, Madrid
9. UNE 100715–1 (2014) Diseño, ejecución y seguimiento de una instalación geotérmica somera. AENOR, Asociación Española de Normalización y Certificación
10. Fraga C, Hollmuller P, Schneider S, Lachal B (2018) Heat pump systems for multifamily buildings: potential and constraints of several heat sources for diverse building demands. *Appl Energy* 225:1033–1053
11. Jeong J, Hong T, Kim J, Chae M, Ji C (2018) Multi-criteria analysis of a self-consumption strategy for building sectors focused on ground source heat pump systems. *J Clean Prod* 186:68–80
12. Zarrella A, Zecchin R, Pasquier P, Guzzon D, De Carli M, Emmi G, Quaggia M (2018) A comparison of numerical simulation methods analyzing the performance of a ground-coupled heat pump system. *Sci Technol Built Environ* 24(5):502–512
13. Zhang X, Li H, Liu L, Bai C, Wang S, Song Q, Zeng J, Liu X, Zhang G (2018) Optimization analysis of a novel combined heating and power system based on biomass partial gasification and ground source heat pump. *Energy Convers Manage* 163:355–370
14. Luo J, Luo Z, Xie J, Xia D, Huang W, Shao H, Xiang W, Rohn J (2018) Investigation of shallow geothermal potentials for different types of ground source heat pump systems (GSHP) of Wuhan city in China. *Renew Energy* 118:230–244

15. Self SJ, Reddy BV, Rosen MA (2013) Geothermal heat pump systems: status review and comparison with other heating options. *Appl Energy* 101:341–348
16. Wang E, Fung AS, Qi C, Leong WH (2012) Performance prediction of a hybrid solar ground-source heat pump system. *Energy Build* 47:600–611
17. Europe's Energy Portal (2018) Fuel and electricity prices. <http://www.energy.eu/>
18. Sorknæs P (2018) Investigation of shallow geothermal potentials for different types of ground source heat pump systems (GSHP) of Wuhan city in China. *Energy* 152:533–538
19. Sarbu I, Sebarchievici C (2016) Solar-assisted heat pump systems. *Renew Energy Sourc Appl Emerg Technol* 1:79–13
20. Isafiade JA, Short M, Bogataj M, Kravanja Z (2017) Integrating renewables into multi-period heat exchanger network synthesis considering economics and environmental impact. *Comput Chem Eng* 99:51–65
21. Karunathilake H, Perera P, Ruparathna R, Hewage K, Sadiq R (2018) Renewable energy integration into community energy systems: a case study of new urban residential development. *J Clean Prod* 173:292–307
22. Alnifro M, Taqvi ST, Ahmad MS, Bensaida K, Elkamel A (2017) Optimal renewable energy integration into refinery with CO₂ emissions consideration: an economic feasibility study. *IOP Conf Ser Earth Environ Sci* 83:012018
23. Instituto para la Diversificación y Ahorro de la Energía “IDAE” (2010) Agua Caliente Sanitaria Central. Ministerio de Industria, Turismo y Comercio, Madrid
24. Sáez Blázquez C, Farfán Martín A, Martín Nieto I, González-Aguilera D (2017) Measuring of thermal conductivities of soils and rocks to be used in the calculation of a geothermal installation. *Energies* 10:795–813
25. Sarbu I, Sebarchievici C, Dorca A (2017) Simulation of ground thermo-physical capacity for a vertical closed-loop ground-coupled heat pump system. In: International multidisciplinary scientific geoconference surveying geology and mining ecology management, SGEM, vol 17(42), pp 557–565
26. Sliwa T, Nowosiad T, Vytyaz O, Sapinska-Sliwa A (2016) Study on the efficiency of deep borehole heat exchangers. *SOCAR Proc* 2:29–42
27. Blázquez CS, Martín AF, Nieto IM, García PC, Pérez LSS, Aguilera DG (2017) Thermal conductivity map of the Avila region (Spain) based on thermal conductivity measurements of different rock and soil samples. *Geothermics* 65:60–71
28. Blázquez CS, Martín AF, Nieto IM, García PC, Pérez LSS, Aguilera DG (2017) Efficiency analysis of the main components of a vertical closed-loop system in a borehole heat exchanger. *Energies* 10:201–216; Special Issue “Low Enthalpy Geothermal Energy”
29. Blázquez CS, Martín AF, García PC, Pérez LSS, del Caso JS (2016) Analysis of the process of design of a geothermal installation. *Renew Energy* 89:1–12
30. Código Técnico de la Edificación “CTE” (2017) DB-HE-1: Limitación de la demanda energética. Ministerio de Economía y Competitividad, Madrid
31. Código Técnico de la Edificación “CTE” (2017) DB-HE-2: Rendimiento de las instalaciones térmicas. Ministerio de Economía y Competitividad, Madrid
32. Agencia Estatal de Meteorología “AEMET” (2017) Servicios climáticos. Ministerio de Agricultura y Pesca, Alimentación y Medio Ambiente, Madrid
33. Instituto para la Diversificación y Ahorro de la Energía “IDAE” (2006) Energía solar térmica. Ministerio de Industria, Turismo y Comercio, Madrid
34. ISO 9806:2017 (2017) Solar energy—Solar thermal collectors—test methods. International Organization for Standardization
35. Okafor IF, Akubue G (2013) F-chart method for designing solar thermal water heating systems. *Int J Sci Eng Res* 3(9)
36. Boletín Mensual de Estadística “BME” (2016) Climatología. Ministerio de Agricultura y Pesca, Alimentación y Medio Ambiente, Madrid
37. Catálogo tarifa bomba de calor (2018) ENERTRES
38. Catálogo de producto y tarifas, Sistema de geotermia (2018) ALB SISTEMAS

39. EN 14511–1:2013 (2013) Air conditioners, liquid chilling packages and heat pumps with electrically driven compressors for space heating and cooling. AENOR, Asociación Española de Normalización y Certificación
40. ISO 13256–1:1998 (1998) Water-source heat pumps—Testing and rating for performance. International Organization for Standardization
41. Instituto para la Diversificación y Ahorro de la Energía “IDAE” (2014) Factores de emisión de CO₂ y coeficientes de paso a energía primaria de diferentes fuentes de energía final consumidas en el sector edificios en España. Ministerio de Industria, Energía y Turismo, Madrid

The Role of Geothermal Heat Pump Systems in the Water–Energy Nexus



Carlos Rey Mahia , Felipe Pedro Álvarez Rabanal , Stephen J. Coupe ,
and Luis Ángel Sañudo Fontaneda

Abstract Unplanned rapid urbanization is considered to be one of the major drivers of change in cities across the world. It leads to an inadequate transformation of urban environments, affecting strategic energy and water management infrastructure, resulting as well in an escalation in energy demand and a greater pressure on stormwater facilities. It is estimated that one third of the total energy demand in the European Union (EU) is associated to air-conditioning in buildings, whilst conventional drainage systems have become unsustainable under the current scenario of climate change. In this context of uncontrolled challenges, the EU is encouraging the incorporation of Nature-Based Solutions (NBS) in order to promote resilient infrastructure and to reduce instability. Sustainable Drainage Systems (SuDS) have been selected as key Stormwater Control Measures (SCM), contributing to a paradigm shift in urban water management. As the need for multifunctional spaces evolves due to the lack of urban land, SuDS are increasingly becoming a potential asset to house renewable energy structures, helping to develop the water–energy nexus. Thus, this chapter deals with the opportunities arising in this new research line combining surface geothermal energy systems and SuDS. Both laboratory and field experiences

C. R. Mahia (✉)

Department of Construction and Manufacturing Engineering, Polytechnic School of Mieres,
University of Oviedo, Calle Gonzalo Gutiérrez Quirós s/n, 33600 Mieres, Spain
e-mail: UO236881@uniovi.es

F. P. Á. Rabanal

Department of Construction and Manufacturing Engineering, Polytechnic School of Mieres,
University of Oviedo, Calle Pedro Puig Adam, Módulo 7, 33203 Gijón, Spain
e-mail: alvarezfelipe@uniovi.es

S. J. Coupe

Centre for Agroecology, Water and Resilience (CAWR), Coventry University, Wolston Lane, CV8
3LG, Ryton on Dunsmore, UK
e-mail: Stephen.coupe@coventry.ac.uk

L. Á. S. Fontaneda

Department of Construction and Manufacturing Engineering, Polytechnic School of Mieres,
University of Oviedo, Calle Gonzalo Gutiérrez Quirós s/n, 33600 Mieres, Spain
e-mail: sanudoluis@uniovi.es

have been analyzed, compiling the lessons learned, identifying the present knowledge gaps, and proposing the future prospects for development. Therefore, paving the way for the effective combination of both technologies.

Keywords Sustainable drainage systems • Water–energy Nexus • Ground source heat pumps • Air conditioning

1 Introduction and Background

1.1 *Challenges in Urban Energy and Water Infrastructures*

In most cities, stormwater is collected and rapidly conveyed off the surface into the sanitation system. This stormwater is mixed with the wastewater generated in the city. This mix is then conveyed to the wastewater treatment plants [1], involving high energy consumption due to the pumping along the network and the subsequent treatment of the flow. Energy is also consumed in the production of the chemical products necessary to treat water. This process leads to the emission of an increasing volume of greenhouse gases [2].

This management is key to provide access to clean water and sanitation, following the 6th 2030 Sustainable Development Goal (SDG) promoted by the United Nations (UN) [3]. 34% of the world's population did not have access to basic sanitation services in 2015; whilst 80% of the wastewater, resulting from human activity, is discharged into the natural streams untreated [4]. Consequently, the UN has declared the need to guarantee environmental sustainability, establishing how our energy and production systems are responsible for greenhouse gases emission. This will cause related problems with water management, among other issues [5].

Increasing population and its densification in urban areas in the upcoming decades [6] will increase the pressure in stormwater measures; and therefore, it will pose the need to implement better stormwater control measures (SCM) in cities across the world.

The International Energy Agency (IEA) has highlighted the need to boost geothermal energy uptake in order to achieve a zero net emissions scenario by 2050 [7]. To this end, the IEA stated that the exchange of information and best practices on the exploitation, development and use of geothermal energy should be promoted [8].

Energy consumption for space heating and air-conditioning in the European Union (EU) accounts for almost one third of the total energy demand [9]. 61% of the boilers used for air-conditioning in EU buildings use natural gas, oil and coal as fuels [10]. In this context, the EU has urged the member countries in recent decades to expand the use of geothermal resources [11]. The European Green Pact reaffirms the need to promote the use of renewable energy sources. Like the IEA, the objective of zero net greenhouse gas emissions by 2050 has been established [12].

The UN through its 2030 sustainable development agenda establishes in its goal number 7 the following: “*Ensure Access to affordable, reliable, sustainable*

and modern energy for all” [3]. Thus, the UN sets the need to foster modern and sustainable energy services, especially in less developed areas and countries, committing themselves towards the development and improvement of renewable energy systems [13].

Furthermore, the World Economic Forum (WEF) estimated that 68% of the world’s population will live in cities by 2050. This will exacerbate the current problems faced by cities, and the authorities are required to respond to these problems through sustainable urban planning and the development of resilient infrastructures [14]. One of the most serious consequences of this population growth is water stress (e.g., water scarcity, flooding issues...). If this scenario continues to develop, almost half of the world’s population could be suffering from water stress by 2030 [15].

The fourth industrial revolution is emerging against this backdrop [16]. One of the main challenges is to collect and reuse rainwater as much as possible before it continues its natural hydrological cycle, whilst using clean and sustainable energy at the same time [15].

1.2 The Water–Energy Nexus: An Opportunity for Resilience

Water and energy are two critical resources, so it is interesting to study the mechanisms of interaction between these two elements, especially when referring to infrastructures [17]. Hence, numerous new research lines have emerged in recent times with the aim of deepening the understanding of these mechanisms [18, 19]. Figure 1 shows the evolution of the number of academic publications in recent years.

The graph above shows the evolution of the academic publications found in Scopus associated with the keywords “water-energy nexus”. Scopus is the largest scientific database for journals, books and conference proceedings, which makes it ideal for

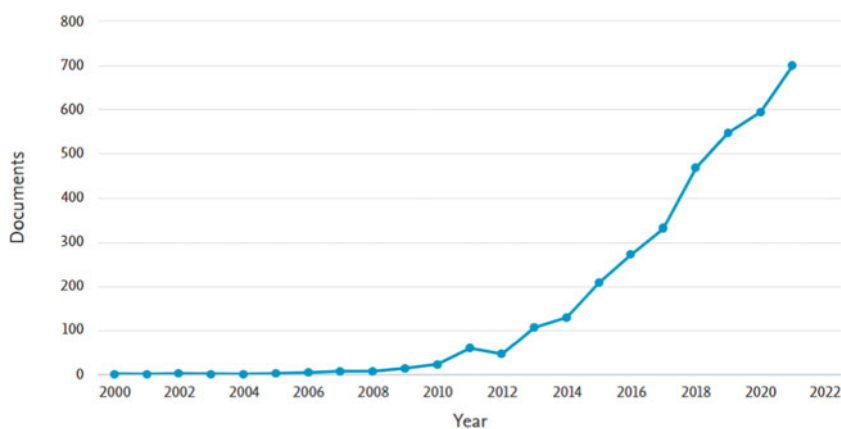


Fig. 1 Evolution of the number of publications on the water-energy nexus

this tentative analysis. As it can be seen in Fig. 1, there has been a strong scientific interest over the last decade in studying and developing this line of work. The scientific articles showed that the water-energy nexus was studied from different viewpoints: 28.9% of the publications were associated with the Environmental Science area, 16.2% with Energy, 12.9% with Engineering, and 10.3% with Social Science. These four areas of knowledge represented the main research fields in which these investigations were published.

These previous researches, explored the relationship between the water-energy nexus and the new challenges facing future cities and societies [20]. However, the involvement of the nexus in more specific problems and issues was also examined [21, 22], such as the implications of the water-energy nexus for sustainable transition in the state of Sao Paulo (Brazil). In Sao Paulo's research, the need to implement appropriate and affordable technologies for energy production and water management was identified, the enhancing green economic growth [23]. Along these lines, other studies have integrated other concepts into the water-energy nexus such as infrastructure life cycle assessment, using indicators such as the Water Stress Index (WSI) and the Blue Water Footprint (BWF) [24].

2 Surface Geothermal Energy Systems

Geothermal energy is described as the energy from the heat of the Earth's interior, stored in rock, water vapour or liquid water [25]. This heat is produced because of the following several physical phenomena taking place in the Earth's core and in the different layers that envelop it [26]:

- Disintegration of radioactive isotopes.
- Initial heat released during the formation of the planet.
- Differential movements of the varying layers.
- Crystallisation of the core.

This type of energy generation consists of using the heat released in the aforementioned processes to produce thermal or electrical energy, geothermal energy being one of the most efficient renewable energy sources [27].

In the current context of the energy model shift, an economic change will take place, promoting new technologies associated with renewable and clean energies [28]. It is estimated that by 2050, half of all households in the EU will be producing renewable energy [29], putting consumers at the core of the energy transition process. Geothermal energy thus establishes itself as a renewable, controllable energy source with great potential for exploitation.

For instance, very low-temperature geothermal energy systems ($<30\text{ }^{\circ}\text{C}$) can be used in virtually all of the earth's crust above ground [30]. These low enthalpy systems are presented as an energy source that help to reduce dependence on fossil fuels, favouring domestic energy self-consumption and promoting a sustainable energy

transition [31]. In addition, these systems could be outlined in many different configurations and designs, making them very versatile and easily adaptable to practically any situation and location [32]. Geothermal energy offers many benefits compared to other types of energy sources in the application to the air conditioning of buildings, including the following listed below [33]:

- Low operation and maintenance costs.
- No equipment is located outdoors, which avoids deterioration.
- Reduced machine room requirements.
- Reduced greenhouse gas emissions.
- Potential use for Domestic Hot Water (DHW) heating.
- Low levels of electricity demand associated with the consumption of the heat pump.

Another advantage of geothermal systems is that they are compact systems, and therefore, require less installation space. Then, this can be essential in buildings with limited space [34].

2.1 Types and Functions

There are different types of geothermal energy, as well as different classifications to categorise them. This section presents some of the most commonly used classifications. A study was also carried out to show the properties of the most appropriate geothermal systems for combination with SuDS elements.

Geothermal systems can be ranked according to the temperature of the geothermal reservoir [26], as shown in Fig. 2.

Thus, there are different types of geothermal exploitation depending on the ground temperature (a.k.a. enthalpy potential) [35, 36]:

- *High enthalpy*: these reservoirs are used for energy production through steam turbines.

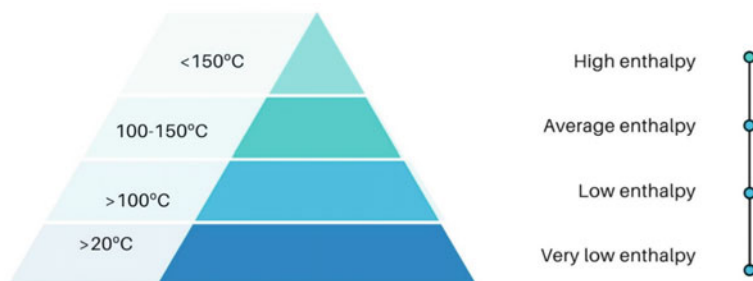


Fig. 2 Classification of geothermal energy according to the temperature of the geothermal reservoir

- *Medium enthalpy*: The reservoir can be used for electricity production, although with a lower yield than high enthalpy reservoirs.
- *Low enthalpy*: they are usually used for thermal use in industry, spas and heating.
- *Very low enthalpy*: thermal exploitation is carried out in deposits for heating and cooling purposes such as air-conditioning, using a heat pump.

A geothermal heat pump is a machine capable of transferring heat from a cold source to a hot source by means of an exchanger (see operating diagram in Fig. 3). For instance, it is capable of extracting heat from a cold source (e.g., the ground) and heating a hot source (e.g., a house), requiring only a small amount of electrical energy. The exchange can also be carried out in the opposite direction [37, 38]. GSHP can be divided according to the type of heat exchange with the outside as per outlined as follows [39]:

- Ground-Coupled Heat Pumps (GCHP) are closed-loop piping systems buried in the ground.
- Ground Water Heat Pumps (GWHP) are open loop systems with water wells.
- Water-Source Heat Pumps (SWHP) are closed-loop piping systems or open-loop systems connected to lakes, streams or other reservoirs.

There are two main types of heat exchange systems using heat pumps (Fig. 4): open loop and closed loop. In open systems, groundwater is extracted; while in closed systems, the fluid circulates through a vertical or horizontal circuit [40].

Horizontal and vertical closed-loop geothermal systems have a number of advantages and disadvantages. Within this system two main types can be distinguished as follows [36]:

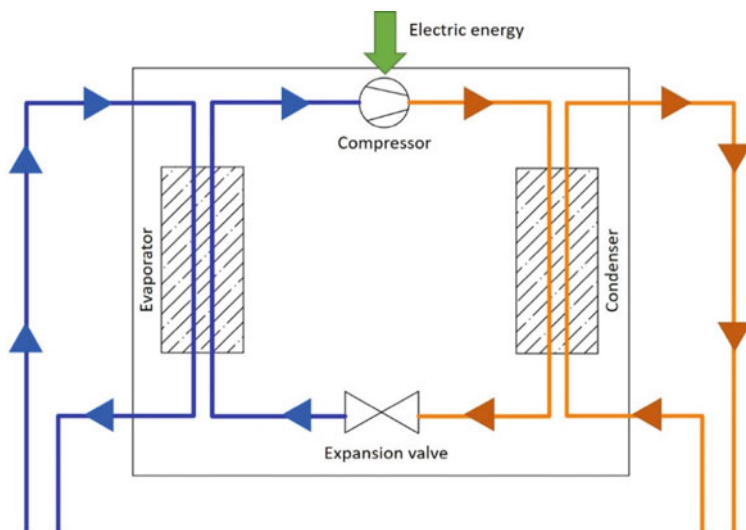


Fig. 3 Schematic diagram of heat pump operation

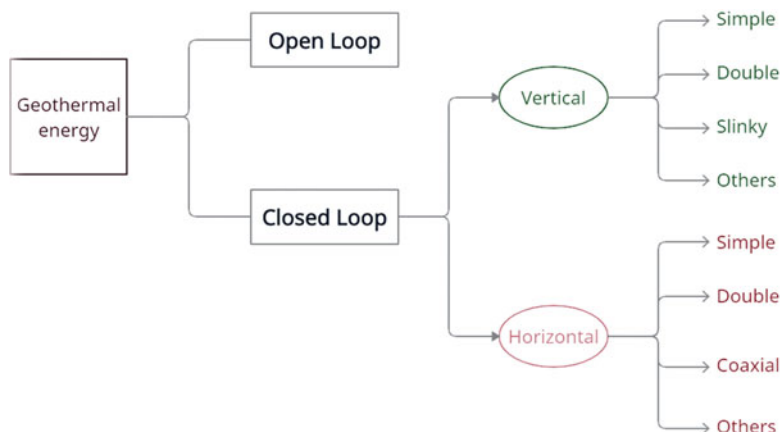


Fig. 4 Classification of geothermal energy according to its geometry

- *Vertical*: These are usually used when the space available is limited. It is necessary to use drilling equipment to make small-diameter boreholes with depths of between 25 and 100 m. The pipes, through which the fluid circulates, are inserted into these boreholes with the number of boreholes required varying according to the characteristics of the building to be air-conditioned, and the type of terrain.
- *Horizontal*: these systems require a larger surface area, limiting the future uses of the surface area in which the heat exchangers are installed. The heat exchangers are placed horizontally at a reduced depth.

Shallow geothermal systems require a longer pipe length to produce the same efficiency as vertical geothermal systems, but have a higher installation cost [41, 42]. Another disadvantage of horizontal geothermal systems is that they are more affected by variations in ambient temperature than vertical geothermal systems due to their proximity to the ground surface [43]. This may result in a lower efficiency of the heat pump.

Surface geothermal energy also has other disadvantages compared to vertical systems, such as the need to have a plot of land or surface area adjacent to the area where the heat pump is to be installed. The uses of this plot where the horizontal heat exchangers are installed are limited [35]. Horizontal systems are also influenced by the growth of vegetation on the plot, the presence of snow, rain or shadows on the plot [32].

There are also other novel arrangements and typologies of geothermal systems [44]. These have not been studied in this section, as their use is not as widespread as those seen so far.

2.2 Variables Affecting Design and Construction

The design of low or very low enthalpy geothermal installations used for the air-conditioning of houses and buildings, depends mainly on five factors outlined below [39, 45]:

- Characteristics of the building: thermal envelope, orientation, surface area, etc.
- Emitting system: underfloor heating, radiators, fan coil, etc.
- Technical room.
- Climatology.
- Geothermal reservoir.

In this section, the focus will be placed on the study of the parameters that influence the design of the geothermal reservoir applied to surface geothermal energy. These design parameters are the ones that influence the combination of surface geothermal energy with Sustainable Drainage Systems (SuDS).

There are broadly three horizontal exchanger arrangements: linear, slinky and helical distribution [46]. Numerous studies have been carried out to determine the best thermal performance on each of these arrangements. The study by Kim et al. [47] evaluated the thermal performance of horizontal slinky type and spiral coil type Ground Heat Exchangers (GHE). They used Thermal Response Test (TRT), showing that the slinky type provides better performance. The authors also analysed the parameters affecting the performance of horizontal GHEs, determining that the pipe diameter did not affect the performance. On the other hand, they found that the type of installation design and the thermal conductivity of the ground were the main factors affecting the performance of the heat pump.

In the same line, Selamat et al. [48] investigated different horizontal GHE designs and materials using numerical modelling. Six different pipe configurations, orientations and materials were explored, namely straight, slant, horizontal, vertical and inverted vertical, HDDE, copper and composite pipe material. Based on the results, the authors commented that the additional pipe length in the slinky configurations was compensated for as the effective period was extended. In addition, the vertical orientation provided a 14% higher effective heat exchange rate compared to the horizontal orientation.

On the other hand, parallel connections require less pumping, which saves energy. However, parallel connections use smaller diameter pipes, which influences heat transfer with the ground by transporting a smaller volume of fluid. In this sense, the slinky arrangement offers a number of advantages, since a greater pipe length (pipe density) occupies less area. This favours heat exchange, optimising the available space [48, 49].

Studies have also been carried out on the influence of the spacing of the trenches in which geothermal heat exchangers are installed. It has been observed that the reduction of the horizontal separation between trenches has an influence on the performance, but that this influence is less than the configuration of the heat exchanger [50].

Another important feature to take into account is the fluid circulating inside the heat exchanger. This is normally water or water with an anti-coolant, depending on the temperature operational range [35, 51].

Finally, a fundamental aspect to consider is the type of ground or material in which the heat exchanger is located, influencing the performance of the heat pump [52]. For instance, a material with a high permeability behaves in a similar way to a soil without moisture. In a saturated material, the rate of heat transfer with the ground increases [53]. Some authors have proposed that a viable option to increase the moisture content of the soil would be to use stormwater, suggesting to direct it to the heat exchanger [51].

The following (Table 1) lists the design parameters identified in the literature, as well as the reference values proposed by these investigations.

Table 1 Geothermal reservoir design parameters in shallow geothermal energy

Design criteria	Recommended value
Pipe installation depth	Installation depth 1–2 m [41, 54]. Depths below 0.35 m are not recommended in order to avoid excessive influence of ambient temperature [55]. Depths above 1.5 m do not significantly improve performance [56]
Exchanger configuration	There are several exchanger configurations, but generally speaking, the slinky configuration is the one showing the best properties [47, 48]
Pipe diameter	Does not affect the performance of the heat pump [47]. However, a compromise between pressure drop and thermal performance must be followed, so that the pressure drop is small (less pumping power) and turbulence is produced to promote heat transfer (small pipe diameters) [35] Typically 32 mm diameter is used for depths of 0.5 to 0.8 m, and 40 mm for depths of 1.2–1.5 m [49]
Exchanger length	Length of 35–60 m of piping per kW of heating or cooling required [41, 54]
Liquid inside the exchanger	The fluid consists of a mixture of water and ethylene glycol (4:1 ratio) to avoid possible freezing problems [51]
Exchanger tube material	The materials used are polyethylene (PE) and polybutylene (PB) [35]
Slope	Maximum ground slope of up to 15%. Installing the collector horizontally parallel to the earth's surface [49]
Distance to the heat pump	Low distance to the heat pump
Land properties	A higher thermal conductivity of the material in which the geothermal heat exchanger is placed improves the heat exchange rate [53]

3 Sustainable Drainage Systems (SuDS)

SuDS are a set of drainage techniques, encompassed within what is known as Green Stormwater Infrastructure (GSI) or Nature Based Solutions (NBS) for stormwater control. SuDS techniques also fall under the umbrella of the philosophy known as Water Sensitive Urban Design (WSUD). SuDS not only help in managing water volumes, but also water quality, while maintaining environmental opportunities and promoting amenity and liveability [57]. The design of SuDS has traditionally rested on four basic pillars: water quantity, water quality, biodiversity and amenity [58].

In this way, SuDS manage surface runoff, mitigate the effects of torrential rain-storm events, while managing the quality by retaining and treating the pollutants contained in them [59]. They also contribute to create better places to live, protecting and restoring natural and degraded urban areas. Thus the implementation of SuDS contribute to a wide range of objectives [57]:

- Protect and improve water quality and biodiversity.
- Maintain and restore the natural flow of water and its hydrological cycle.
- Protection against accidental spills and economic and environmental losses.
- Visually and environmentally attractive landscapes in the city.
- Recharge aquifers.
- Mitigate the heat island effect.

In addition, there are different SuDS techniques, which can be classified according to the primary hydrological function provided [60]:

- *Source Control*: green/blue roofs, permeable pavements.
- *Slowing and conveyance*: filter drains, green swales, rain gardens.
- *Storage*: rainwater harvesting, wetlands, storage tanks.
- *Infiltration*: structural swales, infiltration trenches, filter drains and ponds.

There is a large experience around sustainable rainwater management since centuries ago by ancient civilizations [61]. However, in recent decades, the implementation of SuDS techniques has become increasingly important. There are a high number of experiences developed around these techniques, both in their practical application, and in their academic study [62, 63].

For instance, in Spain, a new regulatory framework favourable to the implementation of SuDS is emerging, drawing on many of the lessons learnt in other countries [64]. Among some of the regulations, that have been modified or developed, is the Regulation of the Public Hydraulic Domain which has introduced the mandatory use of SuDS in new urban developments [65]. A number of design manuals and guides are also emerging at local and regional level, which serve as a basis for technicians to implement these techniques [66, 67]. There are also a wide variety of experiences in both the dissemination of SuDS, as well as in the planning and construction of SuDS [68].

3.1 Types and Functions

There are several types of SuDS with particular characteristics. Some manuals identify up to 13 different types of techniques, which in turn can be further subdivided depending upon their specific functions [69]. This section identifies and briefly describes the most widely used SuDS [70], analysing their properties, as well as the different varieties of each one of them.

Green/Blue Roofs

Green roofs are a multi-layered system installed on the roofs of buildings or services structures [66]. The aim of this SuDS is to capture stormwater for its subsequent use, while treating it through the filtering effect provided by its vegetative cover, the growing media and the soil, and the aggregate materials included in the lower layers of its section. It also provides a great aesthetic and amenity value, delivering ecosystemic value by creating new green areas [69]. Moreover, green roofs are one of the most widely studied and utilised SuDS techniques internationally [70].

Green roofs usually consist of a vegetated surface cover, which is supported by a substrate and a set of drainage layers. A separating geotextile is usually placed under the substrate layer to act as a filter layer together with the granular bed placed under the geotextile [70]. A geomembrane is placed underneath, which protects and waterproofs the surface, preventing possible root damage [69].

This SuDS can be classified into two main types [69]:

- *Extensive green roofs.* In extensive green roofs, the entire roof area is covered with hardy, slow-growing, low-maintenance and, if possible, drought-tolerant vegetation. For instance, mosses, herbs or grasses are often used. The canopies can be flat or sloping and have a light weight.
- *Intensive green roofs.* These roofs are designed to support greater biodiversity, providing major landscape and amenity benefits. A wide variety of plants are often used, including grasses, shrubs and/or trees. These types of roofs can also include water storage elements, i.e. blue cover elements. These types of canopies have a greater weight, so structural considerations must be taken into account.

In addition, there is a third type of roofing, called semi-intensive roofing, which is an intermediate type between the two previous ones [69].

Green roofs have a number of advantages, which can be summarised as follows:

- Green roofs help to lower the temperature of cities, reducing the heat island effect and improving the insulation of the buildings where they are installed, thus reducing their energy consumption [71].
- They contribute to the removal of air pollutants, while reducing stormwater runoff [72], showing that the cumulative retention by a green roof was more than 50% over a 29-month record [73].
- Improve the biodiversity of the environment, creating a new green space in the city [69].

The main limitations of green roofs are as follows [66]:

- Structurally, the building must be able to support the weight of the green roof, which is greater than that of a conventional roof.
- Higher construction and maintenance costs.
- Depending on the climate where the roof is located, it can be difficult to maintain the vegetation in perfect condition.
- The treated surface run-off is limited to that of the roof where it is installed.

Permeable Pavement Systems

Pervious pavements are multi-layered, traffic-resistant structures that allow water to filtrate through all their layers. Structures that do not allow water to pass through all their layers are not considered to be permeable pavements [74].

These can be constructed with the same materials as conventional pavements, modifying the percentage of voids in the pavement, or to be made of specially manufactured materials such as geocells [75] (Fig. 5).

Permeable pavements are usually utilised in light vehicle parking areas and on roads with low traffic intensities [59], although in the last decade they have been implemented in heavy traffic areas, although this requires a careful study and a good design of the various layers of the pavement as well as the road surface. Successful experiences have been carried out in heavy traffic areas such as airport service areas [76].

Permeable pavements can be classified according to the characteristics of the pavement surface. Each of these has several different properties and applications.



Fig. 5 View of a car park with permeable pavement

The following points are a description of each of the different types that are usually described in the scientific literature [77]:

- *Plastic Turf Reinforcing Grid (PTRG)* is made up of flexible plastic interlocking units, called geocells, through which water infiltrates through openings filled with aggregate or topsoil and turf. PTRG is well suited for low stress areas such as pedestrian, cycling or light vehicle-parking areas. PTRG is not suitable for high stress areas such as roads or areas with heavy vehicles.
- *Porous Concrete (PC)*: PC consists of a concrete layer with less fines than a conventional concrete mix. It may also include other modifications to create interconnected voids for drainage purposes. PC has a lower fines content than conventional concrete and has a lower strength and coarser appearance.
- *Porous Asphalt (PA)*: PA is like conventional asphalt (impermeable), but less fine material are used in the mix to provide greater porosity.
- *Slotted Paving Blocks (SPB)*: SPBs are a type of paving system unit that drains water through the joints between pavers filled with small, highly permeable aggregates. The pavers are placed in a thin layer of aggregate bedding on top of a layer of coarser aggregate and the base underneath, this provides uniform support and storage of the draining water.
- *Porous Pavers (PPa)*: PPa are a type of paving system unit that drains water through existing pores in the concrete of the pavers. They have a coarser appearance than SPBs.

The classification of permeable pavements according to the final destination of the water, as mentioned above, is shown below [74, 75]:

Permeable pavement with drainage deferred to the conventional system. These are pavements that have an underground drainage system made up of permeable pipes, with the aim of delaying the flow of rainwater, laminating the peak floods in the sewerage systems to which they are connected.

Permeable pavement with storage. These pavements are designed and built to allow the storage of a certain volume of water in the sub-basin, with the aim of its subsequent use through its reuse for non-drinking uses.

Permeable pavement with infiltration into the ground. These are pavements that allow the infiltration of infiltrated and filtered water into the ground through all the permeable layers of the pavement, including the esplanade, with the aim of allowing the recharge of natural groundwater reserves (Fig. 6).

Permeable pavements have the following advantages over conventional pavements and other sustainable drainage techniques [59, 78]:

- Reduction of surface runoff volumes, improving e.g. road safety.
- Reduction of the percentage of impervious surface, increasing groundwater reserves.

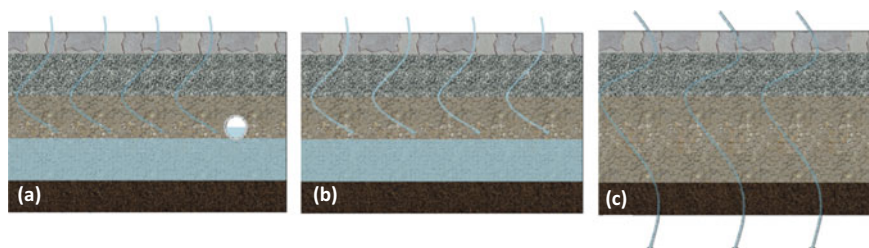


Fig. 6 Hydraulic behaviour of permeable pavements. **a** Deferred drainage to the conventional system, **b** storage, **c** Infiltration into the ground

- Increased time of concentration due to the lamination caused by the passage of water through the different layers.
- Improved water quality due to the filter effect.
- Connection to other SuDS. This is the most complete drainage technique.

Permeable pavements have great advantages, as they are the most complete and versatile drainage technique [79, 80], although they also have a number of disadvantages, which can be summarised as follows:

- Clogging of the permeable surface.
- Degradation.
- Lack of knowledge and mistrust.

These disadvantages can be alleviated with proper knowledge of the technique, as well as with correct and effective maintenance of permeable pavements.

Swales

A green swale is a naturalised artificial depression in the soil that captures and conveys water from the surface runoff originated in adjacent impermeable surfaces or natural land. They can replace natural watercourses degraded by urban development, providing a high ecological value [59]. Swales contribute to manage volume reduction and runoff treatment, while providing ecosystem value [81].

Removal of pollutants from the captured water occurs through biofiltration, sedimentation and infiltration, as main physical processes, filtering pollutants as the runoff water flows through the vegetation [82]. The following variables should be considered in the design of swales to improve pollutant removal: swale length, longitudinal slope, presence of check dams, cross section geometry, vegetation density, vegetation type, soil permeability and designed flow [83].

The pollutant removal capacity of green swales is superior to other conventional drainage systems [84]. Depending on the type of green swale and its characteristics, average reductions in Suspended Solids (SS) of 40–50% can be obtained, in some cases reaching reductions up to 90% [83].

Green swales are generally made up of the following elements, some of which are optional, depending on the design of the swale [67]: geotextile, geomembrane,

usually placed to protect an area from possible infiltration, drainage layer, filter medium.

There are three main types of green swales, which provide a number of specific characteristics [69]:

- *Conveyance and attenuation swales*: These are shallow swales intended to capture and convey runoff water to a treatment and/or infiltration area. They have a limited pollutant removal capacity.
- *Wet swales*: These are like transport and attenuation swales. However, they are designed to hold a certain amount of water. They can be used in areas with small slope, or with poorly draining soils. They can also be used in areas where biodiversity is to be enhanced through a longitudinal component that functions as a wetland.
- *Dry swales*: They are designed to include a filter bed, usually made of aggregate, which is overlain by an underdrainage system. This underdrain provides additional treatment and conveyance capacity below the base of the swale, preventing the system from becoming waterlogged. If infiltration is to be prevented, a liner could be introduced at the base layer.

The main advantages delivered by green swales are cited below:

- Runoff peak reduction, as they minimise flow velocity due to the action of vegetation [82].
- They are adaptable to most soil types, but preferably should be non-compacted soils, to facilitate the growth of roots and biological organisms. It is also important that the soil contains the nutrients and carbon necessary for vegetation growth [70].
- They provide great ecosystemic value, encouraging the growth of diverse plant species [59].
- They have a high capacity to reduce pollutants in surface runoff [81].
- They perform well in the long term, maintaining their hydraulic function even without swale [85].
- Low construction and maintenance costs [66].

The main drawbacks or limitations from this SuDS technique are described below:

- The slope of the trench is a limiting factor, as it cannot be too steep or too high [69].
- If the slope is not adequate, it may suffer from resuspension of solids. Fertilisers should also not be used [66].
- They should be close to the drainage area, as well as have slopes laid down so that they do not pose a hazard [67].

Bioretention systems

Bioretention systems are depressions artificially made in the ground with a variable extension and a vegetated surface, which receive rainwater from the surface runoff generated in their surrounding areas. This runoff accumulates in the system with a variable depth, although it is usually a thin layer of water. The runoff infiltrates into the ground in most of its designs, and when the infiltration capacity is exceeded, the



Fig. 7 View of a bioretention systems type rain garden

surplus is stored in the system until it reaches the maximum level, where it is drained into the conventional drainage system [82, 86].

The main advantage of this type of SuDS is based on the simplicity and low cost of installation, offering great benefits such as improved site aesthetics, runoff control, increased biodiversity, improved air quality, etc. [79], being one of the most efficient techniques for pollutants removal [82] (Fig. 7).

There are different variations of bioretention systems, all of which have their own characteristics, which are described below [69]:

- *Rain garden*: these are small and simple systems, which usually have a single inlet and a small depth. They capture and manage water from a small area, adapting the design to the place where they are located.
- *Raised planter*: these are terraces built on the surface of the ground, which capture rainwater and filter it through their different layers. These systems are widely used in consolidated urban areas for the management of rainwater collected from adjacent roofs.
- *Bioretention tree pit*: these are tree pits in which the surface has been planted in addition to the tree(s). This offers a better performance of the system, allowing to offer improvements in rainwater management.
- *Anaerobic bioretention system*: a system designed to maintain a constant water level in the drainage layer. In this way plants have access to water in dry weather, and this system helps the treatment of certain types of pollutants.

Rainwater Harvesting

This system consists of collecting rainwater, mainly from roofs, although it can also be collected from other impermeable areas. The collected water is directed to



Fig. 8 View of a rainwater harvesting system

cisterns for later use, normally for uses where drinking water is not required [79]. These systems typically include many components that work together to capture and manage rainwater [82]. Rainwater storage cisterns can be located above ground (see Fig. 8) or underground.

Rainwater Harvesting offers a number of benefits where it is implemented [86]: reducing potable water consumption, reducing the need for water distribution infrastructure, providing emergency water storage, reducing the volume of runoff water generated, etc.

Ponds and wetlands

Ponds and wetlands are impermeable depressions in the ground, which store water permanently. Depending on the time of year, the water level will fluctuate, thus having the capacity to buffer rainfall events. They usually have vegetation, as well as various animals, providing a high ecosystemic value. In order to control the water level, they usually have a drainage system, usually towards a natural watercourse [69].

They have a high sedimentation capacity, providing greater opportunities for particle settling and pollutant removal. Even so, designs often include a system for water pre-treatment; hence protecting the fauna and flora present in the wetland [63, 82].

Wetlands are typically implemented in green areas, such as parks, which provide a high amenity value (see Fig. 9). Therefore, wetlands are one of the most comprehensive SuDS from a design pillar standpoint.



Fig. 9 View of a wetland at the North Carolina Museum of Art

3.2 Variables Affecting SuDS Design and Construction

Each SuDS has its own characteristics, and these must be adapted to the site in which they are going to be implemented, as well as, to the casuistry of each design. However, a set of Minimum Design Criteria (MDC) can be established, which can be applied to the design of all SuDS in a particular region. These MDC can in turn be structured according to the SuDS design pillars discussed above (quality, quantity, amenity and biodiversity), as shown in Table 2. These MDCs have been compiled from what has been established by other authors through different scientific publications and manuals [60, 63, 66, 69, 78, 82, 87, 88].

In addition to the MDCs set out in Table 2, several other conditions and constraints must be considered when designing a SuDS. One of these constraints is the maintenance work to be carried out on the different SuDS techniques. These maintenance tasks will depend to a large extent on the type of SuDS, and for this reason an operation and maintenance plan must be established during the design stage. This plan will set the maintenance work to be develop, determining their periodicity. Following up from this reasoning, these activities should be taken into consideration during SuDS design, facilitating them through a correct layout [82].

Table 2 Variables affecting the design and construction of SuDS

Design pillar	Minimum design criteria (MDC)
Water quantity	Analysis of the properties of the basin and study of the flows to be managed
	Protection of natural hydrological systems
	Manage the flood risk and drainage capacity of the catchment
	Flexibility to future changes or variations (drainage)
Water quality	Analysis of the quality of drained water and water quality management
	Protection of the systems against erosion or the entrainment of pollutants
	Adaptation to variations in the managed flow
Amenity	Design of systems that are safe for users and the environment
	Improve aesthetics and multi-functionality, adapting to possible changes
	Dissemination of the systems and their properties
Biodiversity	Protection of native fauna and flora
	Facilitate habitat connectivity and create self-sustaining ecosystems

4 The Combination of Surface Geothermal Energy and SuDS

4.1 Description of the System

The proposed system consists of a combination of surface geothermal elements and SuDS. With this aim, the same system has been proposed in all the studies that have been carried out (see Table 3). This system consists of a heat pump connected to a heat exchanger in a closed circuit, which is usually located underneath the SuDS cross-section.

The image below shows the operating diagram of the system, where it can be used for both air-conditioning and cooling of nearby buildings (Fig. 10).

This system offers a number of benefits over conventional horizontal geothermal systems. It offsets some of the disadvantages discussed above by providing the following benefits from a construction viewpoint:

- It reduces the installation costs of the exchanger, as earthworks are necessary for the construction of the SuDS.
- It allows optimising land use, creating a multifunctional infrastructure.
- Some of the materials used in the SuDS structure serve as insulation against the influence of the weather. This would lead to an increase in the Coefficient of Performance (COP) of the heat pump.

In addition to all these benefits, there are the inherent individual advantages delivered by geothermal energy systems and SuDS, which were discussed in more detail above.

Table 3 Previous studies of the combination of SuDS and surface geothermal energy

Year	Author(s)	Document type	Type of SuDS studied	Type of study	Main contributions
2008	Scholz and Grabowiecki [89]	Article	Pervious paving systems	Laboratory	One of the first experiments on the geothermal use of permeable pavements, providing promising results
2009	Coupe et al. [90]	Conference paper	Pervious paving systems	Laboratory	Determined that water quality in a pervious paving is not affected by the presence of surface geothermal systems
2009	Tota-Maharaj and Scholz [91]	Book chapter	Pervious paving systems	Literature review	
2010	Tota-Maharaj et al. [92]	Article	Pervious paving systems	Laboratory	Study of the proliferation of bacteria and microorganisms, ruling out any significant influence of the geothermal heat exchanger
2010	Tota-Maharaj [93]	PhD Thesis	Pervious paving systems		

(continued)

4.2 Main Experiences

Different studies and experiences on the geothermal development of SuDS can be found in the literature. In this section, publications have been compiled comprehending the most relevant previous studies, analysing them and identifying gaps in the knowledge up to date, distinguishing between laboratory and field experiences.

Laboratory experiments:

Tota-Maharaj et al. [94] developed an experiment consisting of introducing water at different temperatures inside the section of a permeable pavement system, while simulating the effect of external heat on the pavement section.

With this experiment, geothermal energy balances were studied, and a temperature balance model was developed for the sections tested. Parameters such as ambient temperature, the effect of the sun, the water level inside the pavement, amongst other,

Table 3 (continued)

Year	Author(s)	Document type	Type of SuDS studied	Type of study	Main contributions
2011	Tota-Maharaj et al. [94]	Article	Pervious paving systems	Theoretical study	Development of a numerical method for modelling heat fluxes and energy balance from measured temperature data and other environmental factors
2012	Scholz et al. [95]	Article	Pervious paving systems	Theoretical study	Analysis of the application of KSOM to predict microbial contaminant concentrations and study of the system in combination with geothermal elements
2013	del-Castillo-García et al. [96]	Article	Pervious paving systems	Laboratory	Study of the influence of different paving surfaces and different cross-sections on thermal performance
2013	Novo et al. [97]	Article	Pervious paving systems	Field experiment	Study of temperature differences of permeable pavements compared to air temperature, as well as analysis of the deterioration of water quality due to temperature differences
2014	Coupe et al. [98]	Book chapter	Pervious paving systems	Literature review	
2015	Tota-Maharaj et al. [99]	Article	Pervious paving systems	Laboratory and field	Determine the low influence of the geothermal heat exchanger on the water quality of the system
2016	Faraj-lloyd el al. [100]	Book chapter	Pervious paving systems	Literature review	
2017	Charlesworth et al. [55]	Article	Pervious paving systems	Literature review	

(continued)

Table 3 (continued)

Year	Author(s)	Document type	Type of SuDS studied	Type of study	Main contributions
2018	Andrés-Valeri et al. [101]	Conference paper	Green swale	Laboratory	Preliminary study on the geothermal exploitation of green swale
2019	Rey-Mahía et al. [102]	Article	Green swale	Laboratory	Laboratory proof-of-concept on the geothermal utilization of green wet swales
2020	Yildiz et al. [9]	Article	Generic	Laboratory	Determination that the thermo-hydrological conditions within Suds are conducive to efficient soil heat exchange
2022	Erbs-Poulsen et al. [103]	Article	Pervious paving systems	Field	Field study of geothermal use of a permeable pavement
2022	Raaschou-Andersen et al.[104]	Article	Pervious paving systems	Field	Field study of geothermal use of a permeable pavement
2022	Janssen et al. [105]	Article	Ponds	Field	Field pilot for the use of geothermal energy as a cooling system for the outlets of a pond

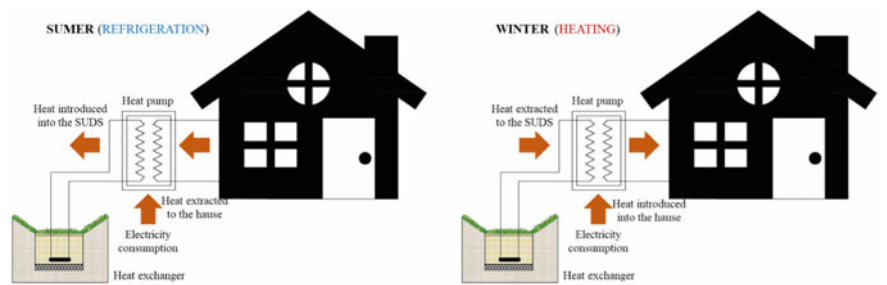


Fig. 10 Schematic of the system proposed for study

were introduced into this model, which made possible to predict the behaviour of the combination of the heat pump and the permeable pavement system.

A study was also carried out with twelve containers with a permeable pavement inside. These were placed both in the laboratory and in the field, with a surface geothermal system inside. The water quality of the system was studied and it was found that the presence of the geothermal heat exchanger had hardly any influence on the system [99].

del-Castillo-García et al. [96] conducted laboratory tests, which were based on heating several standard sections of a permeable pavement by means of a heat source, carrying out tests lasting 72 h. The test sections tested had different surfaces (interlocking concrete blocks, porous concrete and porous asphalt), and it was observed that the insulation capacity of the different surfaces varied. It was also concluded that the tested system was thermally insulating.

Novo et al. [97] developed a field study to identify the temperatures inside a permeable pavement, as well as to evaluate the influence on the water quality inside the pavement under different operating temperatures.

Closer to these days, Rey-Mahía et al. [102] developed a laboratory proof of concept to study the feasibility of the geothermal use of swales. This was one of the first experiments in this line. This test consisted of replicating the operation of a heat pump in three models of green gutters, with the same cross-section. To do this, they placed a geothermal exchanger inside the gutter and recirculated water at different temperatures. The results obtained pointed to the feasibility of this system, although establishing the need for further tests and field trials.

In this vein, Yildiz et al. [9] devised a laboratory experiment to monitor the soil–water–atmosphere interaction, showing the good thermo-hydrological response of SuDS.

With the aim to summarise all these investigations, Table 3 contains a list with previous publications on the geothermal utilisation of SuDS, identifying the most important contributions, as well as other relevant data.

Field experiences:

Hanson EcoHouse, Watford, UK

In 2007, a single-family house was built in Watford, following the parameters of the Passive House methodology. A landscaped area was built around the house, where a permeable pavement area was constructed for rainwater harvesting, as well as for the installation of a geothermal energy exchanger. Geothermal energy was used as the only means of heating the house, while at the same time it was very well insulated, obtaining energy efficiency level 4, the highest level of energy efficiency in the UK [55].

The house had a floor area of 95 m², distributed over two floors. Next to the house, a 65 m² area of permeable pavement was located, where the heat exchanger was placed and connected to an 8 kW heat pump. The heat exchanger was placed 140 mm from the base of the permeable pavement, which means that it was submerged in the water at all times [100].

The operation of the heat pump was monitored during three years, obtaining adequate performance despite the problems that arose, such as power outages, constant opening of doors and windows as the house was a demonstrator, shallow depth of the geothermal system, etc., which caused some of the pipes to freeze during extreme winter weather. Despite all these considerations, this experiment at a full scale provided promising outputs and laying the foundations for this technology [55] for the next years to come.

The Hanson Stewartby Office, Bedford, UK

Following the success of the Hanson EcoHouse experience, it was decided to implement this technology in the refurbishment of the offices of brickworks in Bedford. This system was implemented to air-condition a three-storey building with a total floor area of 6,500 m², using five 130 kW heat pumps, a heat exchanger length of 8.4 km at a depth of 1 m, and a car park area of 7,000 m². With this system, the offices could be heated via underfloor heating with an optimum efficiency of 45 °C. It was estimated that the investment of the system would pay for itself in 5 to 6 years [100, 98].

4.3 Gaps Identified

Several authors have studied the influence of the geothermal system on the water quality in permeable pavement systems. However, these studies have not been carried out on other types of SuDS.

Furthermore, shortcomings have been identified in the design of pervious paving systems in combination with surface geothermal energy, such as those carried out at the Hanson EcoHouse. For example, they suffered from freezing problems because the geothermal heat exchanger was not located at an adequate depth. Studies of the optimal operating characteristics of shallow geothermal energy need to be carried out in SuDS techniques in order to apply them to these designs.

The need for correct thermal designs has also been identified, studying the properties of the materials and standard sections in order to optimise the performance of the heat pump.

SuDS other than pervious paving systems have been studied with good results, so it may be feasible to apply this technology to other drainage techniques.

Different authors have raised the need for more laboratory and field tests as a necessary step into the development of the new generation of multifunctional surfaces using the combination of geothermal energy systems and SuDS.

5 Future Prospects

This chapter has identified the need to strengthen the water-energy nexus in engineered urban surfaces. It has analysed the characteristics and properties of geothermal

energy, going deeper into the design criteria for surface geothermal energy. A study of SuDS has also been carried out, analysing in detail the characteristics of the most widely used and studied SuDS techniques. The MDC applicable to this combined techniques have been proposed.

On the other hand, previous experiences resulting from the geothermal use of SuDS have been studied. As can be seen in the works studied, research has been carried out on the geothermal use of permeable pavements, one of the most widely used SUDS techniques in the world, obtaining very promising results, both in the laboratory tests carried out and in the field tests. The feasibility and efficiency of the system for use in the air conditioning of a single-family house was demonstrated at the Eco House in Watford. This experience was ratified at the Hanson Stewartby Office, demonstrating that this system can also be efficient for the air conditioning of this type of building.

These previous experiences not only lay the foundations for the geothermal utilisation of permeable pavements, but also set a precedent for the possible combination with other SUDS techniques. This has been tested in the laboratory by means of preliminary tests on the geothermal utilisation of green swales, with promising results.

From the analysis of these previous studies, a series of gaps in knowledge have been identified, which should be the focus of future research. In order to do this, further study is needed on the mechanisms of heat transfer that occur in SuDS for their energy use in combination with surface geothermal techniques.

To continue developing this new research field, a series of milestones or steps are proposed in order to address the aforementioned knowledge gaps:

- Identification of the most appropriate SuDS for combination with surface geothermal energy.
- In-depth study of the thermal and mechanical properties of the materials that make up the most commonly used SuDS type sections. Analysing these properties for the type of section as a whole.
- Study of the hydraulic properties of SuDS in combination with geothermal exchangers, as well as their performance in the management of water quality.
- Analysis of the perception of society and the different stakeholders for the combination of these technologies.
- The influence of the geothermal exchanger on the biodiversity present in the SuDS, and how it can influence temperature changes in the SuDS, should be studied.
- Determination of the optimal operating parameters of the heat pumps in combination with SuDS.

It will also be necessary to conduct more experimental campaigns in the field, as the factors involved in the operation of a SuDS in combination with geothermal energy are difficult to replicate faithfully in laboratory studies. More field trials can also help to raise the visibility and acceptance of the operation of these systems by the different stakeholders.

However, it will undoubtedly be necessary to develop the above items in order to be able to plan and execute experimental campaigns in the field correctly. This will ensure that they are successful and do not have the opposite effect.

In this way, this new multifunctional technology will continue to be developed for its possible application in the air conditioning and cooling of single-family homes and buildings, as well as in other urban public uses. In this way, the knowledge on the design of SuDS in combination with energy aspects will be further developed.

Funding This investigation was funded by the FICYT through the GRUPIN project; grant number AYUD/2021/51328, co-financed with EU FEDER funds. Carlos Rey-Mahía would like to thank the University of Oviedo for the Predoctoral Grant with reference PAPI-21-PF-23.

References

1. Grupo de trabajo ST-10 (2018) Congreso nacional del Medio Ambiente. In: Rumbo 2030. Agua y Ciudad. Sistemas Urbanos de Drenaje Sostenible. Fundación Conama, Madrid
2. Bloomberg MR (2010) NYC green infrastructure plan. In: A sustainable strategy for clean waterways
3. United Nations Transforming our world: The 2030 agenda for sustainable development
4. AEAS Informe Sobre Aguas Residuales En España 2017
5. United Nations (2015) The Millennium development goals report. New York, NY, ISBN 978-92-1-101320-7
6. Melchiorri M, Pesaresi M, Florczyk A, Corbane C, Kemper T (2019) Principles and applications of the global human settlement layer as baseline for the land use efficiency indicator—SDG 11.3.1. IJGI 8:96. <https://doi.org/10.3390/ijgi8020096>
7. International Energy Agency (IEA) (2021) Net zero by 2050: a roadmap for the global energy sector. France
8. AIE (2021) Energía Geotérmica. AIE, París. <https://www.iea.org/reports/geothermal-power>
9. Yildiz A, Stirling RA (2021) Thermo-hydrological behaviour of green infrastructure: a comparative field and laboratory study. Geomech Energy Environ 25:100219. <https://doi.org/10.1016/j.gete.2020.100219>
10. Directorate General for Energy (2016) Mapping and analyses of the current and future (2020–2030) heating/cooling fuel deploymentc. European Commission
11. Vlad N (2008) Motion for a resolution on EU research into enhanced geothermal systems. European Parliament, p 2
12. European Council (2019) European council conclusions on climate change. Brussels
13. Bárcena A, Cimoli M, García-Buchaca R, Fidel-Yáñez L, Pérez R (2018) *La Agenda 2030 y los Objetivos de Desarrollo Sostenible: una oportunidad para América Latina y el Caribe*. Comisión Económica para América Latina y el Caribe (CEPAL), Santiago de Chile. ISBN 978-92-1-058643-6
14. World Economic Forum (2016) Inspiring future cities & urban services shaping the future of urban development & services initiative
15. World Economic Forum (2018) Circular economy in cities evolving the model for a sustainable urban future
16. World Economic Forum (2018) Agile cities preparing for the fourth industrial revolution
17. Wang S, Wang S, Dawson R (2022) Energy-water Nexus at the building level. Energy Build 257:111778. <https://doi.org/10.1016/j.enbuild.2021.111778>

18. Borge-Diez D, García-Moya FJ, Rosales-Asensio E (2022) Water energy food Nexus analysis and management tools: a review. *Energies* 15:1146. <https://doi.org/10.3390/en15031146>
19. de Oliveira GC, Bertone E, Stewart RA (2022) Challenges, opportunities, and strategies for undertaking integrated precinct-scale energy-water system planning. *Renew Sustain Energy Rev* 161:112297. <https://doi.org/10.1016/j.rser.2022.112297>
20. Wang X-C, Jiang P, Yang L, Fan YV, Klemeš JJ, Wang Y (2021) Extended water-energy Nexus contribution to environmentally-related sustainable development goals. *Renew Sustain Energy Rev* 150:111485. <https://doi.org/10.1016/j.rser.2021.111485>
21. Chen C, Zhang X, Wang S, Zhang H (2021) Regional-scale water-energy Nexus management by a mixed possibilistic-flexible robust nonlinear programming model. *J Hydrol* 603:126852. <https://doi.org/10.1016/j.jhydrol.2021.126852>
22. Chenoweth J, Al-Masri RA (2021) The impact of adopting a water-energy nexus approach in Jordan on transboundary management. *Environ Sci Policy* 118:49–55. <https://doi.org/10.1016/j.envsci.2021.01.006>
23. Bortoleto AP, Franco Barbosa PS, Maniero MG, Guimarães JR, Vieira Junior LCM (2021) A water-energy nexus analysis to a sustainable transition path for Sao Paulo State, Brazil. *J Clean Prod* 319:128697. <https://doi.org/10.1016/j.jclepro.2021.128697>
24. Rodríguez-Merchan V, Ulloa-Tesser C, Baeza C, Casas-Ledón Y (2021) Evaluation of the water-energy nexus in the treatment of urban drinking water in Chile through exergy and environmental indicators. *J Clean Prod* 317:128494. <https://doi.org/10.1016/j.jclepro.2021.128494>
25. Goldstein B, Hiriart G, Bertani R, Bromley C, Gutiérrez-Negrín L, Huenges E, Muraoka H, Ragnarsson A, Tester J, Zui V, et al (2011) Geothermal energy. In: Edenhofer O, Pichs-Madruga R, Sokona Y, Seyboth K, Matschoss P, Kadner S, Zwickel T, Eickemeier P, Hansen G, Schlomer S, von Stechow C (eds) *Renewable energy sources and climate change mitigation*. Cambridge University Press, Cambridge, pp 401–436. ISBN 978–1–139–15115–3
26. Llopis Trillo G, Rodrigo Angulo V (2008) *Guía de La Energía Geotérmica*
27. Uriarte JL, Muñoz PP, de J (2015) Estudio de alternativas para el aprovechamiento geotérmico en el edificio Juan de la Cosa. p 197
28. Sanahuja JA (2021) Pacto Verde Europeo: el giro ambiental de un actor global. p 28
29. European Union (2019) *Clean energy for all Europeans*. European Commission. ISBN 978–92–79–99843–0
30. Trillo GL, Rodrigo Angulo V (2008) *Guía de La Energía Geotérmica*. Fundación de la Energía de la Comunidad de Madrid (FENERCOM)
31. Bleicher A, Gross M (2016) Geothermal heat pumps and the vagaries of subterranean geology: energy independence at a household level as a real world experiment. *Renew Sustain Energy Rev* 64:279–288. <https://doi.org/10.1016/j.rser.2016.06.013>
32. Self SJ, Reddy BV, Rosen MA (2013) Geothermal heat pump systems: status review and comparison with other heating options. *Appl Energy* 101:341–348. <https://doi.org/10.1016/j.apenergy.2012.01.048>
33. New York City Department of design and construction geothermal heat pump systems manual: a design and installation guide for New York City projects 2012
34. GSHP (2016) Association surface water source heat pumps: code of practice for the UK
35. Asociación Técnica Española de Climatización y Refrigeración (ATECYR) (2012) *Guía Técnica de Diseño de Sistemas de Intercambio Geotérmico de Circuito Cerrado*. Instituto para la Diversificación y Ahorro de la Energía (IDAE), Madrid. ISBN 978–84–96680–60–9
36. España, Ministerio de Industria, C. Y T., España, Ministerio de Ciencia e Innovación, Instituto para la Diversificación y Ahorro de la Energía (2008) *Instituto Geológico y Minero de España Manual de geotermia*. IDAE: Madrid. ISBN 978–84–96680–35–7
37. York Thermal Geothermal Owner's Manual 2022
38. Collins A, Orio CD, Smiriglio S (2002) *Ground heat pump manual*. NYC Department of Design and Construction, New York
39. Kavanaugh S, Rafferty K (2014) *Geothermal heating and cooling: design of ground-source heat pump systems*. ASHRAE, Atlanta, GA. ISBN 978–1–936504–85–5

40. Agència Catalana de L'Aigua (2010) Guia "CLIMACA". In: Climatización de Edificios a Partir de La Energía Del Subsuelo (Baja Temperatura)
41. Aresti L, Christodoulides P, Florides G (2018) A review of the design aspects of ground heat exchangers. *Renew Sustain Energy Rev* 92:757–773. <https://doi.org/10.1016/j.rser.2018.04.053>
42. Pouloupatis PD, Florides G, Tassou S (2011) Measurements of ground temperatures in cyprus for ground thermal applications. *Renew Energy* 36:804–814. <https://doi.org/10.1016/j.renene.2010.07.029>
43. Sarbu I, Sebarchievici C (2014) General review of ground-source heat pump systems for heating and cooling of buildings. *Energy Build* 70:441–454. <https://doi.org/10.1016/j.enbuid.2013.11.068>
44. Deng G, Kang N, He J, Wang S, Liu G, Liu N (2021) An investigation of the performance of groundwater-based heat pipes in heating Lawn systems. *Energy Convers Manage* 244:114492. <https://doi.org/10.1016/j.enconman.2021.114492>
45. García RH-A, Ronco MAR, Sánchez TA (2014) Viabilidad económica de un sistema geotérmico para el almacenamiento de la sidra. University of Oviedo, p 11
46. Cui Y, Zhu J, Twaha S, Chu J, Bai H, Huang K, Chen X, Zoras S, Soleimani Z (2019) Techno-economic assessment of the horizontal geothermal heat pump systems: a comprehensive review. *Energy Convers Manage* 191:208–236. <https://doi.org/10.1016/j.enconman.2019.04.018>
47. Kim M-J, Lee S-R, Yoon S, Go G-H (2016) Thermal performance evaluation and parametric study of a horizontal ground heat exchanger. *Geothermics* 60:134–143. <https://doi.org/10.1016/j.geothermics.2015.12.009>
48. Selamat S, Miyara A, Kariya K (2016) Numerical study of horizontal ground heat exchangers for design optimization. *Renewable Energy* 95:561–573. <https://doi.org/10.1016/j.renene.2016.04.042>
49. Uponor Geotermia (2013) Información Técnica
50. Zhou Y, Bidarmaghz A, Makasis N, Narsilio G (2021) Ground-source heat pump systems: the effects of variable trench separations and pipe configurations in horizontal ground heat exchangers. *Energies* 14:3919. <https://doi.org/10.3390/en14133919>
51. Eloisa Di Sipio, Bertermann D (2017) Factors influencing the thermal efficiency of horizontal ground heat exchangers. *Energies* 10:1897. <https://doi.org/10.3390/en10111897>
52. Go G-H, Lee S-R, Nikhil NV, Yoon S (2015) A new performance evaluation algorithm for horizontal GCHPs (ground coupled heat pump systems) that considers rainfall infiltration. *Energy* 83:766–777. <https://doi.org/10.1016/j.energy.2015.02.086>
53. DiCarlo AA (2021) Novel seasonal enhancement of shallow ground source heat pumps. *Appl Therm Eng* 186:116510. <https://doi.org/10.1016/j.applthermaleng.2020.116510>
54. Florides G, Kalogirou S (2007) Ground heat exchangers—a review of systems, models and applications. *Renew Energy* 32:2461–2478. <https://doi.org/10.1016/j.renene.2006.12.014>
55. Charlesworth SM, Faraj-Llyod AS, Coupe SJ (2017) Renewable energy combined with sustainable drainage: ground source heat and pervious paving. *Renew Sustain Energy Rev* 68:912–919. <https://doi.org/10.1016/j.rser.2016.02.019>
56. Congedo PM, Colangelo G, Starace G (2012) CFD simulations of horizontal ground heat exchangers: a comparison among different configurations. *Appl Therm Eng* 33–34:24–32. <https://doi.org/10.1016/j.applthermaleng.2011.09.005>
57. Fletcher TD, Shuster W, Hunt WF, Ashley R, Butler D, Arthur S, Trowsdale S, Barraud S, Semadeni-Davies A, Bertrand-Krajewski J-L et al (2015) SUDS, LID, BMPs, WSUD and more—the evolution and application of terminology surrounding urban drainage. *Urban Water J* 12:525–542. <https://doi.org/10.1080/1573062X.2014.916314>
58. Cooper N, Cooke S (2015) Assessment and management of unexploded ordnance (UXO) risk in the marine environment. CIRIA, London, UK. ISBN 978–0–86017–760–9
59. Sañudo-Fontaneda LA, Rodríguez-Hernández J, Castro-Fresno D (2012) Diseño y Construcción de Sistemas Urbanos de Drenaje Sostenible (SUDS). School of Civil Engineering of the Universidad de Cantabria

60. Ministerio para la Transición Ecológica Guía de Adaptación al Riesgo de Inundación: SUDS 2019
61. Charlesworth SM, Fontaneda LAS, Mays LW (2016) Back to the future? History and contemporary application of sustainable drainage techniques. In: Charlesworth SM, Booth CA, (eds) Sustainable surface water management. Wiley, pp 11–30. ISBN 978–1–118–89770–6
62. Chan FKS, Griffiths JA, Higgitt D, Xu S, Zhu F, Tang Y-T, Xu Y, Thorne CR (2018) “Sponge City” in China—a breakthrough of planning and flood risk management in the urban context. *Land Use Policy* 76:772–778. <https://doi.org/10.1016/j.landusepol.2018.03.005>
63. Mayor’s Office of Transport and Utilities (2014) City of Philadelphia green streets design manual. Philadelphia
64. Andrés-Doménech I, Anta J, Perales-Momparler S, Rodríguez-Hernández J (2021) Sustainable urban drainage systems in Spain: a diagnosis. *Sustainability* 13:2791. <https://doi.org/10.3390/su13052791>
65. Gobierno de España (2016) Real Decreto 638/2016, de 9 de Diciembre, Por El Que Se Modifica El Reglamento Del Dominio Público Hidráulico
66. Ayuntamiento de Madrid Guía (2018) Básica de Diseño de Sistemas de Gestión Sostenible de Aguas Pluviales En Zonas Verdes y Otros Espacios Libres
67. Momparler SP, Romero EC, Catalán CB, Pitarch IB (2019) Guía básica de diseño de sistemas urbanos de drenaje sostenible para el término municipal de Castelló de la Plana. Ayuntamiento de Castelló de la Plana 88
68. Revista de Obras Públicas (ROP) (2019) Consolidando El Drenaje Sostenible En España
69. Woods-Ballard B, Wilson S, Udale-Clarke H, Illman S, Scott T, Ashley R, Kellagher R (2015) The SuDS manual. CIRIA, London, UK. ISBN 978–0–86017–760–9
70. Jato-Espino D, Sañudo-Fontaneda LA, Andrés-Valeri VC (2018) Green infrastructure: cost-effective nature-based solutions for safeguarding the environment and protecting human health and well-being. In: Hussain CM (ed) Handbook of environmental materials management. Springer International Publishing, Cham, pp 1–27. ISBN 978–3–319–58538–3
71. Santamouris M (2014) Cooling the cities—a review of reflective and green roof mitigation technologies to fight heat island and improve comfort in urban environments. *Sol Energy* 103:682–703. <https://doi.org/10.1016/j.solener.2012.07.003>
72. Theodoridou I, Karteris M, Mallinis G, Tsiros E, Karteris A (2017) Assessing the benefits from retrofitting green roofs in mediterranean, using environmental modelling. GIS and very high spatial resolution remote sensing data: the example of Thessaloniki, Greece. *Proc Environ Sci* 38:530–537. <https://doi.org/10.1016/j.proenv.2017.03.117>
73. Stovin V, Vesuviano G, Kasmin H (2012) The hydrological performance of a green roof test bed under UK climatic conditions. *J Hydrol* 414–415:148–161. <https://doi.org/10.1016/j.jhydrol.2011.10.022>
74. Hernández JR (2008) Estudio, Análisis y Diseño de Secciones Permeables de Firmes Para Vías Urbanas Con Un Comportamiento Adecuado Frente a La Colmatación y Con La Capacidad Portante Necesaria Para Soportar Tráficos Ligeros. Universidad de Cantabria, Santander
75. Fontaneda LÁS (2014) Análisis de La Infiltración de Agua de Lluvia En Firmes Permeables Con Superficies de Adoquines y Aglomerados Porosos Para El Control En Origen de Inundaciones = The analysis of rainwater infiltration into permeable pavements, with concrete blocks and porous mixtures, for the source control of flooding. Universidad de Cantabria, Santander
76. Bruinsma J, Smith K, Peshkin D, Ballou L, Eisenberg B, Lurie C, Costa M, Ung C, Nassiri S, Shi X, et al (2017) Guidance for usage of permeable pavement at airports. Transportation Research Board, Washington, DC. p 24852. ISBN 978–0–309–44649–5
77. Eisenberg B, Collins Lindow K, Smith DR (2015) Permeable pavements. American Society of Civil Engineers (ASCE). ISBN 978–0–7844–1378–4
78. de la Fuente García L, Perales Momparler S, Rico Cortés M, Andrés Doménech I, Marco Segura JB (2021) Guía Básica para el Diseño de Sistemas Urbanos de Drenaje Sostenible en la Ciudad de València. Ayuntamiento de Valencia ISBN 978–84–9089–386–9

79. Washington State Department of Ecology Stormwater Management Manual for Western Washington 2014
80. City of San Francisco San Francisco Stormwater Management Requirements and Design Guidelines. 2016
81. Gavrić S, Leonhardt G, Österlund H, Marsalek J, Viklander M (2021) Metal enrichment of soils in three urban drainage grass swales used for seasonal snow storage. *Sci Total Environ* 760:144136. <https://doi.org/10.1016/j.scitotenv.2020.144136>
82. North Carolina Department of Environmental Quality (2017) USA. Stormwater Design Maintenance
83. Winston RJ, Hunt WF, Kennedy SG, Wright JD (2011) Evaluation of permeable friction course (PFC), roadside filter strips, dry swales, and wetland swales for treatment of highway stormwater runoff. p 111
84. Andrés-Valeri VC, Castro-Fresno D, Sañudo-Fontaneda LA, Rodríguez-Hernandez J (2014) Comparative analysis of the outflow water quality of two sustainable linear drainage systems. *Water Sci Technol* 70:1341–1347. <https://doi.org/10.2166/wst.2014.382>
85. Sañudo-Fontaneda LA, Roces-García J, Coupe SJ, Barrios-Crespo E, Rey-Mahía C, Álvarez-Rabanal FP, Lashford C (2020) Descriptive analysis of the performance of a vegetated swale through long-term hydrological monitoring: a case study from Coventry, UK. *Water* 12:2781. <https://doi.org/10.3390/w12102781>
86. Hinman C, Wulkan B (2012) Low impact development. Technical Guidance Manual for Puget Sound
87. Martín RP (2020) Normas para Redes de Saneamiento. Versión 3(2020):346
88. Jia H, Yao H, Tang Y, Yu SL, Zhen JX, Lu Y (2013) Development of a multi-criteria index ranking system for urban runoff best management practices (BMPs) selection. *Environ Monit Assess* 185:7915–7933. <https://doi.org/10.1007/s10661-013-3144-0>
89. Scholz M, Grabowiecki P (2008) Combined permeable pavement and ground source heat pump systems to treat urban runoff. *J Chem Technol Biotechnol* 84:405–413. <https://doi.org/10.1002/jctb.2054>
90. Coupe SJ, Tota-Maharaj K, Scholz M, Grabowiecki P, Formpave H, Avenue T, Gl G (2009) Water stored within permeable paving and the effect of ground source heat pump applications on water quality. p 11
91. Maharaj KT, Scholz M (2009) Permeable (Pervious) pavements and geothermal heat pumps: addressing sustainable urban stormwater management and renewable energy. *IJGE* 3:447. <https://doi.org/10.1504/IJGE.2009.031334>
92. Tota-Maharaj K, Scholz M, Ahmed T, French C, Pagaling E (2010) The synergy of permeable pavements and geothermal heat pumps for stormwater treatment and reuse. *Environ Technol* 31:1517–1531. <https://doi.org/10.1080/09593331003782409>
93. Tota-Maharaj K (2010) Geothermal paving systems for urban runoff treatment and renewable energy efficiency. University of Edinburgh
94. Tota-Maharaj K, Scholz M, Coupe SJ (2011) Modelling temperature and energy balances within geothermal paving systems. *Road Mater Pavement Design* 12:315–344. <https://doi.org/10.1080/14680629.2011.9695248>
95. Scholz M, Tota-Maharaj K, Grabowiecki P (2012) Modelling of retrofitted combined permeable pavement and ground source heat pump systems. p 11
96. del-Castillo-García G, Borinaga-Treviño R, Sañudo-Fontaneda LA, Pascual-Muñoz P (2013) Influence of pervious pavement systems on heat dissipation from a horizontal geothermal system. *Eur J Environ Civil Eng* 17:956–967. <https://doi.org/10.1080/19648189.2013.837842>
97. Novo AV, Bayon JR, Castro-Fresno D, Rodríguez-Hernandez J (2013) Temperature performance of different pervious pavements: rainwater harvesting for energy recovery purposes. *Water Resour Manage*. <https://doi.org/10.1007/s11269-013-0270-y>
98. Coupe SJ, Faraj AS, Nnadi EO, Charlesworth SM (2014) Integrated sustainable urban drainage systems. In Adeyeye K (ed) *Water efficiency in buildings*. John Wiley & Sons, Oxford, pp 147–163. ISBN 978–1–118–45661–3

99. Tota-Maharaj K, Paul P (2015) Sustainable approaches for stormwater quality improvements with experimental geothermal paving systems. *Sustainability* 7:1388–1410. <https://doi.org/10.3390/su7021388>
100. Faraj-Lloyd A, Charlesworth SM, Coupe SJ (2016) Sustainable drainage systems and energy: generation and reduction. In: Charlesworth SM, Booth CA (eds) *Sustainable surface water management*. Wiley, pp 177–192. ISBN 978–1–118–89770–6
101. Andrés-Valeri VC, Sañudo-Fontaneda LA, Rey-Mahía C, Coupe SJ, Alvarez-Rabanal FP (2018) Thermal performance of wet swales designed as multifunctional green infrastructure systems for water management and energy saving. In: *Proceedings of the 2nd international research conference on sustainable energy, engineering, materials and environment*. MDPI, pp 1433
102. Rey-Mahía C, Sañudo-Fontaneda LA, Andrés-Valeri VC, Álvarez-Rabanal FP, Coupe SJ, Rocés-García J (2019) Evaluating the thermal performance of wet swales housing ground source heat pump elements through laboratory modelling. *Sustainability* 11:3118. <https://doi.org/10.3390/su11113118>
103. Poulsen SE, Andersen TR, Tordrup KW (2022) Full-Scale demonstration of combined ground source heating and sustainable urban drainage in roadbeds
104. Andersen TR, Poulsen SE, Tordrup KW (2022) The climate road—a multifunctional full-scale demonstration road that prevents flooding and produces green energy
105. Janssen E, Seters TV (2022) Thermal mitigation of stormwater management pond outflows using geothermal cooling

Performance Prediction of Hybrid GSHP System Considering Ground Thermal Balance



Shiyu Zhou and Wenzhi Cui

Abstract Thermal imbalance is usually encountered in the application of ground-source heat pumps (GSHP) in cooling or heating load-dominated areas, which results in the performance degradation of the GSHP system. Hybrid ground-source heat pump (HGSHP) combining cooling tower, domestic hot water (DHW), or other auxiliary technologies has been developed to temper the underground heat or cold accumulation in cooling or heating load-dominated zones. This chapter will discuss several typical hybrid ground-source heat pump systems, how to build and validate the numerical model for the HGSHP system based on the TRNSYS code, and prediction and analysis of the long-term performances of the HGSHP systems considering the ground thermal balance via the optimization of the system operation strategies. This chapter focuses on the research of auxiliary heat dissipation that is suitable for heat accumulation systems. Several schemes for alleviating the underground heat accumulation of GSHP and keeping higher system efficiency are proposed and validated by the simulation work. For a typical GSHP system equipped in an office building, the optimum design and operation parameters are given for each scheme, respectively.

Keywords Hybrid GSHP · Thermal balance · System performance · Operation strategy

1 Introduction

Ground source heat pump (GSHP) has been regarded as a highly efficient, renewable energy technology for space heating and cooling [1, 2]. This technology has gained international attention as a mean of energy conservation in the residential and commercial air conditioning of indoor spaces, and then it has been widely used in

S. Zhou

School of Thermal Engineering, Shandong Jianzhu University, Jinan 250101, Shandong, China

W. Cui (✉)

School of Energy and Power Engineering, Chongqing University, Chongqing 400030, China

e-mail: wzcui@cqu.edu.cn

the world [3, 4]. Specifically, in China, the GSHP system has been developed rapidly in recent years [1, 2].

With the in-depth research and application, it has been found that the application of GSHP system in geographical areas in which there is a large difference between the cooling load and the heating load will lead to the evident variation of the ground temperature. That is, there exists a problem of load imbalance in the application of GSHP system in the cooling load dominated areas. The long-time running of the GSHP system will result in a surplus of heat being accumulated in the ground. Consequently, the ground temperature gradually increases, which deteriorates the performance of the GSHP system in terms of capacity and energy efficiency [5, 6], and also other problems, such as the change of thermal and microbial environment, and even the organic carbon reserves in the soil [7]. Therefore, some scholars put forward the application of hybrid ground source heat pump (HGSHP), which is referred to GSHP system assisted with auxiliary heat sink or source [8]. HGSHP can not only improve the operating performance of the system, but also reduce the system initial investment [9]. The following describes several ways to alleviate the imbalance of ground temperature and compound ground source heat pump system.

(1) Schemes to alleviate the underground heat accumulation of GSHP

Schemes to alleviate the underground heat accumulation of GSHP is to use additional power to raise or lower the temperature of rock-soil body. For the problem that the ground temperature of the ground source heat pump system in Hot Summer and Cold Winter Zone increases year by year, only the water circulation system of the buried heat exchanger can be opened in transition season to make the cooling water absorb heat from the ground and then release the heat into the air through the cooling tower.

(2) GSHP system assisted with cooling tower

In the cooling load dominated areas, the most common heat sink of HGSHP system is cooling tower. Cooling tower can be compounded into the GSHP system in two modes, i.e., parallel and series connections. In which, the parallel configuration should be adopted in the newly-built GSHP project, while the series configuration is suitable for the renovated project [10]. Some researches have been conducted on the performance of HGSHP system. Man et al. [11] studied the performance of a HGSHP system installed in hot-weather areas with a practical hourly simulation model. Their simulation results showed that the HGSHP system could effectively solve the heat accumulation problem and reduce both initial and operating costs compared with conventional GSHP system. Hackel and Pertzborn [12] studied three HGSHP systems including two cooling tower assisted systems. Considering the economic and environmental performances of the HGSHP systems, some improved design and operation strategies were proposed in their study. Sagia et al. [13] improved the design of cooling tower in a HGSHP system through the performance comparison among systems with different auxiliary cooling ratios (ACRs). Furthermore, Sayyadi and

Nejatolahi [14] optimized thermodynamic and thermoeconomic performances of a HGSHP system in a multi-objective optimization process using the genetic algorithm.

(3) GSHP system assisted with chiller

The GSHP system assisted with chiller means that the air conditioning refrigeration system is composed of two relatively independent refrigeration systems, namely, the chiller + cooling tower system and the heat pump unit + buried pipe system [15] this system can not only ensure the timely recovery of ground temperature, but also help the system to provide stable cooling under high load conditions. In addition to effectively alleviating underground heat accumulation, this system configuration also has some advantages that conventional ground source heat pump systems and cooling tower auxiliary cooling systems do not have, such as flexible control, mutual standby of host machines, and good system stability [16].

(4) Design and operation parameter optimization based on TRNSYS simulation

There are also a series of articles about the prediction of system long-term performance that usually be accomplished with TRNSYS software. Huang et al. [17] simulated the 20 years' performances of two GSHP cases. The results showed that, benefiting from the proposed multi-objective design optimization strategy, the total system cost in 20 years decreased by 9.5 and 5.2% for the two cases, respectively, comparing with a single-objective design optimization strategy. Chen et al. [18] performed a 20 years' numerical simulation for a solar-assisted GSHP system. The simulation results showed that the long-term yearly average space heating efficiency was improved by 26.3% comparing with a traditional GSHP system. Fan et al. [19] simulated the long term (50 years) performance of a practical hybrid GSHP (HGSHP) system assisted with cooling tower. The results showed that the hybrid GSHP system could effectively solve the heat accumulation problem and the decrease of system performance in the long run. Wang et al. [20] developed a simulation model in TRNSYS to predict the multi years' performance of a hybrid GSHP system assisted with solar energy. The simulation results showed that the system was reasonably designed to resolve the thermal imbalance problem.

In this chapter, the main work to be carried out includes: taking a GSHP system in Chongqing as an example to carry out relevant research, including compound system operation simulation and ground temperature imbalance mitigation simulation.

2 Operation Analysis And Performance Prediction for a GSHP System Compounded With Domestic Hot Water (DHW) System

2.1 Description of the GSHP System

2.1.1 GSHP System

The research object is a multi-storied building with 32F on the ground and 3F under the ground. The building's footprint size is 2123 m² and its orientation can be seen in Fig. 1. The first three floors of 6368 m² on the ground are office area and the stories that above 3F are residential rooms. Therefore, there is not only air conditioning demand in office floors but also domestic hot water (DHW) demand in residential floors for this building. Since the building is located in Chongqing where the climate is characterized by hot summer and cold winter, there is a load imbalance between the cooling and heating. A hybrid GSHP system compounded with DHW system was applied to this building. The designed cooling and heating loads of the office part were 605 and 298 kW, respectively. There were two heat pump units (HPUs) installed, which were used for domestic water-heating and air-conditioning, respectively, as shown in Fig. 2. Table 1 shows the main parameters of the GSHP system.

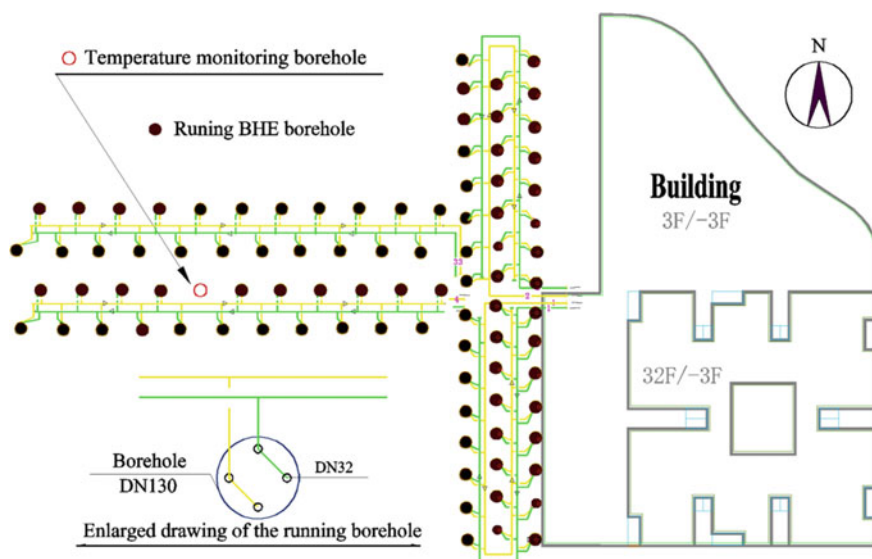


Fig. 1 Layout of the building and BHE system

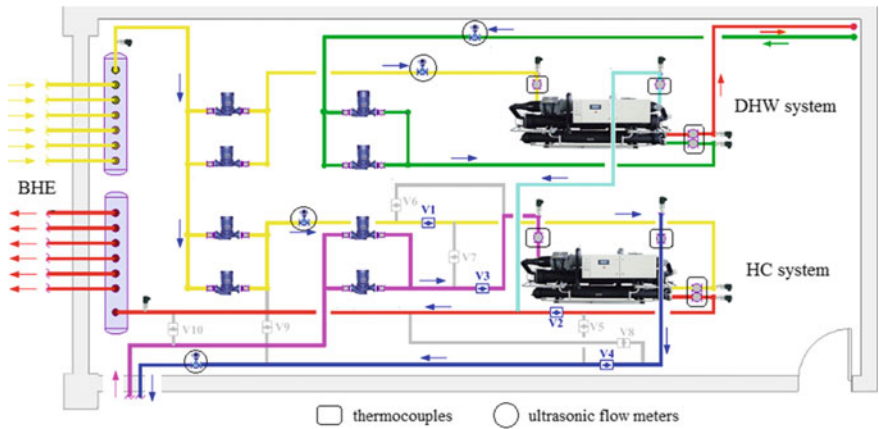


Fig. 2 Composition of the GSHP system

Table 1 Main parameters of the GSHP system

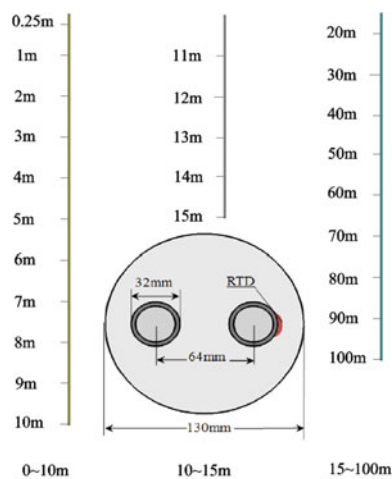
Type	Item	Parameters
Domestic hot water system (DHW)	Heat pump unit	Heating capacity 362 kW, heating power 102.7 kW
	Pump in load side	Flow rate 64 m ³ /h, head 19 m, power 5.5 kW
	Pump in source side	Flow rate 70 m ³ /h, head 22 m, power 5.5 kW
Air-conditioning system (HC)	Heat pump unit	Refrigerating/heating capacity 564.3/623 kW Refrigerating/heating power 121/134 kW
	Pump in load side	Flow rate 129 m ³ /h, head 31 m, power 22 kW
	Pump in source side	Flow rate 150 m ³ /h, head 33 m, power 22 kW
Ground	Soil thermal conductivity	2.5 W/(m K)
	Soil heat capacity	3600 kJ/(m ³ ·K)
	Undisturbed ground temperature	20 °C
Borehole heat exchanger (BHE)	Number of boreholes	90
	Borehole depth and diameter	100 and 0.13 m
	Inner and outer diameters of the U-pipe	25 and 32 mm
	Thermal conductivity of the U-pipe	0.46 W/(m K)

2.1.2 Data Acquisition System

The data acquisition system includes two separate monitoring systems, i.e., a GSHP performance monitoring system and a ground temperature monitoring system. The data acquisition system ran automatically by the control of computers. For the GSHP performance monitoring system, the temperatures were measured by thermocouples ($\pm 0.5\text{ }^{\circ}\text{C}$ accuracy), which were distributed at some specific points at the inlets and outlets of the pipes. The flow rates of water in the source and load side pipes were measured by ultrasonic flow meters (1–5% accuracy). The locations of the thermocouples and ultrasonic flow meters can be found in Fig. 2. The ground temperature monitoring system was set up in an idle borehole which was surrounded by other running boreholes, as shown in Fig. 1. The resistance temperature detectors (RTDs, $\pm 0.1\text{ }^{\circ}\text{C}$ accuracy) were installed on the legs of the U-pipe at specified positions as shown in Fig. 3, i.e., from ground surface to 15 m depth, the RTDs were installed with one meter spacing and 10 m spacing in the depth range from 20 to 100 m.

The DHW system has not been operated so far, hence only running data of the HC (air-conditioning) system could be obtained. The GSHP system ran from 9:00 to 17:00 every day except for the weekends in the cooling and heating seasons which were usually from May 15th to September 15th and December 1th to February 15th, respectively. Since the paper focuses on the long term performance of the GSHP system, the running data between 10:00 and 17:00 period of everyday were averaged for data processing and the bad data were eliminated. Besides, for the reason that the stable running state of the GSHP system usually concentrated in the high load period, the measured data of 46 days from July 15th to August 30th in cooling season, and also that of 42 days from December 4th to January 15th in heating season were chosen for processing.

Fig. 3 Arrangement of RTDs in the borehole



2.2 Operating Characteristic of the GSHP System

2.2.1 Inlet and Outlet Temperatures

Figure 4 shows the variations of the inlet/outlet water temperature on both of load and source sides of the HPU in cooling and heating seasons. For the daily highest dry-bulb (HDB) temperature usually occurs at noon of a day while the air-conditioning system in operation, therefore, the variation of the daily HDB temperature can somewhat reflect the change of air-conditioning load. In order to present the variation of the daily load during air-conditioning season, the HDB temperatures in the corresponding period are also included in Fig. 4.

It can be known from the figure that, the fluctuation trends of the water temperatures are almost the same as that of HDB temperature in both cooling and heating seasons. In cooling season, higher HDB temperature means higher cooling load for the GSHP system, which is an adverse work condition for system running. Therefore, both the inlet temperatures of the load and source sides of the HPU increase. In heating season, on the other hand, the lower HDB temperature implies the higher heating load for the GSHP system, which leads to the decrease of the inlet temperatures of both the load and source sides of the HPU. Furthermore, it can be seen from the whole air-conditioning season that, the water temperatures of the source side increase gradually in cooling season, while decrease gradually in heating season. The reason was partially due to the reduction of the heat exchanging capability of the BHE.

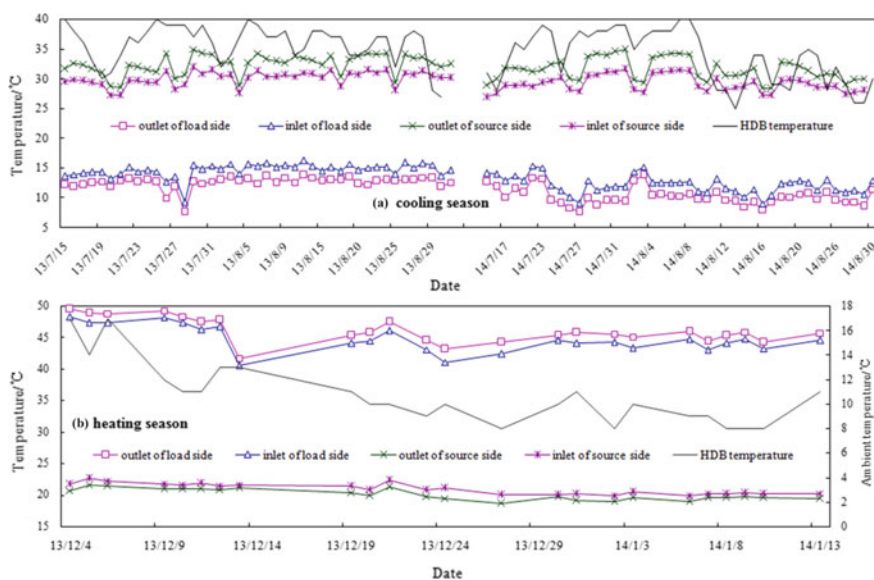


Fig. 4 Variations of the inlet/outlet temperatures of HPU

Table 2 Average inlet/outlet temperatures of HPU (°C)

Operation period	Inlet of source side	Outlet of source side	Inlet of load side	Outlet of load side
Cooling season of 2013/2014	30.1/29.2	32.5/31.5	14.7/12.2	12.7/10.2
Heating season of 2013	20.9	20.0	44.8	46.1

Because the heating load of the GSHP system was far less than the rated heating capacity of the HPU, the system always worked at low load ratio in heating season, resulting in frequent start-stop of the HPU. Therefore, in heating season, there were several days' measured data deviated from the normal value and the number of effective data was relatively small. In heating season, the temperature differences between the inlet and outlet of both load and source sides of HPU were so small that the characteristic of low heating load could be demonstrated. Besides, the inlet temperature of source side was relatively higher, close to the ground temperature and this was not conducive to the heat exchanging under the ground.

Table 2 is the averaged values of these temperature data. It can be seen that, in cooling season, the average inlet/outlet water temperatures of 2014 are lower than that of 2013. This was due to the fact that the cooling load of 2014 was lower than that of 2013, which would be further illustrated in Sect. 3.2.

2.2.2 Amount of Heat

The system load (Q) and quantity of heat exchange under the ground (Q') can both be calculated with Eq. (1):

$$Q = V\rho c\Delta t_w/3600 \quad (1)$$

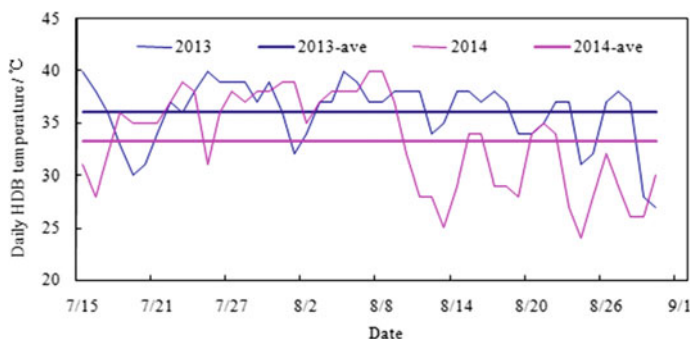
where, V —Flow rate of water in the load /source side, m^3/h . The system worked with constant water flow rates of $141.1 \text{ m}^3/\text{h}$ in load side and $132.3 \text{ m}^3/\text{h}$ in source side, respectively; Δt_w —Temperature difference between the inlet and outlet of load /source side, °C; ρc —Volumetric heat capacity of the water, $\text{kJ}/(\text{m}^3\cdot^\circ\text{C})$.

In order to guarantee the authenticity of the measured data, Eq. (2) was taken to check the energy balance between the load and source sides of the HPU, in which Dev_c and Dev_h represent the energy deviations in cooling and heating seasons, respectively. The computed average values of the system load, underground heat exchange and also the energy deviations between the load and source sides of the GSHP system are shown in Table 3.

$$Dev_c = \left| \frac{Q'_c - Q_c - N_c}{Q'_c} \right|; Dev_h = \left| \frac{Q'_h + N_h - Q_h}{Q_h} \right| \quad (2)$$

Table 3 Averaged amount of heat (kW)

Operation period	Heat exchange under the ground	Air-conditioning load	Deviation %
Cooling season of 2013/2014	392/389	313/299	3.38/5.74
Heating season of 2013	146	205	7.71

**Fig. 5** Comparison of HDB temperatures

where, Q'_c/Q'_h represents quantity of heat exchange under the ground, kW; Q_c/Q_h means air-conditioning load of the GSHP system, kW; N_c/N_h is running power of HPU, kW.

The deviations in cooling and heating seasons are both less than 10%, indicating the validity of the measured data. Besides, the table also shows that the air-conditioning load of 2014 is less than that of 2013, because the average HDB temperature in the cooling season of 2014 was lower than that of 2013, as shown in Fig. 5. The average heating load is about 67% of the average cooling load, while the quantity of heat exchange under the ground in heating season, i.e., heat extracted from the ground is only about 37.5% of that injected to the ground in cooling season. This inevitably aggravates the heat accumulation under the ground, leading to the increase of the ground temperature.

2.2.3 EER and COP

Figure 6 is the running power variations of the HPU (heat pump unit) and HPS (heat pump system). Because the pumps worked with constant flow, the running power of pumps kept almost constant. Therefore, the power variations of the HPU and HPS present the same trend in both cooling and heating seasons. In cooling season, the HDB temperature variation is almost the same as power variation. The higher HDB temperature means the higher cooling load, which definitely need higher power to

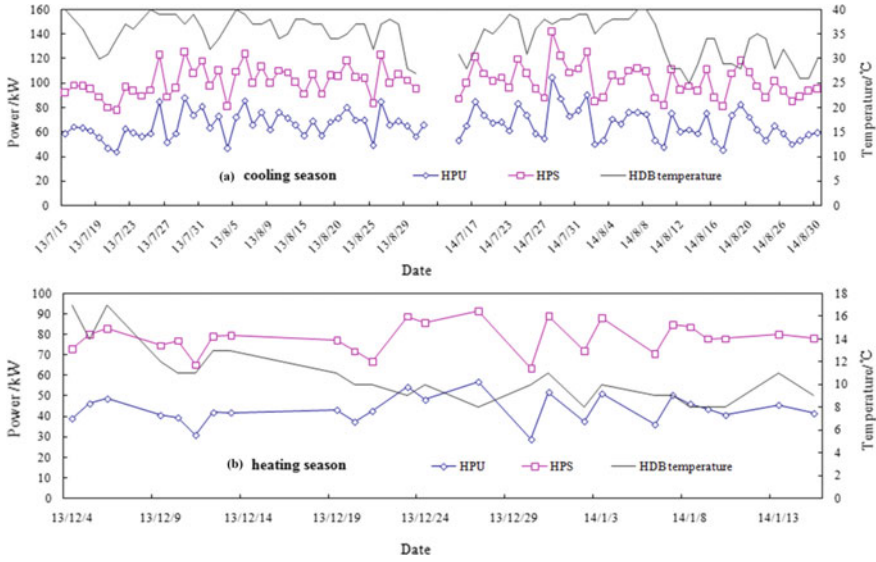


Fig. 6 Running power variations in cooling and heating seasons

meet the cooling load. In heating season, the HDB temperature decreases day by day, meaning that the heating load and also power increase gradually.

The *EER* (Energy Efficiency Ratio) in cooling season and *COP* (Coefficient of Performance) in heating season of HPU and HPS can be calculated according to the following equations:

$$EER_u = Q_c / N_c; EER_s = Q_c / (N_c + \sum N_i) \quad (3)$$

$$COP_u = Q_h / N_h; COP_s = Q_h / (N_h + \sum N_i) \quad (4)$$

In which, EER_u / COP_u represents *EER*/*COP* of HPU; EER_s / COP_s means *EER*/*COP* of HPS; $\sum N_i$ is running power of pump system, kW;

Figure 7 is the calculated *EER* and *COP* in both cooling and heating seasons. It shows that values of *EER* and *COP* fluctuate frequently. In cooling seasons, the ratio of *EER* greater than 5.0 is 35.7% in 2013 for HPU, while that is only 9.3% in 2014. For HPS, the ratio of *EER* greater than 3.0 is 61.9% in 2013, while that is 55.8% in 2014. In heating season, the ratio of *COP* greater than 5.0 is 40% for HPU, while the ratio of *COP* greater than 3.0 is only 20% for HPS.

Table 4 lists the average values of *COP* and *EER*. It can be seen that the system cooling performance in 2014 is inferior to that in 2013, which is supposed due to the increase of the ground temperature. For HPU, the *COP* is equal to *EER* in 2013, and even higher than *EER* in 2014. For HPS, however, the *COP* is remarkably lower than the *EER* values. This is due to the constant flow rate of pump system, i.e., the

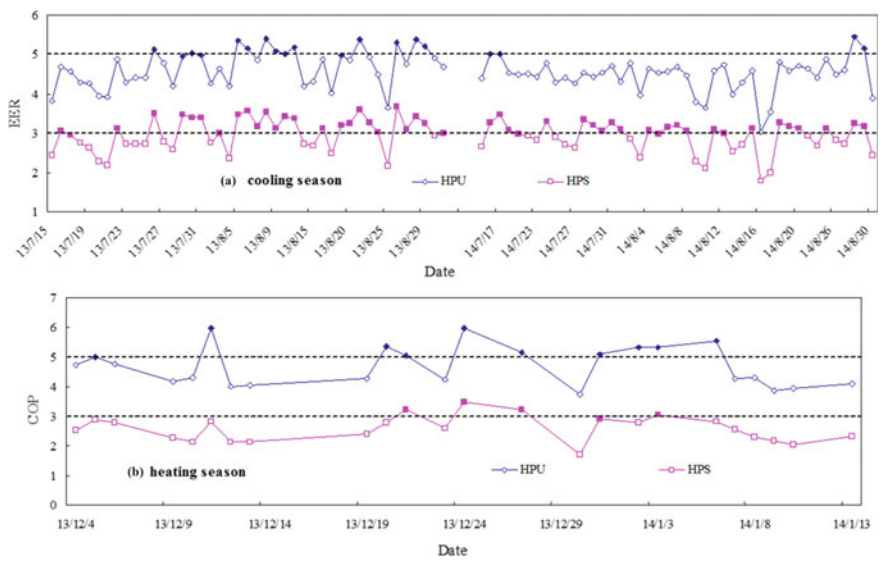


Fig. 7 Variations of *EER* and *COP* in cooling and heating seasons

Table 4 Average *COP* and *EER*

Period	HPU	HPS
Cooling season of 2013/2014 (<i>EER</i>)	4.69/4.47	3.01/2.91
Heating season of 2013 (<i>COP</i>)	4.69	2.59

pump power kept almost constant in both cooling and heating seasons. As shown in Table 3, the heating load is far less than the cooling load, meaning that the heating power is less than cooling power for HPU. Therefore, the possess proportion of pump power in the system power in heating season is much higher than that in cooling season, leading to the decrease of *EER* of HPS.

2.2.4 Ground Temperature

The variation of the monthly average ground temperature at different depths from March 2013 to October 2014 is shown in Fig. 8. It can be seen from the figure that, when the GSHP system started up for cooling in June-2013, the ground temperature began to increase continuously and reached the maximum at the end of the cooling season. Since then, the ground temperature decreased in transitional (mid) season and also the succeeding heating season until the coming of the next cooling season. As expected from the load distribution of the building, the ground temperature could not restore to the undisturbed temperature level before the second cooling season because of the imbalance between the heat injected into and extracted from the ground during a whole year. Therefore, the ground temperatures presented a general upward trend

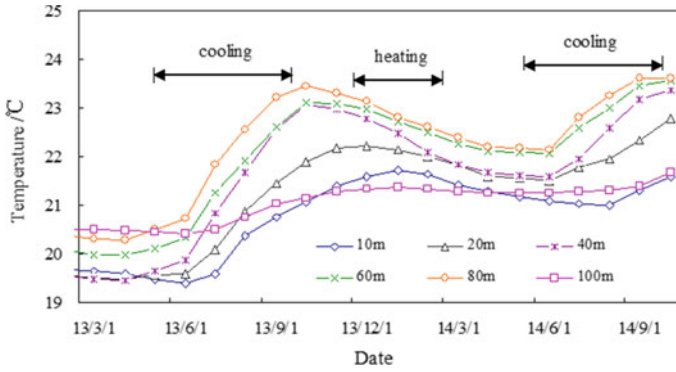


Fig. 8 Ground temperature variations

with the increase of the system operation time, which definitely weakened the heat exchange capability of the ground for cooling, leading to the deterioration of the system cooling performance.

2.3 Performance Prediction of the GSHP System

2.3.1 Mathematical Model of the System

(1) Water-to-water heat pump

Type 668 is a simplified water-to-water heat pump model, based on user-supplied performance data containing heating and cooling capacity related to power consumption. It performs linear interpolating according to the entering source and load temperatures. The COP of the heat pump can be calculated by [21]:

$$COP_h = \frac{Q_h}{P_h}; COP_c = \frac{Q_c}{P_c} \quad (5)$$

$$Q_s = Q_h - P_h, Q_s = Q_c + P_c \quad (6)$$

(2) Ground heat exchanger

The DST model, Type 557, is the most commonly used model in GHE simulation. The program assumes that the boreholes are placed uniformly within a cylindrical storage ground volume, which can be calculated by:

$$V = \pi N_b H (0.525B)^2 \quad (7)$$

The borehole thermal resistance is defined by Hellstrom as [22]:

$$R_b = \frac{\overline{T_f} - \overline{T_b}}{q} \quad (8)$$

where, T_b is the average temperature at borehole wall; T_f is the average fluid temperature in tubes; q is the power pulse per unit length.

The ground temperature distribution is then superposed by global temperature, local solution and steady-flux solution. The detailed calculation of the three temperatures can be found in [22].

Pertzborn et al. [23] conducted a sensitivity study about DST model and concluded that the thermal conductivity and heat capacity of the ground had the greatest impact on the accuracy of the model.

(3) Closed cooling tower

The model (Type 510) relies on the basic premise that the saturated air temperature is the temperature at the air water interface and is also the temperature of the outlet fluid [24]. With this assumption the authors demonstrate that the saturated air enthalpy can be calculated from:

$$h_{sat}(T_{f,out}) = h_a(T_{a,in}) + \frac{\dot{m}_f C p_f (T_{f,in} - T_{f,out})}{\dot{m}_a (1 - \exp[-\lambda_{design}(\gamma_a)^{-0.4}])} \quad (9)$$

where the fan control signal is defined as:

$$\gamma_a = \frac{\dot{m}_a}{\dot{m}_{a,design}} \quad (10)$$

Given the inlet air temperature, humidity and flow rate (all inputs to the model), the fan control signal (an input), the inlet fluid temperature and flow rate (inputs), and the fluid properties (parameter), Eq. (5) can be iteratively solved in order to calculate the outlet fluid temperature.

Besides, in the study, the pump model used in the TRNSYS simulation is constant-frequency, the pump power do not change with time. Therefore, it is unnecessary to describe the mathematical model of the pump. The detailed description of the variable frequency pump can be found in reference [25].

2.3.2 Air-Conditioning Load Calculation

The load calculation work was executed with Designer's Simulation Toolkit (DeST) developed by Tsinghua University [26]. The meteorological data used in the simulation was derived from Chinese standard weather data [27]. The main parameters used in the air-conditioning load calculation are listed in Table 5. In order to cohering the simulation results with the measured results shown in Table 3, the designed indoor temperatures were regulated in the scope of the specification [28]. Therefore, the computed load was different from the initial designed loads of the building. The

calculated building load distribution is shown in Fig. 9. The negative value represents cooling load whose peak value is 597 kW, while the positive value represents heating load whose peak value is 340 kW. The accumulated cooling load is 300235 kW, while the accumulated heating load is 77991 kW.

Table 5 Main parameters set in the load calculation software

Type	Description of the studied building	Additional information
Exterior wall	190 mm Brick + 40 mm Insulation + 40 mm Cement	$K = 0.68 \text{ W}/(\text{m}^2 \cdot \text{K})$
Roof	100 mm Concrete + 40 mm Insulation + 60 mm Cement	$K = 0.81 \text{ W}/(\text{m}^2 \cdot \text{K})$
Window	Insulating glass with 12 mm cavity	$K = 2.83 \text{ W}/(\text{m}^2 \cdot \text{K})$
Glazing ratio	25% for the east wall and the west wall, 19% for the south wall, and 13% for the north wall, respectively	
	Internal loads	
Indoor heat sources	500 persons working in the building Computer load $15 \text{ W}/\text{m}^2$ Lighting load $10 \text{ W}/\text{m}^2$	
Indoor temperatures	21 ~ 23 °C in heating season and 23 ~ 26 °C in cooling season for office rooms 18 ~ 21 °C in heating season and 25 ~ 28 °C in cooling season for other regions, such as corridor	
	Heating and cooling seasons	
Heating season	December 1st to February 15th	
Cooling season	May 15th to September 15th	

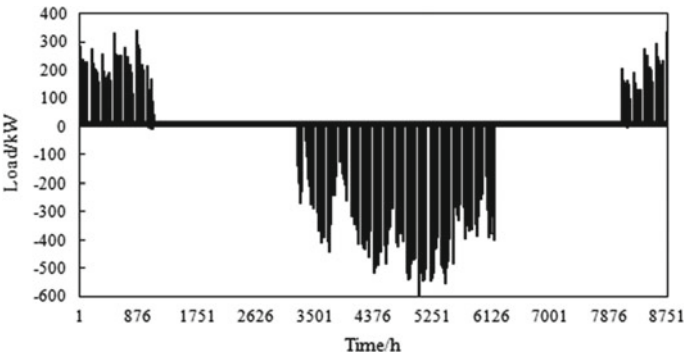


Fig. 9 Load distribution of the studied building

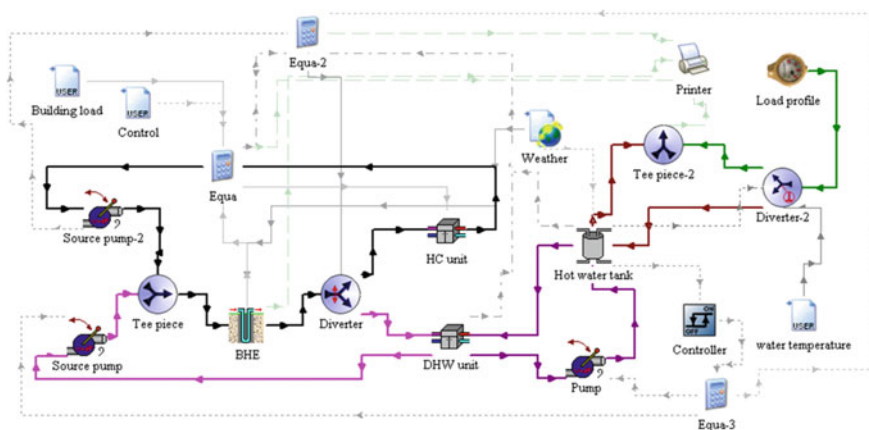


Fig. 10 TRNSYS model of the studied GSHP system

2.3.3 TRNSYS Model Establishment

TRNSYS is a modular simulation software which can be used to simulate and predict the behavior and performance of transient thermal systems. It was developed by Solar Energy Laboratory of the University of Wisconsin-Madison and improved by some research institutes in Europe [29]. The model of the studied GSHP system was established in TRNSYS 17, as shown in Fig. 10. The calculated load in Sect. 2.3.2 was read into by the “Building load” type, and the parameters of other types in the model were set according to Table 1.

2.3.4 Model Validation

(1) Outlet water temperature

Duct Ground Heat Storage (DST) model was adopted to simulate the heat transfer process of BHE in TRNSYS, which was developed by Hellstrom [30]. In the model, the user can define the ground thermal properties and heat exchange characteristics such as soil thermal conductivity, heat capacity and also borehole depth, radius, etc. DST model has been validated in several papers. For example, Fan [19] validated the model by comparing the measured and simulated data of outlet water temperature from the BHE. Raab [31] demonstrated the accuracy of DST model by comparing the measured and calculated temperatures of the heat store areas. Besides, Magraner [32] validated a whole TRNSYS model by comparing the experimental and prediction values of system performance factor. The corresponding parameters of the DST model in this paper were set according to Table 1.

Figure 11 is the comparisons and deviations between the simulated and measured outlet water temperature of BHE in two successive cooling seasons and one heating

season. For the purpose of clarity, the comparisons are listed for only a week period, while the deviations are listed for the whole period of running data process in cooling and heating seasons. It can be seen from the comparisons that, the two temperatures are in good accordance when the system is in the running state. When the system is shut down, however, the two temperatures begin to deviate from each other, especially in the second cooling season and the heating season. The reason for this is that, the measured temperature got close to the indoor temperature because of the thermocouples were installed at the inlet pipe of HPU, while the simulated temperature got close to the ground temperature in the software. The deviations in the figure are also small enough to indicate the good accordance of the two temperatures, except for the heating season, which may be caused by the existing severe difference between the indoor air temperature and the ground temperature in the winter.

(2) Ground temperature

Besides, the average ground temperature was also calculated with the model and used to validate the whole TRNSYS model. The comparison between the simulated and

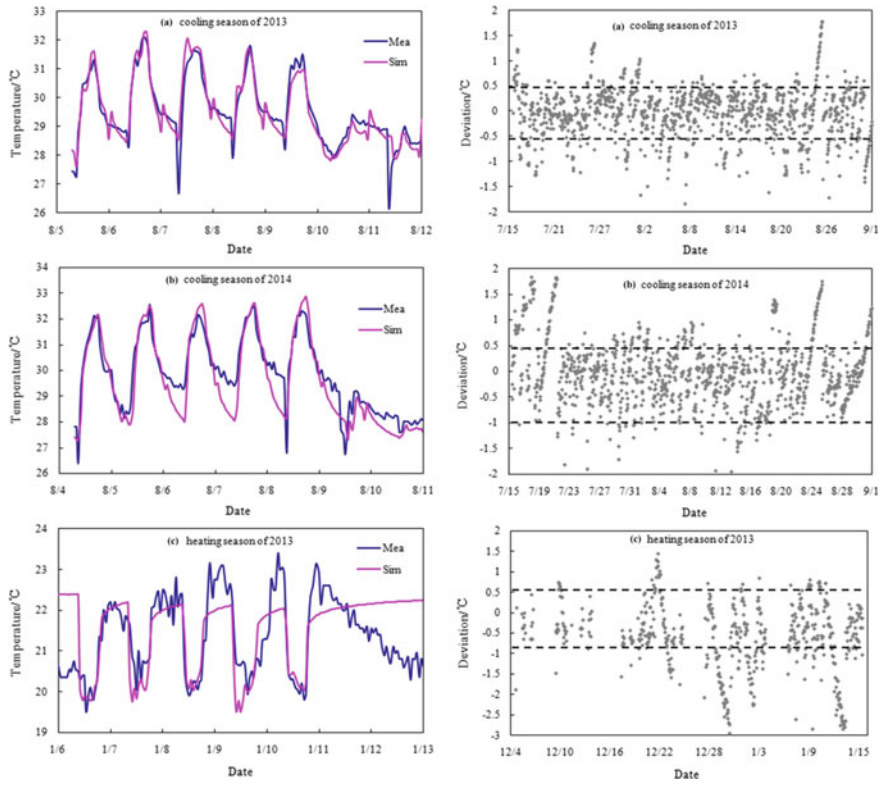


Fig. 11 Comparisons and deviations between the simulated and measured outlet temperature of BHE

measured data is shown in Fig. 12. The figure shows that the deviation in the first year is the maximal and then it decreases gradually. As shown in Table 6, the maximum deviations in the first cooling and heating seasons are 0.78 and 0.69 °C, respectively. While in the second year, they decrease to 0.09 and 0.20 °C, respectively. The reason for the deviation is that, the calculated air-conditioning load (Fig. 9) was adopted in the simulation, which was based on the typical meteorological data extracted from the Chinese standard weather data [27], rather than the real weather data of the simulated year.

There exists difference between the typical and practical weather data. For example, as shown in Fig. 13, the practical daily HDB temperature of 2013 is higher than the typical temperature remarkably in the cooling season, meaning that the real cooling load in 2013 is more than the calculated cooling load. Similarly, the comparisons between the average values of the typical weather data and other years' practical temperature are also shown in Table 6. It can be seen that the deviations are all enough low except for that of 2013. So the simulated and the practical ground temperatures that after 2013 are in good accordance, also indicating the accuracy of the simulation.

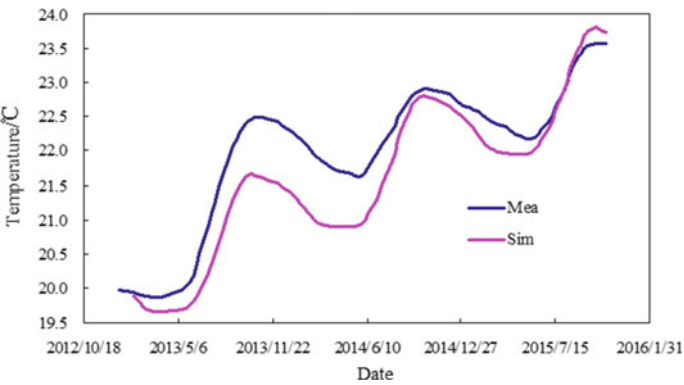


Fig. 12 Comparison between the simulated and measured ground temperature

Table 6 Comparison between average temperatures of practical and simulation (°C)

Type	Average value	CS of 2013	HS of 2013	CS of 2014	HS of 2014	CS of 2015
Ground-temperature	Measured	22.49	21.65	22.88	22.20	23.57
	Simulated	21.61	20.96	22.79	22.00	23.79
	Deviation	0.78	0.69	0.09	0.20	−0.23
Daily-	Practical	32.74	11.78	30.17	11.60	30.66
HDB-	Typical	30.36	10.97	30.36	10.97	30.36
temperature	Deviation	2.38	0.81	−0.19	0.63	0.30

Note 1. CS represents cooling season and HS represents heating season

2. Ground temperatures are peak/valley values in Fig. 12

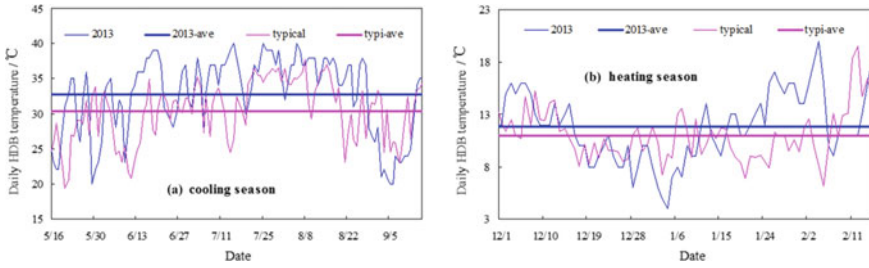


Fig. 13 Comparisons between the practical and typical HDB temperatures

2.3.5 System Performance Prediction

(1) Conventional GSHP system

In order to predict the long-term performance of the GSHP system, a simulation of 20-years operation of the GSHP system was performed with TRNSYS software. As inferred from the calculated air-conditioning load, after several years running of the GSHP system, the ground temperature would increase definitely due to the imbalance between the cooling and heating loads. The increase of the ground temperature will cause the change of the system performance. In order to analyze the variation of the system performance, the annual system performance factor (ASPF) is defined as follows:

$$ASPF = \frac{Q_{tot,c} + Q_{tot,h}}{Q_{tot,s}} \quad (11)$$

In which, $Q_{tot,c}$ is the cumulative cooling load in a whole year, kWh; $Q_{tot,h}$ is the cumulative heating load (including hot-water load) in a whole year, kWh; $Q_{tot,s}$ is the power consumption of the GSHP system in a whole year, kWh.

Since the DHW system has not been operated so far, suppose it will never be operated in the whole simulation period. The simulated results are shown in Fig. 14. It can be seen that, in the 20th year, the average ground temperature will ascend to 30.5 °C from the initial value of 20 °C, while the ASPF value will descend to 2.72 from the initial value of 3.12. The ASPF declining proportion reaches 12.82%, demonstrating the deterioration of the system performance. The increase of the ground temperature is mainly due to the heat accumulation under the ground. In order to improve the system performance, some measures for alleviating the heat accumulation should be applied to form a hybrid GSHP system, such as auxiliary with cooling tower system or DHW system.

(2) Hybrid GSHP system

As stated in the previous sections, DHW system has been equipped into the GSHP system. Therefore, it should be operated timely to attemper the heat accumulation under the ground. Supposing the DHW system will be put into operation in the fourth

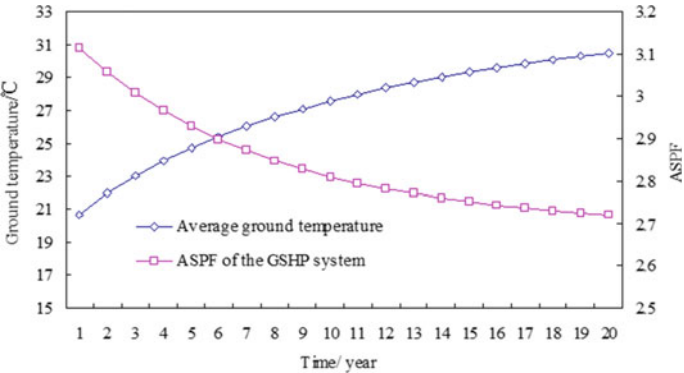


Fig. 14 Variation of the ground temperature and ASPF value of the GSHP system

Table 7 Hourly flow rate of DHW in a day round

Period (h)	0~6	7~9	10~11	12~13	14~18	19~21	22~24
Flow rate (L/h)	0	6084	0	8112	0	10,140	0

year (2016) and the system performance in 20 years was simulated. In the simulation, the municipal water temperature was set as 7 °C in heating season, 25 °C in cooling season and 18 °C in transitional season, respectively. Table 7 lists the hourly flow rate of DHW supply in a day round. The supply temperature of hot water was set as 45 °C, and the volume of hot water tank was 20 m³, which could satisfy at least two consecutive hours of hot water supply. The running of DHW system was controlled by an on/off differential controller whose operational principle can be found in the documentation of TRNSYS software [29].

The simulated results are shown in Fig. 15. It can be seen that once the DHW system is put into operation, the ground temperature ceases from increasing and begins falling year by year. Meanwhile, the ASPF value of the system rises up to 3.4 in the fourth year, and then decreases year by year. However, in the later years until the 20th year, it is still higher than the ASPF values of the first three years. Apparently, the operation of DHW system can not only meet the hot water needs of the residents in this building, but also be benefit for the system operation by improving the system performance. Therefore, the DHW system should be operated as soon as possible in the studied GSHP system.

2.4 Summary

The section investigated the operating characteristics of a GSHP system by analyzing the running data of the system in two successive years. The measured *EER* of the

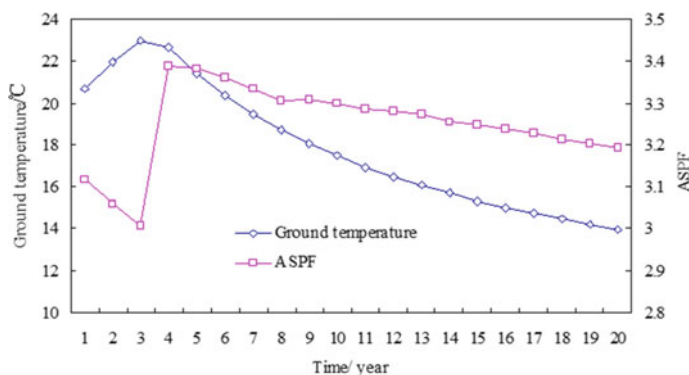


Fig. 15 Variation of the ground temperature and ASPF value of the hybrid GSHP system

system in cooling seasons of 2013 and 2014 are 3.01 and 2.91, respectively, while the *COP* of the system in heating season of 2013 is 2.59. The system performance in the second year was inferior to that in the first year, which was mainly caused by the increase of the ground temperature.

In order to predict the long-term system performance of the GSHP system, a TRNSYS model was constructed according to the practical parameters of the GSHP system. And then, the model was validated by the comparison between the simulated and measured outlet water temperature and also the ground temperature variations. The simulation results showed that the ground temperature would rise up by 10.5 °C and the ASPF value would decrease by 12.82% after 20-years running. As a remedy measure, DHW system was supposed to be operated in the following years. The simulation of 20-years running showed that, both the lower ground temperature and higher ASPF value of system would be obtained.

3 Schemes to Alleviate the Underground Heat Accumulation of the Ground Source Heat Pump

In order to dissipate the surplus heat accumulated under the ground, a scheme that the cooling tower be operated in transitional season is proposed in this section. The scheme can also be applied to the conventional GSHP system, in which a cooling tower needs to be connected to the GHE to form a fluid circulation for heat exchange. As an extension, the other HGSHS system configured with chiller cooling system is also proposed to temper the heat accumulation under the ground. With TRNSYS software, the feasibilities of the two schemes are investigated.

3.1 Design and Operation Parameter Optimization Analysis of GSHP System Assisted with Cooling Tower

The previous analysis demonstrates the fact that there is a serious thermal imbalance between the cooling and heating loads for the studied GSHP system. The ground temperature will increase greatly if the GSHP system keeps running without any auxiliary cooling measures, and the performance of GSHP system will be deteriorated, which has been predicted in the previous section. Therefore, in the following simulation, the GSHP system is considered to be improved by adding cooling tower for auxiliary heat dissipating.

3.1.1 Optimization of Design Parameters

Because the GSHP system has been operated for more than two years and the BHE length was designed according to the cooling load of the system initially, the cooling tower should be attached to the system in series connection mode. In the renovation, a closed cooling tower is adopted to prevent the circulating water from pollution. Figure 16 is the HGSHP system assisted with cooling tower in series connection, which is improved from the GSHP system model that has been verified.

The auxiliary cooling ratio (ACR) can be regulated by changing the diversion ratio of the diverter in Fig. 16. In order to obtain the optimal ACR of the HGSHP system, different diversion ratios are defined for comparison, i.e., $ACR = 10, 30, 50, 70, 90\%$, respectively. Besides, in order to analyze the optimal renovation time in the whole simulation period of 20 years, the cooling tower is supposed to be attached to the system at different stages, including the third year (initial stage), the seventh year (early stage), the eleventh year (interim stage) and the fifteenth year (later stage).

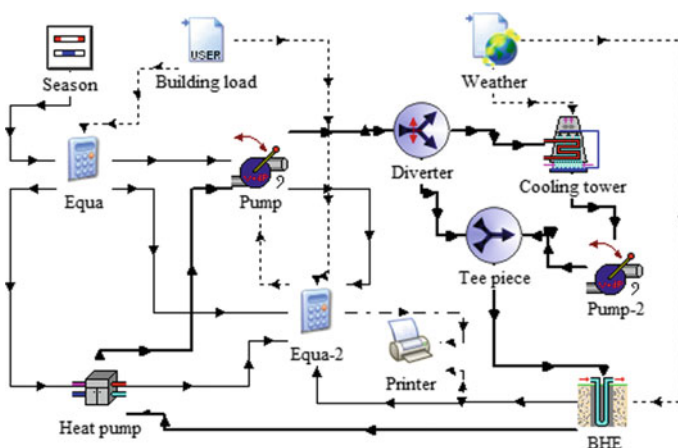


Fig. 16 HGSHP system assisted with cooling tower

Table 8 Designed parameters of auxiliary cooling system

Auxiliary cooling ratio (%)	Flow rate (m ³ /h)	Fan power (kW)	Spray pump power (kW)	Cooling pump power (kW)
10	14	0.9	0.75	1.5
30	42	2.6	1.5	5.5
50	70	3.6	2.2	15
70	99	4.5	2.2	15
90	127	5.2	4	22

The designed parameters of the auxiliary cooling system under different ACRs are shown in Table 8.

The situation for which the cooling tower being operated in the third year is analyzed as an example, Fig. 17 shows the energy consumptions of the heat pump unit and system under different ACRs. In the figure, 0% represents the operating mode of conventional GSHP system. It can be seen that, if the GSHP system is operated for 20 years without cooling tower, both the energy consumptions of heat pump unit and system increase linearly year by year. Once the cooling tower is attached and operated (ACR > 0%), the energy consumption of heat pump unit will be reduced obviously. However, only when the auxiliary cooling ratio is more than 10%, the yearly increasing trend of heat pump power can be reversed. Furthermore, the annual energy consumption of heat pump unit decreases obviously with the increase of ACR. Therefore, the affiliation of cooling tower could effectively reduce the heat that dissipated into the ground, and also alleviate the thermal imbalance under the ground. The higher auxiliary cooling ratio could maintain a lower ground temperature, so that the energy consumption of heat pump unit could be effectively reduced, since there is a mutual coupling relationship between the ground temperature and the energy consumption of heat pump unit.

Figure 17b is the energy consumption of heat pump system during 20 years' operation period. It can be seen that the variation trend of system energy consumption is different from that of heat pump unit. This is due to the fact that operation of cooling tower will consume energy. That extra energy consumption of cooling system offsets part of the energy saving of heat pump unit, which eventually leads to the increase of energy consumption of heat pump system. This implies that there exists an optimal ACR under which the system energy consumption would be the lowest.

Figure 18 is the 20 years' total energy consumption of heat pump system under different auxiliary cooling ratio and different operation time. It can be seen from Fig. 18 that, the system total energy consumption is the lowest when the cooling tower is operated in the third year at the auxiliary cooling ratio of 30%. In order to further reduce the system energy consumption, two control strategies are applied to the HGSHS system. And then, the simulation is carried out to explore the optimal control strategy and parameters.

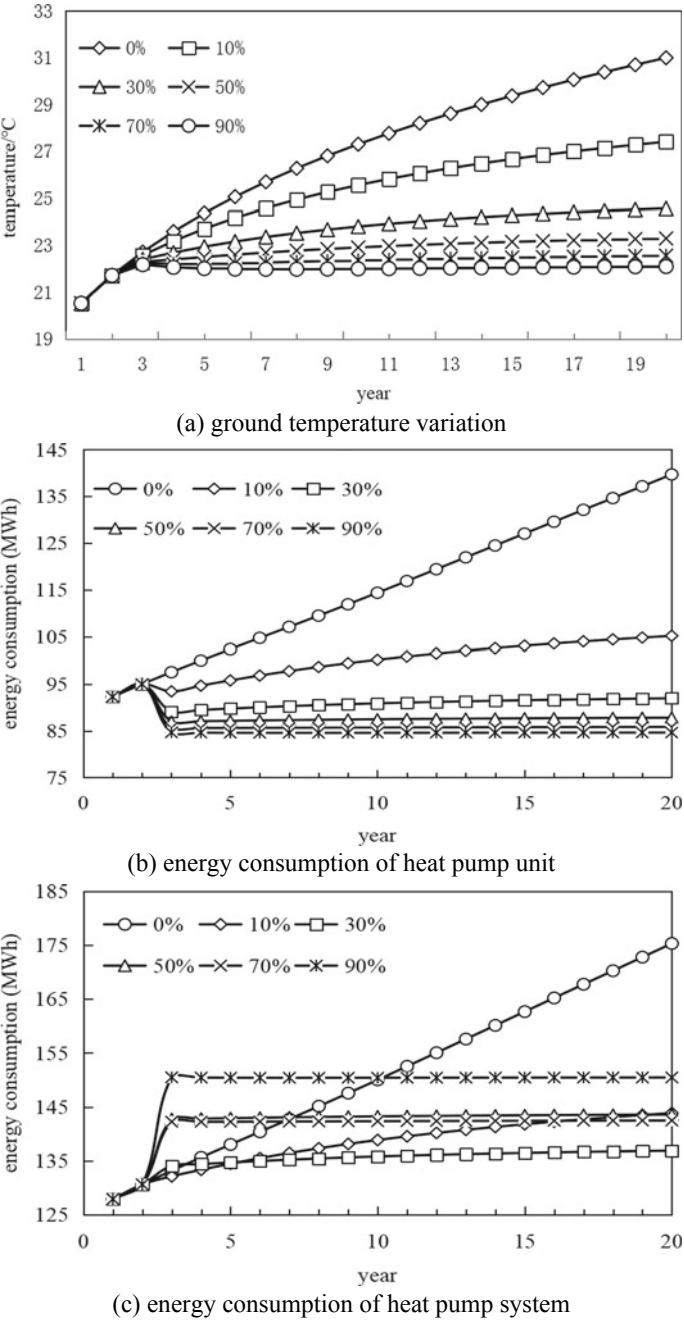


Fig. 17 Variation of energy consumption when the cooling tower is operated in the third year ($\times 10^4$ kWh)

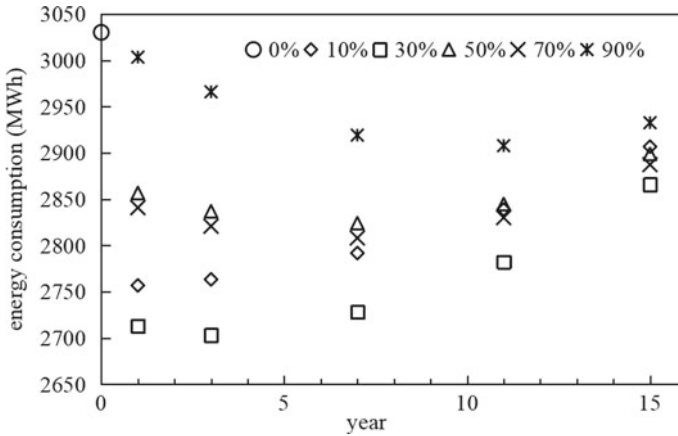


Fig. 18 The total energy consumption of heat pump system

3.1.2 Optimization of Operation Control Parameters

Three control strategies are usually applied in the HGSHP system, i.e., temperature difference control strategy, constant temperature control strategy and fixed running time control strategy [33]. Since the fixed running time control strategy is easily affected by human factors, the following paper only studies the former two control strategies. Basing on the optimal ACR of 30%, the simulation of the HGSHP with different control strategies are conducted in the following paper.

(1) Temperature difference control strategy

The temperature difference control strategy is to start cooling tower when the difference between the cooling water temperature entering heat pump and the ambient dry-bulb (or wet-bulb) temperature exceeds a fixed value. Different control temperatures (ΔT) are set for simulation. It has been found from the previous simulation that, for the adopted cooling tower, the cooling water temperature decrement that can be cooled down by cooling tower is less than 1 °C when ΔT is less than 4 °C. So the set value of ΔT for cooling tower to start up should not be less than 4 °C. In the following simulation, the values of ΔT are set as 0, 4, 6, 8, 10, 12 °C, respectively. In which, the mode of $\Delta T = 0$ °C means that the control strategy does not work.

Figure 19 is the comparison of the total energy consumptions of the heat pump unit and system under different control parameters. It shows that the difference between the energy consumption of heat pump unit and that of system decreases when ΔT increases. This is because both the running time and energy consumption of cooling tower drop down for this situation. While the shorter running time of cooling tower leads to the higher energy consumption of heat pump unit. So the too little running time of cooling tower is not preferred. However, the overmuch running time of cooling tower is also not advisable for that it may enlarge the HGSHP system energy consumption. It can be seen from Fig. 19 that the total energy consumption

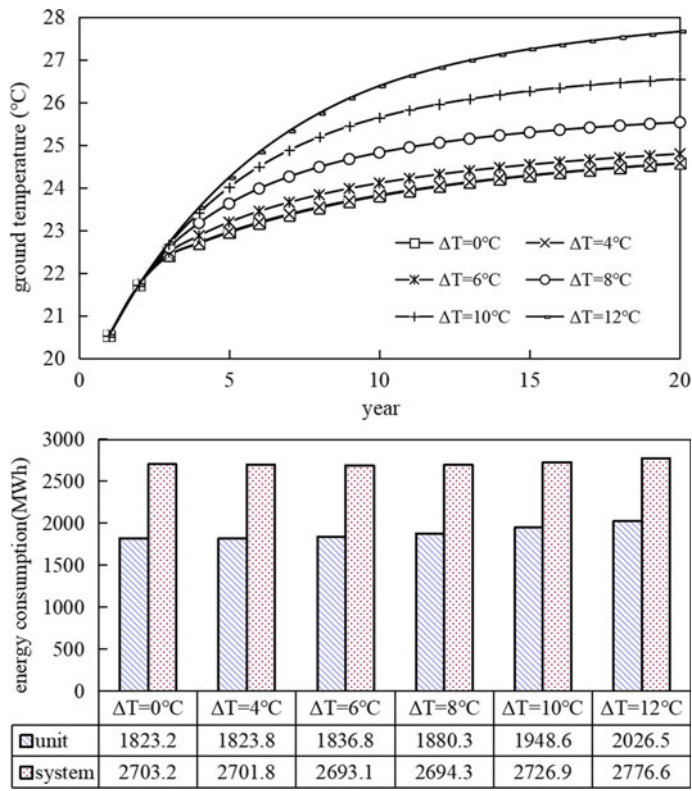


Fig. 19 Comparison of ground temperature and energy consumption under different control parameters

of HGSHS system is the lowest when the cooling tower is operated at the mode of $\Delta T = 6^{\circ}\text{C}$. This indicates that there is a good balance between the energy consumption decline of heat pump unit and the energy consumption increment of cooling system at $\Delta T = 6^{\circ}\text{C}$, which can be deemed as the optimal control parameter for temperature difference control strategy.

(2) Constant-temperature control strategy

The so-called constant-temperature control strategy is that when the outlet water temperature of the BHE is higher than the upper fixed temperature (T_u), the cooling tower is started up for auxiliary heat dissipating, the cooling tower is shut down when the outlet water temperature is lower than the lower fixed temperature (T_l). According to reference [34], the highest outlet cooling water temperature of BHE is recommended to be less than 33°C in cooling season, so the maximum value of T_u was set as 32°C . In order to prevent the frequent starting up of auxiliary cooling system, the temperature difference between T_u and T_l should not be less than 2°C .

Table 9 The ground temperature in the 20th year under different control parameters(°C)

<i>Tl</i>	30 °C	29 °C	28 °C	27 °C	26 °C	25 °C	24 °C	23 °C	22 °C	21 °C	20 °C
<i>Tu</i>											
32 °C	26.48	26.22	26.13	26.01	25.61	25.33	25.16	24.95	24.93	24.73	24.61
30 °C			25.58	25.42	25.32	25.13	25.03	24.87	24.85	24.72	24.59
28 °C					24.98	24.92	24.83	24.74	24.66	24.63	24.58
26 °C							24.68	24.65	24.60	24.59	24.57
24 °C									24.57	24.57	24.56
22 °C											24.56

Table 10 The total power consumption of the system under different control parameters (MWh)

<i>Tc</i>	30 °C	29 °C	28 °C	27 °C	26 °C	25 °C	24 °C	23 °C	22 °C	21 °C	20 °C
<i>To</i>											
32 °C	2711.8	2704.0	2703.4	2703.2	2700.2	2696.6	2695.3	2696.1	2696.6	2698.8	2701.1
30 °C			2690.0	2690.3	2691.3	2692.3	2693.1	2695.7	2696.9	2698.6	2701.3
28 °C					2691.6	2693.0	2694.9	2697.5	2700.0	2701.0	2701.8
26 °C							2698.3	2700.0	2701.6	2702.3	2703.0
24 °C									2702.7	2703.0	2703.2
22 °C											2703.2

Besides, T_1 should be higher than the initial ground temperature of 20 °C, or else, the control strategy will not work.

Table 10 is the 20-years’ energy consumption of the HGSHp system under different control parameters. As can be seen from the table that the total system energy consumption is the lowest when the control parameter is $T_u/T_1 = 30/28$ °C, which can be defined as the optimal control parameters of this strategy. It can also be seen that the total energy consumption of the system at the mode of $T_u/T_1 = 22/20$ °C is the same as that without control strategy, which means the control strategy does not work at this condition.

3.1.3 Summary

In the cooling dominated areas, the long term running of GSHP system will lead to the ground temperature increases gradually, which will conversely reduce the system performance. In order to avoid or solve the performance degradation problem of conventional GSHP system, the section intend to renovate the studied GSHP system by adding a cooling tower for auxiliary heat dissipating. By simulating the 20 years’ running performance of the HGSHp system assisted with cooling tower, the following conclusions are derived: (1) Auxiliary cooling ratio of 30%, together with the operation of cooling tower since the third year has been found to be the most energy-saving design scheme; (2) $\Delta T = 6$ °C is the optimal control parameters of

the temperature difference control strategy, while $T_u/T_1 = 30/28$ °C is the optimal control parameters of the constant temperature control strategy.

3.2 Ground Temperature Active Restoration Scheme

The so-called “active recovery of ground temperature” is to use additional power to raise or lower the temperature of rock-soil body. For the problem that the ground temperature of the ground source heat pump system in Hot Summer and Cold Winter Zone increases year by year, only the water circulation system of the buried heat exchanger can be opened in transition season to make the cooling water absorb heat from the ground and then release the heat into the air through the cooling tower. Due to the low outdoor temperature in the transition season, the air conditioning system is idle. Therefore, the heat accumulated in the underground rock and soil can be released by circulating the cooling tower and the fluid in the buried pipe at this stage.

3.2.1 System Configuration

Two HGSHP systems with different configurations are established in TRNSYS 16 as shown in Fig. 20. One is that cooling tower and GHE are connected in parallel configuration, which is defined as configuration *A*; the other is that cooling tower is connected to GHE in serial configuration, which is defined as configuration *B*. It should be noted that, configuration *A* is the common HGSHP system as depicted in the previous section, while configuration *B* is a conventional GSHP system, to which a cooling tower is connected for heat dissipating purpose. In configuration *A*, GHE is designed according to the heating load, and cooling tower is designed according to the load difference between heating and cooling. In configuration *B*, GHE is designed according to the cooling load, and the cooling tower capacity should be equivalent to that of GHE to ensure the optimum flow rate of the fluid in GHE. The designed parameters of the two configurations are shown in Table 11.

In the proposed scheme, the cooling tower in configuration *A* is operated not only in transitional season but also in cooling season, while the cooling tower of configuration *B* is operated only in transitional season. The simulation period is 20 years.

3.2.2 System Performance Study

In transitional season, the air conditioning systems usually do not run because the ambient temperature is comfortable. The cooling tower efficiency in transitional season is also higher than that in cooling season for this reason. Therefore, the scheme that cooling tower be operated in transitional season to dissipate the heat that has been accumulated under the ground seems to be feasible. However, the problem is whether

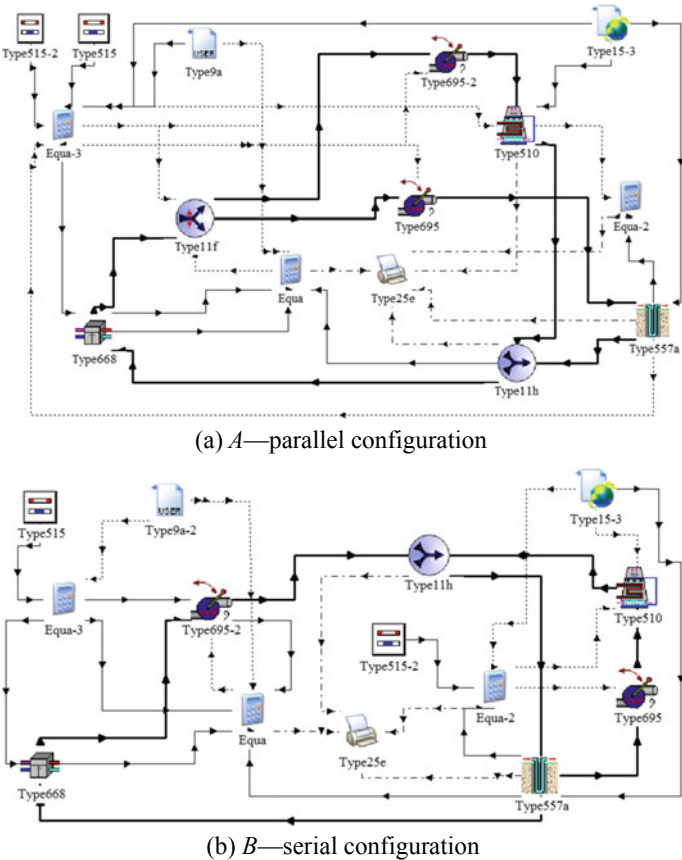


Fig. 20 HGSHS systems with different configurations

Table 11 Designed parameters of HGSHS system

Configuration	Heat pump unit	GHE system	Cooling tower system
<i>A</i> -parallel	flow rate of 150 m ³ /h at source side	50 boreholes of 100 m, Pump 12 kW	60 m ³ /h, cooling tower 5.1 kW
	flow rate of 129 m ³ /h at load side		Pump 12 kW
<i>B</i> -serial		90 boreholes of 100 m, Pump 22 kW	60 m ³ /h, cooling tower 5.1 kW Pump 12 kW

cooling tower can effectively work or not. Since in theory, air wet-bulb temperature is the lowest temperature that cooling water can be cooled to. But the actual cooling water that be cooled is usually higher than air wet-bulb temperature. The difference between cooling water temperature and air wet-bulb temperature is defined as Δt_1 ; In order to prevent the cooling water in the GHE from pollution, closed cooling tower

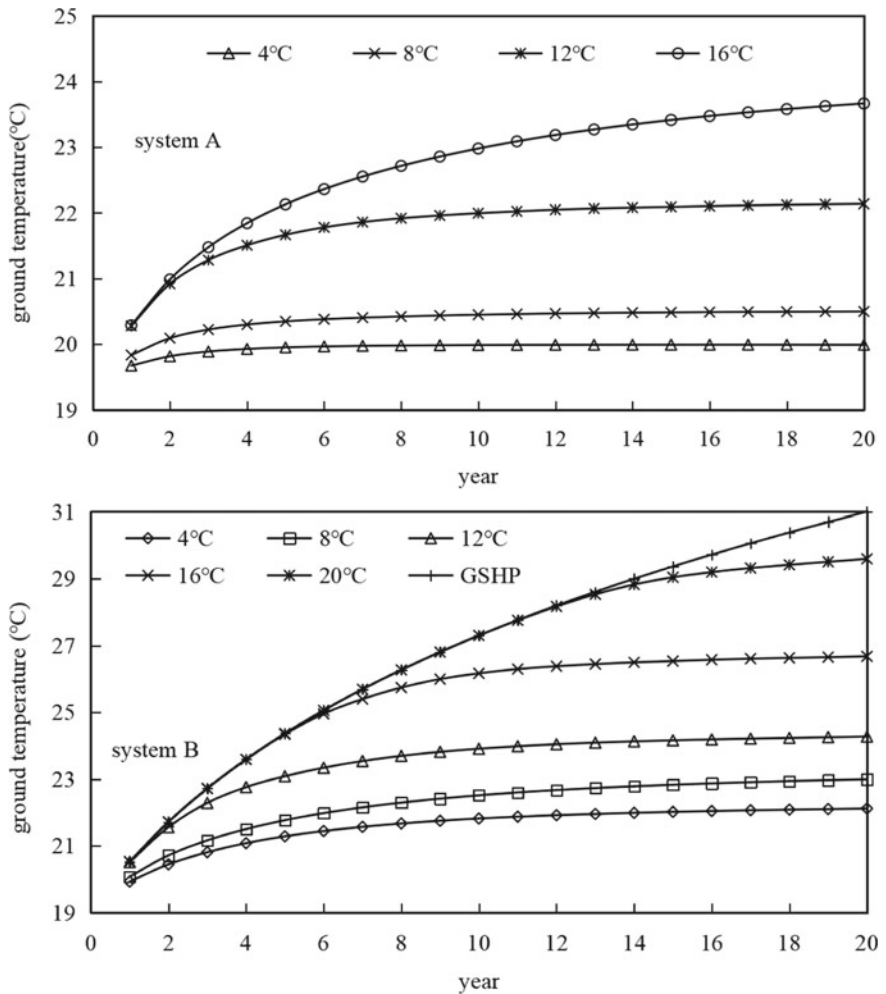
is usually used. The temperature difference between the cooling water in the GHE and that in the closed cooling tower is defined as Δt_2 ; The temperature difference between the cooling water in the GHE and the ground is defined as Δt_3 ; The difference between the air wet-bulb temperature and the ground temperature is defined as Δt . Therefore, the condition for the cooling tower to work effectively is that $\Delta t > \Delta t_1 + \Delta t_2 + \Delta t_3$. Or else, the cooling water cannot be effectively cooled by cooling tower. Within the service life of the GSHP systems, the air wet-bulb temperature changes periodically while the ground temperature increases continuously for the load accumulation. As shown, the temperature difference Δt is always changing.

Δt can be set as the control parameter for cooling tower to start up. It has been found by simulation that, under the system configuration of A and B, the cooling water temperature decrement that can be cooled down by cooling tower is more than 1 °C when Δt is not less than 4 °C. So, the set value of Δt for cooling tower to start up should not be less than 4 °C. On the other hand, when Δt is more than 20 °C (A) and 24 °C (B), respectively. It has been found that, cooling tower would not be started during 20 years' running time for the two systems. So, the set value of Δt for cooling tower to start up should not be more than 16 °C for A and 20 °C for B. In the following sections, the value of Δt is set as, 8, 12, 16 and 20 °C, respectively, and the system performance of A and B are studied under these set values of Δt . In the following analysis, 'GSHP' for B means the situation that cooling tower is not operated in the 20 years' period.

Besides, it should be noted that, the heat that accumulated under the ground in summer is beneficial to the system running in winter, so the cooling tower should not be operated in autumn, but only in spring. In this study, the cooling season is from May 16th to September 15th while the heating season is from November 15th to February 15th, so the possible running time of cooling tower in transitional season is in the period from February 16th to May 15th.

Figure 21 is the variations of the ground temperature (a), ASPF of heat pump system (b) in the 20 years running period. It can be found that, the smaller the set value of Δt is, the smaller the ground temperature increment is. For configuration A, because some of the condensing heat is dissipated by the cooling tower in cooling season, the ground temperature increment is small even if cooling tower is not operated in transitional season. However, for configuration B, because its cooling tower is not operated in cooling season, when $\Delta t = 20$ °C, the ground temperature increment is remarkable. When the cooling tower is operated in transitional season, the ground temperature increment gets down obviously.

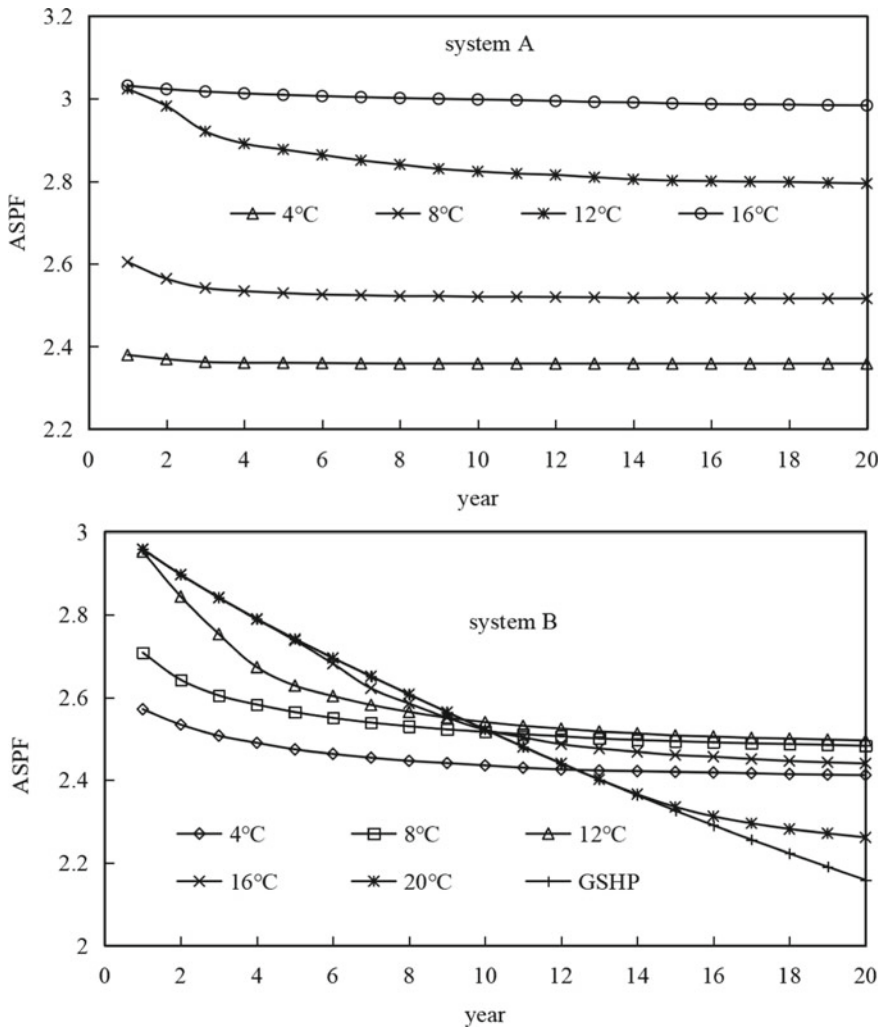
Ground temperature is an important factor that affecting the performance of heat pump unit. With the increase of the ground temperature, the outlet water temperature of GHE increases year by year. This temperature change is good for the heating performance of the heat pump unit, but it is not conducive to the cooling performance of the heat pump unit. In cooling dominated areas, however, the accumulated cooling load is far more than the accumulated heating load in a whole year. So the total power consumption of the heat pump unit increases year by year, which definitely bring down the ASPF of heat pump system.



(a) Variation of the average ground temperature

Fig. 21 Simulation results

The lower increment of the ground temperature is favored in sustainable development and utilization perspective, while the lower power consumption of the GSHP system is preferred in energy conservation view. However, it can be found from the above analyses that, the two considerations cannot be met at the same time. Although the lower set value of Δt can effectively reduce the ground temperature increment, the system performance decreases remarkably. Fig. 21 shows that the ground temperature increment and system performance are moderate when $\Delta t = 8\text{ }^{\circ}\text{C}$ and $\Delta t = 12\text{ }^{\circ}\text{C}$. Therefore, the optimum set value of Δt should be between 8 and 12 $^{\circ}\text{C}$.



(b) Variation of the HGSHP system ASPF

Fig. 21 (continued)

Figure 22 is the total system power consumption in 20 years running period. It can be seen that, when $\Delta t \leq 8^\circ\text{C}$, power consumption of configuration A is more than that of configuration B; when $\Delta t \geq 12^\circ\text{C}$, power consumption of configuration B is more than that of configuration A. Therefore, at the same set value of Δt , when Δt is lower than 8°C , configuration B is better than configuration A in energy conservation perspective. On the contrary, when Δt is higher than 12°C , configuration A performs better than configuration B. Correlating with the previous conclusions that $8\sim 12^\circ\text{C}$ is the optimum set value range, Therefore, from the perspective of system energy

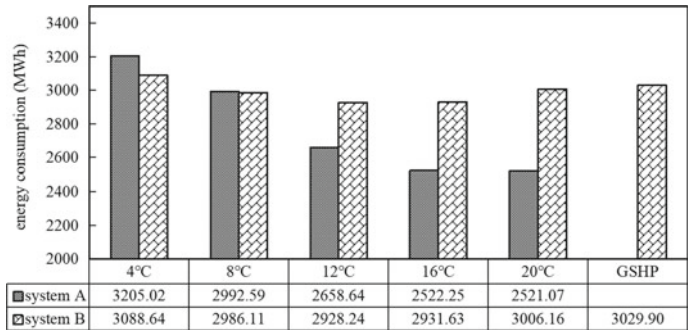


Fig. 22 Summary of the HGSHP system total power consumption

saving, it is not necessary for system A to implement transitional season operation of cooling tower, $\Delta t = 12\text{ }^{\circ}\text{C}$ for configuration B are the optimum system mode.

An existing problem can be found from the previous analysis, i.e., although the lower set value of Δt can effectively reduce the unit power consumption, the running time of cooling tower also increases, which leads to the increase of system power consumption. This demonstrates the fact that, the decrement of the unit power consumption is less than the increment of the cooling tower system power consumption that caused by the value change of Δt . Firstly, this is due to the increment of the cooling tower running time in transitional season. Besides, the problem may be derived by the system configuration. There is only one heat pump unit is adopted in both configuration A and B, and the unit capacity is designed according to the cooling load, which is far more than the actual heating load. Therefore, in heating season, the heat pump unit mostly works at partial load. As well known, the coefficient of performance (COP) of the heat pump unit is relatively low at partial load. As a result, the system performance is poor in heating season. In the following section, a HGSHP system that configured with chiller cooling system is proposed to deal with the problem.

3.3 HGSHP System Assisted with Chiller

3.3.1 System Configuration

This HGSHP system is composed of two relatively independent systems, i.e., one is heat pump configured with GHE system; the other is chiller configured with cooling tower system. In which, the former system is designed according to the heating load while the latter system is designed according to the load difference between heating and cooling. In heating season, the heat pump system is operated for heating the building. In cooling season, when the air-conditioning load is small, one of the systems is operated for cooling; when the load gets heavier, the two systems are

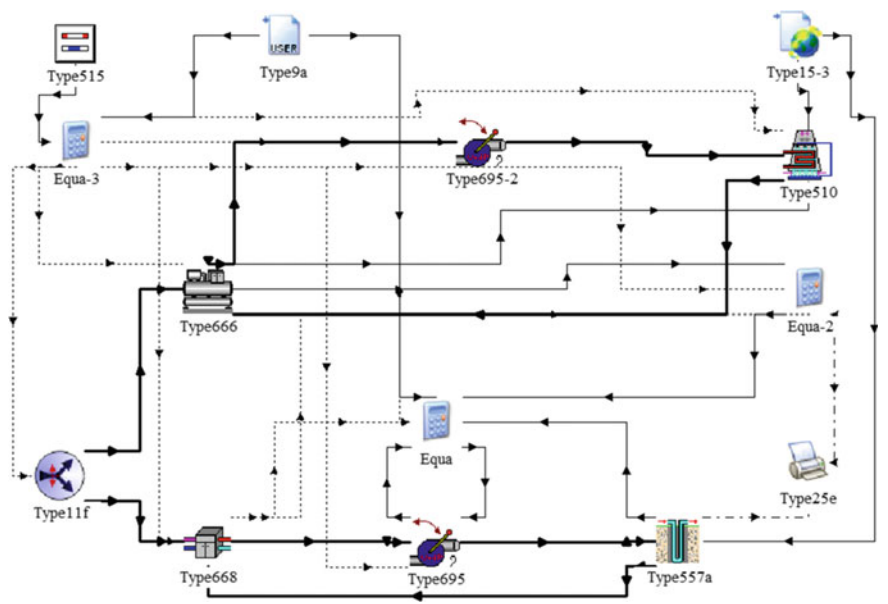


Fig. 23 HGSHP system assisted with chiller

Table 12 System equipment configurations

Unit	Rated capacity	Rated power	Circulating pump	Cooling system
Chiller	349 kW	77 kW	15 kW	Closed cooling tower, 5.8 kW
Heat pump	277/333 kW	51/66 kW	12 kW	50 boreholes of 100 m

operated together for cooling purpose. This HGSHP system can not only ensure enough recovery period of the underground temperature, but also helps to stably provide the required cooling capacity at high-load conditions [15]. The established system with TRNSYS software is shown in Fig. 23, and the system configurations are shown in Table 12.

3.3.2 System Performance Study

AS discussed before, when the load is small, either the chiller or heat pump system can be operated for cooling purpose. Therefore, two operation strategies are proposed for this configuration. One is that chiller system is preferentially operated when the cooling load is small, which is defined as *C-H* strategy. The other is that heat pump system is preferentially operated when cooling load is small, which is defined as *H-C* strategy. The system performances with the two strategies, and also that of GSHP, are shown in Fig. 24. It can be seen that, the ground temperature increments of *C-H*

is the smallest, while that of *H-C* is the *highest*. The increase of ground temperature will cause the decrease of the system performance. In order to assess the variation of the system performance, the annual system performance factor (ASPF) defined in chap. 2.3.5 is used.

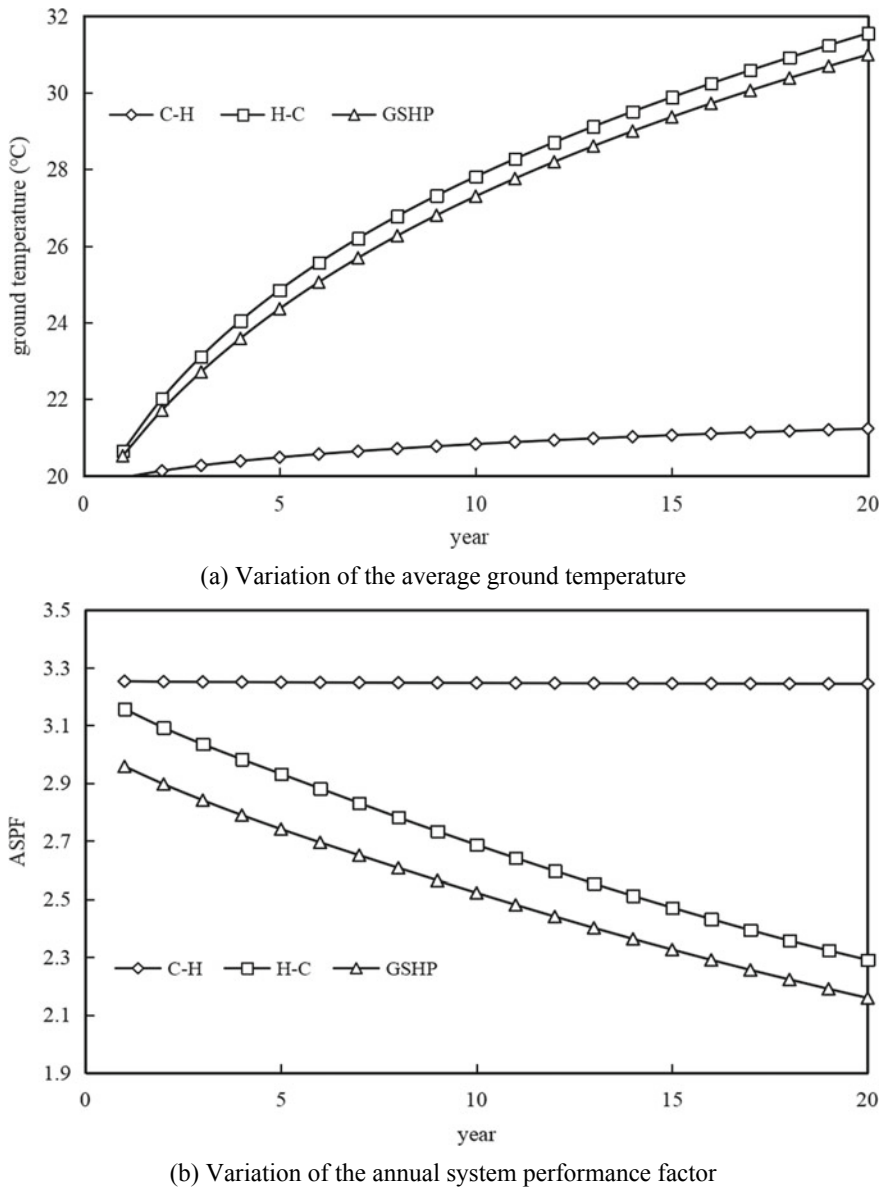


Fig. 24 Simulation results

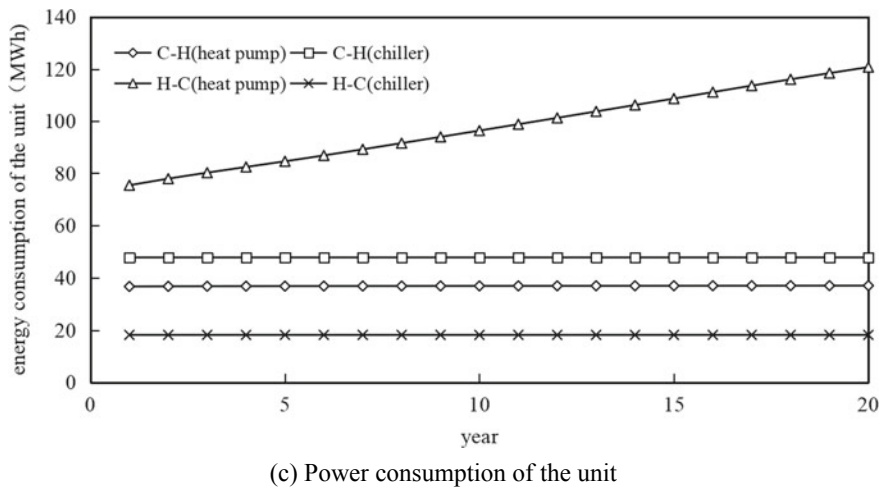


Fig. 24 (continued)

It can be seen from Fig. 24b that, with the elapse of running time, the value of ASPF decreases year by year for all the three systems. In which, the decrement of *H-C* is the most, while the decrement of *C-H* is the least. Figure 24c is the unit power consumption of the two systems. It can be found that only the heat pump unit consumption is increasing year by year, which is caused by the change of ground temperature.

Figure 25 is the total power consumption of the three different system configurations or control strategies in the simulation period.

It can be concluded from the above analysis that, the operation strategy of *C-H* is better than *H-C* in both the ground temperature increment and the energy conservation perspectives. The reason is that the low cooling load period is mainly at

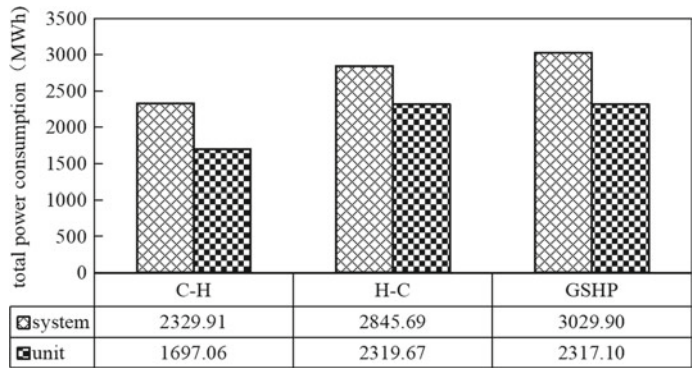


Fig. 25 Summary of power consumption

the beginning and the end of the cooling season. The ambient temperature is closer to the ground temperature in this period compared with that in the high cooling load period. Therefore, the cooling tower efficiency in the low cooling load period is higher than that in the high cooling load period. However, the ground temperature is relatively stable in a specific cooling season, so the heat pump efficiency keeps almost constant in the whole cooling season. Consequently, the chiller system should be operated at first in the low cooling load period, and then the heat pump system should be operated when the cooling load cannot be met only by the chiller system.

It can be seen in Fig. 25 that the unit energy consumption is the main component of the system energy consumption, and the unit energy consumption basically determines the level of the system energy consumption. Since the unit load of each scheme is consistent, the energy consumption of the unit depends on its energy efficiency ratio. Therefore, it is necessary to analyze the energy efficiency of the unit. Figure 26 shows the comparison of the unit energy efficiency ratios of the two operation schemes of the cooling auxiliary system and the conventional ground source heat pump system (GSHP), in which the unit energy efficiency ratios of the first year and the 20th year of operation of the system are compared respectively.

Figure 26a shows the comparison between the conventional heat pump system strategy (GSHP) and the “heat pump chiller” (H-C) strategy. It can be seen that in the first year when the system has just been put into operation, the unit energy efficiency ratio of the conventional heat pump system strategy is higher in both the cooling season and the heating season, mainly because the ground temperature has not changed greatly at this time, and the unit performance is relatively stable. In the 20th year of operation, the heat pump heating energy efficiency ratio of the two strategies has increased slightly, while the refrigeration energy efficiency ratio of the unit has decreased significantly, because the ground temperature under the operation of the two strategies has risen to more than 30 °C. Since the EER of the refrigerator is not affected by the ground temperature, it is only affected by the outdoor meteorological conditions. The simulation uses the meteorological data of typical meteorological years, and its annual fluctuation range is consistent, so the EER of the refrigerator will not change every year. Figure 26b shows the comparison of the unit energy efficiency ratio of the “chiller heat pump” (C-H) strategy and the conventional ground source heat pump system (GSHP). It can be seen that under this operation strategy, the unit energy efficiency ratio has not changed significantly in the first year and the 20th year, because the ground temperature has increased very little under the “chiller heat” operation strategy.

The performance curve coefficient of the unit can be customized by users in the heat pump unit and chiller module in TRNSYS. Therefore, the performance curve in the actual unit sample is used for the simulation of the heat pump unit. Since the ground source heat pump system studied in this paper does not use the chiller in practice, the performance curve of the chiller in this paper is the performance curve of the software. Figure 27 shows the comparison of the refrigeration energy efficiency ratio of the main engine of the auxiliary cooling system and the conventional ground source heat pump system (GSHP) under different load side/source side inlet water temperatures. In the figure, heat pump 1 represents the heat pump unit in the

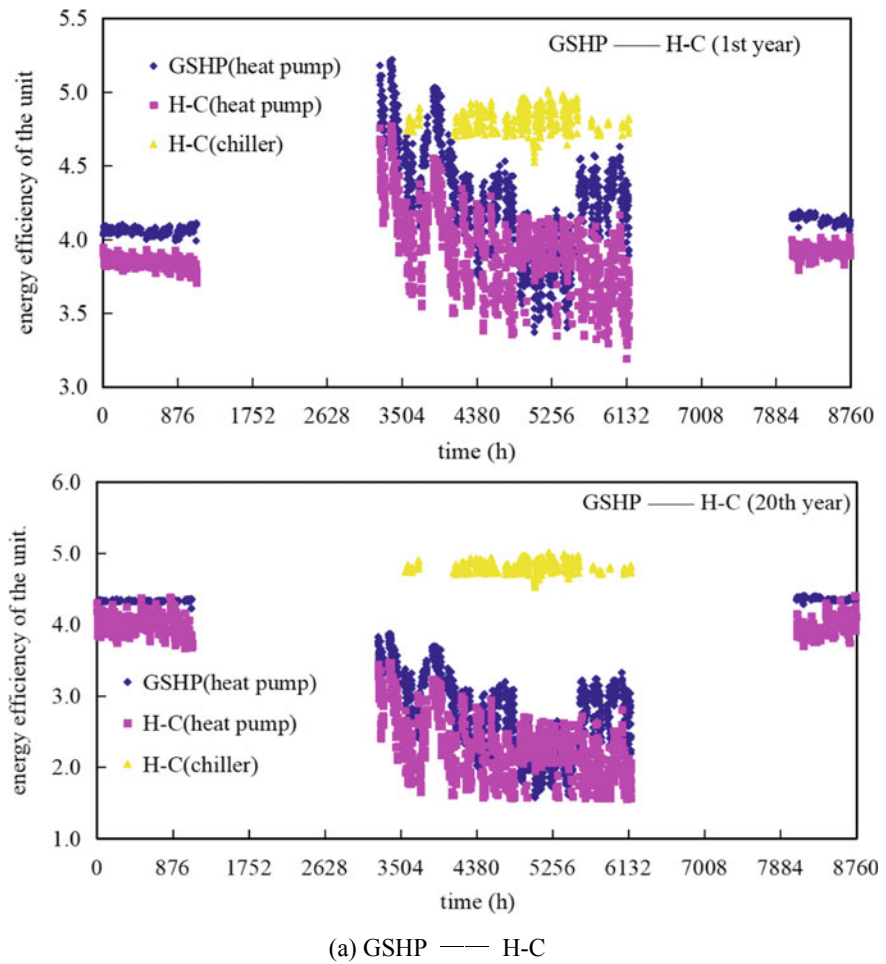


Fig. 26 Comparison with unit efficient of GSHP

conventional ground source heat pump system, and heat pump 2 represents the heat pump unit in the cooling auxiliary ground source heat pump system. Although the performance curve ratio of the heat pump unit in the GSHP system and the heat pump unit in the auxiliary cooling system is the same, the rated energy efficiency ratio is relatively high because the cooling capacity of the heat pump unit in the GSHP system is greater than that of the heat pump unit in the auxiliary cooling system.

As shown in Fig. 27, under the same unit inlet water temperature, the energy efficiency ratio of the heat pump in the GSHP system is always higher than that of the heat pump in the cooling auxiliary system. The energy efficiency ratio under the heating condition of the unit is not listed here, but the relationship between the heating energy efficiency ratios of the two units is the same. Similarly, as can be

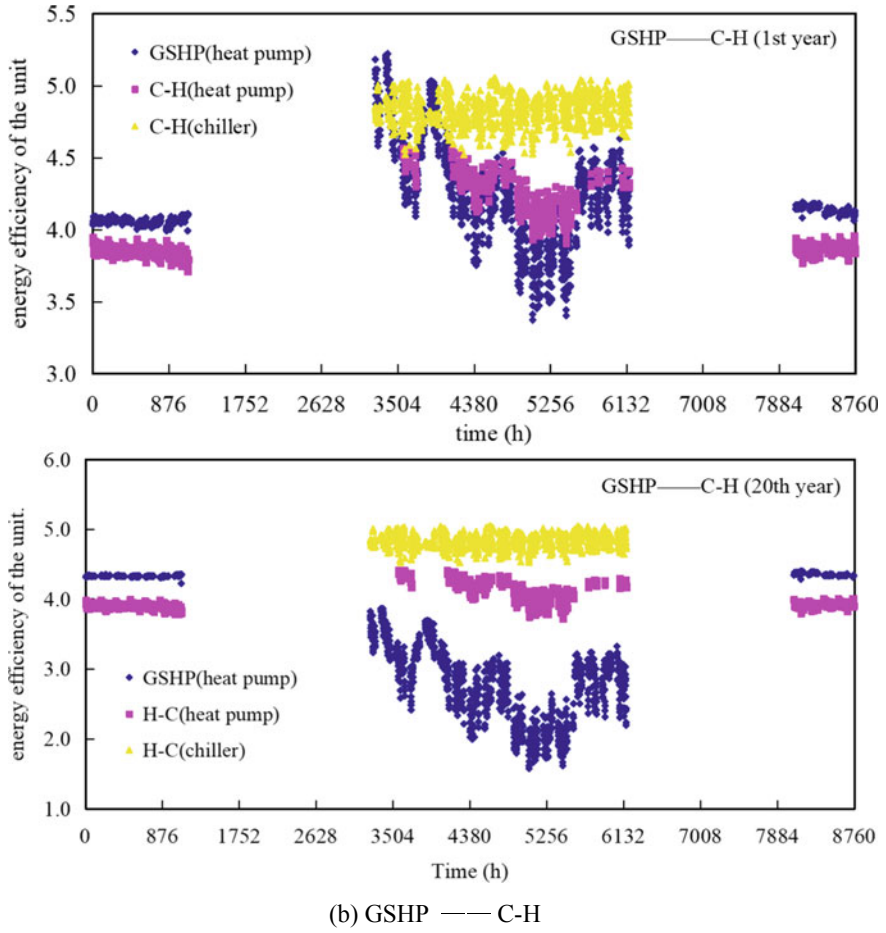


Fig. 26 (continued)

seen from Fig. 27, the EER of the refrigerator is always higher than that of the heat pump, except for some working conditions where the water inlet temperature at the source side is 20 °C. However, when the water inlet temperature at the source side is 20 °C, and the reasonable water inlet temperature at the load side (<13 °C), the energy efficiency ratio of the refrigerator is also higher than that of the heat pump. This explains the relationship between the host energy efficiency ratios of the three systems in Fig. 26.

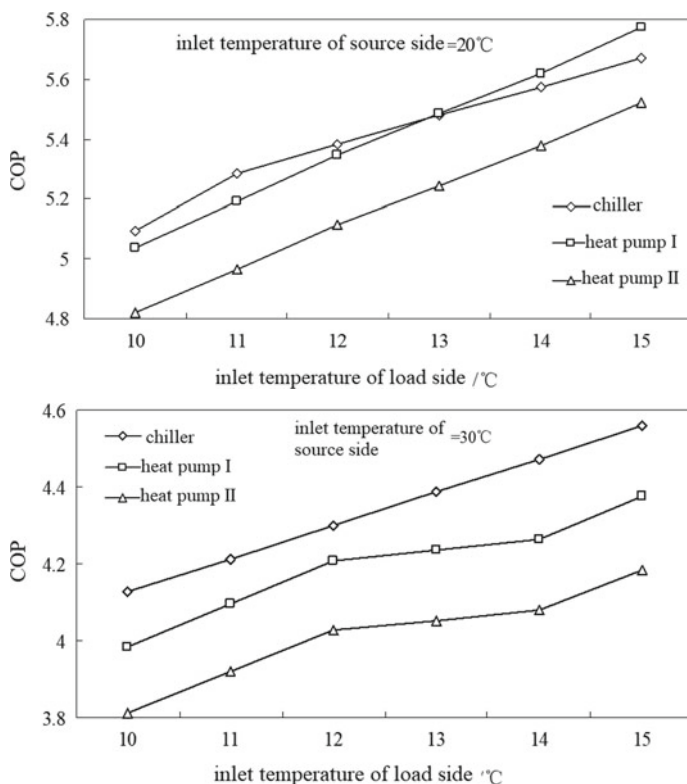


Fig. 27 Comparison of unit energy efficiency ratio

3.4 Summary

Firstly, the auxiliary cooling strategy of the cooling tower is applied to the system, and then the operation strategy of active ground temperature recovery for the transition season operation of the cooling tower and the configuration strategy of the cooling assisted hybrid ground source heat pump system are proposed. The operation effects of the three strategies are simulated and analyzed by TRNSYS software, and the main conclusions are as follows:

- (1) Through analyzing the auxiliary cooling of the cooling tower of the system, it is found that when the cooling tower is started in the third year and the auxiliary cooling ratio is 30%, and the total energy consumption of the system for 20 years of operation is the lowest. On the basis of this design optimization, if the temperature difference control strategy is adopted for the opening of the cooling tower, then $\Delta T = 6^\circ\text{C}$ is the best temperature difference control parameter; If the operation strategy of constant temperature control is adopted, T_o/T_c of $30/28^\circ\text{C}$ is the best control parameter. In addition, the constant temperature

- control strategy is more energy-saving than the temperature difference control strategy.
- (2) Aiming at the problem of underground heat accumulation in the system, a strategy of active ground temperature recovery in the transition season of the cooling tower is proposed, and the effectiveness of the scheme in ground temperature recovery is verified by simulation analysis. Furthermore, the simulation analysis of the proposed chiller assisted hybrid ground source heat pump system shows that it is more energy-saving if the chiller is preferentially turned on at low load.

References

1. Omer AM (2008) Ground-source heat pumps systems and applications. *Renew Sustain Energy* 12:344–371
2. Blum P, Campillo G, Munch W, Kolbel T (2010) CO₂ savings of ground source heat pump systems—a regional analysis. *Renew Energy* 35:122–127
3. Zhai X, Qu M, Yu X, Yang Y, Wang R (2011) A review for the applications and integrated approaches of ground-coupled heat pump systems. *Renew Sustain Energy Rev* 15:3133–3140
4. Self SJ, Reddy BV, Rosen MA (2013) Geothermal heat pump systems: status review and comparison with other heating options. *Appl Energy* 101:341–348
5. Lee CK, Lam HN (2012) A modified multi-ground-layer model for borehole ground heat exchangers with an inhomogeneous groundwater flow. *Energy* 47:378–387
6. Zheng XH, Zhang L, Liang WQ, Qian H (2013) The geothermal field analysis of cooling and heating load imbalance for GSHP. *Appl Mech Mater* 281:533–536
7. Han JW, Dong L (2013) Study on the environmental impacts of GSHP. *Sichuan Build Sci* 39:331–333 (in Chinese)
8. Kavanaugh S, Rafferty K (1997) Ground-source heat pumps: design of geothermal systems for commercial and institutional Buildings. ASHRAE, Atlanta
9. Qi Z, Gao Q, Liu Y, Yan Y, Spitler J (2014) Status and development of hybrid energy systems from hybrid ground source heat pump in china and other countries. *Renew Sustain Energy Rev* 29:37–51
10. Cui W, Zhou S, Liu X (2015) Optimization of design and operation parameters for hybrid ground-source heat pump assisted with cooling tower. *Energy Build* 99:253–262
11. Man Y, Yang H, Fang Z (2008) Study on hybrid ground-coupled heat pump systems. *Energy Build* 40:2028–2036
12. Hackel S, Pertzborn A (2011) Effective design and operation of hybrid ground-source heat pumps: three case studies. *Energy Build* 43:3497–3504
13. Sagia Z, Rakopoulos C, Kakaras E (2012) Cooling dominated hybrid ground source heat pump system application. *Appl Energy* 94:41–47
14. Sayyadi H, Nejatolahi M (2011) Thermodynamic and thermoeconomic optimization of a cooling tower-assisted ground source heat pump. *Geothermics* 40:221–232
15. Jeon J, Lee S, Hong D, Kim Y (2010) Performance evaluation and modeling of a hybrid cooling system combining a screw water chiller with a ground source heat pump in a building. *Energy* 35:2006–2012
16. Xu YJ (2011) The applications of hybrid ground source heat pump system and study on operation control strategies in Chongqing. Chongqing university
17. Huang S, Ma Z, Wang F (2015) A multi-objective design optimization strategy for vertical ground heat exchangers. *Energy Build* 87:233–242

18. Chen X, Lu L, Yang H (2011) Long term operation of a solar assisted ground coupled heat pump system for space heating and domestic hot water. *Energy Build* 43:1835–1844
19. Fan R, Gao Y, Hua L, Deng X, Shi J (2014) Thermal performance and operation strategy optimization for a practical hybrid ground-source heat-pump system. *Energy Build* 78:238–247
20. Wang E, Fung A, Qi C, Leong W (2012) Performance prediction of a hybrid solar ground-source heat pump system. *Energy Build* 47:600–611
21. Mitchell JW, Braun JE (1997) Design analysis, and control of space conditioning equipment and systems, solar energy laboratory. University of Wisconsin, Madison
22. Hellstrom G (1991) Ground heat storage. University of Lund, Sweden, Department of Mathematical Physics
23. Pertzborn A, Hackel S, Nellis G, Klein S (2011) Experimental validation of a ground heat exchanger model in a hybrid ground source heat pump. *HVAC&R Res* 17:1101–1113
24. Weifel GZ, Dorer V, Koschenz M, Weber A (of EMPA) (1995) Building energy and system simulation programs: model development, coupling and integration. In: *International Building Performance Simulation Association Conference Proceedings*. IBPSA
25. Muhammad HK (2006) Modeling, simulation and optimization of ground source heat pump systems(Master thesis). Oklahoma State University, Stillwater, Oklahoma
26. Jiang Y et al (2006) Building environmental system simulation and analysis-DeST. China Architecture & Building Press, Beijing
27. China Meteorological Administration, National Meteorological Information Center. Climate Standard Data of China (1971–2000). <http://cdc.cma.gov.cn/>
28. ASHRAE (2007) HVAC Applications, SI ed., ASHRAE, Atlanta, GA
29. Klein et al (2004) TRNSYS 16. A transient system simulation program, user manual, solar energy laboratory. University of Wisconsin, Madison
30. Hellstrom G (1989) Duct ground heat storage model. Department of Mathematical Physics, University of Lund, Sweden, Manual for Computer Code
31. Raab S, Mangold D, Muller-Steinhagen H (2005) Validation of a computer model for solar assisted district heating systems with seasonal hot water heat store. *Sol Energy* 79:531–543
32. Magraner T, Montero A, Quilis S, Urchueguia JF (2010) Comparison between design and actual energy performance of a HVAC-ground coupled heat pump system in cooling and heating operation. *Energy Build* 42:1394–1401
33. Yavuzturk C, Spitler JD (2000) Comparative study to investigate operating and control strategies for hybrid ground source heat pump systems using a short time step simulation model. *ASHRAE Trans* 106(2):192–209
34. Yang J, Xu L, Hu P, Zhu N, Chen X (2014) Study on intermittent operation strategies of a hybrid ground-source heat pump system with double-cooling towers for hotel buildings. *Energy Build* 76:506–512

5th Generation District Heating and Cooling Networks as a Heat Source for Geothermal Heat Pumps



Robin Zeh, Matthias Schmid, Björn Ohlsen, Stefan Venczel,
and Volker Stockinger

Abstract Renewable heating and cooling energy can be distributed with low temperature district heating and cooling networks connected to several renewable heat sources. These fifth generation district heating and cooling networks (5GDHC) deliver energy to settlements up to whole city districts. Because of the low temperature levels, the energy is distributed with almost no distribution losses and made usable to the consumer with decentralized heat pumps. Several renewable heat sources like large-scale geothermal collector systems, frozen soil storages or external dry cooler can be used. Moreover, sewage water and waste heat at low temperature levels can serve energy for 5GDHC. Especially, the use of geothermal heat sources like the large-scale geothermal collector system or the frozen soil storage enable the possibility to shift heating and cooling loads seasonally, contributing to flexibility in the heating network. In addition, the soil can be cooled below freezing point due to the strong regeneration potential caused by the solar irradiation. Geothermal collector systems with more than one layer can be used to generate excessive cooling by freezing individual areas within the collector system to provide cooling energy for residential buildings, office complexes or industrial applications. Planning these systems requires expertise and understanding regarding the interaction of these technologies in the overall system.

Keywords 5GDHC · Large-scale geothermal collector systems (LCS) · Frozen soil storage (FSS) · External dry cooler (EDC) · Renewable heat sources · Very shallow geothermal potential (vSGP)

R. Zeh (✉) · M. Schmid · V. Stockinger
Nuremberg Tech, Keßlerplatz 12, 90489 Nuremberg, Germany
e-mail: robin.zeh@th-nuernberg.de

B. Ohlsen · S. Venczel · V. Stockinger
Energie PLUS Concept GmbH, Blumenstraße 1, 90402 Nuremberg, Germany

1 5th Generation District Heating and Cooling Networks as a Heat Source for Geothermal Heat Pumps

1.1 *Classification of District Heating and Cooling Networks*

Commercial district heating (DH) networks were first utilized to mainly use the excess heat from electricity production of large power plants. Because of the combined use of heat and electrical power the efficiency of those power plants increased. Furthermore, the power plant's waste heat supplied cities and industries with heating energy at very high temperature levels. The first commercial DH networks were built in the USA during the 1880s [1]. Since that DH was continuously improved and spread around the world. The efficiency increased during the last 100 years and nowadays they can be distinguished based on circulation fluid, thermal application, network size and energy source.

The first generation of DH networks (1GDH) used pressurised steam as a heat carrier [2–4]. There was no insulation on the pipes which resulted in a lot of energy losses. With the second generation of DH networks (2GDH) the heat carrier changed to superheated water. There was a large spread of this systems around Europe since 1930. Large DH networks were built in big cities next to central power plants. These networks used insulated network pipes for the first time to reduce heat losses to increase the overall efficiency. With the third generation of DH networks (3GDH) a lot more energy sources were used at temperature levels of around 100 °C. Industrial waste heat and other high temperature excess heat can be used for these networks. With lower temperature levels and better insulation, efficiency has increased significantly since 1980. Most of the existing networks in large cities can be classified into 2GDH or 3GDH. Since the need of highly efficient DH networks due to climate change the fourth generation of district heating networks (4GDH) has been established since the 2020s. The network temperatures were lowered as far as possible to reduce heat losses and to enable the integration of way more excess heat sources at lower temperature levels. Because of this 4GDH networks are highly efficient renewable systems with temperature levels less than 100 °C. The temperature levels of 4GDH networks are as close as possible to the level of the end user's temperature demand [4]. The evolution of the generations of DH networks can be seen in Fig. 1.

The development of DH networks since the 1880s indicates the trend from centralized fossil heat sources with low efficiency up to decentralized renewable energy sources at low temperature levels in smart thermal grids with almost no heat losses [3]. In those smart thermal grids renewable energy can be shared within the whole district and the network itself can be used as a heat storage [3, 5]. In Table 1 the main features and differences from the different DH generations are compared. Now the fifth generation of DH network first introduces the double usage of heating and cooling within one network just because of its very low temperature levels, thus it is called fifth generation of district heating and cooling (5GDHC). The temperature is lowered below the ambient temperature of the pipes surrounding soil to temporarily reduce heat losses.

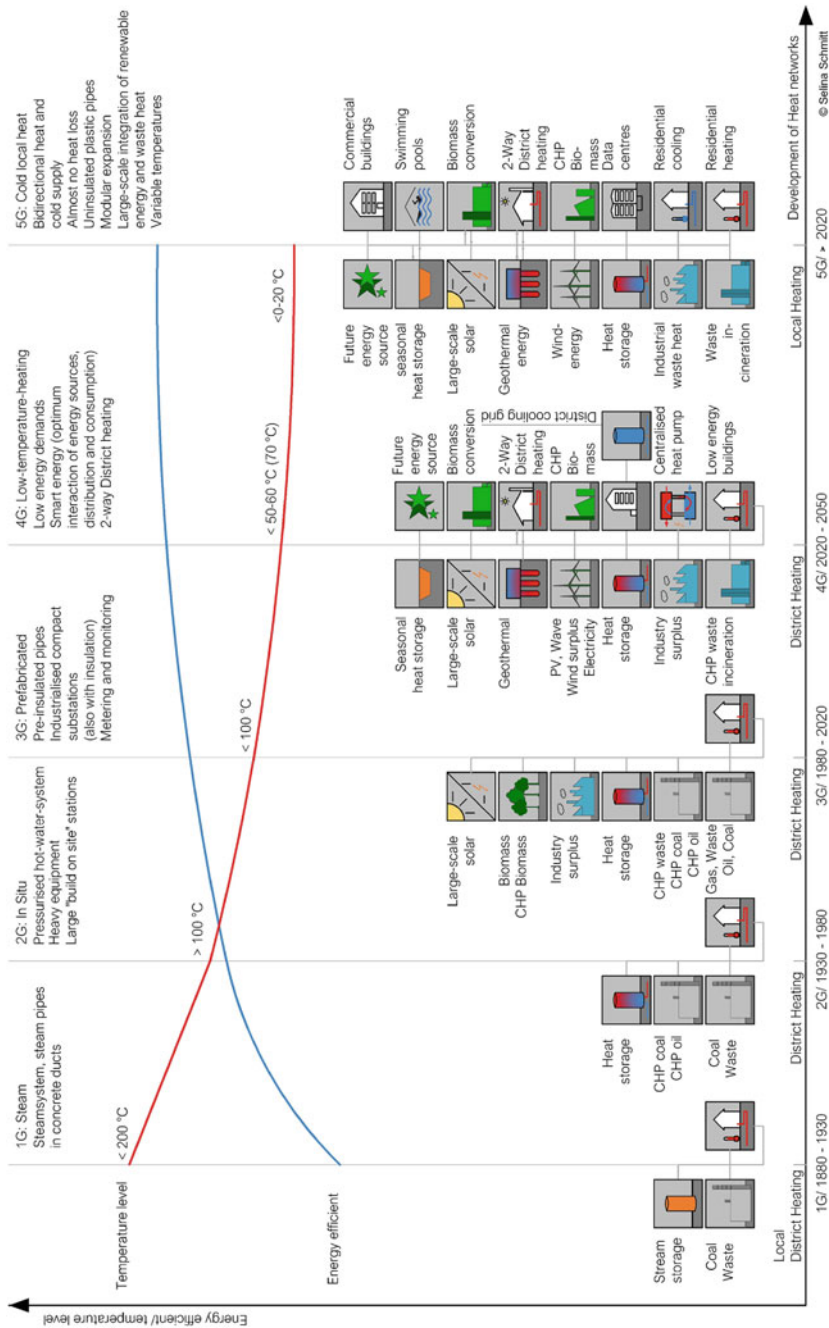


Fig. 1 District heating networks from the first to the 5th generation during the last 150 years (*Source* Zeh et al. [3], further development of the graphic in accordance with Lund et al. 2014 [2] (p. 9))

Table 1 Typical features of district heating networks from 1st to 5th generation (*Source [3]* with data use from [2, 6, 7 (p. 1206 ff)])

	1G	2G	3G	4G	5G
Mostly used	1880–1930	1930–1980	1970—now	Currently used	Currently used
Motivation	Comfort, reduced risk	Fuel and cost savings	Reliable heat supply	Renewable energy	Renewable energy, efficiency, cooling
Temperature level	<200 °C	>100 °C	>70 °C	90–40 °C	20–<0 °C
Temperature spread	20–60 K	20–40 K	20–40 K	20–40 K	3–6 K
Heat carrier	Steam	Pressurized hot water	(pressurized) hot water, often below 100 °C	Water	Antifreeze
Source of heat (examples)	Coal, CHP, boilers	Coal, oil, CHP, boilers	CHP, boilers, waste, fossil-fired boilers	Waste heat, solar thermal energy, biomass, deep geothermal energy	Waste heat, geothermal energy, sewage water, river water
Heat distribution	Steam pressure	Centralized pumps	Centralized pumps	(de-) centralized pumps	(de-) centralized pumps
Heat distribution losses	Very high	High	Moderate	Moderate	Low/heat gain
Pipe materials	(On-site insulated) steel pipes	(On-site insulated) steel pipes	Pre-insulated steel pipes	Pre-insulated steel/polymer pipes	Non-insulated polymer pipes
Heat transfer	Condensers	Tube-and-shell heat exchangers	Plate heat exchangers	Plate heat exchangers	Heat pumps
Heating system (radiators)	High-temperature radiators using steam or water (>90 °C)	High-temperature radiators using district heating water direct or indirect (90 °C)	Medium-temperature radiators using district heating water direct or indirect (70 °C), floor heating	Low-temperature radiators (50 °C) using water indirect, floor heating	Floor heating

With highly efficient smart thermal grids which belong to 4GDH the direct use of the waste heat sources at very low temperatures $<40\text{ }^{\circ}\text{C}$ is mostly not possible. The direct use of the heat within the network is not attainable because its temperature level is higher than the source temperature. Because of this, the 5GDHC networks were introduced in Europe as a descendant of the 4GDH since the 2020s. 5GDHC are decentralized and bidirectional networks with fluid temperatures around the surrounding soil temperature. This leads to almost no heat losses during the distribution. In addition, it can achieve significant heat gains through the energy distribution process itself by using very low temperature levels via the 5GDHC [3, 8, p. 26, 9].

Since the integration of 5GDHC a lot of these systems were built around Europe. Right now, there are no stringed guidelines for planer and designer yet [6]. With investigations in research and development a lot of theoretical and practical analysis were done to understand the implementation of different heat sources with different temperature levels [10].

1.2 Comparison of Different Terms and Definitions of 5GDHC

With new developments, it is often the case that a new product or an idea is developed and given a name by its developer or inventor. This name is often also the established name for this product or idea, until it comes to the next clear further development. With products or ideas, which are developed at the same time by different persons, it often comes to the fact that each of these developers develops its own name. The different names or terms are then side by side until one of the terms prevails and becomes the generally accepted term.

This is currently happening with the latest generation of DH networks. Due to different projects with different technologies and network temperatures, there are several different terms and partly even different definitions for these new types of DH networks.

Buffa et al. [6] list several terms that are currently in use. Thus, there is Low temperature District Heating and Cooling (LTDHC), (Bidirectional) Low temperature networks (LTNs), Cold District Heating (CHD) (“Kalte Fernwärme” or “Kalte Nahwärme” in German and “Teleriscaldamento Freddo” in Italian), Anergy networks or Anergy grid (“Anergienetz” in German).

Some of these terms are easily confused with existing definitions of 4GDH systems such as Low temperature District Heating (LTDH) and Ultra-low temperature District Heating (ULTDH), defined by Østergaard and Svendsen [11] as 4GDH systems with supply temperatures of $50\text{ }^{\circ}\text{C}$ and $35\text{ }^{\circ}\text{C}$, respectively.

Buffa et al. [6] therefore explicitly recommend that these different terms be unified under the collective term “Fifth-Generation District Heating and Cooling” (5GDHC).

Besides the mere definition of the term, the definition of the term is also different. Lund et al. [4] compared several definitions for 5GDHC, some of which are presented below.

Boesten et al. [9] define 5GDHC as “decentralized, bi-directional, close-to-ground temperature networks that use direct exchange of hot and cold return flows and thermal storage to balance thermal demand as much as possible.”

Brennenstuhl et al. [12] cite the reduction of network losses and cost savings for insulation as advantages of the low temperatures of the 5GDHC. The low temperatures allow the integration of heat from vertical heat exchangers, low-temperature waste heat, or horizontal ground collectors. In some cases, the network temperature is below the soil temperature, thus the distribution network acts as a horizontal heat collector.

Barone et al. [13] refer to DH networks with temperatures of about 30 °C and heat pumps/chillers as fifth generation.

For Allen et al. [14], typical 5GDHC temperatures are between 15–25 °C and use decentralized heat pumps (HP) that temper water for heating or cooling.

Wirtz et al. [15] refer to DH networks with 5–30 °C as 5GDHC. For them, the temperature difference between hot and cold pipe is 5–10 K. They see it as a great advantage to be able to feed low-grade waste heat (e.g. from space cooling) directly into the system without having to raise the temperature first.

The most appropriate definition is provided by Buffa et al. [6], they define 5GDHC as, “[...] a thermal energy supply grid that uses water or brine as a carrier medium and hybrid substations with Water Source Heat Pumps (WSHP). It operates at temperatures so close to the ground that it is not suitable for direct heating purpose. [...] The possibility to reverse the operation of the customer substations permits to cover simultaneously and with the same pipelines both the heating and cooling demands of different buildings. Through hybrid substations, 5GDHC technology enhances sector coupling of thermal, electrical and gas grids in a decentralised smart energy system.”

This definition includes the major functional difference between 4 and 5GDHC, namely the need for decentralized heat pumps. In addition, the bidirectional nature of the network with the possibility of cooling becomes clear. In addition, the temperature level is mentioned as close to the ground, which makes it unnecessary to declare it exactly.

There are also critical voices regarding the term 5GDHC. Lund et al. [4] argue that generations represent certain sequential development. 4GDH thus represent a general evolutionary development of the three previous generations, but better aligned with the unique characteristics of renewable and recycled heat. 5GDHC can be considered a different technology than the previous generations because heat production by the heat pump occurs only at the consumer. As a result, the supply temperature can be customized and there is the possibility of cooling. Currently, there is a great variety of technological solutions in DH networks. To call a group within this diversity a generation should therefore require broader goals and characteristics rather than other technical solutions.

Furthermore, Lund et al. [4] criticize that the term 5GDHC represents a progression over 4GDH. However, improved energy efficiency is not present, which was the case during the transition from previous generations to 4GDH. For this reason, the 5GDHC term does not appear to be compatible with the established terms of the

first four generations. They therefore argue that 5GDHC should be seen as a parallel development to 4GDH and should rather be seen as part of the larger 4GDH family with different technology options.

Only the future will show on which term and which definition the majority will agree.

1.3 5GDHC Network Types (*active, passive, hybrid*)

The supply network within a 5GDHC can be realized in different ways. The most common network types are the active and passive network type which mainly differ by the use of central network pumps. Furthermore, there is also a mixture of these two types which combines various properties to a hybrid network. In the following, the three different network types are introduced. The presented information is based on [3, p. 4–5].

1.3.1 Active 5GDHC

Similar to conventional DH systems, central pumps are installed inside an energy center. An active 5GDHC is suitable for spatially extensive construction areas with more than 50 to up to hundreds of consumers. Different remote heat sources can be linked via a pipe system bidirectionally resulting in an exchange of heating and cooling energy. Another reason for considering an active 5GDHC is due to limited space for large pipe diameters like used in a passive network. Moreover, supplying smaller areas is a suitable scope for an active 5GDHC.

Central network pumps generate a flow through the heating network. Therefore, the delivery head in the pump can be freely selected. Thus, the pressure loss is not the main planning variable compared to a passive network. This construction method makes even smaller pipe diameter possible. By using central network pumps the active network gets a modular character by expanding the network with additional heat sources or network sections in the future. Considering this modular character, it is necessary to be aware of this during the initial planning phase of the energy center and the heat pumps in order to gain a temperature spread of about 3–6 K. The energy center consists of

- the central network pumps,
- pressure equalization tanks,
- motorized butterfly valves
- and the network degassing system.

By installing several identical pumps in parallel or operated alternately maintenance measures are enabled and simultaneously possible malfunctions are prevented.

House substations are installed at the consumer's side. These substations contain a control and regulation unit by using a motorized butterfly valve to prevent a permanent

flow and thereby constant pressure losses. If there is a thermal energy request a flow is generated through the heat pumps. The corresponding operating points must be considered during the planning phase for minimizing pressure losses in the overall system and decreasing wear as well as energy demand of the central pumps.

1.3.2 Passive 5GDHC

Contrary to an active network the fluid flow in a passive network is induced by feed pumps integrated in the heat pumps. Therefore, the pressure loss is the main design parameter for network planning. The design depends on

- piping,
- house substation,
- distributor,
- line regulating valve,
- heat source,
- heat transfer medium, etc.

By using the heat pump's integrated feed pump it must overcome the pressure loss in the overall system to ensure a circulation. The maximum flow of the heat transfer medium is achieved if all heat pumps are in operation. As the system depends mainly on the network's pressure loss, it is recommended to select large pipe diameters and only short pipe lengths. Large pipe diameters cause the need for more free space when laying in the street. Although, the pipe system of other trades like water, electricity, wastewater must be kept in mind.

Due to the use of the integrated feed pump the energy center can be built very small and no further electric energy is required. A necessary energy center consists only of pressure maintenance, refilling and ideally degassing. Advantage of this network type is a long-term cost-effective and energy-efficient operation due to the elimination of central network pumps. On the other hand, this type cannot be easily expanded for more consumers in the future. Moreover, the integration of other heat source or network sections is also limited.

In general, a typical passive 5GDHC is established with a magnitude of maximum 100 heat consumers as small pipe lengths are required. Moreover, the lower the customer-specific heat demand, the more customers can be supplied with this network type.

1.3.3 Hybrid 5GDHC

A hybrid network is a combination of an active and passive network. With the help of a hybrid network, an attempt is made to combine the advantages of the two network types. The background to these considerations is to reduce auxiliary energy and to ensure an equally high level of supply security. The investigations of a hybrid network are being advanced and being investigated first in the research project "ErdEis II"

(Grant Number: 03ET1634, funded by the German Federal Ministry for Economic Affairs and Climate Action) [16]. The characteristics of the respective network types can be summarized to only a low provision of auxiliary energies during operation in passive network. At the same time, the decentralized, integrated feed pumps of the heat pumps are limited to a certain network size due to the increasing pressure losses. Extensions of the network are economically and technically difficult to realize.

The characteristics of active networks allow the network to be constantly expanded and new consumers to be connected. This results in a change from decentralized feed pumps to centralized feed pumps in the energy center. The disadvantage is the constant operation of the network pumps in order to be able to guarantee the security of supply. This in turn results in higher electrical energy consumption for pump operation. The remedy is to combine both types. In the research project “ErdEis II”, a hybrid network is being investigated that combines both types. The network is primarily operated via decentralized, integrated network pumps in the heat pumps of the consumers. However, this requires a precise analysis of the pressure losses in the system. A hydraulic separator is used to create a bypass between the supply and return lines, which can be controlled by an automatic motorized valve. If load peaks occur in the network so that the pressure losses increase, which in turn would lead to a drop in the flow rate if the system were operated only via the decentralized feed pumps, the bypass opens. When the bypass is open, central feed pumps switch on in an energy center, which supports the passive network with an active component and overcomes the pressure losses. The security of supply is therefore guaranteed.

2 Energy Sources to Supply a Geothermal Heat Pump via 5GDHC

2.1 Very Shallow Geothermal Potential

In general, the geothermal potential is divided into two different layers. The first layer up to a depth of 400 m is defined as the shallow geothermal source. Below a depth of 400 m the corresponding layer is known as the deep geothermal source [17, p. 1]. For 5GDHC networks a shallow geothermal source fits perfectly according to the low temperature level. For a more practical exploitation of this energy source, it is suitable to separate the layer of the shallow geothermal source into the less deep geothermal source which is defined as the very shallow geothermal potentials (vSGP) [3, p. 5]. The layer of the vSGP is defined up to a depth of 10 m [18]. A visualization of the geothermal subdivisions can be depicted in Fig. 2.

A big influence for the vSGPs are soil parameters compared to vertical shallow geothermal systems which are even more dependent on the geologic rock strata regarding the heat extracting potential. The main thermal properties for soil are the thermal conductivity, thermal diffusivity, and heat capacity. The properties are mainly

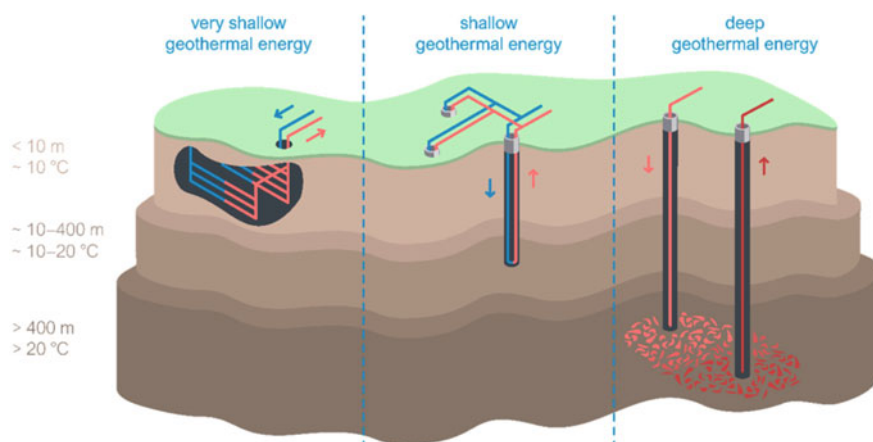


Fig. 2 Very shallow, shallow and deep geothermal potential subdivisions (Source Zeh et al. [3])

influenced by the physical soil parameters like bulk density, water content and soil texture defined by the size distribution [19, 20].

Besides the soil parameters solar irradiation and precipitation have a more crucial impact on the vSGP [18, 21]. The less deep the geothermal source is the lower is the influence of the earth's interior heat input (terrestrial heat flow). On the other hand, the less deep the geothermal source the higher is the impact due to solar irradiation [3, p. 6]. The exploitation of vSGP is mainly accomplished by using horizontally installed geothermal systems at the earth's surface. These horizontal ground heat exchangers (GHE) are shaped like a geothermal collector in the classic single pipe installation or tube mats. There are also other special designs such as trench collectors, heat baskets, and other comparable modular collector systems. The only limitations of these systems are the use of geothermal source until a depth of 10 m [3, p. 6].

Regarding an economical context, geothermal systems have lower operational costs for heating and cooling compared to other systems [22]. Furthermore, horizontal ground heat exchangers are beneficial in lower installation costs and much lower drilling technology requirements [23].

2.2 Large-Scale Geothermal Collector System

One very shallow geothermal heat source for 5GDHC networks which can be used in temperate conditions is called a large-scale geothermal collector system (LSC). Those special ground heat exchanger is separated by normal systems by its size and performance [3, p. 7] but is built in the same depth layers of around 1.5–3 m. In Germany a lot of LSC systems have been built since 2020 and they typically supply whole settlements with both heating and cooling energy via a 5GDHC [12, p. 3]. They can be built next to the settlement below agricultural used fields [3] or directly

below the buildings [24, 25]. Large-scale geothermal collector systems are defined by the following parameters (Fig. 3). At least one of them must be fulfilled to be considered LSC:

- $\geq 1,000 \text{ m}^2$ area
- $\geq 25 \text{ kW}$ maximum source power
- $\geq 50 \text{ MWh/a}$ source heat extraction

The main difference of an LSC to normal GHE systems is in the size. Normal ground heat exchangers are mostly built for one individual buildings. A typical LSC system can extract source heat for more than 100 buildings. Because of this the second main difference is the complexity. Smaller systems mostly use simple hydraulic installations and are directly connected to the heat pump. The hydraulic components of an LSC need to be calculated and designed to optimize the pressure loss of the system. There are also way more distribution shafts which control the heat extraction to be consistent over the entire system. Inside an LSC there are a lot of individual ground heat exchangers connected to one big system. Because of this there is also some heat extraction affects between the heat exchangers which influences the heat extraction behaviour of the LSC. This is very important and requires a more detailed planning with the help of simulation programs.

Most of the LSC systems use modular trench collectors which are connected to each other via distribution shafts. With the use of modular heat exchanger systems and the use of the Tichelmann system the pressure loss for each modular collector system is the same. This enables an equal heat extraction. Also, the hydraulic of the whole

**large-scale geothermal
collector system (LSC):**

- $\geq 1,000 \text{ m}^2$
- $\geq 25 \text{ kW}$
- $\geq 50 \text{ MWh/a}$

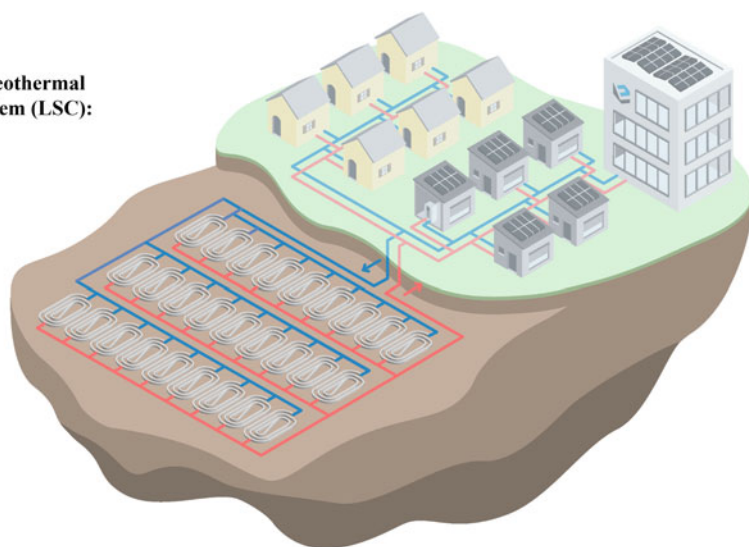


Fig. 3 Parameters to describe an LSC. At least one of the criteria must be fulfilled to be considered LSC (Source Zeh et al. [3])

system can be calculated more easily. Using horizontal GHE's multilayer collector systems can be built to get a higher specific heat extraction. In those cases, each layer is controlled separately via the distribution shafts to maintain the advantages of this LSC design for seasonal heat and cold storage.

2.2.1 Advantages and Disadvantages of a LSC

By using the very shallow geothermal potential with a large-scale geothermal collector system there is a high regeneration potential through the climate caused by solar irradiation and precipitation. Because of this the soils temperature can be cooled down by heat extraction below freezing. This is only possible for a short period of time to enable natural regeneration later. By using the phase change from soils water to ice more energy can be extracted. There is a lot of energy which can be extracted by changing the water's phase condition at consistent zero degrees. This can lead to high specific heat extraction. After freezing the soils water the temperature starts sinking below zero degrees. It is very important not to cool down the soil too far, because natural regeneration would not be enough. In these cases, regeneration energy from waste heat or other heat sources is necessary. Most of the yet built LSC systems run at the end of the heating period with some freezing around the LSC. After complete regeneration during the summer month, the LSC can provide heating energy for the next heating period. With GHE's in depths of 1.5–2 m it is almost impossible to cool down the surrounding soil that far that it cannot be regenerated naturally in locations with temperate latitudes (four seasons, sufficient precipitation) [3, 26].

Within a LSC there are some efficiency losses caused by mutual influences of the GHE's. They occur in the centre of the system. This can lead to stronger freezing in this area. Because of the surface regeneration caused by solar irradiation and precipitation every part of the system can be regenerated naturally in those depth layers. Because of this the yield of the LSC can be calculated very accurate with easy and low-cost soil analysis of the upper soil layer and simulations.

Another advantage caused by the soils freezing around the GHE's can be used by multilayer LSC systems. With a double layer collector system, the lower layer can be used in some cases as a seasonal heat and cold storage. During the heating season both layers equally extract heating energy. Both layers start freezing. It is important that the soils freezing of the two layers would not connect. During spring and early summer months only the upper layer is used for serving heating energy. In this period the natural regeneration only leads to higher soil temperatures at the upper layer. The lower layer is shut off solar irradiation and precipitation and remains freezing/cold. In the summer months when cooling energy is needed, mostly the lower layer of the double layer LSC is used for serving the cooling energy. During this the lower layer is regenerated with the excess heat by providing cooling energy for residential buildings, office complexes or industrial applications within a 5GDHC [27]. At the end of the summer months both layers remain regenerated (natural regeneration in the upper layer and excess heat regeneration in the lower layer). By using the cooling

energy with excess heat, the surrounding soil can somewhat be overheated to serve energy for the next heating season [3].

The main disadvantage of a LSC is in the heat potential which depends on the location with its soil and climate conditions. In addition, the heat potential is subject to seasonal fluctuations. The lowest geothermal potential with a single layer LSC is available during the winter months. But at that time the highest heating demand in a settlement is required. This leads in most cases to higher area demand than other geothermal systems like borehole heat exchangers).

Pros:

- Strong natural regeneration caused by climate conditions
- Using the soil's moisture for phase change for higher specific heat extraction
- Easy and low-cost analysis of the upper soil layer
- Accurate calculation with simulation models
- Heating and cooling energy by using a multilayer LSC

Cons:

- Location with temperate climate conditions is required (four seasons, sufficient precipitation)
- Efficiency losses within the single GHE's inside the LSC
- Lowest geothermal potential during highest heat demand
- High area demand

2.2.2 Application Scenarios of a LSC

If the 5GDHC is operating with very low system temperatures some heat sources are in constant competition to each other like the LSC or other ground heat exchangers, solar thermal energy, biomass, or waste heat sources (industrial waste heat, wastewater heat, etc.). If not every building can have its own heat source due to space constraints a centralised LSC at available open areas may be a good choice. It can be placed below agricultural used fields, below a rainwater retention basin, below sport fields or in compensation areas to enable dual use of these areas.

In combination with a 5GDHC the LSC can deliver both, heating and cooling energy for the settlement. By using dual layer LSC's the heat extraction can lead to local icing of the soil which leads to higher specific heat extraction per square meter of the soil surfaces [3, 28, 29]. Because of this the use of multilayer LSC leads to area savings if the settlement needs both heating and cooling energy. It must be ensured that the normal freezing and thawing does not cause the soil to permanently lose moisture. Because of this, regions with very dry soil conditions are unsuitable for this, unless additional moisture can be introduced into the soil via special structures like drainage systems.

In most areas with special legal requirements a LSC is possible to use. For example, borehole heat exchangers are usually subject for special restrictions. In Germany in special the use of vertical borehole heat exchanger may be prohibited due to

groundwater protection or due to mining law. For LSC the requirements are much less strict which leads to regenerative low-temperature heating and cooling systems also in those special legal situations.

A LSC can also be used as an intermediate storage unit within a 5GDHC with different low temperature heat sources. Heating or cooling energy can be stored temporarily and then provide it when necessary. This requires a very special hydraulic system.

2.3 *Frozen Soil Storage*

In Sect. 2.2 the large-scale geothermal collector systems were presented as a heat source that delivers a lot of energy but also requires some larger areas. Especially in urban areas, it is more difficult to meet these requirements. For this reason, the frozen soil storage (FSS) was developed. The components, like the modular GHE, the distribution shafts and antifreeze can be the same as for the LSC, but the GHE are arranged differently. Instead of one or two large collector layers, several layers are arranged on top of each other. The aim is to increase the specific heat extraction per square meter. This is achieved by tapping the ground at a greater depth. In addition, the ground between and around the collectors is increasingly frozen in order to make even greater use of the latent heat than with a LSC. In Fig. 4 the structure of a FSS and the integration within a 5GDHC is shown.

The layers are arranged one above the other at a distance of approximately 1 m at a depth of around 1.5 m. To be able to use the slope of the excavation pit, the collector layers are arranged in a funnel shape. This reduces the amount of excavated soil significantly.

By arranging several layers on top of each other, the thermally tapped soil volume can be increased. As with the LSC, the top layer shields the lower layers mostly from natural regeneration from solar irradiation and precipitation.

For this reason, active regeneration of the lower layers is necessary. The FSS can thus be seen as a mixture of heat source and heat accumulator. The FSS is a heat source as it absorbs environmental heat from solar irradiation, precipitation, the surrounding soil, and groundwater flows. On the other hand, it also serves as a latent heat storage. By freezing the soil, a large amount of heat can be stored at a low temperature level with a relatively small area requirement. Figure 5 shows the operating mode of an FSS over the course of a year.

In winter, heat is extracted from the FSS and the soil around and between the collector layers is frozen. The heat is transported to the buildings via a 5GDHC. In the buildings there are decentralised heat pumps which help to raise the heat to a utilizable temperature level and supply the heating circuit of the building and heat the domestic hot water.

In spring, the FSS—especially the top layer—is naturally regenerated by solar irradiation, precipitation and the higher outside temperatures. Heat also flows in from the soil below and around the FSS, but to a much lesser extent.

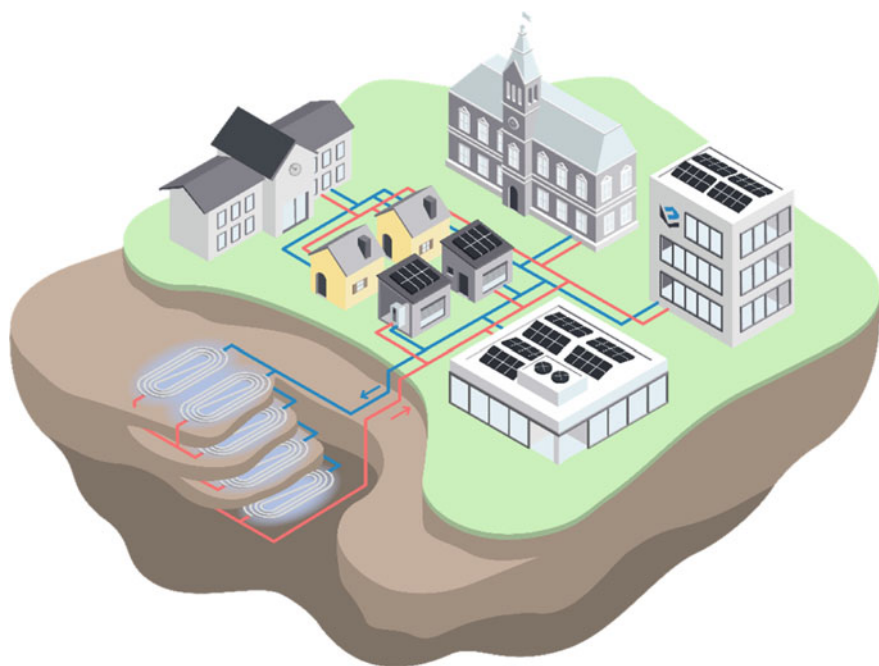


Fig. 4 Schematic use of the frozen soil storage within a 5GDHC (*Source* Energie PLUS Concept GmbH)

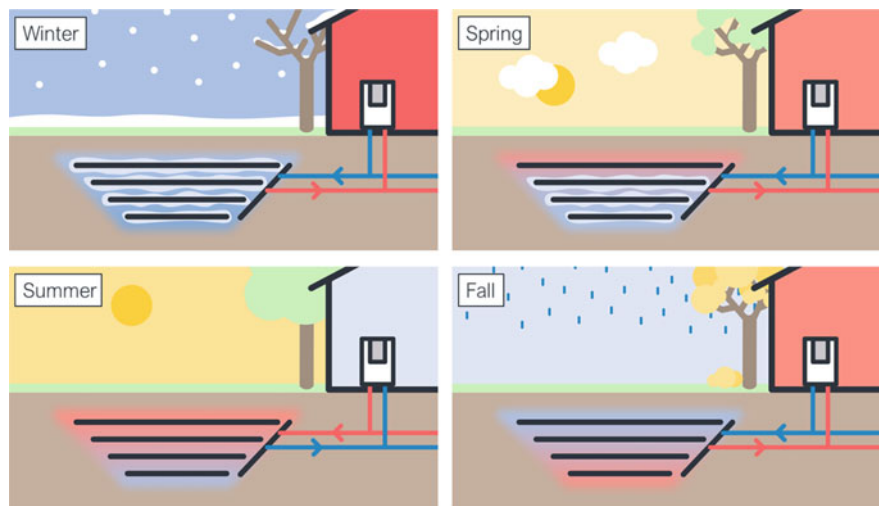


Fig. 5 Operation mode of the frozen soil storage [30] (*Source* Energie PLUS Concept GmbH)

In summer, the natural regeneration increases and regenerates the FSS from above. Additionally, there is a need for cooling energy in the buildings during summer. Since the 5GDHC does not exceed a temperature of approx. 17 °C, it can be used for cooling without any further significant energy input. With the help of a heat exchanger in the heat pump, the buildings can be cooled in a cost-effective and environmentally friendly way. Especially the lower layers of the FSS, which are shielded from above and are still partly frozen by this time, can provide sufficient cooling potential throughout the summer month. Conversely, the lower layers can be actively regenerated and heat can be stored seasonally by defrosting the soil.

In the fall, the heating season is beginning and heat is extracted from the FSS again. The ground cools down and is frozen in a controlled manner in the further course of the heating period.

Thus, the FSS provides heating in winter and cooling in summer.

2.3.1 Advantages and Disadvantages of a FSS

The advantages and disadvantages of a FSS are similar to those of a LSC (see Sect. 2.2.1). For this reason, only advantages and disadvantages compared to the LSC will be discussed here.

The biggest advantage over an LSC is the smaller footprint. By stacking multiple layers on top of each other and making greater use of latent heat, the required area can be reduced. The exact area saving potential is difficult to quantify because it is very site dependent (soil type, soil moisture, groundwater depth, climate, heating and cooling demand profile).

Although the multi-layer construction method results in less floor space being required, more collector modules are needed overall, as the modules work most effectively in the single-layer construction method. Thus, an FSS costs more than a comparable LSC in terms of heat extraction.

The FSS requires active regeneration of the bottom layers in summer. This can be seen as an advantage or disadvantage depending on the heat and cold demand. It is an advantage if there is a high cooling demand in summer, which would otherwise have to be covered by additional energy input. Without cooling demand or additional waste heat sources, it turns out to be a huge disadvantage.

Pros (compared to a LSC):

- Lower area demand
- High specific energy extraction
- Heating and cooling

Cons (compared to a LSC):

- Requirement of active regeneration
- Higher specific costs per heat extraction

2.3.2 Application Scenarios of a FSS

Like the LSC, the FSS can be used when a large common heat source is needed for heat pumps.

Due to the active regeneration required for the FSS, it should always be built together with another heat source. 5GDHCs are ideal for this purpose, as waste heat from a wide range of sources can be incorporated into them. In this way, the FSS can be regenerated in summer and provides cooling at the same time.

Similar to the LSC, it can be placed below a rainwater retention basin, below sport fields or in compensation areas to enable dual use of these areas.

Its space-saving design makes it suitable for construction areas with few open spaces. However, if enough space is available, the LSC should rather be used, as it is more cost-efficient in terms of investment.

2.4 5GDHC as an Energy Source Itself

The network pipes of an 5GDHC can provide heating and cooling energy by itself just by laying in the ground. This is because the pipes work as a large rolled out horizontal ground heat exchanger. If the fluid temperature is lower than the soils natural temperature the pipes can extract heating energy from its surrounding soil. In most distribution networks, especially 4GDHC and 3GDHC the fluid temperature is higher than the soils temperature. This leads to energy loss. To reduce these losses, the feeding pipes where insulated. With a 5GDHC at ground temperature there is no need for insulation. Is the network temperature higher than its surrounding soil temperature there are also energy losses. But this may be a positive side effect in cases when cooling energy is required.

With the use of very low temperature heat sources like LSC, FSS or vertical GHE the temperature level of the fluid is mostly lower than the soils temperature. Depending on the piping length, the fluid temperature, and the season, the 5GDHC can deliver a noticeable share of the systems source energy. The higher the temperature difference to the surrounding soil and the longer the distance of the distribution pipes the more heat can be extracted. But the amount of the heat gains cannot be quantified in general terms. In addition, the temperature differences and pipe lengths, the surrounding soil conditions (soil type, moisture, thermal conductivity), climatic conditions (air temperature, solar irradiation, precipitation) and the main heat source of the network have a great impact [3]. With simulation tools the estimated heat gains can be calculated which have a big impact in the size of the other heat sources. In less dense residential structures, the heat gains through the 5GDHC itself can provide up to 50% of the annual source energy. The rest needs to be served via low temperature heat sources with temperature levels around the soil's temperature.

2.4.1 Advantages and Disadvantages of using a 5GDHC as a Heat Source

Using a 5GDHC as a heat source itself has a lot of advantages. The size of the centralized heat sources can be reduced significantly just by calculating the heat gains through the network. This reduces the initial costs as well as the operation costs and leads to area savings of the heat sources. With the high fluid volume in the distribution pipes the network itself can absorb fluctuations in heat production and usage which results in a storage effect. In less dense residential structures, the heat gains through the network itself can lead to a significant amount of source heat. By using the 5GDHC as a heat source there are no heat losses.

On the other hand, the use of a 5GDHC as a heat source itself requires a lot of knowledge and simulation of the surrounding soil and its conditions. The planning of the central heat sources must be coupled with the planning of the 5GDHC which leads to interdisciplinary understanding. This makes the planning process way more complex than with 4GDHC. It is also necessary that the heat sources work with fluid temperature levels around the soil temperature. Otherwise, there are no heat gains through the distribution network via temperature differences. Because of the temperature level, the efficiency of the heat pumps is little lower than with higher fluid temperatures.

Pros:

- Heat gains through the network up to 50% of the source energy demand
- smaller central heat sources (reduction of costs)
- storage effect
- no heat losses
- no insulation on the network pipes

Cons:

- very complex planning process
- knowledge of the soil conditions
- fluid temperature level around the soil temperature
- lower efficiency of the HP

2.4.2 Application Scenarios of a 5GDHC as a Heat Source

With very low fluid temperatures at a 5GDHC it can be used as a heat source itself. To ensure a high overall efficiency it is necessary that the heat pumps run at an efficient level. Because of this a very high building standard in the supplied buildings is needed. In most cases this is only possible with new build buildings. Energy improvements in already existing ones need to be done first. In most cases 5GDHC is used in complete new built areas with very highly efficient building structure. This reduces the energy density within the networks length and enables a sufficient heating and cooling supply. Rural areas with other renewable energy potentials are recommended.

In urban areas 5GDHC can also be used, but the percentage of the potential heat gains are less dominant caused by the denser energy demand.

2.5 External Dry Cooler

In addition to the geothermal heat sources the air can also be used as a sustainable heat source for a 5GDHC. One way to harness the energy contained in the air is the use of an external dry cooler (EDC). In its original application, it is designed for cooling processes and is therefore often used in buildings with a high cooling demand. The generated waste heat is released from the warmed heat transfer medium to the ambient air via heat exchanger surfaces within the EDC, with the help of an air flow generated by fans. Usually, a water–glycol or water–bioethanol mixture is used as the heat transfer medium. In smaller systems, the refrigerant of the chiller is also used directly. The heat and cooling functioning of an EDC are shown in Fig. 6.

The structure of an EDC is quite simple. It consists of three main components: A housing, a finned heat exchanger and the fans. Due to space cooling processes in the building, waste heat accumulates at a chiller, which is led to the EDC via a water circuit. Here, the water which is at a high temperature level is led through copper pipes within the heat exchanger. To increase the heat exchanger surface, fins are placed along the piping. Fans are mounted on the top of the housing. This creates an air flow through the heat exchanger to cool down the heat transfer medium in the pipes.

By this process a corresponding amount of heat is released into the ambient air depending on the ambient conditions (temperature, moisture, etc.). The ambient air temperature must therefore be colder than the medium for cooling purposes. On the other hand, the EDC can also be used as a heat source for 5GDHC with ambient air temperature warmer than the networks fluid temperature. The energy thus obtained from the air is then transferred to a 5GDHC and can be used for heating purposes via heat pumps that are connected to the network.

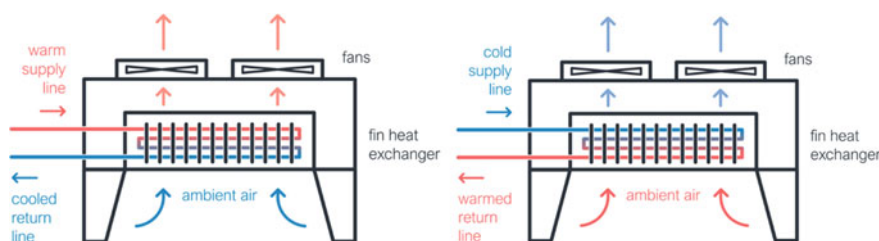


Fig. 6 Scenarios of an EDC as a source for heating and cooling energy (*Source* Energie PLUS Concept GmbH)

2.5.1 Advantages and Disadvantages of an EDC

The major advantages of EDCs are their small space requirement and modularity. It is possible to place the EDC on flat roofs or similar objects next to the 5GDHC, thus making them largely invisible to the end user. In addition, it is possible to interconnect identical EDCs and expand them cost-effectively in the case of future grid extensions.

Another advantage of EDCs is primarily in the investment costs. They are significantly lower compared to other technologies. The EDC can be operated bidirectionally, i.e. for both heating and cooling. Particularly in large mixed districts with a high waste heat potential, the original mode of operation of the EDC can be used.

The main disadvantage of an EDC is the emission of sound. Due to the installed fans and high-volume flows through the heat exchanger, noticeable audible noise emission can increase. Therefore, care must be taken to comply with the official guidelines regarding noise emission in the building area and, if necessary, a sound-insulated has to be found.

Due to the fluctuating ambient air temperatures during the year in temperate regions, a pure heat supply via the outside air is not suitable for efficiency reasons. Especially in the winter months, the operation of an EDC as a heat source is often not economical. Due to thermodynamic conversion processes icing on the fins of the heat exchanger even in the low positive temperature range can cause. This would lead to reduced efficiencies and damages to the EDC. In addition, the annual coefficient of performance of heat pumps is strongly depending on the source temperatures. However, in the case of an EDC the ambient temperatures are very low in the period of highest heat demand.

The operation of the EDC during the summer months can offer optimal conditions for generating source heat from ambient air. However, during this phase the heat demand is usually very low. The generated surpluses during that period can be used within a 5GDHC for regeneration purposes of other heat sources or at heat storages. For this reason, EDC should never be the only heat source for a 5GDHC network but always be operated in combination with other heat sources. The networks temperature should not rise to much in order of space cooling supply to the connected buildings.

Pros:

- Small space requirements and modularity
- Cost efficient
- Heating and cooling
- Regeneration energy for ground heat exchanger

Cons:

- Sound emissions
- Fluctuating air temperature
- Lowest efficiency at highest heat demand

2.5.2 Application Scenarios of EDCs

There is a big potential in using an EDC in combination with one or more environmental heat sources i.e., ground heat exchangers with heat storage potential. This is because the EDC shows its strengths in the transitional periods in spring and autumn. During that time the heat demand of households is in the partial load range, while the ambient air temperature enables the absorption of air heat. In addition, heat surpluses can be stored inside a geothermal heat exchanger (vertical or horizontal) which improves the heat extraction potential for the next heating period.

2.6 *Examples of 5GDHC with different Heat Sources in Germany*

In Germany there are a lot of 5GDHC networks built since 2010. Some of them are part of research projects for further development of these technologies. Different heat sources are used and tested. The following examples describe 5GDHC for heat pumps by using large-scale geothermal collector systems or frozen soil storages.

2.6.1 LSC with Active 5GDHC in Bad Nauheim (KNW-Opt)

The information of the chapter is based on the paper in [31]. Since 2018 a 5GDHC with a LSC in Germany was planned and built in Bad Nauheim. In early 2019 the double layer collector system with 11,000 m² per layer (1.5 m and 3.0 m depth) has been installed. It is connected to the 6 km long (one way) active 5GDHC network. The system provides around 2.3 GWh of source heat per year to more than 400 residential units. During this time, it was the largest known geothermal collector system in Germany. Since 2020 the project is supported via the research project KNW-Opt (Grant Number: 03EN3020, funded by the German Federal Ministry for Economic Affairs and Climate Action). Figure 7 gives an overview of the total project site.

The LSC was built below an agricultural cultivated field (Fig. 8) 600 m away from the district. Because of the earth's double usage food and energy can be generated at the same time.

With decentral HP's the source heat from the LSC and the 5GDHC is made usable to the new built single- and multifamily buildings (Fig. 9). In addition, due to the temperature levels of this system cooling during the summer period is possible. Early investigations have shown that the earth's temperatures between the two collector layers is going to drop below freezing point in the late winter months, which results in significant icing around and between the collector pipes. It is not that much that normal ground freezing at the top of the soil and the collector's icing can connect which would lead to soil changes (lifting and sinking). This low tempered soil remains

Fig. 7 Schematic view of the project site with its LSC and 5GDHC (Source Zeh et al. [31])

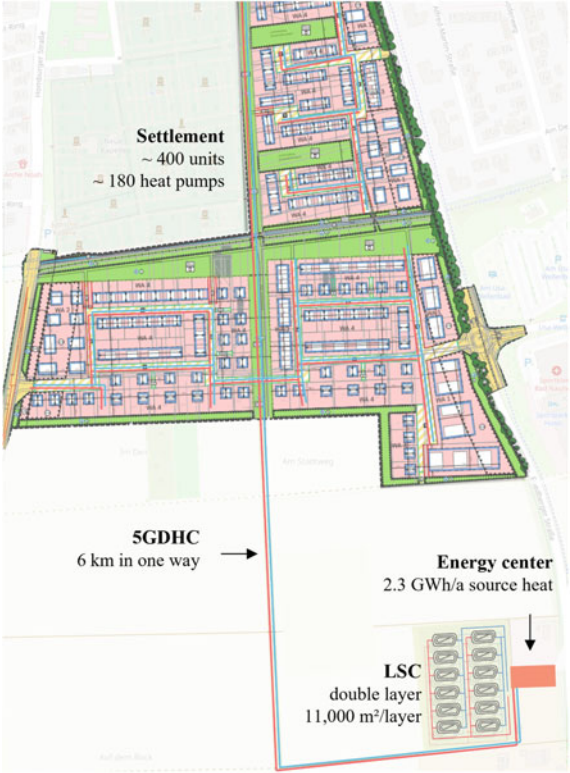


Fig. 8 Building site of the LSC during 2019 (Source Steinhäuser GmbH & Co.KG)



Fig. 9 District with 400 residential units under construction (16.03.2022) (Source Zeh et al. [31])

in the lower layer of the collector until the summer months and can serve cooling energy. This was made possible because the two layers can be controlled individually. From spring up to early summer months mostly the upper layer is used for serving source heat. Solar irradiation and precipitation will force the upper layer to fast regeneration. In the summer months mainly the lower layer is mainly used to serve the buildings cooling demand. During that the excess heat from the buildings serves the regeneration energy for the lower layer. It is also possible that energy can be stored in the lower layers surrounding soil to serve heating energy during the winter period. In this time both layers are going to be used.

The supplied settlement with the 5GDHC is connected to the double layer collector via a 600 m long feeding pipe (DN400) which works as an extension of the LSC. The total network length is more than 13 km in total. Therefore, three redundant feeding pumps were installed inside the energy center (Fig. 10) to ensure a permanent fluid flow. At maximum heat consumption two of the three pressure-controlled pumps are running at full capacity. One pump is installed redundantly to ensure heat supply at every time. Because of this the use of the feeding pumps is going to rotate by time to keep the wear equal.

Figure 11 shows the analysis of the hourly efficiency of one monitored HP. The coefficient of performance (COP) is compared with the average monthly source temperature which is measured directly at the HP. The daily COP of the HP is shown in the boxplot diagram for monthly analysis.

The boxes center line shows the average COP during that month. During the summer period the HP is only running for hot water production which results in lower efficiencies even though the source temperature is relatively high. Since October, the need of space heating increases. At that time the HP runs at its best efficiency because of high source temperatures. During winter months the COP decreases following



Fig. 10 Energy center with three redundant feeding pumps (Source Zeh et al. [31])

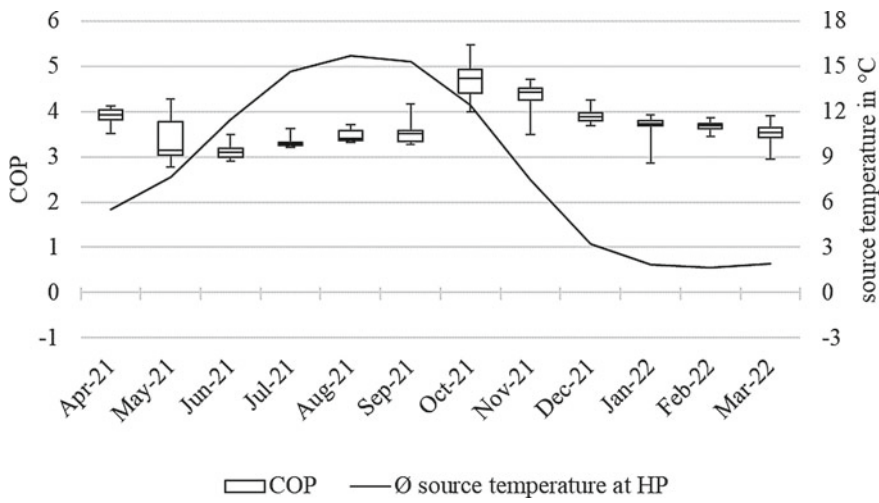


Fig. 11 Analysis of one HP's monitoring data and its source temperatures from April 2021 to March 2022 (Source Zeh et al. [31])

the source temperature but with a temporal delay. The seasonal coefficient of performance (SCOP) of this one HP is at 3.9. This means that 1 kWh of electricity produces 3.9 kWh of heating energy within the HP.

For Fig. 12 the measured source temperature of 24 HP's was analyzed and compared to the LSC's source temperature since April 2021. It turns out that the source temperature at the HP's is always higher during the whole heating season than

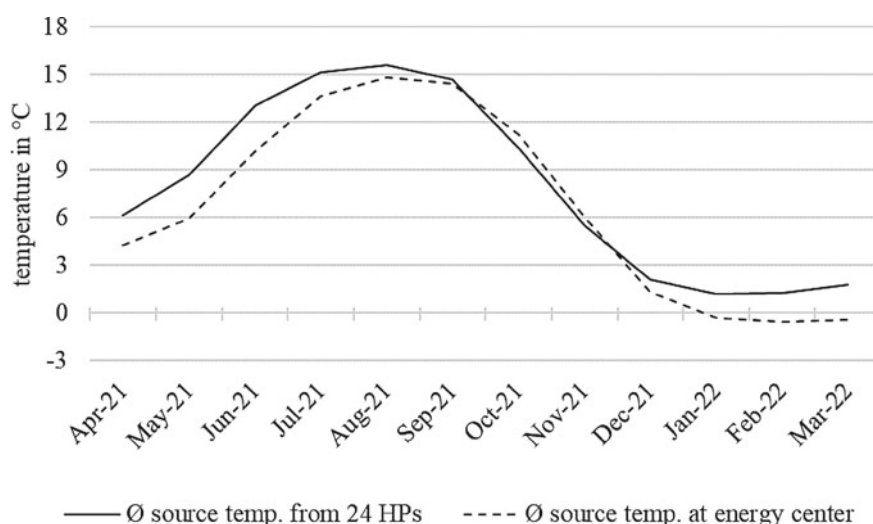


Fig. 12 Comparison of source temperature at different locations (at the energy center, average of 24 buildings) (Source Zeh et al. [31])

the LSC's source temperature. This shows the enormous potential of the 5GDHC network which is working as a heat source itself. The farther the heat source is located away from the settlement and the lower the fluid temperature, the more energy can be gained through the network itself. During planning phase, the simulation data showed that the network itself can deliver around 40% to 50% of the source's energy demand. While the collector system is running around freezing temperatures the network can deliver source energy at a temperature level of around 2 °C higher, which results in higher efficiencies of the HP's. During summer months the average source temperature at the HPs and the source temperature at the collector level are going to be equal caused of solar regeneration and cooling.

2.6.2 FSS with Hybrid 5GDHC in Schleswig (ErdEis II)

The information of the chapter is partly based on the paper in [30]. Since 2019, as part of the "ErdEis II" research project (Grant Number: 03ET1634, funded by the German Federal Ministry for Economic Affairs and Climate Action), a FSS has been implemented for the first time. In Schleswig, a town in northern Germany, a new construction area with approx. 60 residential units and a fire station is to be built. The buildings have decentralised heat pumps and will be supplied via a 5GDHC with very shallow geothermal energy. The first residential buildings were built in 2022. The fire station is already supplied by the 5GDHC. The total heat demand for heating and domestic hot water is projected to about 500 MWh per year. Due to the low temperatures of the



Fig. 13 Installation of the large-scale collector below the green area (*Source* Energie PLUS Concept GmbH)

5GDHC, it is possible to cool the buildings in summer and at the same time use the waste heat to regenerate the geothermal fields (FSS and LSC).

The construction area is supplied with source heat via two FSS and two LSC. In addition, a total of 40 m² of photovoltaic and thermal (PVT) collectors installed on the roof of the fire station, which feed additional heat into the 5GDHC, especially in summer.

The two LSCs each have a collector area of 1,000 m². Figure 13 shows the installation of the LSC below the green area.

The two FSS are identical in design and each FSS has a total collector area of around 1,000 m², divided into four layers. The layers are square and adapted to the slope, i.e. they become smaller towards the bottom. The top layer, which is the largest, has an area of about 340 m². Both the FSS and the LSC have a covering of about 1.5 m. Figure 14 shows the installation of the FSS under the green area. In Fig. 15, a vertical section shows the GPS data of the collector modules of the FSS, the light blue line represents the ground surface.

In order to investigate the behaviour under different installation conditions, one FSS and LSC each were installed under a green area and the other two under a rain retention basin. In this way, it can be investigated how advantageous the installation under a rain retention basin is. According to German law [32], rain should be infiltrated close to the site or discharged into a water body. The further increase of settlement and traffic areas therefore causes the demand for rain retention basins to increase further [33].

The aim of the research project is to test the functioning of the FSS and to develop strategies for its operation in combination with other heat sources. Especially the PVT collectors are an optimal complement to the FSS. They provide heat during the transition periods and during summer, which can be used to regenerate the lower



Fig. 14 Installation of the Frozen Soil Storage below the green area (*Source* Friedrich-Alexander University Erlangen-Nürnberg)

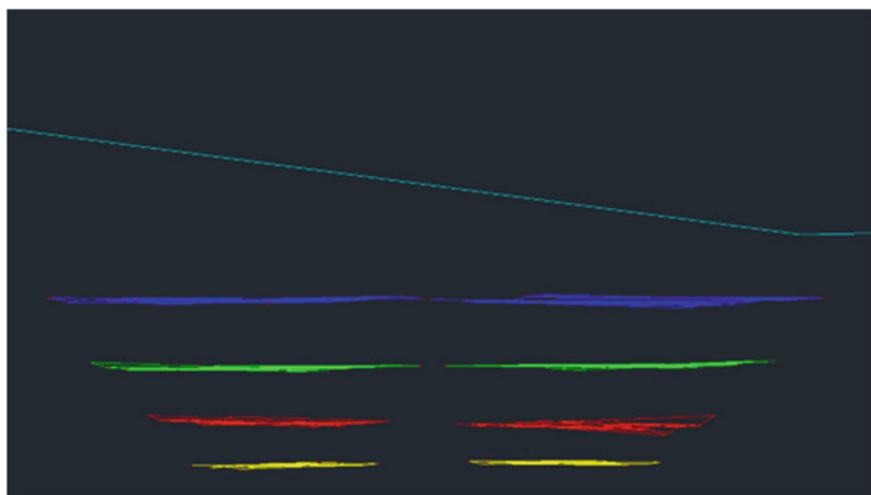


Fig. 15 GPS data of the collector modules of the FSS in a vertical section (*Source* Energie PLUS Concept GmbH)

layers of the FSS. In operation, it will become clear how the dynamic relationships between the FSS, LSC, PVT collectors and the 5GDHC will look like.

In order to be able to test different operating strategies, an elaborate hydraulic concept was developed. This makes it possible to direct the waste heat from the buildings and the PVT collectors to individual parts of the geothermal fields in a targeted manner during the transition periods and in summer. For example, the lower

layers of the FSS can be regenerated in a targeted manner. Similarly, all geothermal fields can be opened and closed independently.

If the FSS and LSC are sufficiently regenerated in summer, the waste heat from the PVT collectors can also be directed downstream of the geothermal fields into the flow of the heat pumps to raise the flow temperature as much as possible. In this way, the coefficient of performance and thus the electricity consumption of the heat pumps can be improved.

If the cooling demand of the buildings is higher, the LSC and the top layer of the FSS can be used for cooling initially at the beginning of summer. This way, there is enough cooling potential in the lower layers of the FSS until the end of summer. The 5GDHC was planned as a so-called hybrid network. For a large part of the year, the network is operated passively, which means that the decentralized heat pumps in the buildings can independently overcome the pressure loss across the network and the heat sources. At times of high volume flows in the network or when only individual heat sources are operated, the network switches to active operation due to the increased pressure loss. In this mode, central circulation pumps are switched in to support the decentralized heat pumps in overcoming the pressure loss.

2.6.3 Large-Scale Geothermal Collector System Below a Multi-Used District (+EQ-Net II)

The information of the chapter is based on the paper in [34]. From 2017 to 2020 the residential and commercial building puls^G was built south of Munich in the town of Geretsried. The building puls^G is framed in an urban context. It contains a full-range provider on the first floor with a floor area of approx. 2,000 m². The second-floor houses seven commercial units with a floor space of approx. 1,000 m². Moreover, the floors three to seven have 66 residential units ranging from 30 m² to 130 m². This residential and commercial building can be seen in Fig. 16. During the research project + EQ-Net II (Grant Number: 03EN1046, funded by the German Federal Ministry for Economic Affairs and Climate Action) an operational optimization of the multivalent plant technology is to be carried out by analyzing measurement data of the extensively installed monitoring.

The energy center in the basement contains a multivalent plant technology using CHPs, water-water heat pumps connected to a large-scale geothermal system, brine-water heat pumps connected to an exhaust air heat recovery system and a photovoltaic system on the building's roof. The large-scale geothermal system consists of 13 individual geothermal collectors exploiting the local vSGP. In total a withdrawal area of approx. 2,100 m² is established below the building's underground car parking. The executed installation method of the geothermal collectors can be seen in Fig. 17.

The GHE's are cast in single-grain concrete to ensure a thermal influence of the local groundwater flow. Due to a missing impact of solar irradiation and precipitation of the sealed area the local groundwater flow has a major influence on the geothermal collector's regeneration. Besides the regeneration via the groundwater flow, there are interfaces that enable the storage of waste heat of the full-range provider's cooling



Fig. 16 Residential and commercial building puls^G (*Source* Nuremberg Tech)

Fig. 17 Installation method of the GHE's (*Source* University of Applied Sciences Munich)



unit in the geothermal system. Moreover, the geothermal collector system provides cooling energy for the seven commercial units in the building. The resulting thermal energy on a higher temperature level can also be stored in the geothermal system. Due to this complex connection between energy extraction, energy storage and regeneration, the analysis of the regulation and energy flow of the geothermal collectors is a main task of the research project + EQ-Net II. Based on the results the control of the geothermal collector system should be optimized. In a first step, the analyzed monitoring data shows that the large-scale geothermal collector provides a non-negligible amount of thermal energy for the supply of the building's thermal energy demand. In the year 2021, the building's thermal energy demand was covered by approximately 30% with source energy of the geothermal collector system. However, a first analysis of the geothermal collectors' performance showed a wide range of specific source energy extraction values among the geothermal collectors. A differentiation of the extracted source energy in waste heat, cooling energy and energy input of the groundwater flow is not carried out. The diagram in Fig. 18 shows the different source energy extraction among the 13 geothermal collectors in 2021. The average source extraction of all geothermal collectors is approximately 66 kWh/m^2 .

As presented in the diagram, there is a wide gap between geothermal collectors, mainly geothermal collector 1, 6, 2, 3, 5, with an over averaged performance. Geothermal collectors 8, 9, 11, 10 and 12 show an under-average performance. The reason for this behavior lies in a different mass flow distribution at each collector branch.

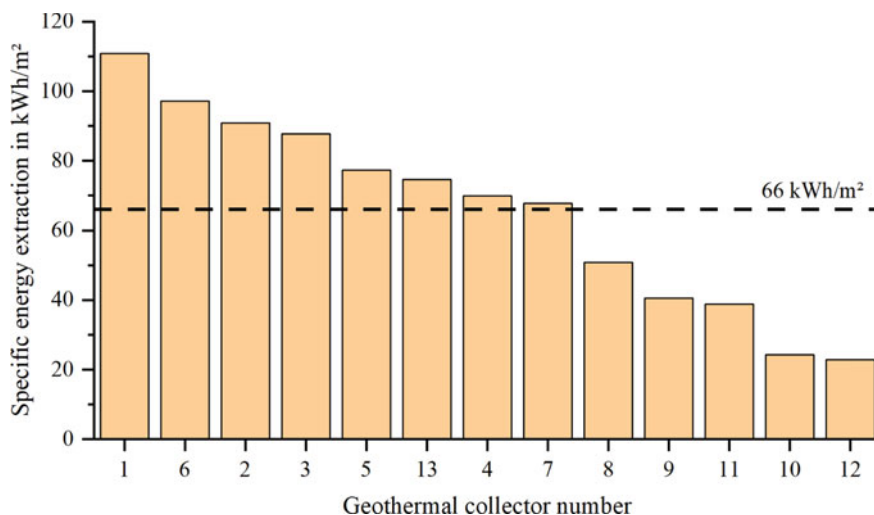


Fig. 18 Specific source energy extraction in 2021 among the 13 geothermal collectors (Source Schmid, Stockinger [34])

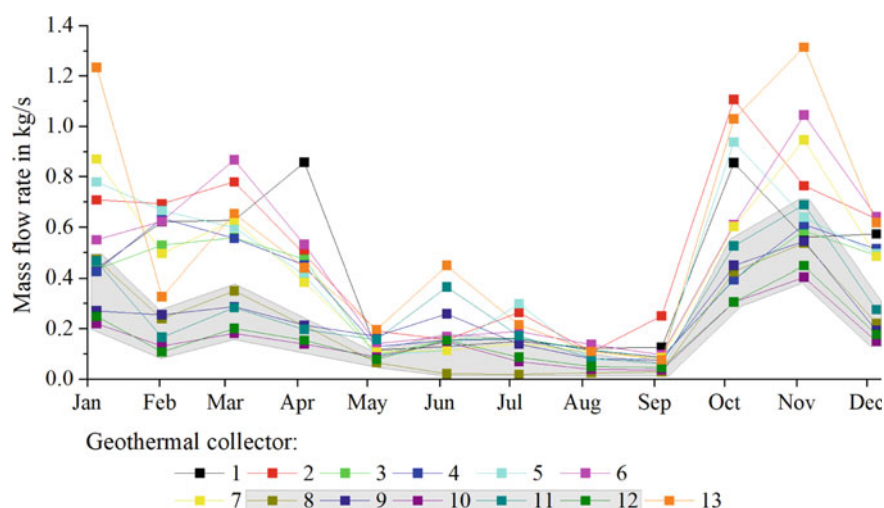


Fig. 19 Mean Mass flow rates in each geothermal collector in 2021 (Source Schmid, Stockinger [34])

By analyzing the mass flow rates flowing through each geothermal collector one can recognize a correlation between the low specific energy extraction and the low mass flow rates in geothermal collectors 8, 9, 11, 10 and 12. This is shown in Fig. 19.

In conclusion, analyzing and evaluating data from a monitoring project can discover optimization potentials in a LSC. A wrong distribution of mass flow rates in the LSC can lead to lower specific energy extractions and thus to a lower performance. An optimization measure can be derived by checking the hydraulic system and “open” the nozzles for the geothermal collector branches with a low performance.

References

1. Rezaie B, Rosen MA (2012) District heating and cooling: Review of technology and potential enhancements. *Appl Energy* 93:2–10. <https://doi.org/10.1016/j.apenergy.2011.04.020>
2. Lund H, Werner S, Wiltshire R, Svendsen S, Thorsen JE, Hvelplund F et al (2014) 4th Generation district heating (4GDH). Integrating smart thermal grids into future sustainable energy systems. *Energy* 68:1e11. <https://doi.org/10.1016/j.energy.2014.02.089>
3. Zeh R, Ohlsen B, Philipp D, Bertermann D, Kotz T, Jocić N, Stockinger V (2021) Large-scale geothermal collector systems for 5th generation district heating and cooling networks. *Sustainability* 13:6035. <https://doi.org/10.3390/su13116035>
4. Lund H, Ostergaard PA, Nielsen TB, Werner S, Thorsen JE, Gudmundsson O, Arabkoohsar A, Mathiesen BV (2021) Perspectives on fourth and fifth generation district heating. *Energy* 227:120520. <https://doi.org/10.1016/j.energy.2021.120520>
5. Stănișteanu C (2017) Smart thermal grids—a review. <https://doi.org/10.1515/SBEEF-2016-0030>

6. Buffa S, Cozzini M, D'Antoni M, Baratieri R (2019) 5th generation district heating and cooling systems: a review of existing case in Europe. *Renew Sustain Energy Rev* 104:504–522. <https://doi.org/10.1016/j.rser.2018.12.059>
7. Weidlich I, Kaltschmitt M, Streicher W, Wiese A (2020) Wärmenetze, in *Erneuerbare Energien*, Berlin, Heidelberg, Springer Vieweg, pp 1203–1225. 2020. https://doi.org/10.1007/978-3-662-61190-6_16
8. Zeh R, Stockinger V (2018) Kalte Nahwärme—Wärme- und Kälteversorgung der Zukunft für Quartiere. *Ingenieur Spiegel* 1:24–25
9. Boesten S, Ivens W, Dekker SC, Eijndems H (2019) 5th generation district heating and cooling systems as a solution for renewable urban thermal energy supply. <https://doi.org/10.5194/adgeo-49-129-2019>
10. Bünning F, Wetter M, Fuchs M, Müller D (2017) Bidirectional low temperature district energy systems with agent-based control: performance comparison and operation optimization. *Appl Energy*. <https://doi.org/10.1016/j.apenergy.2017.10.072>
11. Østergaard D, Svendsen S (2017) Space heating with ultra-low-temperature district heating—a case study of four single-family houses from 1980s. In: *Proceedings of the 15th international symposium on district heating and cooling*, Energy Procedia, vol 116, pp 226–235. <https://doi.org/10.1016/j.egypro.2017.05.070>
12. Brennenstuhl M, Zeh R, Otto R, Pesch R, Stockinger V, Pietruschka D (2019) Report on a plus-energy district with low-temperature DHC network, novel agrothermal heat source, and applied demand response. *Appl Sci* 9(23). <https://doi.org/10.3390/app9235059>
13. Barone G, Buonomano A, Forzano C, Palombo A (2020) A novel dynamic simulation model for the thermo-economic analysis and optimisation of district heating systems. *Energy Convers Manage* 220:113052. <https://doi.org/10.1016/j.enconman.2020.113052>
14. Allen A, Henze G, Baker K, Pavlak G, Long N, Fu Y (2020) A topology optimization framework to facilitate adoption of advanced district thermal energy systems. In: *IOP conference series: earth and environmental science* (Vol 588, No 2, p 022054). IOP Publishing. <https://doi.org/10.1088/1755-1315/588/2/022054>
15. Wirtz M, Kivilip L, Remmen P, Müller D (2020) 5th generation district heating: a novel design approach based on mathematical optimization. *Appl Energy* 260:114158. <https://doi.org/10.1016/j.apenergy.2019.114158>
16. 6. Zwischenbericht ErdEis II, EnEff: Wärme: ErdEisII: Erdeisspeicher und oberflächennahe Geothermie, 11.02.2022
17. Hähnlein S, Bayer P, Ferguson G, Blum P (2013) Sustainability and policy for the thermal use of shallow geothermal energy. *Energy Policy* 59:914–925. <https://doi.org/10.1016/j.enpol.2013.04.040>
18. Bertermann D, Klug H, Morper-Busch L, Bialas C (2014) Modelling vSGPs (very shallow geothermal potentials) in selected CSAs (case study areas). *Energy* 71:226–244. <https://doi.org/10.1016/j.energy.2014.04.054>
19. Bertermann D, Schwarz H (2017) Laboratory device to analyse the impact of soil properties on electrical and thermal conductivity. *Int Agrophysics* 31:157–166. <https://doi.org/10.1515/intag-2016-0048>
20. Schwarz H, Bertermann D (2020) Mediate relation between electrical and thermal conductivity of soil. *Géoméch. Geophys Geo-Energy Geo-Resources* 6:1–16. <https://doi.org/10.1007/s40948-020-00173-x>
21. Bertermann D, Klug H, Morper-Busch L (2015) A pan-European planning basis for estimating the very shallow geothermal energy potentials. *Renew Energy* 75:335–347. <https://doi.org/10.1016/j.renene.2014.09.033>
22. Martinopoulos G, Papakostas K, Papadopoulos AM (2018) A comparative review of heating systems in EU countries, based on efficiency and fuel cost. *Renew Sustain Energy Rev* 90:687–699. <https://doi.org/10.1016/j.rser.2018.03.060>
23. Boban L, Miše D, Herceg S, Soldo V (2021) Application and design aspects of ground heat exchangers. *Energies* 14:2134. <https://doi.org/10.3390/en14082134>

24. STWB SB (2020) 7,65 Millionen Euro vom Bund für energieeffiziente Wärme im Bamberger Konversionsquartier Lagarde. Presseinformation: Stadtwerke Bamberg GmbH
25. Hahn J, Lauterbach S, Jensch W (2021) Netzdienliche Quartiere—Von der Konzeption bis zum Betrieb. in INUAS Konferenz Urbane Transformationen, München, HM Hochschule München, pp 50–53. <https://www.researchgate.net/publication/349595030>
26. Stäudinger V, Jensch W, Stockinger V (2019) ErdEis—Erdeisspeicher und oberflächennahe Geothermie,“ Hochschule München. <https://www.researchgate.net/publication/334988393>
27. Sulzer M, Hangartner D (2014) Grundlagen-/Thesen Kalte Fernwärme (Anergienetze). Hochschule Luzern Technik & Architektur, pp 1–10
28. Hirsch H, Petzold H, Grunewald J (2019) Efficiency and area demand of multilayer ground heat exchanger using phase change of water. CESBP. <https://doi.org/10.1051/mateconf/201928202027>
29. Hirsch H, Hüsing F, Rockendorf G (2019) Modellierung oberflächennaher Erdwärmeübertrager für Systemsimulationen in TRNSYS. Dresden: BauSIM 2016
30. Ohlsen B, Stockinger V (2022) Possible applications of a Frozen Soil Storage and linking with other heat sources. European Geothermal Congress
31. Zeh R, Stockinger V (2022) Monitoring of a large-scale geothermal collector system and a SGDHC in Bad Nauheim. European Geothermal Congress
32. Section 55 (2) of the German Federal Water Act (Wasserhaushaltsgesetz)
33. Brombach H (2010) Im Spiegel der Statistik: Abwasserkanalisation und Regenwasserbehandlung in Deutschland. Korrespondenz Abwasser Abfall 57(1):183
34. Schmid M, Stockinger V (2022) Monitoring and first analysis of a large-scale geothermal collector system under a residential and commercial building. European Geothermal Congress

Techno-Economic Assessment of Shallow Geothermal Heat Pump System with Energy Piles



Yuanlong Cui, Jie Zhu, and Hui Tong

Abstract Shallow geothermal heat pump system has been extensively applied to commercial and residential buildings owing to its high-energy efficiency and low operating cost. The book chapter aims to investigate the energy performance of the energy piles for a shallow geothermal heat pump system, and analyse the influence of “thermal short-circuiting” between two pipes of a U-tube based on the finite volume method. Additionally, the economic feasibility analysis is performed by using the Monto Carlo simulation approach. It is found that the heat pump (heating and cooling) could achieve annual average COP of 3.63 and EER of 4.62. Meanwhile, when the shank spacing could be controlled between 0.06 and 0.10 m and the fluid flow rate is in a range of 0.5–0.7 m³/h, this contributes to avoiding the low outlet fluid temperature and decreasing the influence of “thermal short-circuiting”. Furthermore, the life cycle cost evaluation demonstrates that the system net present value is approximately £26,095 with 4.31 years of payback period at the market discount rate of 8.75% for a 20-year operating period, which is sensitive to the main parameters including electricity price, capital investment and energy production. And also, it is indicated that the low discount rate and high energy production are beneficial to the system with the high NPV and cash flows.

Keywords Energy pile · Techno-Economic model · Heat pump COP · Net present value · Payback period

1 Introduction

The quick growth of population and accelerating process of urban modernization cause a greater requirement for energy consumption. In comparison to the 1990 year,

Y. Cui (✉) · H. Tong
School of Architecture and Urban Planning, Shandong Jianzhu University, 1000 Fengming Road,
Jinan 250101, China
e-mail: cuiyuanlong22@sdjzu.edu.cn

J. Zhu
Department of Architecture and Built Environment, The University of Nottingham,
Nottingham NG7 2RD, UK

it is recorded that the energy consumption until 2050 could be raised by 275% [1]. Nevertheless, a great part of energy utilization for power, space heating and cooling comes in the form of burning fossil fuels [2], which are restricted available and threaten to the environment [3]. Hence, energy pile (EP), as a renewable technology, not only provides structure loads but also extracts soil thermal energy for building energy demands [4]. Specifically, EP is realized via combining geothermal heat exchanger pipes into a reinforced concrete pile as shown in Fig. 1, which contributes to saving the extra borehole drilling cost required by the normal geothermal heat pump (GHP) system [5]. Additionally, the thermal property of concrete EP is better compared to traditional GHP materials [6].

The merit of EP system is its dual functions as building structural element and heat exchanger. In the meantime, concrete is employed as an ideal heat transfer medium between soil and heat exchanger due to its high thermal conductivity and thermal energy storage capacity [7, 8]. It is demonstrated that the EP unit could save about 75% energy compared with the traditional air conditioning unit [9–11]. In the past decades, there are a large of EP units installed in Europe, particularly in Germany, Austria, United Kingdom and Switzerland, such as international solar centre in Berlin [12], multi-purpose hall in Austria [13], Keble College in Oxford [14] and Dock Midfield Zurich airport [15].

Recently, the performance enhancement of the EP system has received more attentions, owing to the fact that it is one of the most effective measures for building air conditioning, hence, some research works have been performed to investigate its heat transfer features. Han et al. [16] assessed the technical, economic and environmental

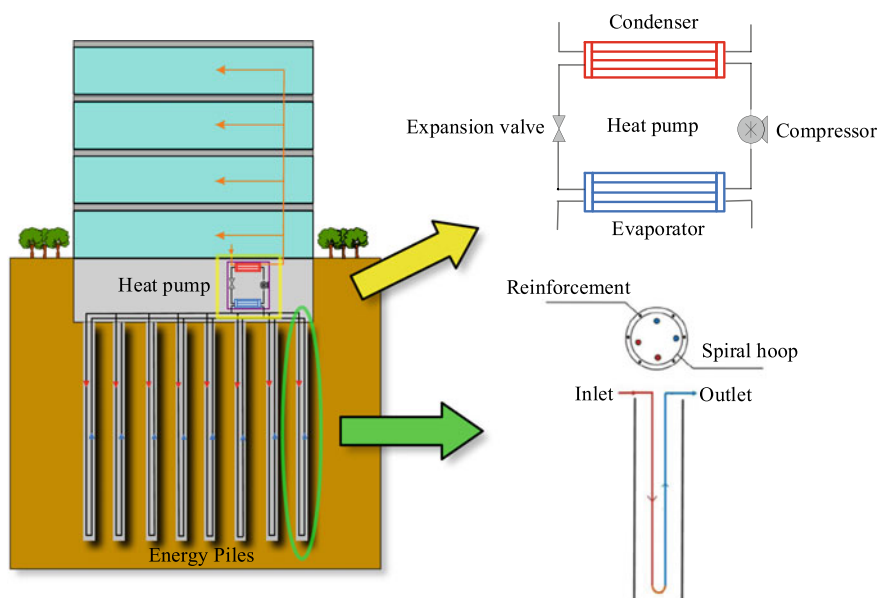


Fig. 1 The schematic diagram of EP unit

profits of energy pile unit applied in building based on different weather conditions in China, and demonstrated that the energy saving varies from 19 to 45%, resulting in 21–40% of cost-saving and 25–36% of CO₂ emission decline. Zhong et al. [17] investigated experimentally and numerically the thermal performance of energy pile system, and revealed that 70–80% of thermal energy can be delivered when the 1/3 of piles are operated, whereas when the 1/2 of the piles are activated 50–60% of thermal energy could be provided. Mousa et al. [18] developed a 3D finite element model to investigate the influences of phase change material (PCM) on the EP performance, and found that the utilizing of multiple PCM contributes to increasing the system performance and heat pump coefficient of performance (COP) reaching 26% and 5.28%, respectively, due to high latent heat capacity of the PCM. Bimaganbetova et al. [19] analysed the thermal–mechanical effects of EP, and concluded that the thermal mechanical loading contributes to decreasing the critical tensile stresses and changing stress distributions on the surface of the pile owing to air pressure. Lee et al. [20] investigated a EP integrated with novel steel pipe heat exchangers (SPHXs) to enhance the thermal performance as replacing for deformed rebars to reinforce concrete. It is demonstrated that the heat extracted from soil could reach 159.5 W/m, which is 30% superior than that of the normal cast-in-place EP system. Ng et al. [21] performed an experimental test of EP unit to study the influences of pile spacing on the serviceability of floating EP units based on the non-symmetrical thermal loading. It is concluded that the 5 diameter pile spacing has the minimise thermal interaction to meet the serviceability criteria within thermally sensitive soft clay.

Due to the advantages of the EP system, lots of researches concentration on the economic evaluation through various economic indicators, life cycle assessment (LCA) [22], discounted cash flow analysis (DCFA) [23], Bin method [24], Monte Carlo method [25], life cycle cost (LCC) [24], simple payback period (SPB) and discounted payback period (DPB) [26, 27]. Specifically, Zhou et al. [28] implemented an economic sensitivity analysis of EP system based on the Taguchi method in China, and concluded that the values of net present value (NPV) could be enhanced from 8567.7 to 15,063.9 CNY, with an increment rate of 75.82%. Ren et al. [27] assessed an economic profit of the EP systems with both polyethylene (PE) and steel heat exchangers in China, and found that the capital of the PE heat exchangers is higher than steel one by 35.2%, and the payback periods of the PE and steel heat exchangers are around 3.45 and 1.83 years, respectively. Arat and Arslan [29] carried out an NPV assessment for a EP system to provide heating for a town centre in Turkey based on the life cycle method, and found that the NPV varies from US\$ 1192.81 to US\$ 23.20 million. Morrone et al. [26] analysed the cost effectiveness between EP and traditional units for NPV and payback period (PP) in Italy, and revealed that the cost of EPs unit in Naples could be saved about 20% with 8 years of PP, whereas the saving in Milan could reach about 10% with 4 years of PP, respectively, compared normal system.

Based on the above-mentioned techno-economic assessments of various EP systems, many researches have been investigated in terms of the energy performance and economic analysis, the long-term performance assessment is one of the

challenges to integrate the system into domestic building. Additionally, the main obstacles in using life cycle method involve life of assets, erratic economic alteration, uncertainty factors concerning interest and discount rates, as well as future maintenance expense, NPV and payback period. The aim of this paper is to evaluate the techno-economic features of an EP system for a long-term operating period. The system seasonal operating performance, soil heat extracted/rejected rates, annual heating and cooling energy generation, the effects of the thermal circulating and fluid flow rate on heat transfer rate are all obtained via the Engineering Equation Solver (EES) software. Moreover, the system LCC assessment is performed based on the @Risk software considering the time value of the money to investigate the NPV and cumulative energy cost savings for 20 years of service lifetime. The key factors are taken into account in the complete LCC analysis, these include inflation rate, income tax rate, discount rate, interest rate, capital investment (CI), loan payment (LP), system energy cost (SEC), maintenance cost (MC), periodic cost (PC), present value (PV) of money and cumulative EP system savings (EPS). Meanwhile, the payback period is also obtained according to the values of cash flows and cumulative system energy cost (SEC) savings.

2 Numerical Models

In order to establish a 3D transient heat transfer model, the working fluid flow region and energy formulations of inlet and outlet pipes are established separately owing to the different flow directions.

2.1 *Single BHE Model*

2.1.1 Equivalent Geometry Approximation

The heat transfer model is developed based on the “equivalent pipe approach” as illustrated in Fig. 2. Specifically, the U-tube circular cross-section is substituted by a rectangular one, and the equivalent pipe sides are determined to guarantee the equal heat transfer rates after the transformation.

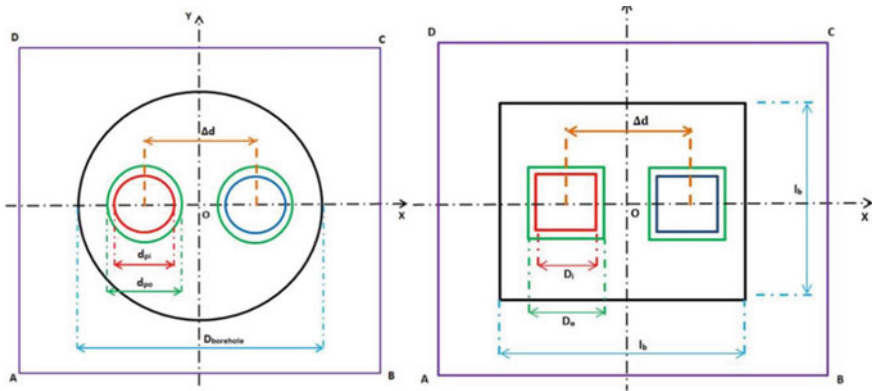


Fig. 2 Schematic diagram of equivalent pipe approach

The thermal capacity of the working fluid is the same within the two regions:

$$\rho_f c_f \frac{\pi d_{pi}^2}{4} = \rho_f c_f D_i^2 \quad (1)$$

$$D_i = \frac{\sqrt{\pi}}{2} d_{pi} \quad (2)$$

$$\rho_p c_p \frac{\pi (d_{po}^2 - d_{pi}^2)}{4} = \rho_p c_p (D_o^2 - D_i^2) \quad (3)$$

$$D_o = \sqrt{\frac{\pi}{4} (d_{po}^2 - d_{pi}^2) + D_i^2} \quad (4)$$

The equivalent fluid temperature gradient in the two regions is given as:

$$\mu \rho_f c_f \frac{\pi d_{pi}^2}{4} = \mu' \rho_f c_f D_i^2 \quad (5)$$

where ρ_f , ρ_p are the densities of working fluid and pipe material (kg/m^3); c_f , c_p are the thermal capacities of working fluid and pipe material, ($\text{J/kg} \cdot ^\circ\text{C}$); D_i , D_o are the lengths of inner and outer equivalent sides (m); d_{po} , d_{pi} are the pipe inner and outer diameters (m); μ , μ' are the working fluid velocities within the U-tube and equivalent pipe (m/s).

The thermal resistance in the circle section is expressed as:

$$R_c = \frac{1}{\frac{1}{h\pi d_{pi}} + \frac{1}{2\pi k_p} \ln \frac{d_{po}}{d_{pi}}} \quad (6)$$

The thermal resistance in the rectangular section is written as:

$$R_s = \frac{2(D_i + D_o)}{\frac{1}{h_s} + \frac{D_o - D_i}{2k_p}} \quad (7)$$

Hence, the heat convection coefficient of the rectangular pipe is given as:

$$h_s = \frac{1}{\frac{2(D_o + D_i)}{h_c \pi d_{pi}} + \frac{D_o + D_i}{\pi k_p} \ln \frac{d_{po}}{d_{pi}} - \frac{D_o - D_i}{2k_p}} \quad (8)$$

where R is the thermal resistances ($^{\circ}\text{C}/\text{W}$); k is the thermal conductivity ($\text{W}/\text{m}^{\circ}\text{C}$); δ is the wall thickness (m); h is the heat convection coefficients ($\text{W}/\text{m}^2 \cdot ^{\circ}\text{C}$).

To ensure the equivalent thermal capacity for the borehole, the square borehole area is expressed as:

$$\rho_g c_g \left(\frac{\pi d_b^2}{4} - 2 \times \frac{\pi}{4} d_{po}^2 \right) = \rho_g c_g (l_b^2 - 2 \times D_o^2) \quad (9)$$

$$l_b = \sqrt{\frac{\pi d_b^2}{4} - \frac{\pi}{2} d_{po}^2 + 2D_o^2} \quad (10)$$

where d_b is the borehole diameter (m); ρ_g is the density of grout (kg/m^3); l_b is the side length of equivalent borehole (m).

2.1.2 Energy Balance in the Solid Region

Heat transfer in energy pile is classified into two separated regions, one is solid region, and one is working fluid region. The solid region includes soil, grout and pipe. Henceforth, the energy balance equation within the solid section are written as:

$$\rho_{\text{soil}} c_{\text{soil}} \frac{\partial T_s}{\partial t} = \frac{\partial}{\partial x} (k_{\text{soil}} \frac{\partial T_s}{\partial x}) + \frac{\partial}{\partial y} (k_{\text{soil}} \frac{\partial T_s}{\partial y}) + \frac{\partial}{\partial z} (k_{\text{soil}} \frac{\partial T_s}{\partial z}) \quad (11)$$

$$\rho_{\text{grout}} c_{\text{grout}} \frac{\partial T_g}{\partial t} = \frac{\partial}{\partial x} (k_{\text{grout}} \frac{\partial T_g}{\partial x}) + \frac{\partial}{\partial y} (k_{\text{grout}} \frac{\partial T_g}{\partial y}) + \frac{\partial}{\partial z} (k_{\text{grout}} \frac{\partial T_g}{\partial z}) \quad (12)$$

$$\rho_{\text{pipe}} c_{\text{pipe}} \frac{\partial T_p}{\partial t} = \frac{\partial}{\partial x} (k_{\text{pipe}} \frac{\partial T_p}{\partial x}) + \frac{\partial}{\partial y} (k_{\text{pipe}} \frac{\partial T_p}{\partial y}) + \frac{\partial}{\partial z} (k_{\text{pipe}} \frac{\partial T_p}{\partial z}) \quad (13)$$

2.2 Multiple EPs Model

The numerical model is discretized by finite volume method (FVM). To be more specific, each EP consists of a series of cubes in three different directions (x, y and z). The cube is regarded as the control volume and its six neighboring nodes are identified as east, west, south, north, bottom and top, and the computational nodes are placed at the centre of each cell cube. The governing equation is discretized via the fully implicit approach.

$$\begin{aligned} &\Theta(m, n, k) \cdot \Gamma(m, n, k, t + 1) = \\ &\Theta_w(m, n, k) \cdot \Gamma(m - 1, n, k, t + 1) + \Theta_e(m, n, k) \cdot \Gamma(m + 1, n, k, t + 1) \\ &+ \Theta_s(m, n, k) \cdot \Gamma(m, n - 1, k, t + 1) + \Theta_n(m, n, k) \cdot \Gamma(m, n + 1, k, t + 1) \quad (14) \\ &+ \Theta_b(m, n, k) \cdot \Gamma(m, n, k - 1, t + 1) + \Theta_t(m, n, k) \cdot \Gamma(m, n, k + 1, t + 1) \\ &+ \Theta^0(m, n, k) \cdot \Gamma(m, n, k, t) \end{aligned}$$

where the Γ is temperature node at different cell cube; the superscript “0” refers to the states at the previous time step; the corresponding coefficients are:

$$\begin{aligned} \Theta_w(m, n, k) &= \frac{k_{\text{grout}} \cdot \Delta y_n \cdot \Delta z_k}{(\delta z)_b}, \quad \Theta_e(m, n, k) = \frac{k_{\text{grout}} \cdot \Delta y_n \cdot \Delta z_k}{(\delta z)_e}, \\ \Theta_s(m, n, k) &= \frac{k_{\text{grout}} \cdot \Delta x_m \cdot \Delta z_k}{(\delta y)_s}, \quad \Theta_n(m, n, k) = \frac{k_{\text{grout}} \cdot \Delta x_m \cdot \Delta z_k}{(\delta y)_n}, \\ \Theta_b(m, n, k) &= \frac{k_{\text{grout}} \cdot \Delta x_m \cdot \Delta y_n}{(\delta z)_b}, \quad \Theta_t(m, n, k) = \frac{k_{\text{grout}} \cdot \Delta x_m \cdot \Delta y_n}{(\delta z)_t}, \\ \Theta^0(m, n, k) &= \frac{c_{\text{grout}} \cdot \rho_{\text{grout}} \cdot \Delta x_m \cdot \Delta y_n \cdot \Delta z_k}{\Delta \tau} \end{aligned}$$

2.3 Boundary and Initial Conditions

2.3.1 Boundary Conditions

The boundary condition is defined as: when $z = 0$, the temperature of inlet pipe is equal to the working fluid temperature as shown:

$$T_{\text{inlet}}(0, t) = T_{\text{fluid}}(t) \quad (15)$$

When $z = 0$, the heat flux at the exit of outlet pipe is defined as:

$$\frac{\partial T_{\text{outlet}}(0, t)}{\partial z} = 0 \quad (16)$$

For the conjugated surface between the fluid and inner wall of pipe:

Inlet pipe:

$$h_s [T_{fl}^{\text{inlet}} - T_{\text{pipe}}^{\text{inner}}(x, y)] \Big|_{x=-\frac{\Delta d \pm D_i}{2}, -\frac{D_i}{2} \leq y \leq \frac{D_i}{2}} = k_{\text{pipe}} \frac{\partial T_{\text{pipe}}}{\partial x} \Big|_{x=-\frac{\Delta d \pm D_i}{2}, -\frac{D_i}{2} \leq y \leq \frac{D_i}{2}} \quad (17)$$

$$h_s [T_{fl}^{\text{inlet}} - T_{\text{pipe}}^{\text{inner}}(x, y)] \Big|_{\frac{\Delta d \pm D_i}{2} \leq x \leq -\frac{\Delta d \pm D_i}{2}, y = \pm \frac{D_i}{2}} = k_{\text{pipe}} \frac{\partial T_{\text{pipe}}}{\partial x} \Big|_{-\frac{\Delta d \pm D_i}{2} \leq x \leq -\frac{\Delta d \pm D_i}{2}, y = \pm \frac{D_i}{2}} \quad (18)$$

Outlet pipe:

$$h_s [T_{f2}^{\text{outlet}} - T_{\text{pipe}}^{\text{inner}}(x, y)] \Big|_{x=-\frac{\Delta d \pm D_i}{2}, -\frac{D_i}{2} \leq y \leq \frac{D_i}{2}} = k_{\text{pipe}} \frac{\partial T_{\text{pipe}}}{\partial x} \Big|_{x=-\frac{\Delta d \pm D_i}{2}, -\frac{D_i}{2} \leq y \leq \frac{D_i}{2}} \quad (19)$$

$$h_s [T_{f2}^{\text{outlet}} - T_{\text{pipe}}^{\text{inner}}(X, Y)] \Big|_{x=\frac{\Delta d \pm D_i}{2}, -\frac{D_i}{2} \leq y \leq \frac{D_i}{2}} = k_{\text{pipe}} \frac{\partial T_{\text{pipe}}}{\partial x} \Big|_{x=\frac{\Delta d \pm D_i}{2} \leq X \leq -\frac{\Delta d \pm D_i}{2}, y = \pm \frac{D_i}{2}} \quad (20)$$

For the conjugated surface between pipe external wall and grout:

Inlet pipe:

$$k_{\text{pipe}} \frac{\partial T_{\text{pipe}}}{\partial x} \Big|_{x=-\frac{\Delta d \pm D_0}{2}, -\frac{D_0}{2} \leq y \leq \frac{D_0}{2}} = k_{\text{borehole}} \frac{\partial T_{\text{borehole}}}{\partial x} \Big|_{x=-\frac{\Delta d \pm D_0}{2}, -\frac{D_0}{2} \leq y \leq \frac{D_0}{2}} \quad (21)$$

$$T_{\text{pipe}} \Big|_{x=-\frac{\Delta d \pm D_0}{2}, -\frac{D_0}{2} \leq y \leq \frac{D_0}{2}} = T_{\text{borehole}} \Big|_{x=-\frac{\Delta d \pm D_0}{2}, -\frac{D_0}{2} \leq y \leq \frac{D_0}{2}} \quad (22)$$

$$k_{\text{pipe}} \frac{\partial T_{\text{pipe}}}{\partial y} \Big|_{x=-\frac{\Delta d \pm D_0}{2}, -\frac{D_0}{2} \leq y \leq \frac{D_0}{2}} = k_{\text{borehole}} \frac{\partial T_{\text{borehole}}}{\partial y} \Big|_{x=-\frac{\Delta d \pm D_0}{2}, -\frac{D_0}{2} \leq y \leq \frac{D_0}{2}} \quad (23)$$

$$T_{\text{pipe}} \Big|_{-\frac{\Delta d + D_0}{2} \leq X \leq -\frac{\Delta d - D_0}{2}, y = \frac{D_0}{2}} = T_{\text{borehole}} \Big|_{-\frac{\Delta d + D_0}{2} \leq X \leq -\frac{\Delta d - D_0}{2}, y = \pm \frac{D_0}{2}} \quad (24)$$

Outlet pipe:

$$k_{\text{pipe}} \frac{\partial T_{\text{pipe}}}{\partial x} \Big|_{x=\frac{\Delta d \pm D_0}{2}, -\frac{D_0}{2} \leq y \leq \frac{D_0}{2}} = k_{\text{borehole}} \frac{\partial T_{\text{borehole}}}{\partial x} \Big|_{x=\frac{\Delta d \pm D_0}{2}, -\frac{D_0}{2} \leq y \leq \frac{D_0}{2}} \quad (25)$$

$$T_{\text{pipe}} \Big|_{x=\frac{\Delta d \pm D_0}{2}, -\frac{D_0}{2} \leq y \leq \frac{D_0}{2}} = T_{\text{borehole}} \Big|_{x=\frac{\Delta d \pm D_0}{2}, -\frac{D_0}{2} \leq y \leq \frac{D_0}{2}} \quad (26)$$

$$k_{\text{pipe}} \frac{\partial T_{\text{pipe}}}{\partial x} \Big|_{x=\frac{\Delta d \pm D_0}{2} \leq x \leq -\frac{D_0}{2}, y = \pm \frac{D_0}{2}} = k_{\text{borehole}} \frac{\partial T_{\text{borehole}}}{\partial x} \Big|_{-\frac{\Delta d \pm D_0}{2} \leq x \leq -\frac{D_0}{2}, y = \pm \frac{D_0}{2}} \quad (27)$$

$$T_{\text{pipe}} \Big|_{-\frac{\Delta d + D_0}{2} \leq X \leq -\frac{\Delta d - D_0}{2}, y = \pm \frac{D_0}{2}} = T_{\text{borehole}} \Big|_{-\frac{\Delta d + D_0}{2} \leq X \leq -\frac{\Delta d - D_0}{2}, y = \pm \frac{D_0}{2}} \quad (28)$$

For the conjugated surface between grout and soil:

$$k_{\text{borehole}} \frac{\partial T_{\text{borehole}}}{\partial x} \Big|_{x=\pm \frac{l_b}{2}, -\frac{l_b}{2} \leq y \leq \frac{l_b}{2}} = k_{\text{soil}} \frac{\partial T_{\text{soil}}}{\partial x} \Big|_{x=\pm \frac{l_b}{2}, -\frac{l_b}{2} \leq y \leq \frac{l_b}{2}} \quad (29)$$

$$T_{\text{borehole}} \Big|_{x=\frac{\Delta d \pm D_o}{2}, -\frac{D_o}{2} \leq y \leq \frac{D_o}{2}} = T_{\text{soil}} \Big|_{x=\frac{\Delta d \pm D_o}{2}, -\frac{D_o}{2} \leq y \leq \frac{D_o}{2}} \quad (30)$$

$$k_{\text{borehole}} \frac{\partial T_{\text{borehole}}}{\partial x} \Big|_{-\frac{l_b}{2} \leq x \leq \frac{l_b}{2}, y=\pm \frac{l_b}{2}} = k_{\text{soil}} \frac{\partial T_{\text{soil}}}{\partial x} \Big|_{-\frac{l_b}{2} \leq x \leq \frac{l_b}{2}, y=\pm \frac{l_b}{2}} \quad (31)$$

$$T_{\text{borehole}} \Big|_{-\frac{l_b}{2} \leq x \leq \frac{l_b}{2}, y=-\frac{l_b}{2}} = T_{\text{soil}} \Big|_{-\frac{l_b}{2} \leq x \leq \frac{l_b}{2}, y=\pm \frac{l_b}{2}} \quad (32)$$

For the conjugated surface at the bottom of soil domain:

$$k_{\text{soil}} \frac{\partial T_{\text{soil}}}{\partial z} \Big|_{z=-L} = 0 \quad (33)$$

For the bottom connecting section between inlet and outlet pipes:

$$T_{f1}(z = -L, t) = T_{f2}(z = -L, t) \quad (34)$$

For the soil surface boundary condition:

$$-k_{\text{borehole}} \frac{\partial T_{\text{borehole}}}{\partial z} \Big|_{z=0} = h_{\text{air}} [T_{\text{air}} - T_{\text{borehole}}] \Big|_{z=0} \quad (35)$$

$$-k_{\text{soil}} \frac{\partial T_{\text{soil}}}{\partial z} \Big|_{z=0} = h_{\text{air}} [T_{\text{air}} - T_{\text{soil}}] \Big|_{z=0} \quad (36)$$

2.3.2 Initial Conditions

The initial condition is presented as:

$$T_{\text{fluid}}(z, t) = T_{\text{pipe}}(x, y, z, t) = T_{\text{grout}}(x, y, z, t) = T_{\text{soil}}(x, y, z, t)(t = 0) \quad (37)$$

Soil surface temperature $T_{\text{soil}}(x, y, z, 0)$ is treated as the undisturbed ground temperature. The analytical solution of ground temperature distribution is optimized by Kasuda [30], it is a sinusoidal wave function of the time and the depth, and is shown as below:

Table 1 Initial conditions and geometrical parameters

Description	Value
Branch outside diameter (d_{po})	0.032 m
Branch inside diameter (d_{pi})	0.0131 m
Shank spacing (Δd)	0.06 m
pipe thickness (s)	0.0029 m
EP diameter ($D_{borehole}$)	0.3 m
EP depth (h)	10 m
Initial ground surface temperature ($T_{surface}$)	10.4 °C
Soil body temperature (soil far field boundary) ($T_{soil\ body}$)	14.95 °C
Soil bottom temperature (soil far field boundary) ($T_{soil\ bottom}$)	15.45 °C
Fluid Inlet temperature ($T_{fl,in}$)	1.2 °C
Fluid rate (v)	$0.38 \times 10^{-3} \text{ m}^3/\text{s}$

$$T_{soil}(Z, t_{year}) = T_{mean} - T_{amp} \cdot \exp\left(-Z \times \sqrt{\frac{\pi}{365}}\right) \cdot \cos\left[\frac{2\pi}{365} \cdot \left(t_{year} - t_{shift} - \frac{Z}{2} \times \sqrt{\frac{365}{\pi \cdot \alpha}}\right)\right] \tag{38}$$

where $T_{soil}(Z, t_{year})$ is the undisturbed ground temperature at time (t) and depth (Z) (°C); T_{mean} is mean surface temperature (average air temperature) (°C); T_{amp} is amplitude of surface temperature [(maximum air temperature – minimum air temperature)/2] (°C); Z is depth below the surface (surface = 0) (m); α is thermal conductivity of the soil (J/kg · °C); t_{year} is current time (day); t_{shift} is day of the year when the coldest air temperature occurs. These initial conditions and geometrical parameters are listed in Tables 1 and 2.

3 Economic Model

The LCC is the sum of all expenses associated with an energy delivery system over a selected period or its service lifetime, with consideration of the time value of money. In the LCC, the expected future expenses are brought back to the present costs (discounted) through calculating how much have to be invested at a market discount rate. The LCC assessment process can be applied to evaluate financial benefit of the EP unit with EPs, the main parameters, for example, interest rate, income tax rate, capital investment (CI), loan payment (LP), system energy cost (SEC), maintenance cost (MC), periodic cost (PC), extra property tax (EPT), incoming tax savings (ITS), net present value (NPV) of money and cumulative EP system savings (EPS), are all

Table 2 Thermal property

Description	Value
Fluid (Glycol and mixed with water)	
Density (ρ_f)	1035 kg/m ³
Kinematic viscosity (ν_f)	4.94×10^{-6} m ² /s
Heat capacity ($C_{p,f}$)	3795 J/(kg · °C)
Thermal conductivity (λ_f)	0.58 W/(m · °C)
Pipe(High density polyethylene)	
Density (ρ_p)	950 kg/m ³
Heat capacity ($C_{p,l}$)	2300 J/(kg · °C)
Thermal conductivity (λ_p)	0.45 W/(m · °C)
Filling (Grout)	
Density (ρ_g)	1860 kg/m ³
Heat capacity (C_g)	840 J/(kg · °C)
Thermal conductivity (λ_g)	2 W/(m · °C)
Soil	
Density (ρ_s)	2260 kg/m ³
Heat capacity (C_s)	1300 J/(kg · °C)
Thermal conductivity (λ_s)	1.5 W/(m · °C)

evaluated in the LCC analysis. The LCC assessment of the EP unit consists of seven parts: SEC, CI, LP, MC, PC, ITS and NPV, while the core part is the NPV calculation which is utilised to compare cash flows at different time intervals. The structure of the LCC assessment is shown in Fig. 3.

The LCC on the basis of the NPV for the EP UNIT can be given as:

$$LCC = C_{SEC} + C_{CI} + C_{LP} + C_{MC} + C_{ITS} + C_{PC} \quad (39)$$

where LCC is the EP unit entire life cycle cost in NPV (£); C_{SEC} is the EP unit energy cost in PV (£); C_{CI} is the unit initial costs including the construction and engineering design expenses (£). In this study, only the construction expenses are taken into account; C_{LP} is the annual loan payment in PV (£); C_{MC} is the EP system maintenance cost in PV (£); C_{ITS} is the EP unit income tax savings expense in PV (£); C_{PC} is the EP unit periodic cost in PV (£).

The SEC is also known as the fuel cost saving which is determined based on the electricity price and consumption. The electricity consumption of the system depends on heating and cooling loads of the building. The annual SEC is given as:

$$C_{SEC} = c_{SEC} \times \frac{1}{(1 + d_{SEC})^N} \quad (40)$$

$$c_{SEC} = E_{generation} \cdot \beta \quad (41)$$

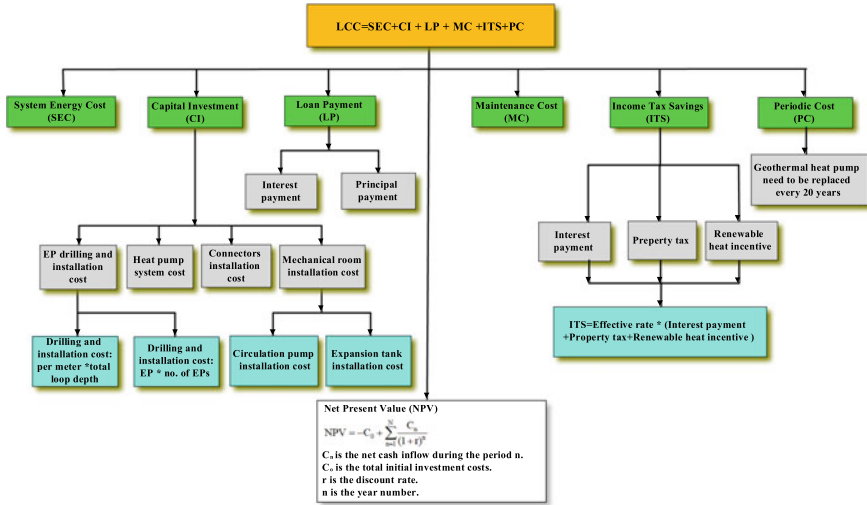


Fig. 3 The structure of the life cycle cost

where C_{SEC} is the EP unit energy cost in PV (£); c_{SEC} is the GCHP annual electricity cost (£); d_{SEC} is the inflation rate of electricity price (%); N is the period of economic assessment; $E_{generation}$ is the energy generation (heating and cooling) from the EP unit (kWh); β is the electricity price (£/kWh).

The CI model is developed via three cost sections in the following:

$$CI = C_{ic} + C_{in} + C_{co} \quad (42)$$

where C_{ic} is the initial expense of main equipment (£); C_{in} is the installation expense, labour expense, auxiliary equipment expense (£); C_{co} is the commissioning or subscription expense (£).

The LP is also referred to as the mortgage payment per annum which involves principle and interest payments to install the system.

The PV of LP is given by:

$$C_{LP} = G \cdot \frac{r_{LP} \cdot (1 + r_{LP})^z}{(1 + r_{LP})^z - 1} \quad (43)$$

where C_{LP} is the loan payment per annum (£); G is the principal payment (£); r_{LP} is the yearly interest rate (%); z is the number of loan payment years.

The present worth of MC per annum is exhibited as:

$$C_{MC} = c_{MC} \times \frac{1}{(1 + d_{MC})^k} \quad (44)$$

where C_{MC} is the present worth of the k th year EP maintenance expense (£); c_{MC} is the first year maintenance expense of EP (£); d_{MC} is the inflation rate of maintenance (%); k is the period of maintenance payment.

The PC denotes the replacement cost of main system parts. For the EP unit, only the heat pump is required to be replaced every 20 years [31]. Therefore, the PC in PV is written as:

$$C_{PC} = c_{PC} \times \frac{1}{(1 + d_{PC})^s} \quad (45)$$

where C_{PC} is the present worth of the s th year EP system periodic expense (£); c_{PC} is the first year EP unit periodic expense (£); d_{PC} is the inflation rate of replacement (%); s is the year number of periodic payment.

The EPS can be written as:

$$C_{EPS} = C_{SEC} - C_{LP} - C_{MC} - C_{PC} - C_{EPT} + C_{ITS} \quad (46)$$

where C_{EPT} is the extra property tax (£); C_{ITS} is the income tax savings (£).

The C_{EPT} in PV is expressed as:

$$C_{EPT} = c_{EPT} \times \frac{1}{(1 + \gamma_{EPT})^\alpha} \quad (47)$$

where c_{EPT} is the annual extra property tax cost of the EP unit (£); γ_{EPT} is the inflation rate of extra property tax (%); α is the period of extra property tax.

The C_{ITS} in PV is written as:

$$C_{ITS} = C_{ETR} \times (C_{IP} + C_{EPT} + C_{RHI}) \quad (48)$$

where C_{ETR} is the effective tax rate (%); C_{IP} is the interest payment (£); C_{RHI} is the renewable heat incentive bonus for heat generation in the UK (£).

The NPV is estimated to evaluate the whole gain of the system. If a payment repeats every year at an inflate rate of r per annum, the NPV is written by the following equation:

$$NPV = -C_{CI} + \sum_{N=1}^{N'} \frac{C_N}{(1 + r)^N} \quad (49)$$

where C_N is the net cash inflow during the N period (£); C_{CI} is the entire capital investment expense (£); r is the discount rate (%).

4 Results and Discussion

4.1 Energy Performance

The average system energy output from the heat pump (heating and cooling) and ground energy extracted and rejected are illustrated in Fig. 4. Specifically, the monthly thermal energy production is low in October and April, and the minimum monthly energy output of the EP system is about 1593.94 kWh in April while the maximum value is around 2285.24 kWh in December. Additionally, from February to April, the EP system operates in most of time, hence the soil has never sufficient time to recover.

Meanwhile, the soil temperature neighbouring the EP is comparatively low resulting in a low temperature of working fluid entering into the heat pump evaporator, correspondingly a low COP. The minimum value of monthly heat extracted from the soil is around 1148.99 kWh in April, and the maximum value is approximately 1890.20 in December. The minimum cooling output of EP system is 1000.25 kWh in September while the maximum value is about 1521.78 kWh in July. Furthermore, the monthly heat rejected into the soil is also depicted, the minimum rejected heat is 894.85 kWh in September whereas the maximum value is 1279.01 kWh in July.

It can be observed from Fig. 5 that the monthly heating electrical energy consumption and system performance variation in the heating and cooling seasons. To be more specific, the monthly power consumptions of the EP unit are 440.69, 578.40, 643.73, 596.18, 555.67, 516.33 and 427.33 kWh from October to April, with associated with mean monthly COPs reaching 3.65, 3.6, 3.55, 3.58, 3.62, 3.65 and 3.73, respectively. By contract, the monthly cooling electrical power consumptions of the EP unit are 215.10, 241.13, 281.10, 266.02 and 190.80 kWh from May to September, with associated with mean monthly EERs achieving 4.65, 4.58, 4.55, 4.61 and 4.69, respectively. The system yearly average COP and EER are 3.63 and 4.62, respectively. The monthly cooling electrical energy consumptions are 215.10, 241.13, 281.10, 266.02 and 190.80 kWh from May to September, with corresponding average monthly EERs achieve 4.65, 4.58, 4.55, 4.61 and 4.69, respectively. So the system annual average EER is 4.62.

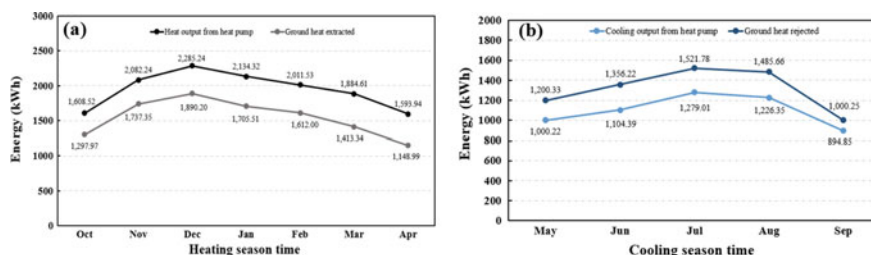


Fig. 4 Energy output: **a** heating season; **b** cooling season

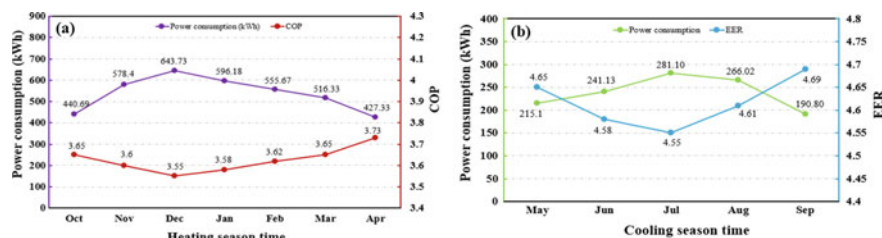


Fig. 5 Electrical energy consumption and system performance: **a** heating season; **b** cooling season

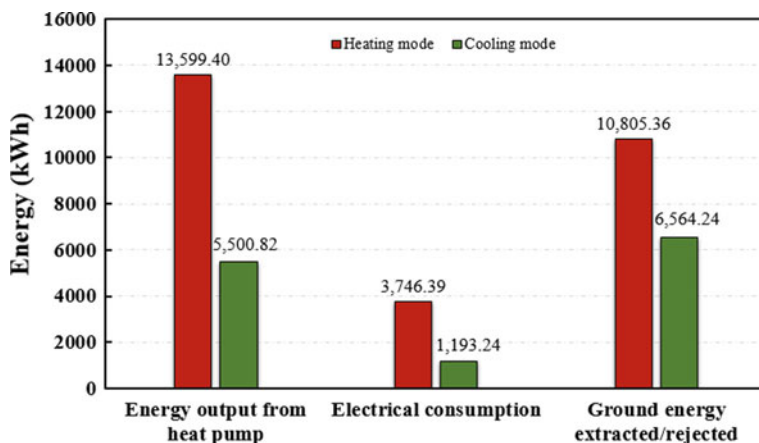


Fig. 6 Total energy production, power consumption and soil energy extracted/rejected

Figure 6 illustrates that the total heat output of the EP system is 13599.40 kWh and the heat extracted from soil is 10805.36 kWh, resulting in the electrical consumption of 3746.39 kWh. However, the cooling output is 5500.82 kWh and the heat rejected into the soil is 6564.24 kWh, leading to 1193.24 kWh of the power consumption. Consequently, the yearly heating and cooling energy output of the EP system is predicated to be around 19,100 kWh and the total power consumption achieves 4939.63 kWh. This indicates that the energy output through the EP unit could cover the building energy demands.

4.2 Effects of Fluid Flow Rate

The fluid flow rate has a vital influence on the outlet fluid temperature and heat extraction rate of the EP unit. The low flow rate contributes to providing the high outlet fluid temperature for heat pump, but the heat transfer rate is low because of the low convective heat transfer coefficient between the pipe and fluid. Moreover, the high flow rate

could enhance heat transfer rate but the fluid outlet temperature is low, this means that the high fluid flow rate results in more electrical consumption for the pump circulating. Hence, it is necessary to sustain the working fluid flow rate within a reasonable range. In order to deal with the influence of flow rate, various flow rates including 0.1, 0.3, 0.5, 0.7, 0.9 and $1.2 \text{ m}^3/\text{h}$ are adopted to assess the heat transfer rates and fluid outlet temperature as described in Fig. 7. The initial inlet fluid temperature is defined as -4°C . It is demonstrated that the flow rate has little influence on heat transfer rate below a certain level. When the flow rate is low, the thermal resistance of the EP has a low convective heat transfer between the pipe and fluid, while the convective heat transfer coefficient could be improved when the flow rate is increased. Additionally, the convective heat transfer has the less influence in the entire process of heat transfer when the flow rate is controlled within a certain degree, so the overall heat transfer rate appears a low increasing trend with the fluid flow rate.

Figure 8 presents the working fluid temperatures variations within the U-tube based on different flow rates. When the outlet fluid temperature and flow rate are defined as -0.15°C and $0.1 \text{ m}^3/\text{h}$, the fluid temperature increments are 3.85°C . Similarly, when the outlet fluid temperature and flow rate are defined as -0.81°C and $1.2 \text{ m}^3/\text{h}$, the fluid temperature increments are 3.19°C . This indicates that there is the fluid heat loss is produced by heat exchange between two pipes of the U-tube, which is called as “thermal short-circuiting”.

Specifically, the fluid temperature within the downward pipe rises along the pipe whereas its temperature within the upward pipe grows slowly at first, and then reduces due to the effect of “thermal short-circuiting” as displayed in Fig. 8. The highest fluid temperature is 0.49°C showing at the middle of the upward pipe at the flow rate of $0.1 \text{ m}^3/\text{h}$, and the maximum temperature difference is 4.49°C between the inlet and outlet pipe at the same moment. Nevertheless, the outlet fluid temperature is -0.15°C , but the actual temperature difference between the inlet and outlet could reach 3.85°C , therefore, the short-circuiting loss rate is 14.26% [$(4.49 - 3.85)/4.49 = 14.26\%$]. It is demonstrated that the effect of “thermal short-circuiting” would be

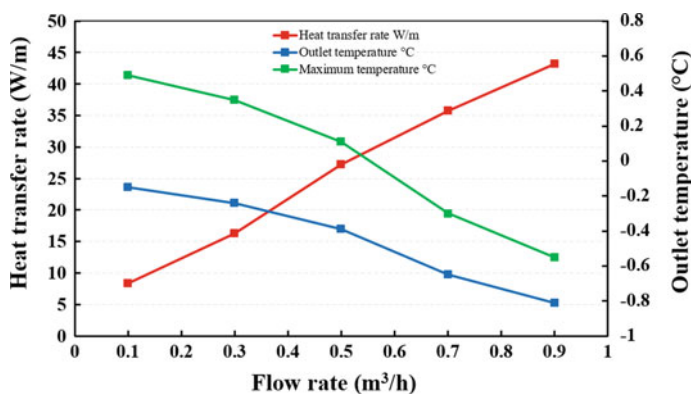


Fig. 7 Influences of fluid flow rate

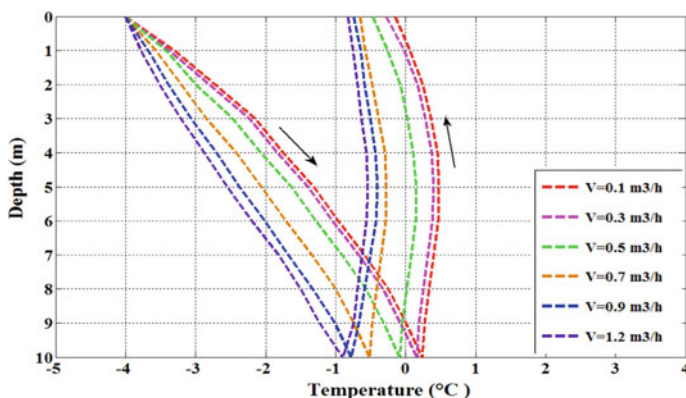


Fig. 8 Fluid temperature distribution in the U-tube

more serious when the flow rate is low because of the large temperature variation, which should be given fully consideration in practical engineering.

4.3 Economic Analysis

The entire system initial cost is £9033 with 10% down payment, the remaining part of the initial investment is financed when the interest rate is defined as 8.2% for the 20 years' period. It is expected to pay normal maintenance cost for the system annually with an inflation rate of 4.5% [32]. Energy pricing mechanism in the UK is a combination of regulated and market-driven prices [27]. The electricity price is obtained as £0.1097/kWh based on the UK government [33]. In terms of UK energy prices regulated via Ofgem [34], the RHI rate for the systems between 4 and 10 kW is £0.1986/kWh. The maintenance cost for EPs is assessed to be £150 per annum. The average effective income tax rate is assessed to be 20% over the service lifetime period. The expenses of EP unit include high density polyethylene pipe material, auger drilling, installation cost and maintenance costs, are shown in Table 3. Details of the component prices, economic expenses and parameters are given in Table 4.

It is illustrated from Table 5 that the yearly progresses of SEC and MC of the EP system over 20 years' operating period. To be more specific, the SEC in the first year is about £2095.27 ($19,100 \times £0.1097/\text{kWh}$) and the second year's SEC is about £2220.99 [$19100 \times £0.1097/\text{kWh} \times (1 + 6\%)$] based on the inflation rate of electricity price. By the end of the 20th year, the value could achieve £6339.45 [$19100 \times £0.1097/\text{kWh} \times (1 + 6\%)^{19}$]. Similarly, the MC in the first year and 20th year are £150 and £346.18, respectively. Additionally, the LP and interest payment in the first year are £840.39 and £666.64, thereby the principal payment and remaining principal could obtain £173.75 ($£840.39 - £666.64$) and £7955.95 ($£9033 \times 10\% - £173.75$), respectively. In terms of the ITS and EPS, the progressions of the ITS and

Table 3 Cost breakdown of EP unit

Item	Value
<i>EP pipe</i>	
Pipe drilling cost	£2.63/m × 413 m
Loop installation into pile reinforcement cages	£640
Estimated pipe installation cost	£1726
<i>Heat pump system</i>	
Heat pump & commissioning	£5600
Working fluid cost	£174
Estimated heat pump unit cost	£5774
<i>Other equipment installation</i>	
Header circuit insulation	£186
Brass fittings	£386
4 port brass manifold with flow control	£361
Estimated other equipment cost	£933
<i>Labour cost</i>	
Header circuit labour	£600
<i>Total capital cost</i>	£9033
<i>Estimated maintenance cost</i>	£150

Table 4 Parameters used for economic analysis

Item	Value
Electricity price	£0.1097/kWh
RHI for GCHP	£0.1986/kWh
Down payment	10%
Inflation rate of electricity price	6%
Interest rate of principal	8.2%
Inflation rate of maintenance	4.5%
Council rate for property tax	2%
Inflation rate of extra property tax	4%
Income tax rate	20%
UK discount rate	8.75%

EPS for the 20-year running period are depicted in columns 10 and 11. The ITS for the first year and 20th year are about £928.11 and £847.51, respectively. Meanwhile, the EPS for each year is the sum of the items containing MC, LP, SEC, ITS and EPT. The yearly EPS is brought to present worth by the UK market discount rate of 8.75%. The deposit charge is £903.3 which is a negative present value, and it is displayed as Year 0. The EPS becomes a positive value achieving about £1852.33 after the first year and the EPS reaches £5619.77 until the 20th year. Furthermore, the NPV of the

EP unit is determined about £26,095.14 at the market discount rate of 8.75% over 20 year's running period. The economic evaluation indicates that the cash flow turns positive at the end of the first year and sustains positive permanently by the end of the service lifetime. This attributes to the replacement of the heat pump which is only taken into account in the 20th year, and also the initial and maintenance costs of the EP unit are much less as well in this case.

It is obtained from Fig. 9 that the cumulative SEC saving (£9166) exceeds the CI (£9033) by the end of the fourth year. The cumulative EPS becomes positive after one year due to the low capital and little maintenance costs. The cumulative system saving (£9531.53) surpasses the remaining principal balance (£7106.28) by the end of the sixth year. The calculation process of the LCC analysis is given in Table 5. Meanwhile, the payback period is approximately 4.3 years as shown in Fig. 9. This is deemed an acceptable payback period (< 10 years) for an engineering project of this nature, and serves to demonstrate the clear benefit of adopting such a system in the UK context.

4.3.1 Sensitive Analyses of NPV and Payback Period

In the following, the comparison analyses are implemented with respect to the NPV and payback period with different parameters. The distribution graphs of cumulative probability versus NPV and payback time for the EP system over the entire LCC period are displayed in Figs.10 and 11 respectively. The legend gives the minimum, maximum, average, number of iterations and standard deviation of NPV and payback period in this case.

The vertical lines in Fig. 10 represent the NPV of present case (£26,095) and average value (£33,053). One row of percentages on the top of the diagram shows the probabilities relative to the NPV. To be more specific, the top row describes the probability with regards to the LCC of the EP unit which is divided into three sections. When the NPV is less than the present case value, it accounts for 28.6%; when the NPV is located between the NPV of the present case value and average value, it makes up 25.2%; when the NPV is greater than the average value, it accounts for a proportion of 46.2%. By comparison, the vertical lines in Fig. 11 denote the minimum and average values in the payback period. Based on one row of percentages on the top of the graph, there is a probability of 44.2% that the payback period of the system is more than 4.31 years, and 55.8% of the payback time is between 1.61 and 4.31 years, while 0% of the payback period is less than 1.61 years.

4.3.2 NPV Variation with the Uncertain Input Factors

The NPV variations with the uncertain input parameters are described in Fig. 12. It is revealed that the uncertainty associated with electricity price has the largest influence on the NPV whereas the inflation rate of maintenance cost has the least influence among the uncertain input parameters. Notably, the low electricity price makes the

Table 5 The economic assessment of the EP system over 20 years' service lifetime

Year	Energy generation (kWh/year)	SEC (£)	LP (£)	Interest payment (£)	Principal payment (£)	Remaining principal (£)	MC (£)	EPT (£)	ITS (£)	EPS (£)	Present worth of EPS (£)	Cumulative EPS (£)	Cumulative SEC savings (£)
0						8192.70				(903.30)	(903.30)	(903.30)	
1	19100	2095.27	(840.39)	666.64	173.75	7955.95	(150)	(180.66)	928.11	1852.33	1703.29	949.03	2095.27
2	19100	2220.99	(840.39)	652.39	188.00	7767.94	(156.75)	(187.89)	926.70	1962.67	1659.54	2911.69	4316.26
3	19100	2354.25	(840.39)	636.97	203.42	7564.52	(163.80)	(195.40)	925.13	2079.78	1617.07	4991.47	6670.50
4	19100	2495.50	(840.39)	620.29	220.10	7344.43	(171.18)	(203.22)	923.35	2204.07	1575.83	7195.55	9166.00
5	19100	2645.23	(840.39)	602.24	238.15	7106.28	(178.88)	(211.35)	921.37	2335.99	1535.76	9531.53	11,811.23
6	19100	2803.94	(840.39)	582.71	257.68	6848.60	(186.93)	(219.80)	919.16	2475.98	1496.83	12,007.51	14,615.18
7	19100	2972.18	(840.39)	561.59	278.80	6569.80	(195.34)	(228.59)	916.69	2624.55	1458.98	14,632.06	17,587.36
8	19100	3150.51	(840.39)	538.72	301.67	6268.13	(204.13)	(237.74)	913.94	2782.19	1422.18	17,414.26	20,737.87
9	19100	3339.54	(840.39)	513.99	326.40	5941.73	(213.32)	(247.25)	910.89	2949.49	1386.38	20,363.75	24,077.41
10	19100	3,539.92	(840.39)	487.22	353.17	5588.56	(222.91)	(257.14)	907.52	3126.99	1351.56	23,490.75	27,617.32
11	19100	3752.31	(840.39)	458.26	382.13	5206.43	(232.95)	(267.42)	903.79	3315.34	1317.67	26,806.09	31,369.63
12	19100	3977.45	(840.39)	426.93	413.46	4792.97	(243.43)	(278.12)	899.66	3515.17	1284.68	30,321.26	35,347.08
13	19100	4216.10	(840.39)	393.02	447.37	4345.60	(254.38)	(289.24)	895.11	3727.19	1252.57	34,048.45	39,563.18
14	19100	4469.06	(840.39)	356.34	484.05	3861.55	(265.83)	(300.81)	890.08	3952.11	1221.29	38,000.56	44,032.24
15	19100	4737.20	(840.39)	316.65	523.74	3337.81	(277.79)	(312.84)	884.55	4190.73	1190.83	42,191.29	48,769.44
16	19100	5021.44	(840.39)	273.70	566.69	2771.12	(290.29)	(325.36)	878.46	4443.86	1161.16	46,635.15	53,790.88
17	19100	5322.72	(840.39)	227.23	613.16	2157.96	(303.36)	(338.37)	871.77	4712.38	1132.25	51,347.52	59,113.60

(continued)

Table 5 (continued)

Year	Energy generation (kWh/year)	SEC (£)	LP (£)	Interest payment (£)	Principal payment (£)	Remaining principal (£)	MC (£)	EPT (£)	ITS (£)	EPS (£)	Present worth of EPS (£)	Cumulative EPS (£)	Cumulative SEC savings (£)
18	19100	5642.09	(840.39)	176.95	663.44	1494.53	(317.01)	(351.91)	864.42	4997.21	1104.08	56,344.73	64,755.69
19	19100	5980.61	(840.39)	122.55	717.84	776.69	(331.27)	(365.98)	856.36	5299.32	1076.63	61,644.05	70,736.30
20	19100	6339.45	(840.39)	63.69	776.70	-0.015	(346.18)	(380.62)	847.51	5619.77	1049.86	67,263.82	77,075.75
Total											26,095.14		

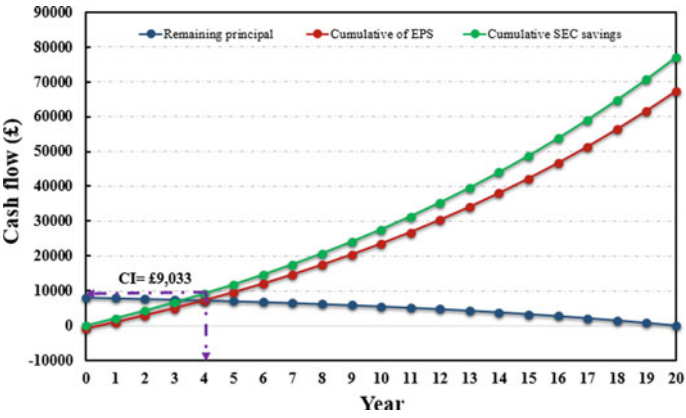


Fig. 9 Cash flow variation

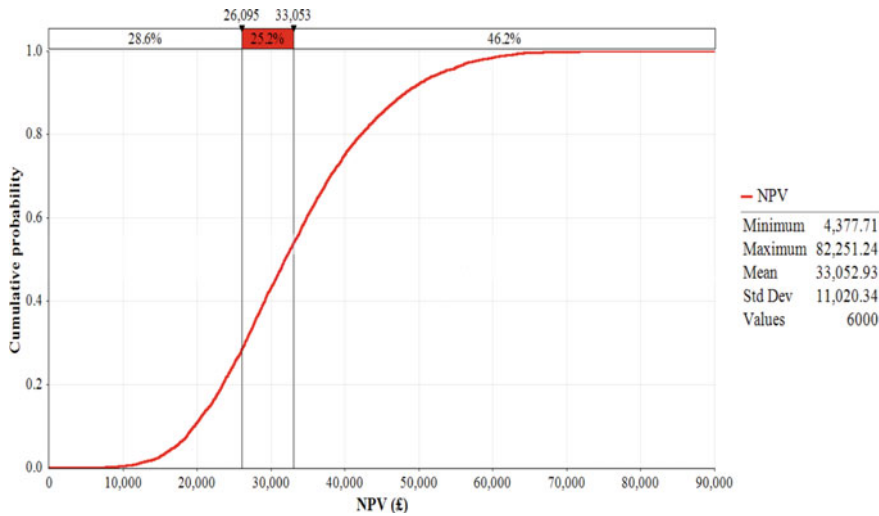


Fig. 10 NPV distribution

NPV to be £20,308.66, 38.6% lower compared to the baseline of £33,068.19. On the contrary, the high electricity price makes the NPV as high as £49,255.99 (50.0% higher). Likewise, the uncertainty in energy production is closely related to the variety of financial credits achieved from enhancing the NPV. Thus, the range of energy production by the EP unit induces a NPV variation from £23,078.62 to £42,588.94. If the lower initial expense are attained, the NPV would achieve £36,816.40, by comparison, the higher initial cost induces a longer period to realise a positive NPV of £28,663.53.

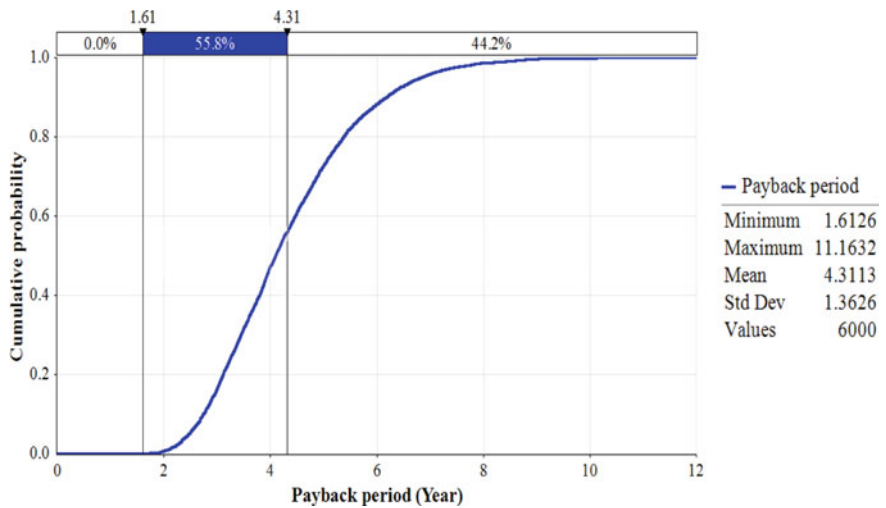


Fig. 11 Payback period distribution

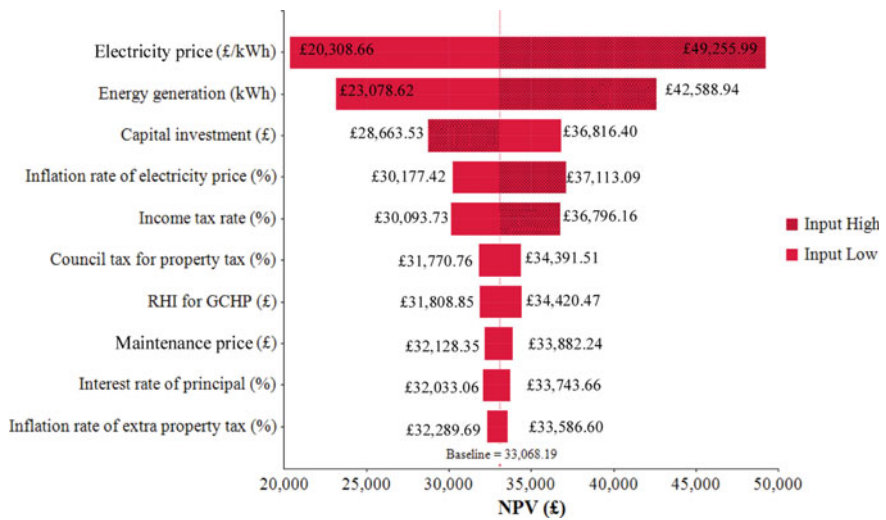


Fig. 12 Tornado chart of NPV variation with uncertain input parameters

Figure 13 describes the NPV variations against energy production, discount rate, investment cost and electricity price. The horizontal and vertical lines (respective mean values) split the graph into four quadrants with the change of electricity price from £0.06 to £0.22/kWh as depicted in Fig. 13a. The NPV changes from £10,000 to £33,066 accounting for the largest proportion of 43.0% when the electricity price enhances from £0.08 to £0.1349/kWh, and also the smallest proportion of 10.7% takes

place when the electricity price further rises from £0.1349 to £0.22/kWh. Similarly, the scope of the energy output from 13,000 to 24,000 kWh affects the savings, cash flows and NPV as displayed in Fig. 13b. When energy output changes from 18,699 to 24,000 kWh, the NPV varies from £10,000 to £33,066 and takes up the biggest proportion of 34.3%, while the NPV lies in the range of £10,000–£33,066 making up the smallest ratio of 17.0% when the energy output is controlled ranging from 13,000 to 18,699 kWh.

Figure 13c describes that the NPV variation associates with the initial expense when the price fluctuation of the EP unit is considered, and the influence of capital cost is more evenly distributed in the NPV quadrants in comparison with the energy production and electricity price. For example, when the initial investment of the EP unit is enhanced from £6000 to £10,178 and from £10,178 to £15,000, approximately 23.7 and 26.7% of the NPVs decrease underneath the mean value of £33,066, respectively.

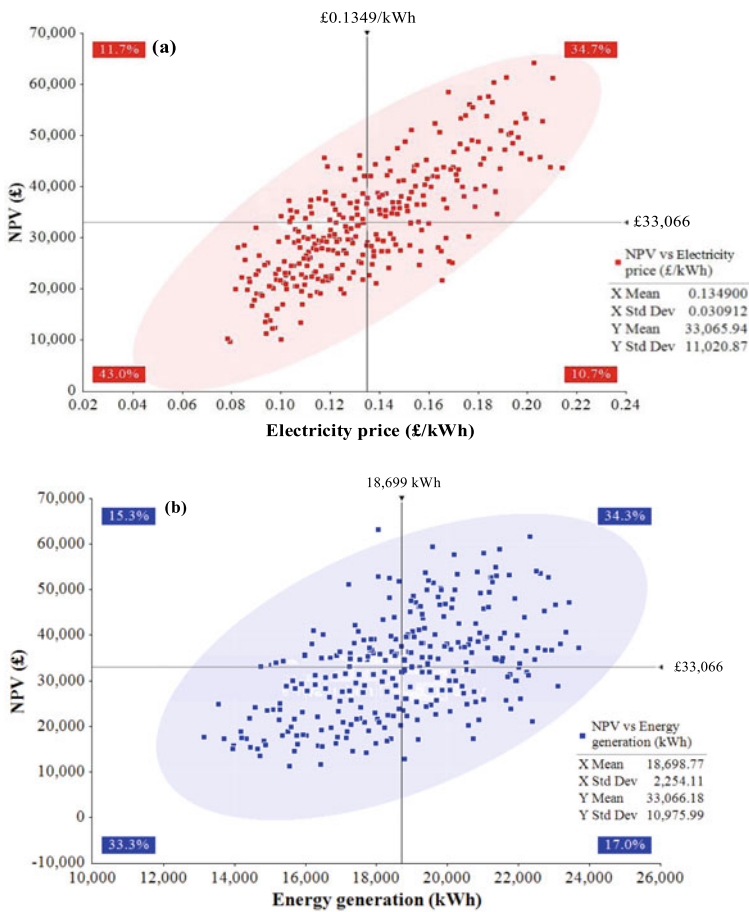


Fig. 13 NPV variations: **a** electricity price; **b** energy production; **c** initial cost; **d** discount rate

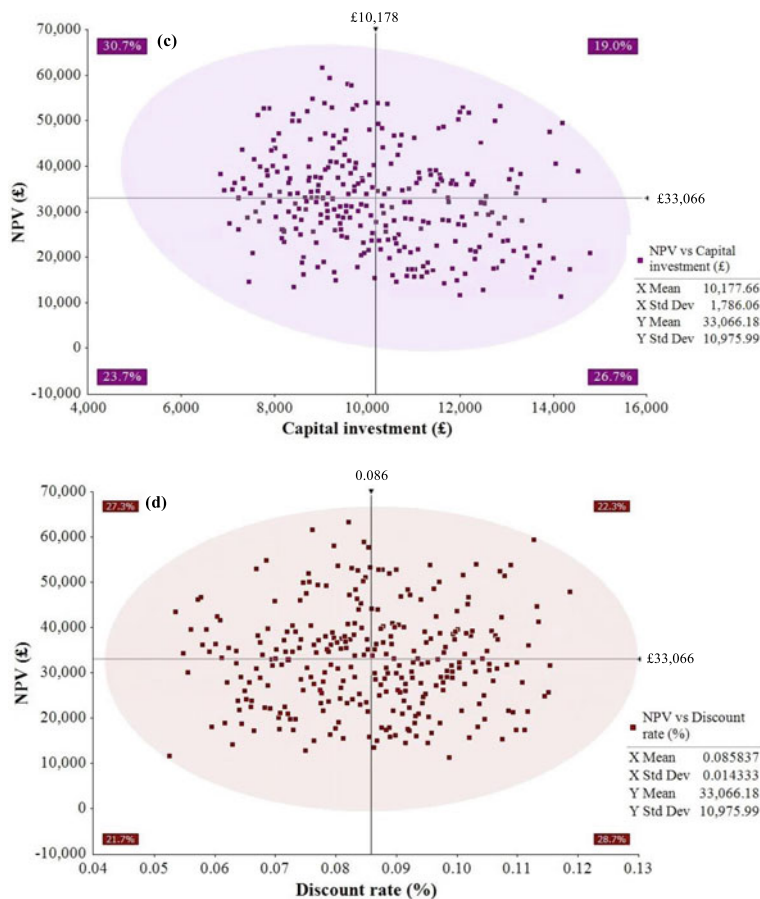


Fig. 13 (continued)

This means that initial expense of the EP unit is vital to the final judgement of investment as the higher EP system price causes the higher loan payment. Consequently, the capital investment of the EP unit should be controlled as low as possible for the better market potential. Furthermore, it can be seen from Fig. 13d that the discount rate also leads to an even distribution of the NPV value. In other words, higher discount rate weakens the energy output and present worth of cash flow, and reduces the NPV. The lower discount rate is beneficial to the investment of the EP unit.

4.3.3 Payback Period Variation with the Uncertain Input Parameters

The payback period is sensitive to several crucial parameters, involving electricity price, initial investment and energy production as illustrated in Figs. 16–18. It can be

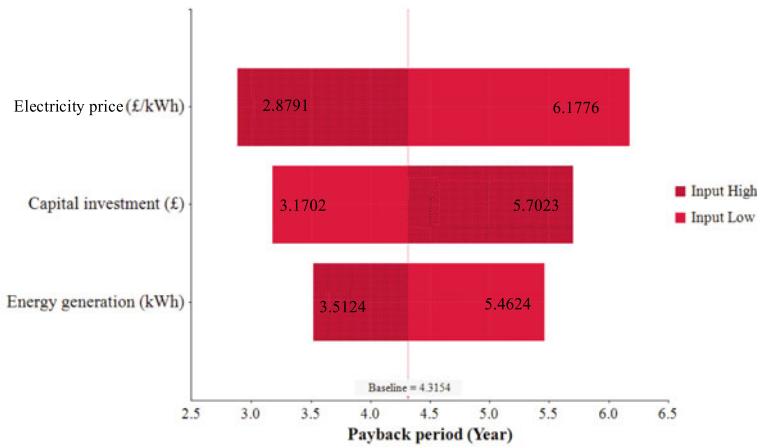


Fig. 14 Tornado chart of payback period variation with uncertain input parameters

found from Fig. 16 that the low electricity price decreases the running and electricity expenses, and enhances the payback period up to approximately 6.18 years relative to the baseline of around 4.31 years. Moreover, the high electricity price contributes to shortening the payback period reaching 2.88 years. In the meantime, uncertainty in energy production is closely related to the financial credit achieved from power consumption. Thus, the range of energy output through the EP system causes a payback period ranging from 3.51 to 5.46 years. In other words, when a low initial cost can be attained, the payback period is around 3.17 years whereas higher initial investment makes a longer term to realize positive NPV reaching 5.70 years (Fig. 14).

It can be found from Fig. 15 that the high electricity price has a good opportunity (38.7 versus 6.7%) to shorten payback time to underneath 4.31 years. However, in lights of a lower electricity price, there is a possibility of 36.0% that payback time is over the average value as presented in Fig. 15a. Scenarios in the lower half of Fig. 15bb have low payback period (< 4.31 years) whereas those in the left-hand side of the figure have lower initial cost that is less than £10,178. As a result, the payback time is located in the lower left quadrant with a possibility of 40.0%. The correlation between the energy production and payback time displays a pretty even distribution in the four quadrants as described in Fig. 15c. The possibility of decreasing the payback time underneath the average value (4.31 years) is 57.3%, with 20.3% for energy production lower compared to 18699 kWh and 37% for energy output in excess of 18,699 kWh.

4.3.4 Payback Period Variation with NPV

It can be demonstrated from Fig. 16 that 38.0% of probability NPV value is lower in comparison to the average value of £33,066 when the payback time is overhead the

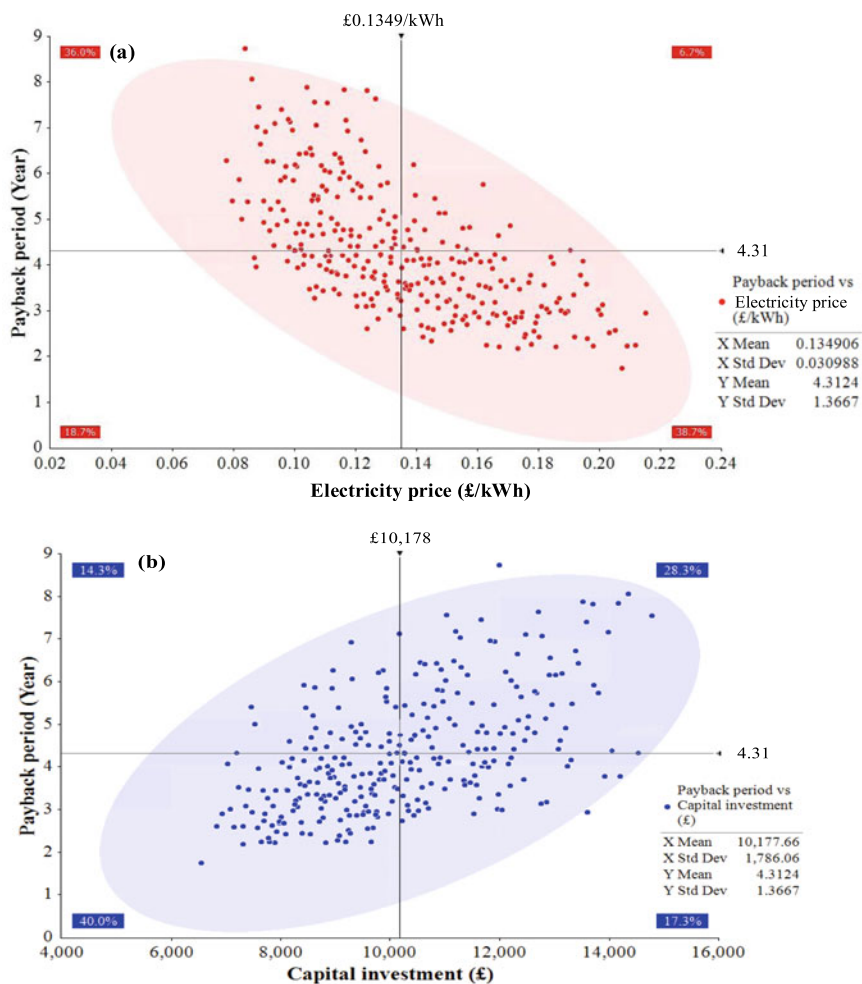


Fig. 15 Payback period against variations: **a** electricity price; **b** initial expense; **c** energy production

value (4.31–8.50 years). Only 4.7% of opportunity NPV is higher compared to the average value, indicating the long payback time is detrimental to the entire NPV. If payback period can be realized less than 4.31 years, there is a possibility of 45.0% that the NPV value is higher compared to the average value while an opportunity of 12.3% for lower value. This means that the high NPV value (the upper left side of the figure) could be realised when the payback time is cut down in the study.

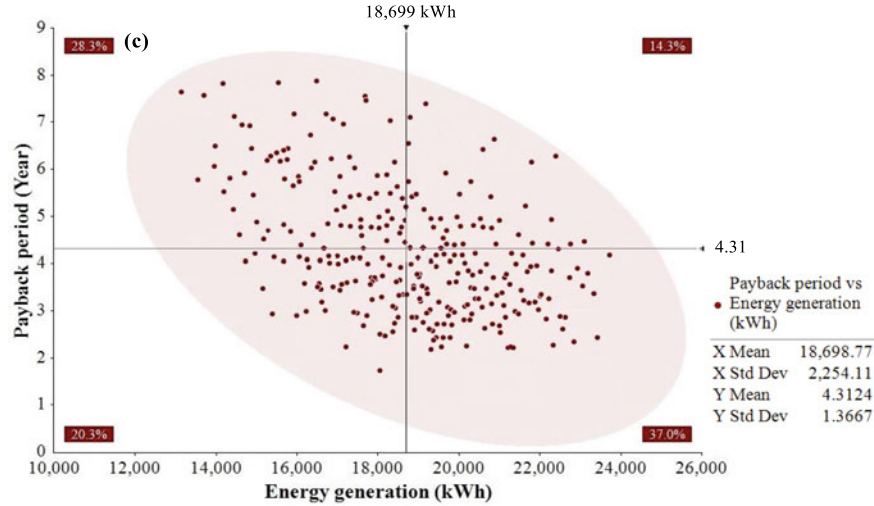


Fig. 15 (continued)

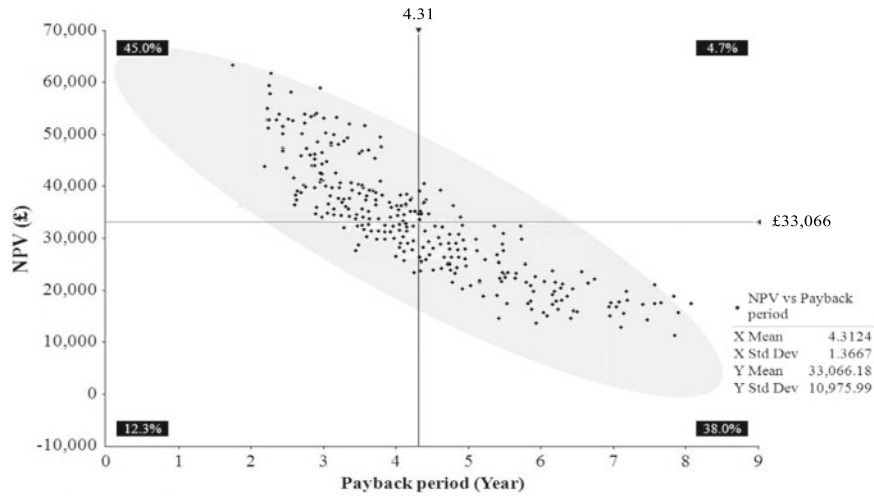


Fig. 16 NPV variation with payback time

5 Conclusions

A techno-economic evaluation on EP unit in the context of the UK is exhibited in this study. A 3D numerical model is employed to analyse the monthly heating and cooling energy production, soil energy extracted and rejected, power consumption, EER and COP. Meanwhile, the influences of the fluid flow rate and thermal short-circuiting

on EP system performance are investigated based on the finite volume approach. Additionally, the economic analysis of the EP system is assessed via the @Risk software, a complete LCC method with consideration for the time value of money is adopted and some important parameter influences on the LCC are illustrated, including interest rate, CI, SEC, LP, EPS, EPT, NPV and ITS. As a result, some crucial conclusions are summarized in the following:

- The heating and cooling energy production of the EP system could fulfil the building energy demands with the yearly COP of 3.63 and EER of 4.62 on average.
- The effect of “thermal short-circuiting” would be more serious when the flow rate is low because of the large temperature fluctuation between inlet and outlet fluid.
- The net present value of the EP system changes from £24,000–£30,000 over a 20 years’ service lifetime, and also the payback period is controlled in the range from 4 to 10 years in general.
- The NPV of the EP system is £26,095.41 at the market discount rate of 8.75% during the running period, and the cumulative EPS becomes positive by the end of the first year, afterwards it sustains positive until the LCC is completed.
- The cumulative SEC saving (£9166) surpasses the capital investment (£9033) by the end of the fourth year, the cumulative EPS (£9531.53) exceeds the remaining principal balance (£7106.28) by the end of the fifth year.
- The low discount rate conduces to decreasing the NPV and initial expense of the EP unit, and the payback period is sensitive to electricity price, initial cost and energy production.

References

1. Aresti L, Christodoulides P, Florides G (2018) A review of the design aspects of ground heat exchangers. *Renew Sustain Energy Rev* 92:757–773
2. Wang G, Wang W, Luo J, Zhang Y (2019) Assessment of three types of shallow geothermal resources and ground-source heat-pump applications in provincial capitals in the Yangtze River basin China. *Renew & Sustain Energy Rev* 111:392–421
3. Mujtaba A, Jena PK, Bekun FV, Sahu PK (2022) Symmetric and asymmetric impact of economic growth, capital formation, renewable and non-renewable energy consumption on environment in OECD countries. *Renew Sustain Energy Rev* 160:112300
4. Gan F, Huang G, Zhang H, Lu J, Zhuang C, Cheng L, Xu N, Liao Z (2020) Ring coils heat source numerical modeling and thermal interference characteristics analysis of truncated cone helix energy pile. *Energy Build* 228:110438
5. Ding X, Peng C, Wang C, Kong G (2022) Heat transfer performance of energy piles in seasonally frozen soil areas. *Renew Energy* 190:903–918
6. Cui Y, Zhu J, Twaha S, Riffat S (2018) A comprehensive review on 2D and 3D models of vertical ground heat exchangers. *Renew Sustain Energy Rev* 94:84–114
7. You T, Wang B, Wu W, Shi W, Li X (2015) Performance analysis of hybrid ground-coupled heat pump system with multi-functions. *Energy Convers Manage* 92:47–59
8. Rammal D, Mroueh H, Burlon S (2018) Impact of thermal solicitations on the design of energy piles. *Renew Sustain Energy Rev* 92:111–120

9. Zhang W, Cui P, Liu J, Liu X (2017) Study on heat transfer experiments and mathematical models of the energy pile of building. *Energy and Buildings* 152:643–652
10. Saeidi R, Noorollahi Y, Esfahanian V (2018) Numerical simulation of a novel spiral type ground heat exchanger for enhancing heat transfer performance of geothermal heat pump. *Energy Convers Manage* 168:296–307
11. Fadejev J, Simson R, Kurnitski J, Haghighat F (2017) A review on energy piles design, sizing and modelling. *Energy* 122:390–407
12. Laloui L, Donna A (2011) Understanding the behaviour of energy geo-structures. In: *Proceedings of ICE, Civil Engineering* vol 164. pp 184–191
13. Brandl H (2013) Thermo-active ground-source structures for heating and cooling. *Procedia Eng* 57:9–18
14. Suckling TP, Smith PEH (2002) Environmentally friendly geothermal piles at Keble College, Oxford, UK. In: *International conference on piling and deep foundations*. pp 445–452
15. Pahud D, Hubbach M (2007) Measured thermal performances of the energy pile system of the dock midfield at Zürich airport. Available at <https://pangea.stanford.edu/ERE/pdf/IGAstandard/EGC/2007/195.pdf> Accessed on 06 2007
16. Han C, Zhu C, Shen Y, Yu X (2022) Energy, environmental and economic performance evaluation of energy pile system under different climate conditions. *Energy Convers Manage* 252:115041
17. Zhong Y, Narsilio GA, Makasis N, Scott C (2022) Experimental and numerical studies on an energy piled wall: The effect of thermally activated pile spacing. *Geomech Energy Environ* 29:100276
18. Mousa MM, Bayomy AM, Saghir MZ (2022) Long-term performance investigation of a GSHP with actual size energy pile with PCM. *Appl Therm Eng* 210:118381
19. Bimaganbetova M, Zhang D, Kim J, Shon CS, Lee D (2022) Structural responses of energy storage pile foundations under thermal-mechanical loadings. *J Build Eng* 45:103539
20. Lee S, Park S, Kim D, Ahn D, Choi H (2021) Dual performance of novel steel pipe heat exchangers equipped in cast-in-place energy pile. *Energy Build* 234:110725
21. Ng CWW, Farivar A, Gomaa SMMH, Shakeel M, Jafarzadeh F (2021) Performance of elevated energy pile groups with different pile spacing in clay subjected to cyclic non-symmetrical thermal loading. *Renew Energy* 172:998–1012
22. Huang B, Mauerhofer V (2016) Life cycle sustainability assessment of ground source heat pump in Shanghai China. *J Clean Prod* 119:207–214
23. Gabrielli L, Bottarelli M (2016) Financial and economic analysis for ground-coupled heat pumps using shallow ground heat exchangers. *Sustain Cities Soc* 20:71–80
24. Lu Q, Narsilio GA, Aditya GR, Johnston IW (2017) Economic analysis of vertical ground source heat pump systems in Melbourne. *Energy* 125:107–117
25. Zhu Y, Tao Y, Rayegan R (2012) A comparison of deterministic and probabilistic life cycle cost analyses of ground source heat pump (GSHP) applications in hot and humid climate. *Energy Build* 55:312–321
26. Morrone B, Coppola G, Raucci V (2014) Energy and economic savings using geothermal heat pumps in different climates. *Energy Convers Manage* 88:189–198
27. Ren C, Deng Y, Cao SJ (2018) Evaluation of polyethylene and steel heat exchangers of ground source heat pump systems based on seasonal performance comparison and life cycle assessment. *Energy Build* 162:54–64
28. Zhou K, Mao J, Li Y, Zhang H (2020) Performance assessment and techno-economic optimization of ground source heat pump for residential heating and cooling: A case study of Nanjing China. *Sustain Energy Technol Assess* 40:100782
29. Arat H, Arslan O (2017) Exergoeconomic analysis of district heating system boosted by the geothermal heat pump. *Energy* 109:1159–1170
30. Kusuda T, Achenbach PR (1965) Earth temperatures and thermal diffusivity at selected stations in the United States. *ASHRAE Trans* 71(1):61–74
31. Cui Y, Zhu J, Meng F (2018) Techno-economic evaluation of multiple energy piles for a ground-coupled heat pump system. *Energy Convers Manage* 178:200–216

32. Buker MS, Mempoio B, Riffat SB (2014) Performance evaluation and techno-economic analysis of a novel building integrated PV/T roof collector: An experimental validation. *Energy Build* 76:164–175
33. Energy price—Parliament UK House of commons library (2018) Available at <https://researchbriefings.parliament.uk/ResearchBriefing/Summary/SN04153> [Accessed on 02 2018]
34. Ofgem Domestic renewable heat incentive <https://www.ofgem.gov.uk/environmental-programmes/domestic-rhi>